DEVELOPMENT OF A DECISION SUPPORT SYSTEM FOR OPTIMAL INSTRUMENTATION OF CONCRETE FACED ROCKFILL DAMS

A THESIS SUBMITTED TO
THE GRADUATE SCHOOL OF NATURAL AND APPLIED SCIENCES
OF
MIDDLE EAST TECHNICAL UNIVERSITY

BY

ONUR ARI

IN PARTIAL FULFILLMENT OF THE REQUIREMENTS
FOR
THE DEGREE OF DOCTOR OF PHILOSOPHY
IN
CIVIL ENGINEERING

SEPTEMBER 2016

Approval of the thesis:

DEVELOPMENT OF A DECISION SUPPORT SYSTEM FOR OPTIMAL INSTRUMENTATION OF CONCRETE FACED ROCKFILL DAMS

submitted by **ONUR ARI** in partial fulfillment of the requirements for the degree of **Doctor of Philosophy in Civil Engineering Department, Middle East Technical University** by,

Prof. Dr. Gülbin Dural Ünver _____
Dean, Graduate School of **Natural and Applied Sciences**

Prof. Dr. İsmail Özgür Yaman _____
Head of Department, **Civil Engineering**

Prof. Dr. A. Melih Yanmaz _____
Supervisor, **Civil Engineering Dept., METU**

Examining Committee Members:

Assoc. Prof. Dr. Nuri Merzi _____
Civil Engineering Dept., METU

Prof. Dr. A. Melih Yanmaz _____
Civil Engineering Dept., METU

Assoc. Prof. Dr. Ferhat Akgül _____
Engineering Sciences Dept., METU

Assist. Prof. Dr. Müsteyde Baduna Koçyiğit _____
Civil Engineering Dept., Gazi University

Assist. Prof. Dr. Aslı Numanoğlu Genç _____
Civil Engineering Dept., Atılım University

Date: 05.09.2016

I hereby declare that all information in this document has been obtained and presented in accordance with academic rules and ethical conduct. I also declare that, as required by these rules and conduct, I have fully cited and referenced all material and results that are not original to this work.

Name, Last Name : ONUR ARI

Signature :

ABSTRACT

DEVELOPMENT OF A DECISION SUPPORT SYSTEM FOR OPTIMAL INSTRUMENTATION OF CONCRETE FACED ROCKFILL DAMS

Arı, Onur

Ph.D., Department of Civil Engineering

Supervisor: Prof. Dr. A. Melih Yanmaz

September 2016, 219 pages

In this study, an algorithm for optimal design of instrumentation systems for concrete faced rockfill dams was developed. The aim of this algorithm is to determine the number and the location of individual instruments for stress monitoring. It was intended to develop a user-friendly and flexible algorithm that would be applicable in reliable and economic design of instrumentation systems for concrete faced rockfill dams. The first developmental step was the generation of a model cross-section for a concrete faced rockfill dam. Possible loadings were applied to this model cross-section. With the execution of a number of analyses for various dam heights via computer-assisted finite element analyses, some stress contours were obtained. These stress contours of different dam heights were analysed to end up with a representative stress distribution model. Then the governing dimensionless equations were formed for obtaining the magnitudes and location of different stress zones as a function of dam height. These zones provided information about the general trend of the overstressed areas. By expansion of the analyses, an algorithm for proper location and number of such equipment was obtained. An optimization algorithm to be used for horizontal placement of sensors in one of the standard sections were developed and the results were analysed. A vertical placement algorithm based on error minimization was also

developed and two algorithms were combined. The final optimization scheme was demonstrated for a number of dams and the sensitivity of the algorithm was also analysed. It can be said that this optimization scheme provides a basis for the design of an instrumentation system for concrete faced rockfill dams considering both the economy and the effectiveness in terms of data quality of the instrumentation system.

Keywords: Dam Safety, Dam Monitoring, Dam Instrumentation, Optimum Instrumentation, Concrete Faced Rockfill Dam

ÖZ

ÖN YÜZÜ BETON KAPLI KAYA DOLGU BARAJLARIN İZLEME SİSTEMLERİNİN EN UYGUN TASARIMI İÇİN BİR ALGORİTMA GELİŞTİRİLMESİ

Arı, Onur

Doktora, İnşaat Mühendisliği Bölümü

Tez Yöneticisi: Prof. Dr. A. Melih Yanmaz

Eylül 2016, 219 sayfa

Bu çalışmada, ön yüzü beton kaplı kaya dolgu barajların izleme sistemlerinin optimum tasarımı için bir algoritma geliştirilmiştir. Bu algoritmanın amacı, bağımsız yük ölçerlerin sayısını ve yerlerini belirlemektir. Ön yüzü beton kaplı kaya dolgu barajların izleme sistemleri için kullanımı kolay ve esnek bir algoritma geliştirilmesiyle bu sistemlerin tasarımlarının daha güvenilir ve ekonomik yapılabileceği öngörülmektedir. İlk adımda, bilgisayar destekli sonlu elemanlar analizi için model kabul edilen ön yüzü beton kaplı kaya dolgu bir baraj kesiti geliştirilmiştir. Bu bağlamda, değişken yükseklikteki baraj kesitlerine olası yüklemeler uygulanmıştır. Bu analizlerin değişken baraj yüksekliklerine uygulanması sonucunda eş-yük eğrileri elde edilmiştir. Bu eş-yük eğrilerinin değişken baraj yükseklikleri ve yükleme koşullarına uygulanmasının sonucunda ise temsili bir yük dağılım modeli oluşturulmuştur. Böylece eş-yük eğrileri boyut ve büyüklüklerini baraj yüksekliğine göre veren denklemler elde edilmiştir. Eş-yük eğrileri, baraj gövdesindeki aşırı yüklenmiş bölgelerin genel eğilimleri ile ilgili bilgiler vermiştir. Analizlerin genişletilmesi ile aygıtların gövde içindeki en uygun yerleri ve sayıları elde edilmiştir. Sensörlerin standart bir kesit içinde yatay doğrultuda yerleştirilmesi için bir optimizasyon algoritması geliştirilmiş ve elde edilen sonuçlar değerlendirilmiştir. Dikey doğrultuda sensör yerleşimi için kullanılacak hata küçültme

tabanlı bir algoritma da geliştirilmiş ve bahsedilen iki algoritma birleştirilmiştir. Sonuçta elde edilen optimizasyon planı çeşitli baraj kesitlerinde denenmiş ve algoritmanın hassasiyeti de analiz edilmiştir. Bu optimizasyon planının ön yüzü beton kaplı kaya dolgu barajların izleme sistemlerinin hem ekonomik, hem de izleme sisteminden elde edilecek verinin kalitesini göz önünde bulunduran bir şekilde tasarlanması için temel oluşturacağı öngörülmektedir.

Anahtar Kelimeler: Baraj Güvenliği, Barajların İzlenmesi, Baraj Ölçüm Sistemleri, En Uygun Ölçüm Sistemi, Ön Yüzü Beton Kaplı Kaya Dolgu Baraj

To My Mother and Father...

ACKNOWLEDGEMENTS

This study was supported by The Scientific and Technological Research Council of Turkey (TUBITAK) 2211-C Scholarship.

I would like to express my deepest gratitude to my supervisor Prof. Dr. A. Melih Yanmaz for his guidance, endless patience, and incredible support. Without his vision and ambition, this study would not have been possible.

Many thanks to my dissertation progress committee members Assoc. Prof. Dr. Nuri Merzi and Assoc. Prof. Dr. Ferhat Akgül for their valuable suggestions, comments and support.

It is with pleasure to express my genuine gratefulness to the Rt Hon. Kerem Ar and Dr. Musa McYılmaz for their exceptional brotherhood, encouragement, and endless support even sometimes from miles away.

Last but not the least, I would like to thank my mother and father for their endless love and patience.

TABLE OF CONTENTS

LIST OF TABLES

TABLES

LIST OF FIGURES

FIGURES

LIST OF SYMBOLS

a	parameter used in modelling of horizontal effective stress distribution
B	base width of the dam
B_c	crest width of the dam
B^*	width of a horizontal layer
b	parameter used in modelling of horizontal effective stress distribution
C_C	cost of cable
C_E	cost of equipment
C_P	cost of penalty
C_S	cost of sensor
C_T	total cost of instrumentation system
c	parameter used in modelling of horizontal effective stress distribution
d	parameter used in modelling of horizontal effective stress distribution
e	parameter used in modelling of horizontal effective stress distribution
f	parameter used in modelling of horizontal effective stress distribution
g	parameter used in modelling of horizontal effective stress distribution
H_b	base thickness of the dam
H_f	dam height from foundation level
H_t	dam height from thalweg level

h^*	height of a point on a horizontal projection from the foundation level
N	number of instruments on a horizontal projection
N_T	total number of instruments within a dam cross-section
M	number of horizontal projection on a dam cross-section
P'_h	projected horizontal effective force
P'_v	projected vertical effective force
$P'_v(N)$	modelled vertical effective force function
P'_{vt}	true vertical effective force function
S_d	horizontal run for 1 m-rise at downstream side slope
S_u	horizontal run for 1 m-rise at upstream side slope
x	horizontal distance of a point from (0, 0)
x_f	horizontal distance of the last point on a horizontal projection from (0, 0)
x_s	horizontal distance of the first point on a horizontal projection from (0, 0)
y	height of a point on a vertical projection from the foundation level
σ'_h	horizontal effective stress on a point
σ'_v	vertical effective stress on a point
σ'_{vmax}	maximum vertical effective stress on a layer
σ'_{vmin}	minimum vertical effective stress on a layer
γ	specific weight of water

CHAPTER 1

INTRODUCTION

1.1 General

Growing demand to energy and water leads to a great increase in dam construction activities. Dams may exhibit potential risk of failure depending on structural type, aging effects, and local site characteristics. In the case of collapse of a dam, valuable farm areas may be flooded, various types of private or public properties may be severely damaged and last but not the least, many fatalities may occur. In order to protect the people and the properties, it can be said that a dam must be as safe as possible. Although, the lessons learned from past events forced designers to develop sophisticated approaches, there still exists an unknown level of risk related with the dam body itself and the appurtenant structures. Due to the uncertain nature of hydro-meteorological data, foundation properties, material deficiencies, and constructional quality, every dam project imposes a potential risk, which can be reduced only if various sources of uncertainties are identified and handled in modelling (Yanmaz and Arı, 2011). This would result in economic savings.

1.2 Statement of the Problem

There is a growing tendency for constructing Concrete Faced Rockfill Dams (CFRDs) worldwide due to their apparent advantages regarding saving in construction duration and no-requirement to impermeable core. Similar to the case of other types of dams, an effective instrumentation system should be implemented to CFRDs to obtain information about the structural behaviour throughout the lifetime of these structures. The layouts of bodies of some existing CFDSs reported in the literature were examined according to the distribution of various types of instruments. However, no specific

guidelines regarding arrangement practices for instruments were found. Therefore, this gap in the literature is considered to be the triggering point of this study, which is carried out specifically for CFRDs.

This study attempts to find a logical answer to the questions that may arise during the design phase of a CFRD. The main question is related with the locations of the sensors to measure a structural health indicator of a dam. The secondary question would emerge quickly as well, which is related with the number of sensors within a structure. The aim is to provide a sound and logical decision support system which can provide the solution to the dam monitoring system designers considering the required amount of information from the sensor network with the lowest possible cost.

1.3 Scope of the Study

In this study, an algorithm for optimal design of monitoring and instrumentation system for CFRDs was developed. The aim of this algorithm is to determine the number and the location of individual instruments for stress-strain monitoring throughout the dam body. This selection is greatly dependent on the evaluation of the structural behaviour of this type of dam. It is intended to develop a user-friendly and flexible algorithm that would be applicable in reliable and economic instrumentation system design of concrete faced rockfill dams.

The first developmental step was the generation of a model cross-section for a concrete faced rockfill dam with respect to stress contours. To this end, a particular loading was applied to a model cross-section of variable height. A realistic execution of the software depends mainly on the description of foundation material properties, contact details between the dam and foundation and concrete upstream facing, and the assumptions made. The software PLAXIS was used for this purpose throughout this study.

Chapter 2 provides brief information about CFRDs, such as history, advantages over other types of dams, and design principles. Chapter 3 gives brief information about the items that should be monitored in CFRDs and summarizes the sensor types to be used in monitoring systems of CFRDs. The scope of the study and the development of the model are explained in detail in Chapter 4. The algorithm outputs and the effects of seepage, earthquake loading, and the alternative placement of sensors are also discussed in Chapter 4. In Chapter 5, the comparison and verification of the algorithm outputs with the instrumentation of existing CFRDs are presented. Finally, the conclusions and recommendations for further studies are provided in Chapter 6.

CHAPTER 2

CONCRETE FACED ROCKFILL DAMS

2.1 Brief Information about CFRDs

A Concrete Faced Rockfill Dam (CFRD) is a kind of embankment dam having an impervious concrete slab on the upstream face of underlying rockfill body in order to achieve watertightness rather than employing an impervious clay core. The hydrostatic load of the reservoir improves the overall stability of the dam body. With the properly constructed upstream concrete facing, the fill materials and zones of a CFRD are not saturated which prevents the occurrence of the pore water pressure within the dam body. CFRDs are gaining popularity from day to day because of their benefits. That is why initiative type selection studies of dam projects include CFRD alternative as the recent trend. Their advantages are listed as relatively low construction costs compared to other types of dams, simplicity in embankment formation, general suitability to different natural and foundation conditions, and shorter construction period. Other key factors favouring selection of concrete faced rockfill dams are their better performance in humid climates and no dependency on impervious soil reserves (Özkuzukıran et al., 2006).

A list of CFRDs in Turkey under service or during planning and construction stages is given in Table 2.1 in which E is energy, MW is municipal water, and IW is irrigation water.

Table 2.1 Concrete faced rockfill dams in Turkey

Dam	Province	River	Purpose
Aladereçam	Gümüşhane	Karaovacık	E
Alaköprü	Mersin	Dragon	E + MW
Arkun	Artvin/Erzurum	Çoruh	E
Atasu	Trabzon	Galyan	E + MW
Çokal	Tekirdağ	Kocadere	IW
Dim	Antalya	Dim	E + MW + IW
Gökçebel	Gümüşhane/Giresun	Gelevar	E
Gördes	Manisa	Gördes	MW + IW
Ilısu	Mardin	Dicle	E
Kandil	Kahramanmaraş	Ceyhan	E
Kavşak Bendi	Adana	Seyhan	E
Kürtün	Gümüşhane	Harşit	E
Marmaris	Muğla	Kocaalan	MW + IW
Sarıgüzel	Kahramanmaraş	Ceyhan	E
Silvan	Diyarbakır	Batman	E+IW
Torul	Gümüşhane	Harşit	E

In spite of the aforementioned advantages of CFRDs, design of the impervious upstream facing requires great attention. Since the design of CFRDs is generally based on the expert judgment and engineering experience (Cooke, 1984), various properties of this face slab should be studied extensively with utmost care. A typical cross-section of a CFRD is given in Figure 2.1.

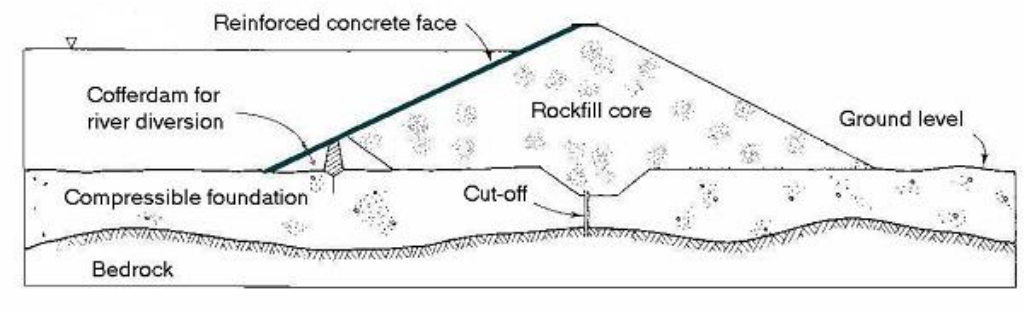

Figure 2.1 A typical CFRD cross-section (Chau Chin, 2004)

2.2 History of CFRDs

CFRD application originated from gold mining region of Sierra Nevada in California by 1850s. Gold miners developed the construction technique of dumped rockfill dams in order to provide cooling water for their drilling equipment. In early times, these dumped rockfill dams had been waterproofed by wooden upstream facings, which were by time replaced by concrete facing (ICOLD, 1989). The first dam which can be considered as a CFRD is Chatsworth Dam which was constructed in California in 1895.

The second development period of CFRD is named as the transition period (ICOLD, 2005). During this period, a number of problems were faced by the engineers. Three most observed problems during that era were the excessive settlement of the relatively high CFRDs, insufficient compaction, and serious seepage from the concrete face slab and plinth. New Exchequer Dam in California completed in 1965 is accepted as the last example of the CFRDs constructed during the transition period (Ergeneman, 2012).

The modern era of the CFRDs was initiated with the advancement of vibratory roller compactors. Better compaction with more efficient controlling of water content of the

fill material leaded to an obvious increase in dam performance. The developments in compaction techniques and the zoning of CFRDs have greatly reduced the settlements of dam body and thus helped to the concrete face slab to stay intact and prevented water seepage.

As a summary, starting from the wooden-face dumped rockfill dams built during the California Gold Rush, development and application of CFRDs was limited up to 1960's (Cooke, 1984). This was due to the limitation of machinery and materials. Starting from 1970's many CFRDs have been designed and constructed (Sherard and Cooke, 1987) due to the economic and technical advantages. The development of material, construction techniques and software analysis possibilities accelerated. Shuibuya Dam in China, passed the 200 m limit and is the highest concrete faced rockfill dam in the world with 233 m height (Özkuzukıran, 2005).

2.3 Characteristics of CFRDs

In design-wise approach, CFRDs do not require any specific site and foundation conditions different from the impervious core rockfill dams (Sherard and Cooke, 1987). However, some components of CFRDs are exclusive to this type of dams and provide both watertightness and stability.

2.3.1 Plinth

A plinth is an important part of a CFRD, located below the upstream concrete facing and foundation. It acts as a transition between the upstream face slab and the foundation which houses some filter materials. Its main role is to prevent foundation level seepage. Copper and rubber waterstops provide the watertightness and continue to provide it up to a predefined level of differential movement of plinth and concrete slab (Korkmaz, 2009). A plinth is also anchored to the foundation rock by the grouting

application. The grouting does not only fix the base of plinth to the ground, but also reduces the seepage beneath it. A typical plinth application is shown in Figure 2.2.

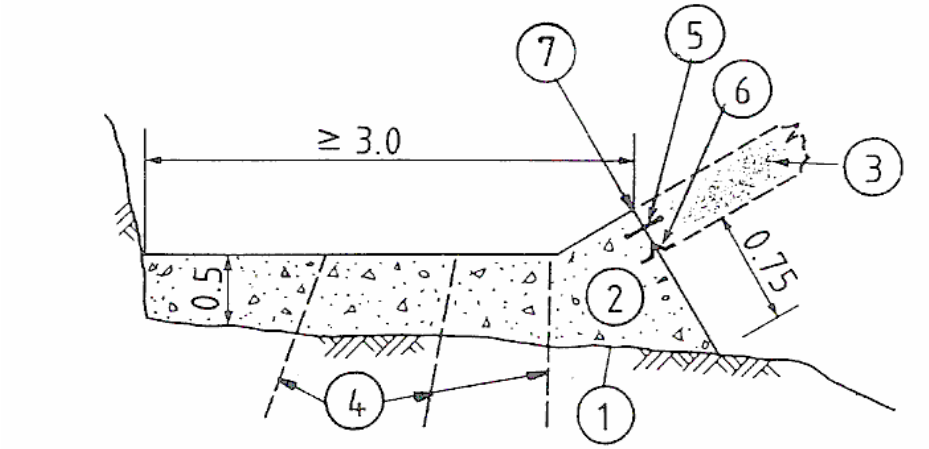

1 Rock surface
2 Reinforced concrete
3 Face sealing
4 Grouting holes
5 PVC waterstop
6 Copper waterstop
7 Plinth line

Figure 2.2 A typical plinth cross-section (ICOLD, 2005)

The dimensioning of the plinth has a significant effect on the stability. If the plinth has excessive height, a number of problems might be observed, such as loss of stability under full reservoir loads. ICOLD (1989) recommends to conduct sliding and overturning analyses. As a general rule of thumb, high plinths should be avoided in order to reduce the chance of seepage due to the excessive movements observed at plinth. The thickness of the plinth can be determined from Ergeneman (2012):

$$T = 0.3 + 0.003H_t \tag{2.1}$$

where, T is the thickness of the plinth in meters and the H_t is the height of the dam from thalweg in meters.

2.3.2 Face Slab

The face slab is the primary element of the CFRDs. It provides watertightness by blocking the water to seep through the dam body. Since no other element is placed inside the dam body, the design of the face slab requires great attention. Face slab can be considered as reinforced concrete plate which is supported by the fill material and is normally under compression (ICOLD, 2005). In Figure 2.3, construction of the upstream concrete face slab of Shuibuya Dam is presented.

Figure 2.3 Concrete face slab of Shuibuya Dam (Materon, 2013)

Although face slabs are considered under compression, the settlement of the dam body might create moment because of the loss of the support of the fill material. In order to reduce the effect of this problem, face slabs are reinforced. Face slabs are constructed in predetermined panel widths in order to reduce the effect of shrinkage during construction (ICOLD, 2005). In general, panel widths are chosen between 12 m and 18 m. Two successive face slab panels are equipped with waterstops in order to ensure the watertightness. Horizontal and vertical waterstops of the face slab of Kavşak Bendi Dam are presented in Figure 2.4.

Figure 2.4 Close-up view of the face slab of Kavşak Bendi Dam

The cracks on the face slab can be divided into three categories as cracks caused by the shrinkage of the concrete (Type-A), cracks caused by the settlement of the supporting fill material (Type-B), and cracks caused by the differential settlement of the dam body (Type-C) (Mori, 1999).

The Type-C cracks are the most common type of cracks. According to Marulanda and Pinto (2000), these cracks are related with the unexpected deformation of the fill body. The Type-C cracks of the face slab of Xingo Dam were as wide as 15 mm and located to the close vicinity of the left abutment (Souza et al., 1999). Those cracks were then filled with fine silt and sand (ICOLD, 2005). The cause of Type-C face slab cracking at Ita Dam was the use of less dense supporting material at distances away from the perimeter joint (Pinto, 2001).

Although small cracks can be filled by fine silt, sand, or fly ash, the cracks which are wider than 30 mm requires a different solution. Wu et al. (2000) recommends to treat wider cracks with a fly ash and a grouting mixture of cement and sand.

The concrete mix design of the face slab requires great attention. The concrete mix should be durable throughout the lifetime of the structure and help to minimize the shrinkage during curing period (ICOLD, 2005). Limiting the water content of the concrete mix will help to obtain a durable concrete (Jiang and Zhao, 2000). Durability of the concrete against freezing and thawing can be achieved by air entrainment. Jiang and Zhao (2000) recommends that the entrained air should be between 4 and 7 percent.

2.3.3 Perimeter Joints

Perimeter joints are the main joints which are placed between the face slab and the plinth. The function of the perimeter joint is to allow the relative movements between the face slab and the plinth to some degree while maintaining the watertightness under various loading cases and reservoir water levels (ICOLD, 2005).

A perimeter joint consists of a number of elastic seals and filler materials to support the seals. A detailed cross-section of the perimeter joint of Salvajina Dam is presented in Figure 2.2.

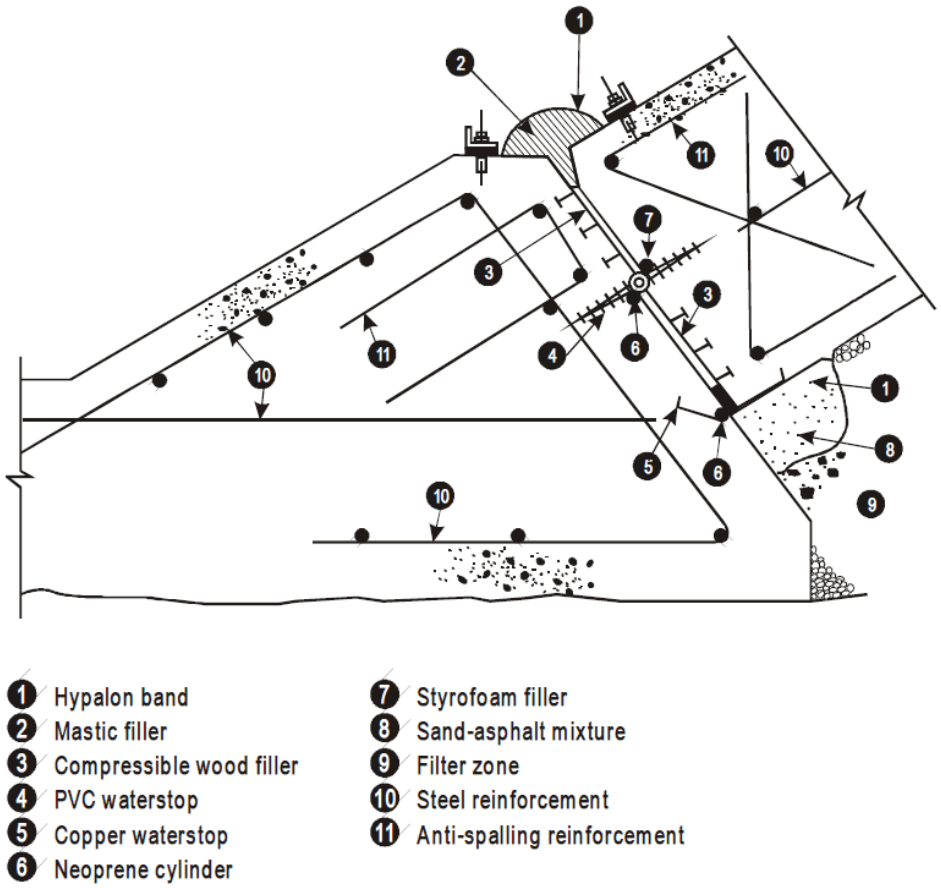

Figure 2.5 Perimeter joint detail of Salvajina Dam (ICOLD, 1989)

The development of the perimeter joints of CFRDs were started with Cethana Dam (Australia). The perimeter joint of Cethana Dam was designed with two subsequent waterstops. After five years of operation, the leakage reduced to 10 litres per second (Pinto and Mori, 1988). The attempts of reducing the waterstops of perimeter joints from two to one led to a drastic increase in the leakage rates of Alto Anchicaya Dam. In order to cope with this problem, mastic joint sealant was applied to the Alto Anchicaya Dam (ICOLD, 2005). Lessons learned from Alto Anchicaya Dam led to the development of three-layer perimeter joints.

2.3.4 Body Zoning

The body fill of a CFRD comprises many zones. Some of these zones act as a filter and bumper material between face slab, whereas the others support the load (ICOLD, 2005). General zoning and the material types of the zones are provided in Figure 2.6.

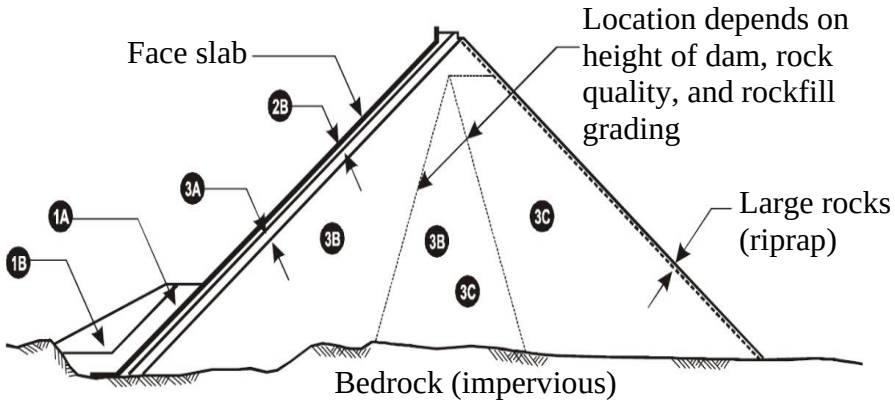

1A: Cohesionless fine-grained soil
1B: Random fill (silt, sand, gravel, etc.)
2A: Perimeter zone filter (not shown)
2B: Face slab support layer (sand and gravel)
3A: Selected rockfill (max. 0.4 m)
3B: Quarry rockfill (max. 1 m)
3C: Quarry rockfill (max. 2 m)

Figure 2.6 CFRD Zoning (ICOLD, 1994)

The 1A zone consists of fine sand, cohesionless silt, or fly-ash and the maximum particle size in this zone is 150 mm. The purpose of the 1A zone is to wash through the possible cracking on the face slab and clog the filter materials beneath the face slab. The 1B zone protects the 1A zone and is made of random fill of silt, sand, and gravel.

The 2A and 2B zones are also called as protective zones. The 2A zone acts as a filter for 1A zone material if any problem arises at perimeter zones. The 2B zone thickness

is between 2 to 4 m and supports the face slab with a low permeability. The 2B zone should be protected with utmost care during construction either by shotcrete application or concrete curbs (ICOLD, 2005).

The 3A zone is a transition zone which prevents the 2B zone to be washed away to 3B zone material. Zones 3B and 3C are the main rockfill zones of the dam body, whereas 3D zone is also called the riprap zone which protects the downstream face of the dam from environmental erosion.

Zones at the mid-axis of Kürtün Dam and Nam Ngum 2 Dam are presented in Figure 2.7 and Figure 2.8, respectively. It can be noticed that these material zones and grading changes in different dams, because the CFRD designs are mainly empirical and rely on the past experiences and expert judgements.

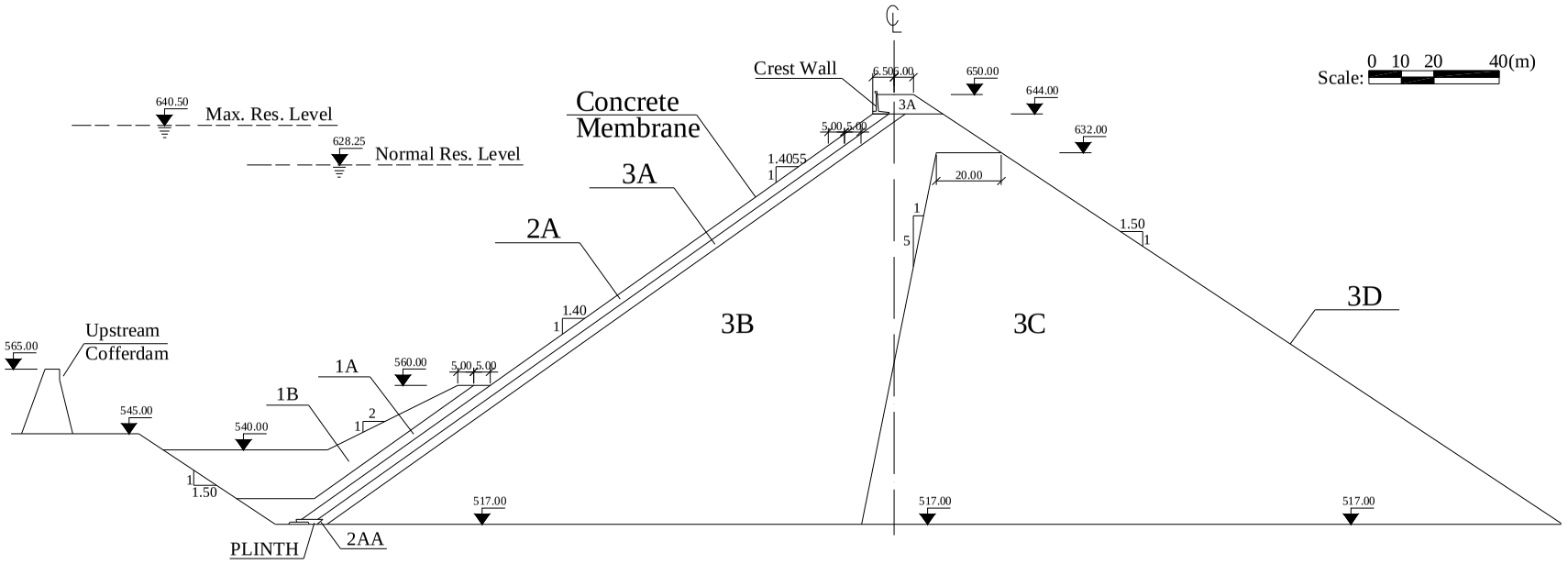

Figure 2.7 Zoning of Kürtün Dam (Özkuzukıran, 2005)

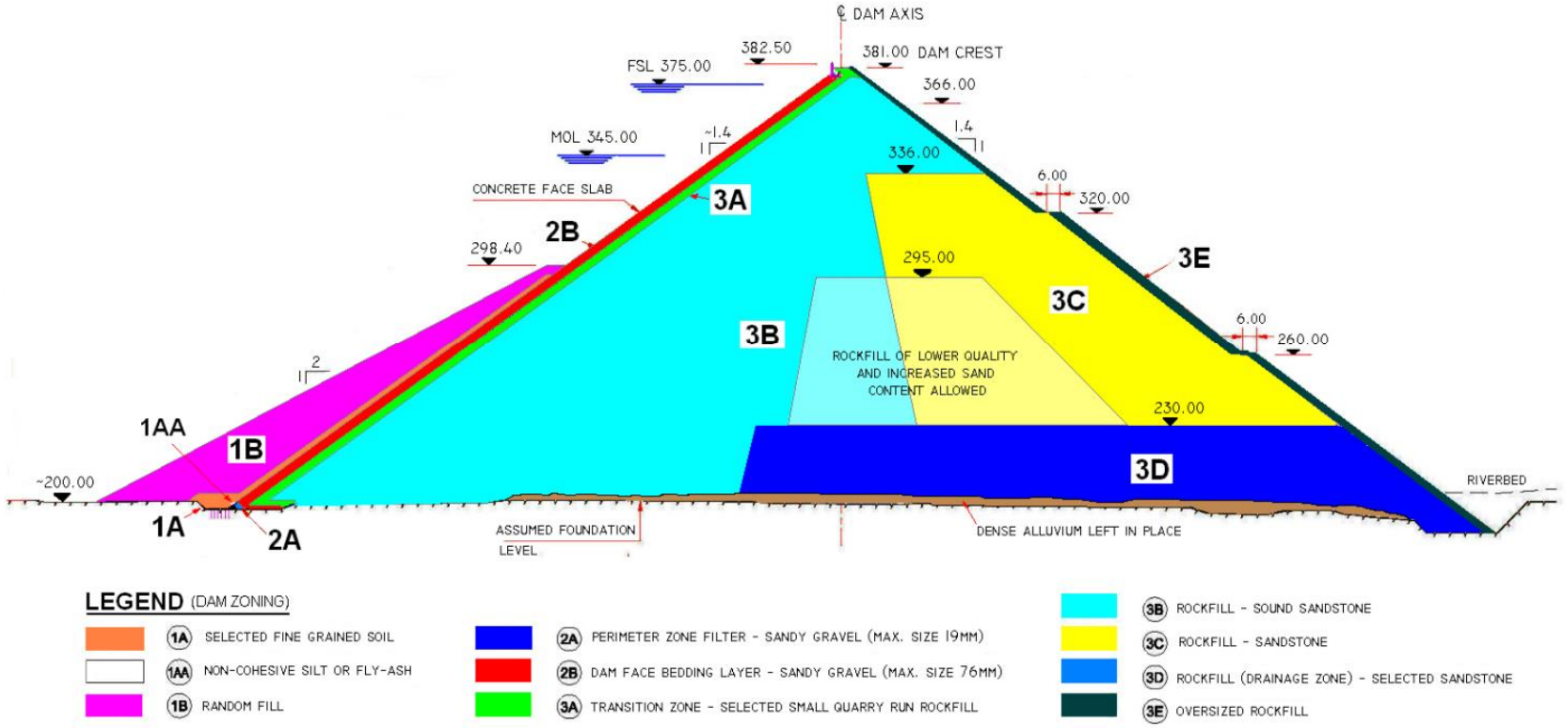

Figure 2.8 Zoning of Nam Ngum 2 Dam (Straubaar et al., 2009)

2.4 CFRD Design Principles

Design of CFRDs comprises a number of essential analyses (ICOLD, 2005), such as:

- Static stability analysis
- Dynamic stability analysis
- Prediction of the settlement and the face slab deformation
- Prediction of the leakage.

Static stability analysis starts with the determination of the properties of the fill materials available in close vicinity. Since a dam construction requires vast amount of material, most of the time it would not be feasible to transport the fill material with desired properties. In the light of the material properties, the designer can, therefore, conduct slope stability analysis and determine the dimensions of the dam body and the side slopes.

Dynamic analysis would provide the anticipated behaviour of the dam during an earthquake and should be conducted if the dam site is susceptible to high seismicity. Although the rockfill dams are generally considered as safe structures against earthquakes, dynamic analysis provides an estimate of a possible crest settlement of the dam under the loading of a severe earthquake. According to ICOLD (2005), CFRDs should be designed by defensive design concept which dictates a sufficient freeboard to compensate a possible crest settlement after an earthquake. A number of widely used methods can be used to determine the crest settlement, such as Makdisi and Seed Method (Makdisi and Seed, 1977) and Bureau's Method (Bureau, 1997).

Settlements immediately after the construction lead to a decrease in freeboard which might increase the risk of overtopping. Settlements can be simply predicted with the

modulus of the elasticity of the rockfill material. However, the rockfill material is not perfectly elastic and Mohr-Coulomb material models might not work well. Some empirical approaches, such as the decision support system of Pinto and Marques (1998) can be used to predict the face slab deformation easily. However, with the advancement in finite element method and increased computing power, complex models, such as hardening soil models would provide more successful results.

Leakage performance of a CFRD is considered as the key parameter in determination of the success of the design. Although the leakage can be estimated with usual flow through porous medium concept, more detailed methods also take the effect of the discontinuities within the foundation and the dam body into account (Giesecke et al., 1991).

As a summary, CFRD design comprises of modelling of a vast number of variables. Before the advancement of computer-assisted design and analyses, some expert systems were developed by researchers. As a result of this, the CFRD designs were dependent on the expert opinions and judgements. The designs were developed with the lessons learned from the past experiences. However, the rapid rise of the computing power in the last few decades helped designers to introduce the effect of more variables to the problem.

Although the design procedures have evolved with the powerful computers and advanced software packages, the performance of the contemporary design applications still needs to be verified. With the advancement in technology, extremely sensitive and accurate sensors are available nowadays. These sensors not only validate the design, but also provide essential support for structural health monitoring. The next chapter gives detailed information about the purpose and the types of the sensors which are now accepted as vital for monitoring of the CFRDs.

CHAPTER 3

MONITORING SYSTEMS OF CONCRETE FACED ROCKFILL DAMS

3.1 Items to be Monitored at CFRDs

3.1.1 Introductory Remarks

CFRDs are prone to overtopping, sliding, seepage induced failures, excessive settlement, and slab cracking. Therefore, it is possible to assess life-long behaviour of CFRDs with the proper instrumentation system which is designed to capture, log, and process the vital structural health indicators of the dam.

3.1.2 Seepage

CFRDs are seepage-critical structures. In design phase, the upstream concrete facing is assumed to be fully watertight during the lifetime of the structure. However, even a small settlement or movement could lead to crack formation or joint openings on the upstream facing. With the absence of an impervious core, the seepage rate would then increase rapidly.

Anthiniac et al. (2002) state that every CFRD experiences some degree of leakage and the general trend among dam owners is to accept that increased leakage. It is also stated that this inevitable leakage would not cause a major safety concern because of the leakage-proof nature of the design and the materials. However, ICOLD (2005) stresses out that if a CFRD is built according to the state-of-the-art methods and meticulous workmanship, the leakage rates may be as low as 1 lt/sec.

The change in the hydrostatic water pressure within the dam body can provide information about the possible leakage from the face slab or perimeter joint. So it is beneficial to measure the hydrostatic water pressure within the dam body and at the foundation of the dam.

Measurement of the rate and the turbidity of the seepage flow will also provide valuable information about the change of the leakage with respect to reservoir level. Turbidity measurement would provide clues about the location of the initiation of the leakage.

3.1.3 Settlement, Deformation, and Movement

Overtopping is a general weak point of embankment dams. CFRDs have a sound upstream facing but the downstream slope is generally unprotected as other types of embankment dams. Settlement of the dam body is one of the causes of overtopping, which may lead to a reduction in the freeboard (FERC, 1999).

Saturation of either foundation or embankment body will result in excessive settlement, which further impacts the concrete facing. Since upstream concrete face slab is an important integral part of the CFRDs, the condition of the face slab should be monitored periodically by means of joint opening and alignment monitoring.

Deformation of the structural elements provides vital information about the behaviour of the dam. Monitoring of the deformation also provides information about the internal stress changes within the dam body. Overall geometry changes which are measured from the outside of the dam would provide evidence about the differential movement of the dam foundation.

3.2 Types of Sensors

The basic instrumentation concept of CFRDs with the instruments and their purposes are summarized in Table 3.1.

Table 3.1 Instruments of CFRD (Moll and Straubhaar, 2011)

Instrument	Measured Parameter
3D Joint Meters	Movement of concrete face slab joints and perimeter joint
2D Joint Meters	Movement of concrete face slab joints
1D Joint Meters	Movement of concrete face slab joints
Inclinometers and Tiltmeters	Deflection of concrete face slab
Rebar Strain Gauges	Strain in concrete face slab
Concrete Strain Gauges	Strain in concrete face slab
No-Stress Strain Gauges	Reference strain in concrete
Embankment Extensometers	Transverse movement of the dam body
Settlement Cells	Settlement of the dam body
Surface Monuments	Movement of the surface
Strong Motion Accelerometers	Earthquake acceleration
Total Pressure Cells	Total pressure at dam body and foundation
Piezometers	Water pressure in dam / dam foundation and seepage
Seepage Measuring Weir	Seepage through the dam body and abutments

3.2.1 Total Pressure Cells

Total pressure cells have been used in dams since late 1950s and were appreciated in terms of their reliability over five years and consistent performance by Thomas and Ward (1969). Total pressure cells measure the changes of direct (effective) pressure acting over them. They are made of two steel plates firmly fixed each other from the edges to form a pad and is filled with an incompressible fluid (Arı, 2008). One end of the total pressure cell is equipped with a pressure transducer which measures the change in the pressure acting on the cell, and thus the oil. Some pressure cells are also equipped with thermistors for the determination of temperature in close vicinity of the sensor.

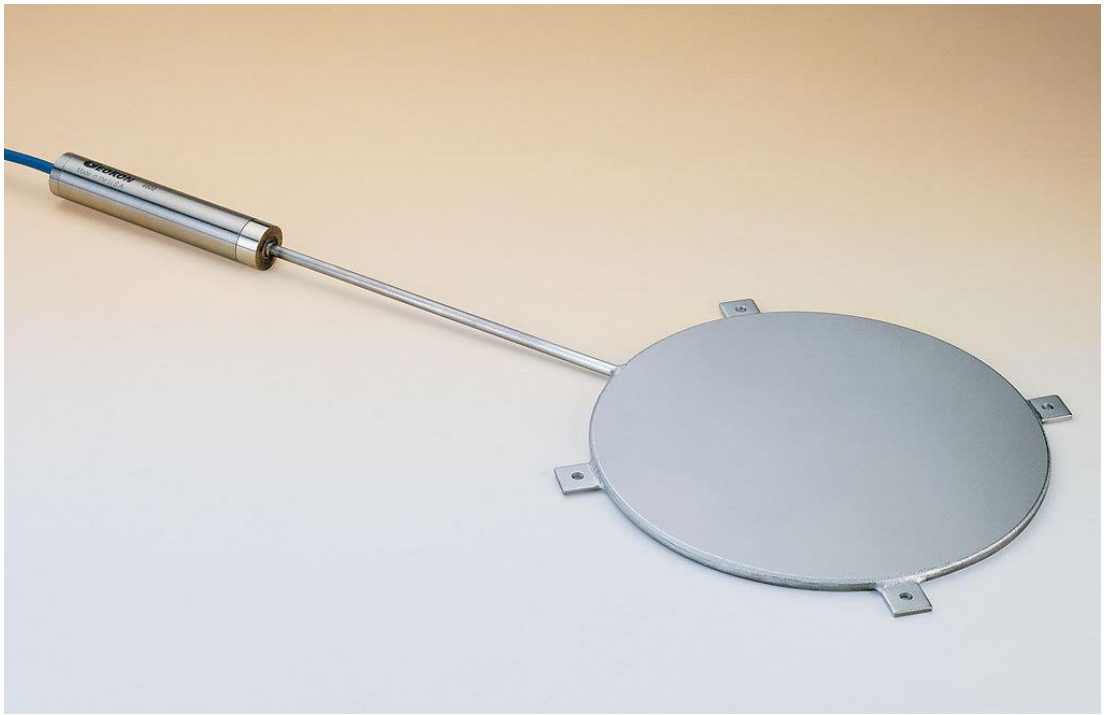

Figure 3.1 Standard type total pressure cell (Geokon, 2016-a)

Total pressure cells can be located to any place within dam body and foundation where the stress variations are of interest (Szostak-Chrzanowski and Massiéra, 2006). Their design varies according to the material types of which they are intended to stay in

contact. Standard total pressure cells are used for the measurement of the pressure within embankments (Figure 3.1). Pressure cells with a rigid back side are named as contact type total pressure cells and they are used to measure the pressure at the contact area of concrete (Figure 3.2).

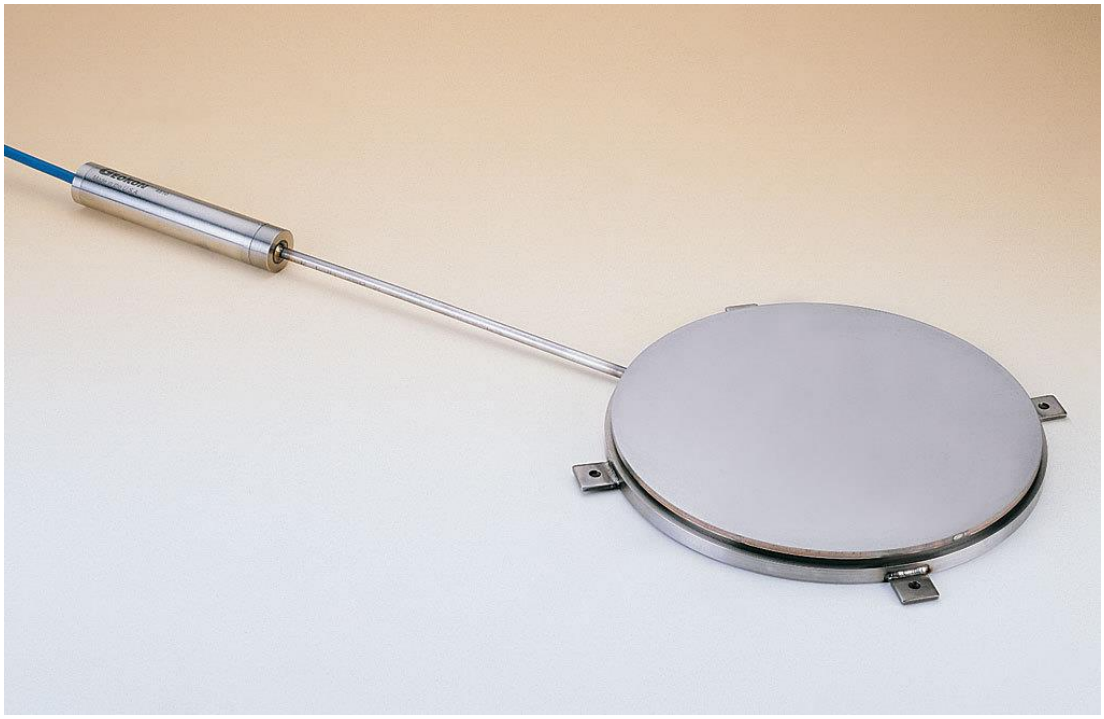

Figure 3.2 Contact type total pressure cell (Geokon, 2016-b)

3.2.2 Strain Meters

Strain meters are used to monitor the strain in one degree; although they can be mounted in a group for measuring the strains in more than one axis. They can be used to monitor the behaviour of the stress changes as well. Strain meters are used to monitor the stress and strain on the reinforcement bars used in the face slab (Yanmaz and Arı, 2008).

Embedment strain meters are embedded into a freshly poured concrete of piles, columns, beams, or face slabs in CFRDs. They measure the strain changes within the concrete. A typical embedment strain meter is presented in Figure 3.3.

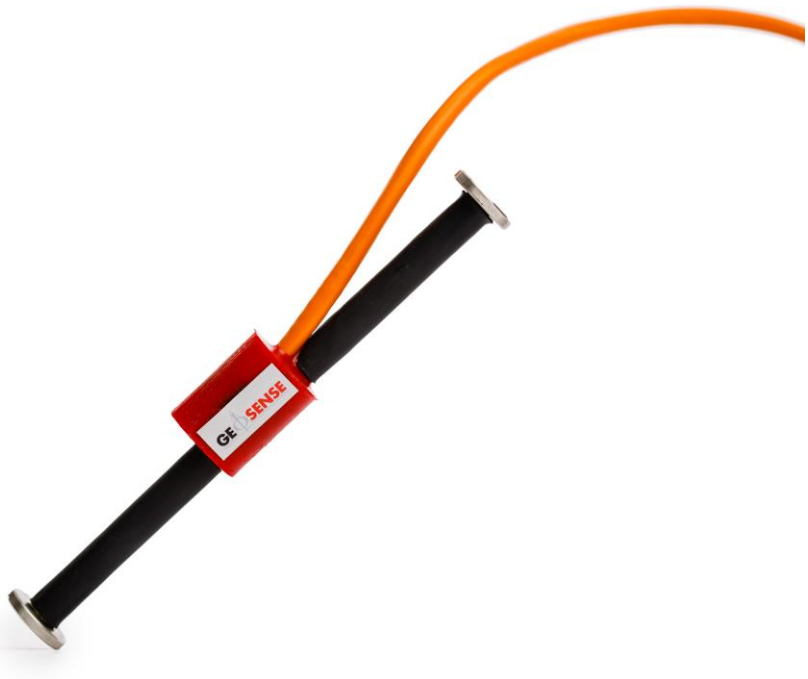

Figure 3.3 Embedment strain meter (Geosense, 2013)

Strain meters are also used for determination of the strain on the reinforcement bars or steel elements. Weldable surface-mount strain meters are suitable for monitoring the steel structural elements, whereas the spot weldable strain meters are used to measure the strain on the reinforcement bars. Typical surface-mount and spot weldable strain meters are presented in Figure 3.4 and Figure 3.5, respectively.

Figure 3.4 Weldable surface-mount strain meter (Slope Indicator, 2013)

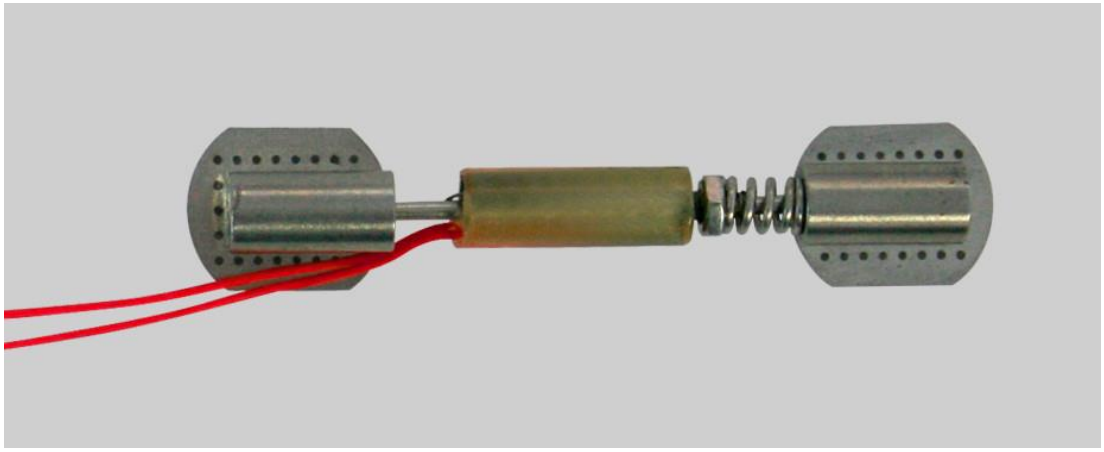

Figure 3.5 Spot weldable strain meter (RST Instruments, 2015)

3.2.3 Settlement Cells

Settlement cells are very useful during the construction phase of the dam. They also play an important role during initial filling of the reservoir, since most of settlements are observed at the initial filling of the dams. Settlement cells are also used for

monitoring the vertical movements of the dam body and foundations throughout the lifetime of the structure. During the design of all dams, some settlement is anticipated by the designer by means of either computer-assisted analyses or empirical formulation. Settlement cells are very helpful for verification of the design methods and parameters just after the completion of the dam. A typical vibrating wire settlement cell is presented in Figure 3.6.

Figure 3.6 Vibrating wire settlement cell (Soil instruments, 2014)

Settlement cells can either be hydraulic or electronic (vibrating-wire). The vertical movement within the dam body changes the location of the settlement cell. This

change is then measured by the settlement cell by measurement of the hydrostatic pressure in the chamber of the instrument.

3.2.4 Joint Meters

As mentioned before, face slab of a CFRD consists of many individual panels. All panels are mounted to each other; however, these mountings should allow relative movements to some extent. In order to monitor the opening or closing movement of the joints, joint meters are used. A typical one-dimensional joint meter is presented in Figure 3.7.

Figure 3.7 Joint meter (Sisgeo, 2016)

Joint meters can be one, two, or three dimensional. Generally, one or two dimensional joint meters are used to monitor the relative displacement of the individual panels, whereas three dimensional joint meters are preferred to monitor the perimeter joints.

3.2.5 Inclinometer

Inclinometers are employed in CFRDs in order to measure the deformation of the face slab. Inclinometers are basically composed of rugged steel or PVC pipes firmly mounted onto the face slab. The pipes have special grooves for driving the measuring probe inside it (Figure 3.8).

Figure 3.8 Inclinometer casing (Roctest, 2016-a)

Just after construction of the face slab and before initial filling, it can be said that the face slab is perfectly flat and there is no deviation on the inclinometer casing. After loading of the face slab, inclinometer casing also deforms with face slab, hence it is firmly mounted. The measuring probes are very sensitive and can record the slightest irregularity while moving inside the inclinometer tubing (see Figure 3.9).

Figure 3.9 Inclinometer probe (Roctest, 2016-b)

3.2.6 Piezometers and Weirs

Piezometers are mainly employed to measure the pore water pressure. There are several different types of piezometers from early standpipes to vibrating-wire piezometers which are as small as a fountain pen. They are accurate and simple way to measure the pore water pressure if the correct filter tips are used and installed properly.

In CFRDs, piezometers are mainly placed at foundation level but can also be installed within the dam body. ICOLD (2005) states that the use of piezometers is optional

unless the embankment fill comprises a non-drained material. A number of piezometers for different applications are presented in Figure 3.10.

Figure 3.10 Vibrating wire piezometers (Telemac, 2016)

Weirs are used to measure the rate of the seepage from the face slab and perimeter joint through the dam body. They can be placed where the seepage measurement requires a critical importance. Turbidity measuring sensors are also very beneficial for determining the exact location of the initiation of the leakage. A v-notch weir with its sensor is presented in Figure 3.11.

Figure 3.11 V-Notch weir and vibrating wire sensor (itmsoil, 2013)

3.3 Monitoring System Layouts of Existing Dams

Current practices formed by expert judgements have been studied in order to form a basis for the algorithm to be generated as a result of this study. That is why the evaluation of the instrumentation configuration of some existing dams may provide useful information. The instrumentation layout of maximum cross-sections of various CFRDs throughout the world are presented in the following figures.

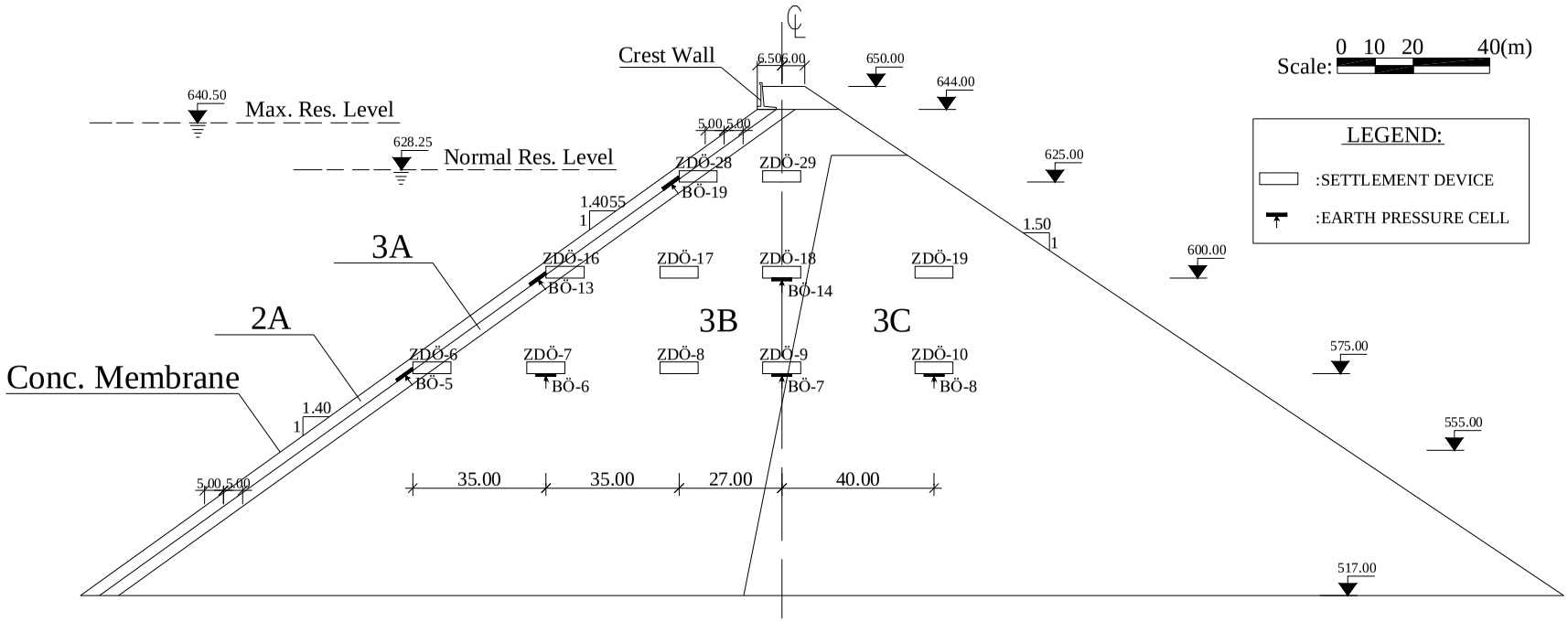

Figure 3.12 Settlement measuring devices and pressure cells in cross-section KM: 0+120.00 of Kürtün Dam (Özkuzukıran, 2005)

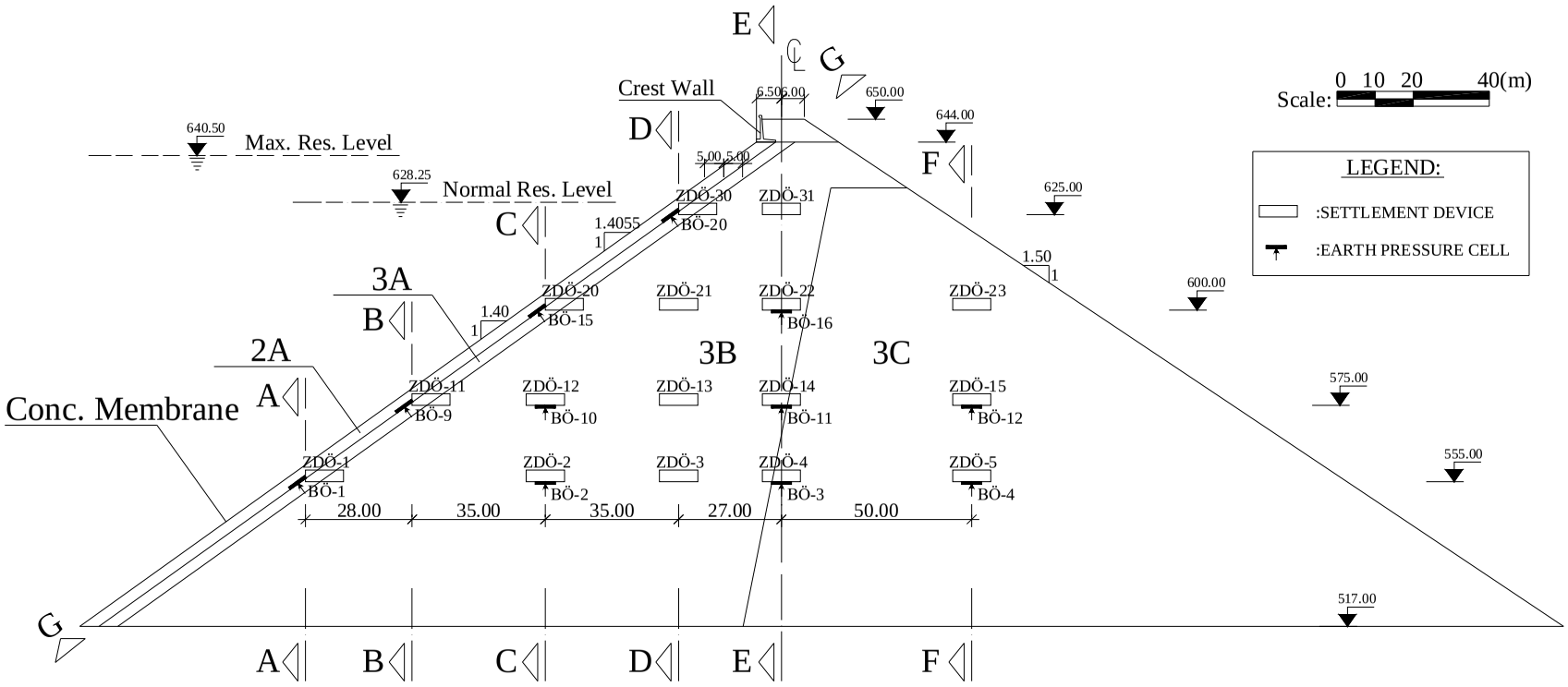

Figure 3.13 Settlement measuring devices and pressure cells in cross-section KM: 0+180.00 of Kürtün Dam (Özkuzukıran, 2005)

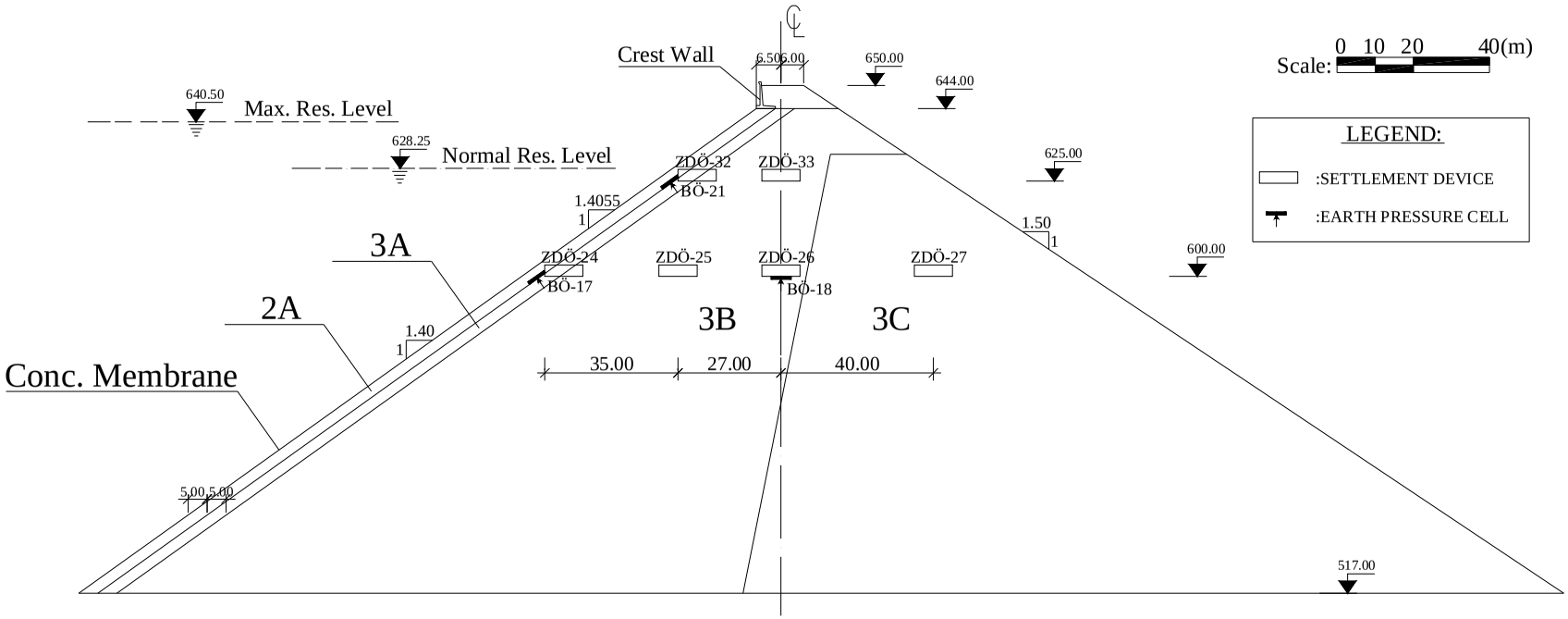

Figure 3.14 Settlement measuring devices and pressure cells in cross-section KM: 0+240.00 of Kürtün Dam (Özkuzukıran, 2005)

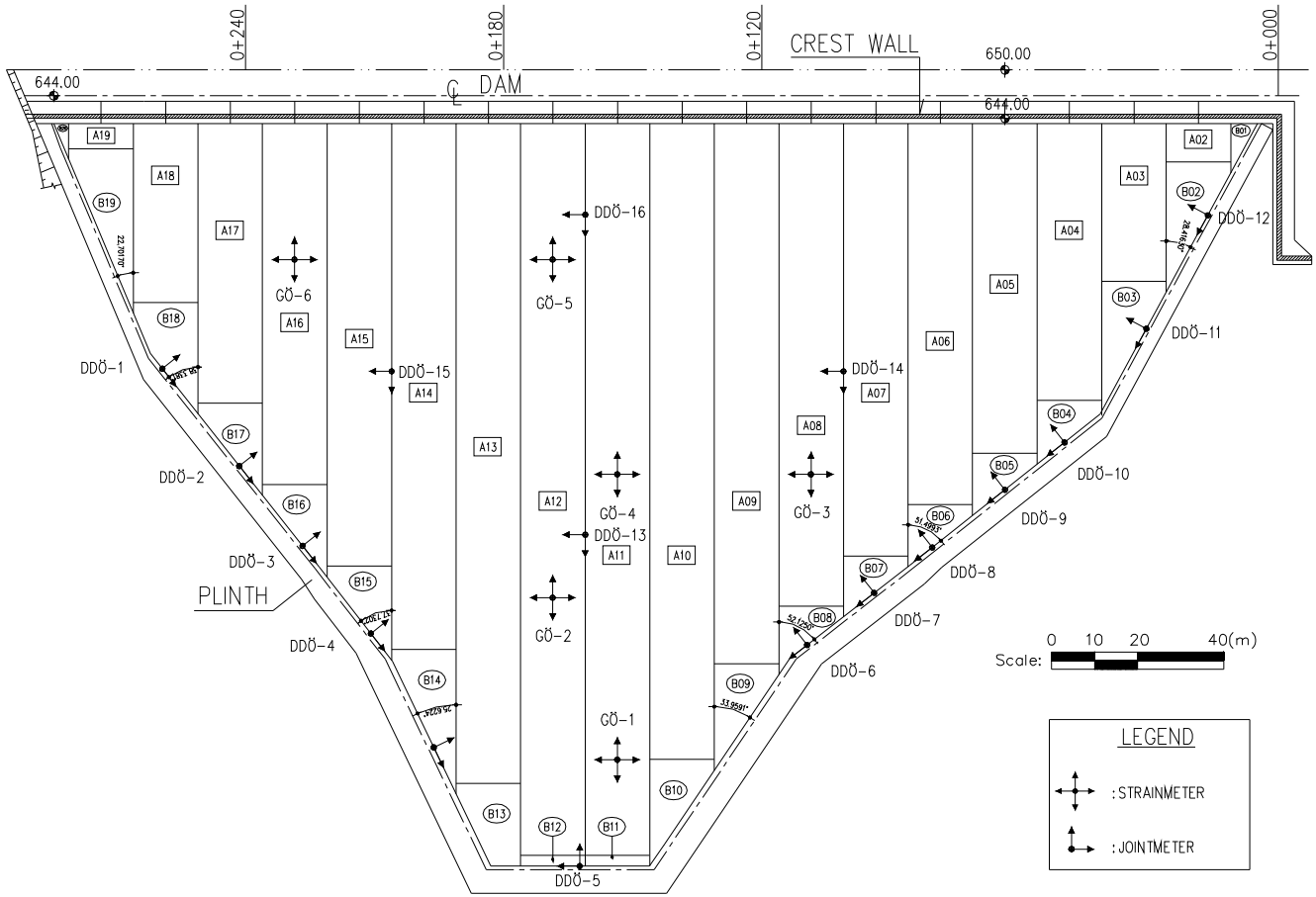

Figure 3.15 Locations of jointmeters and strainmeters at concrete face of Kürtün Dam (Özkuzukıran, 2005)

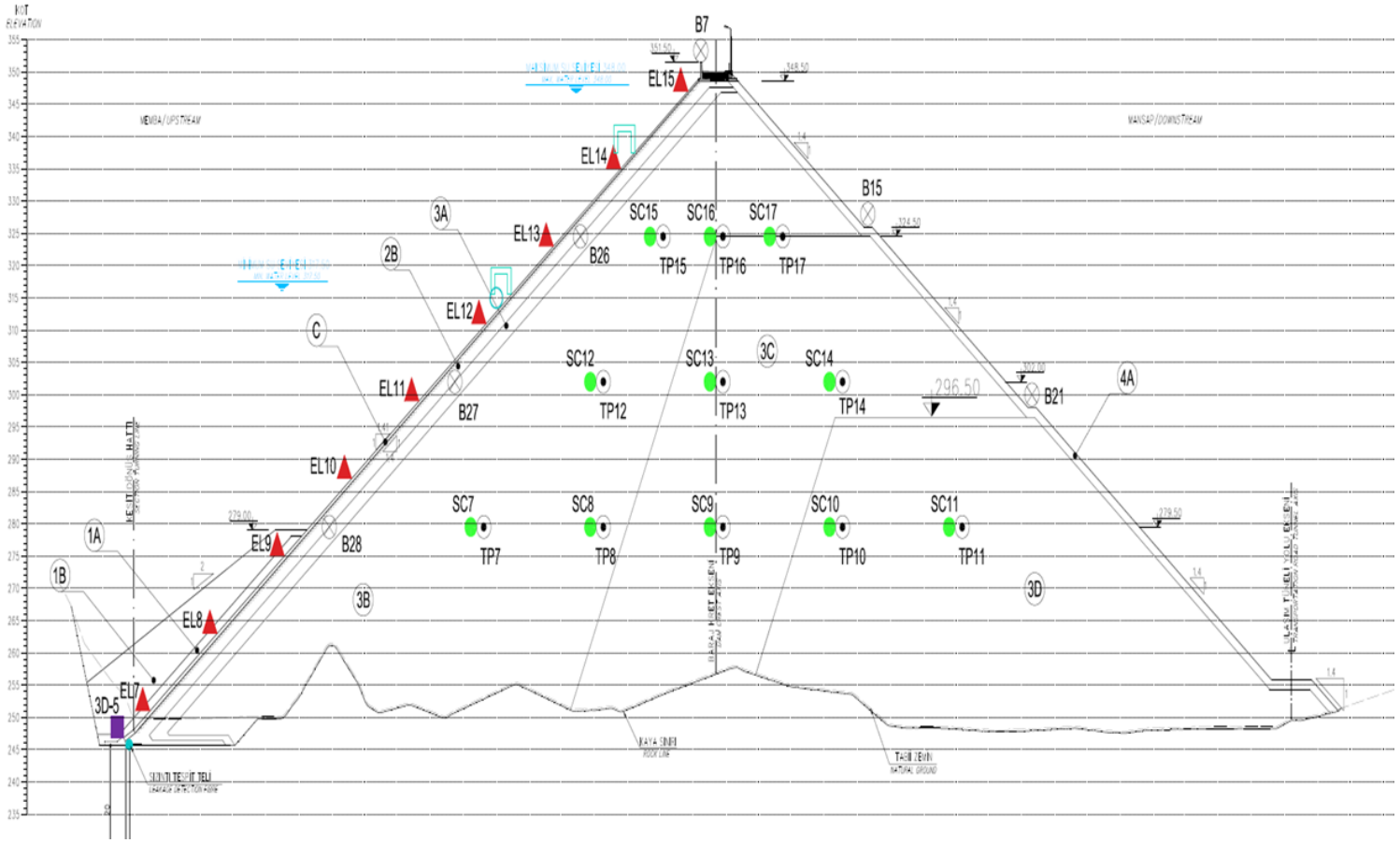

Figure 3.16 Tanyeri Dam (103.5 m) (Stucky Teknik, 2012)

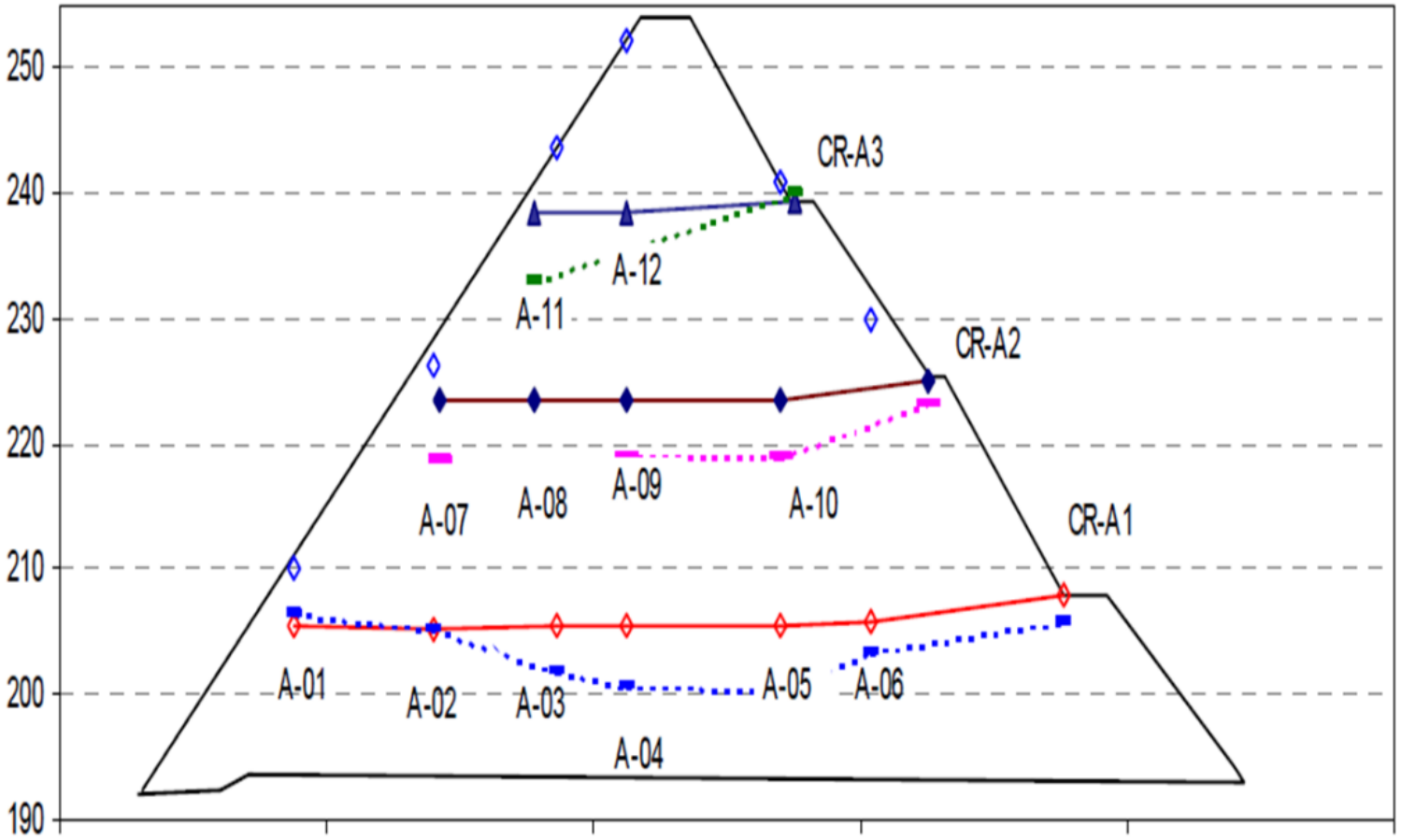

Figure 3.17 Berg River Dam (67 m) (Thamae, 2007)

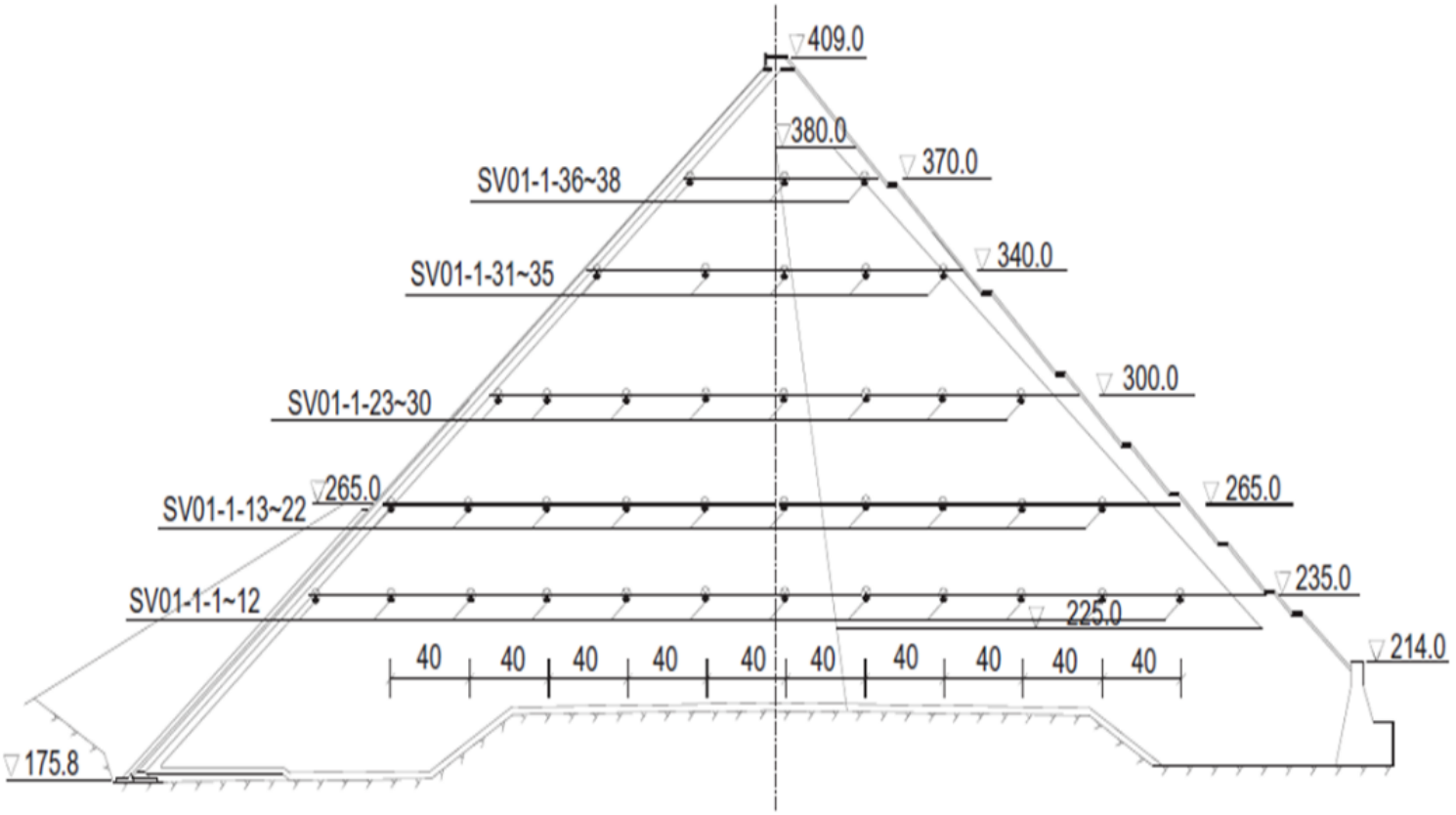

Figure 3.18 Shuibuya Dam (233 m) (Wei et al, 2010)

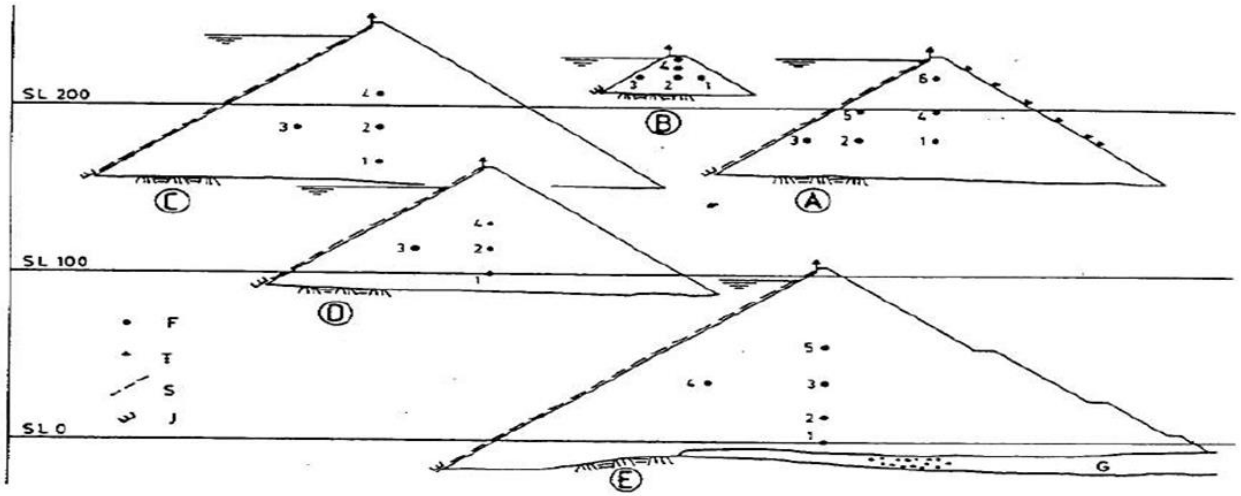

Fig. 3

Pieman River Dams — Sections

Barrages de la rivière Pieman — Coupes

A. Mackintosh dam
B. Tullabardine dam
C. Murchison dam
D. Bastyan dam
E. Lower Pieman dam
F. Settlement cell
T. Survey target
S. Inclinometer
J. Perimetric joint meter
G. River gravel

A. Barrage de Mackintosh
B. Barrage de Tullabardine
C. Barrage de Murchison
D. Barrage de Bastyan
E. Barrage de Lower Pieman
F. Cellules hydrauliques de tassement
T. Repères topographiques
S. Inclinomètre
J. Appareil de mesure du joint périmétral
G. Gravier de rivière

Figure 3.19 Pieman River Dams (ICOLD, 1989)

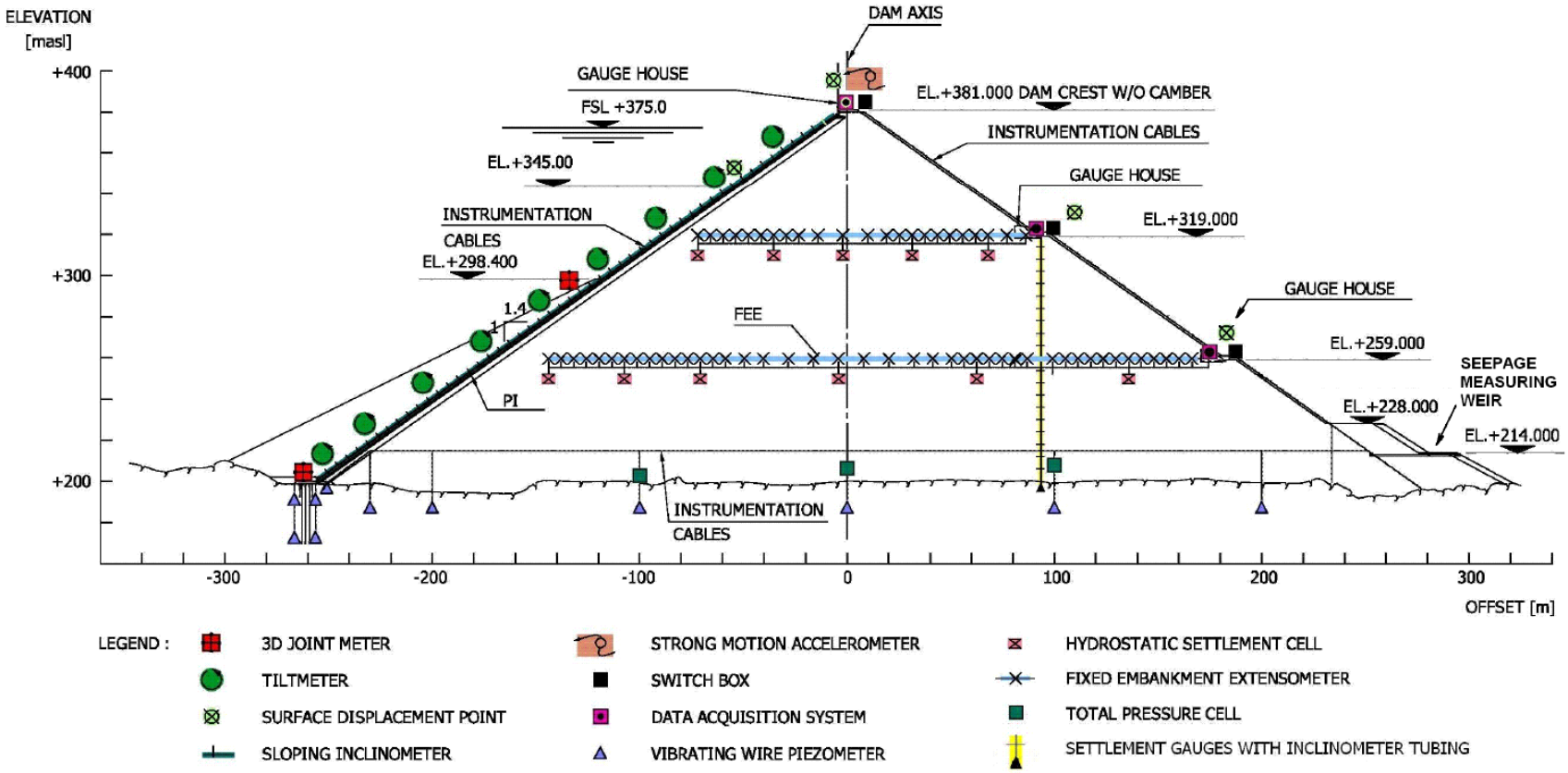

Figure 3.20 Nam Ngum 2 Dam (181 m) (Straubaar et al., 2009)

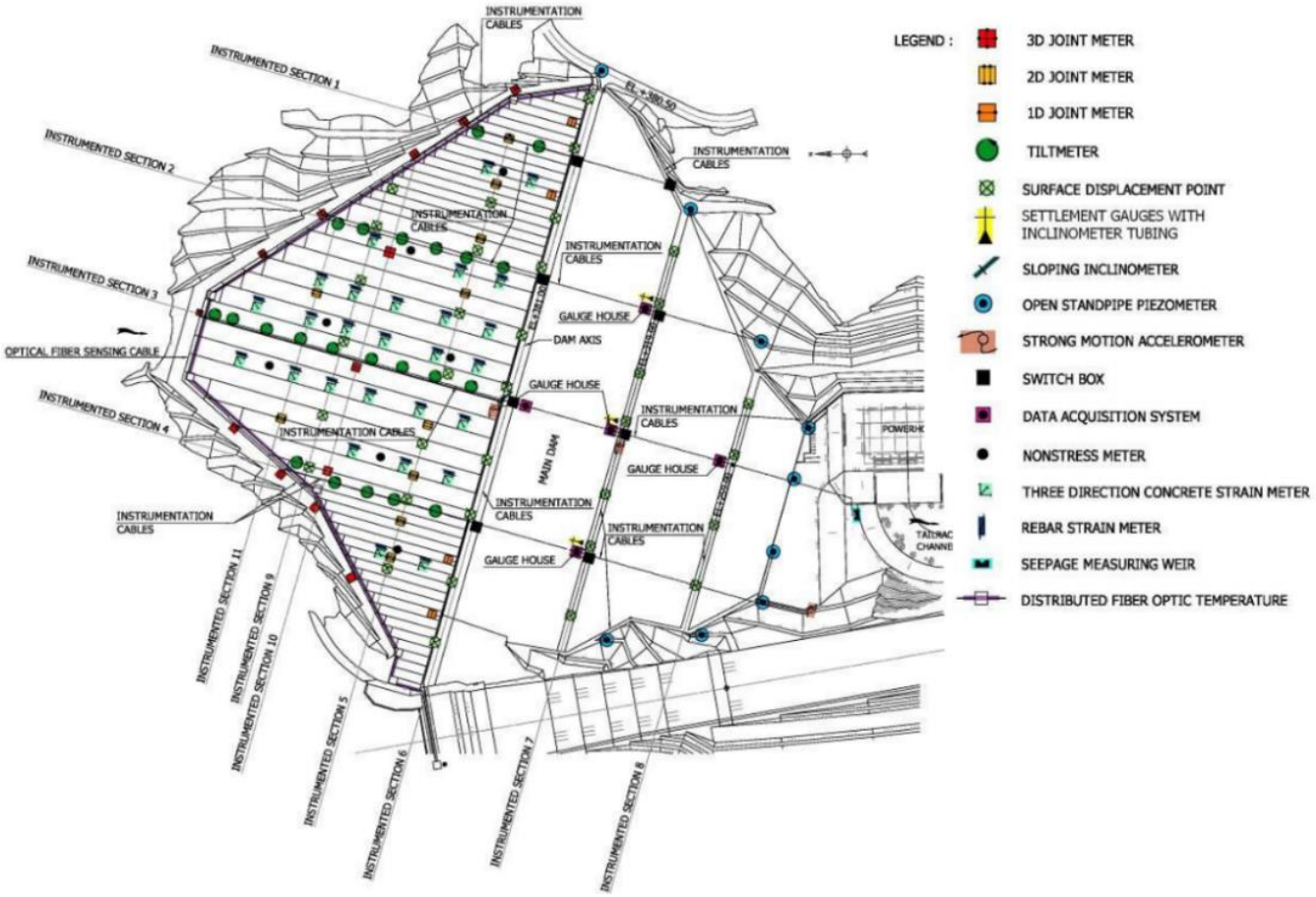

Figure 3.21 Nam Ngum 2 Dam (top view) (Straubaar et al., 2009)

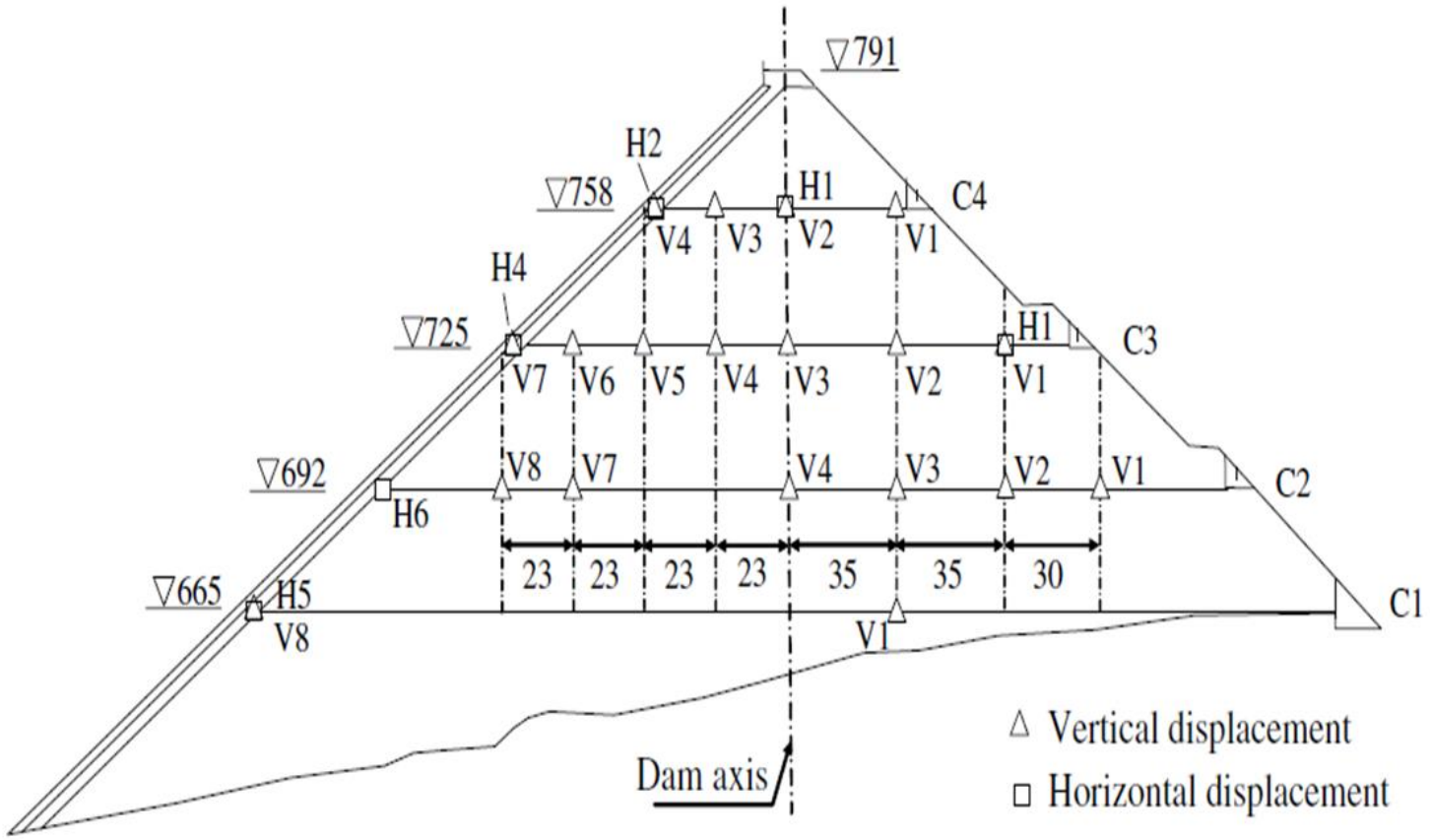

Figure 3.22 Tianshengqiao – I Dam (178 m) (Zhang et al., 2004)

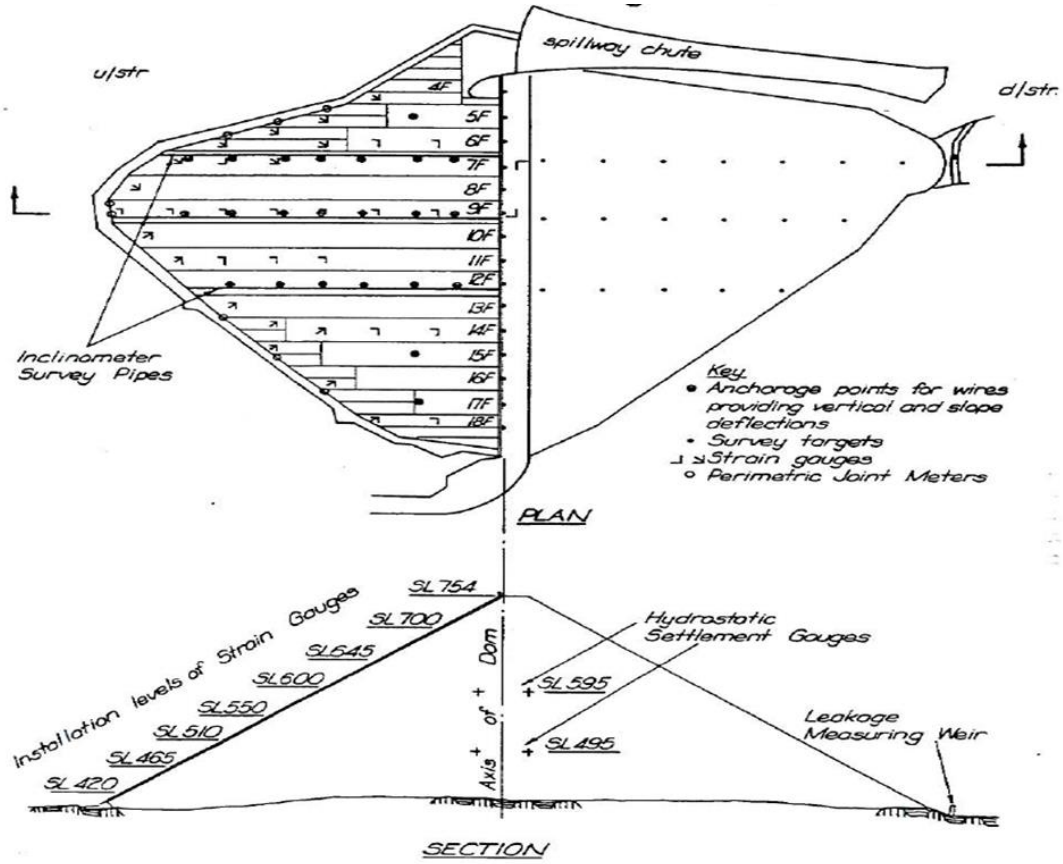

Figure 3.23 Cethana Dam (110 m) (ICOLD, 1989)

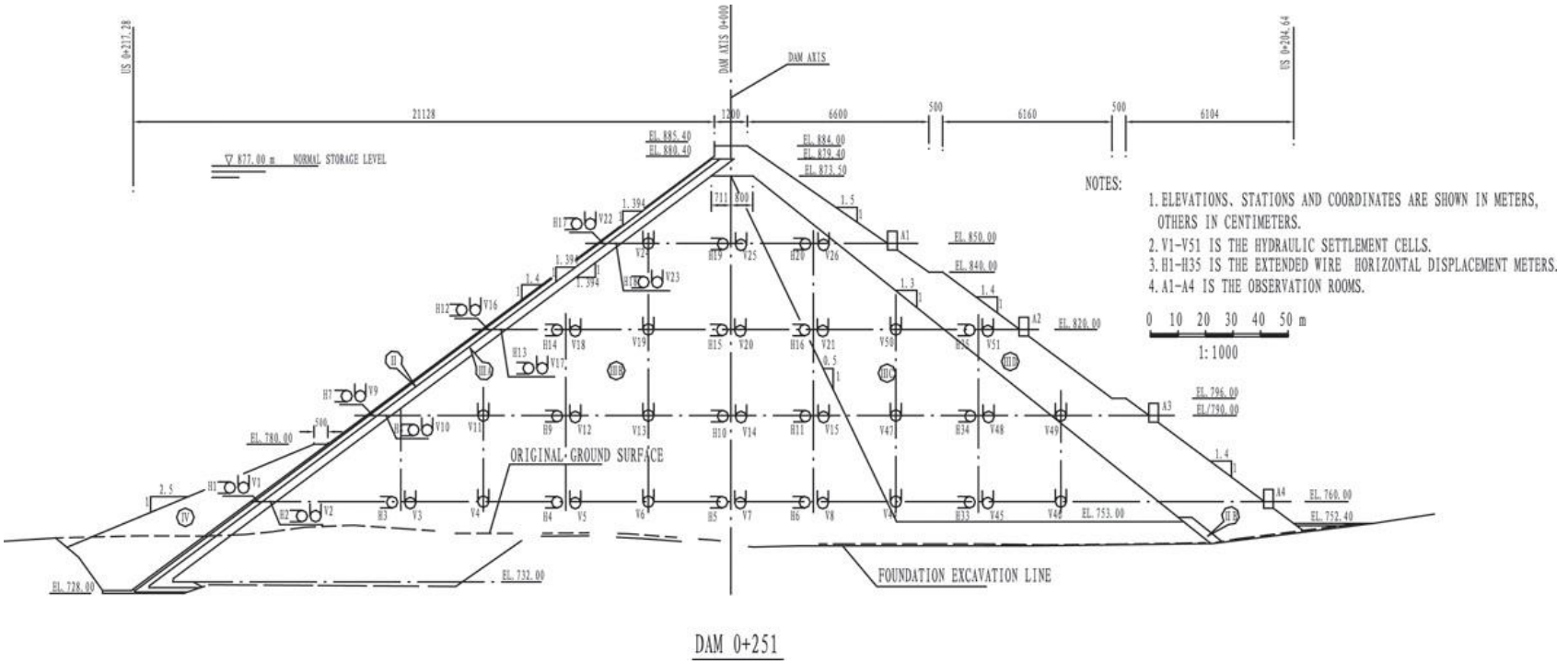

DAM 0+251

Figure 3.24 Zipingpu Dam (156 m) (Chen and Han, 2009)

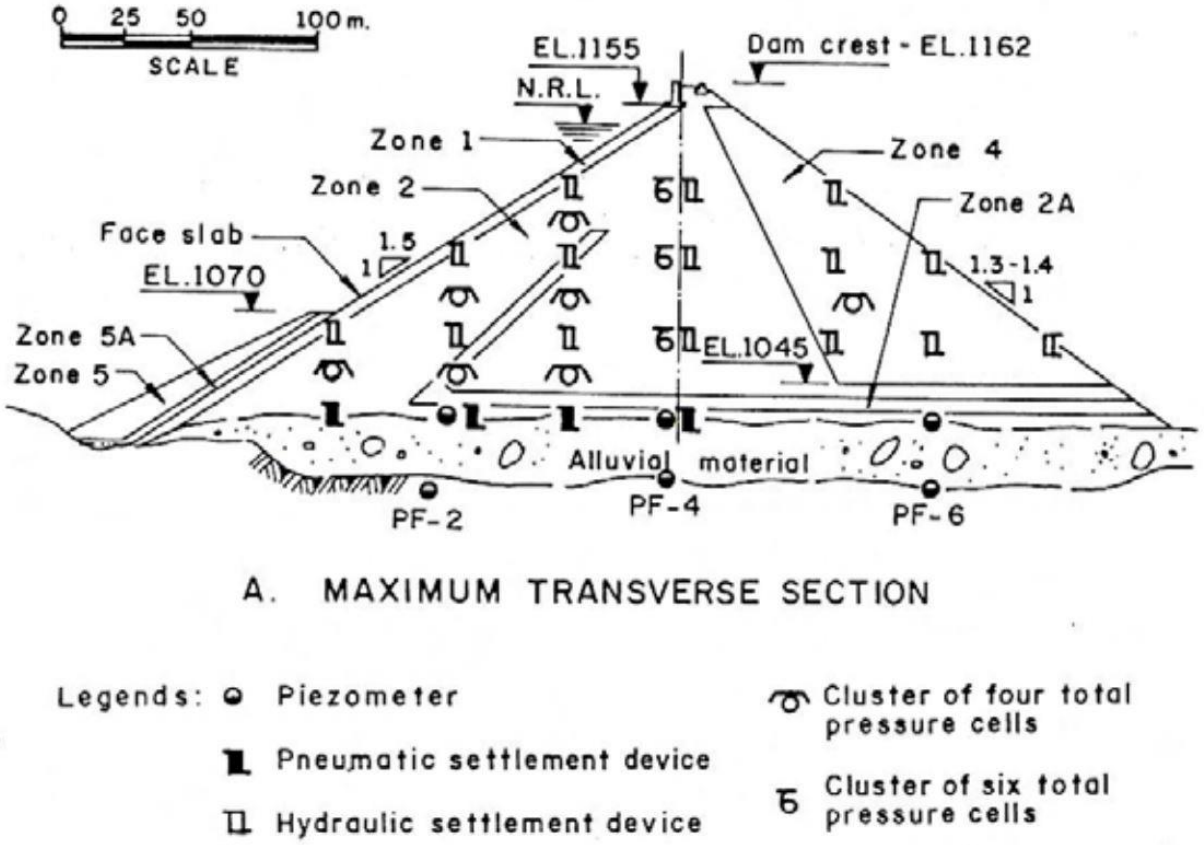

Figure 3.25 Salvajina Dam (148 m) (Hacelas et al., 1985)

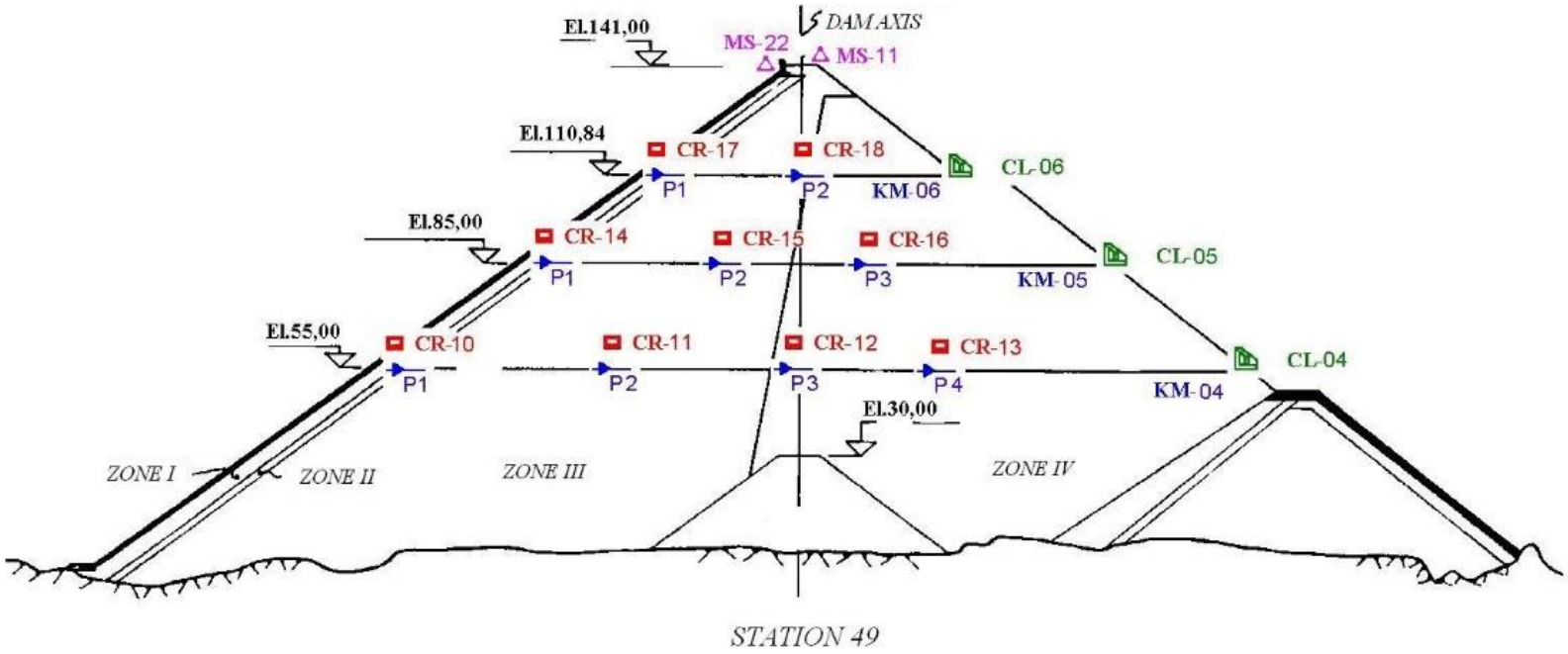

Figure 3.26 Xingó Dam (150) (Souza et al., 2009)

3.4 Analysis of the Trends of Existing Configurations

A number of existing CFRDs were analysed according to their number of horizontal layers where sensors are placed, *M*, and total number of sensors, N_T, to search a possible relationship between the dam height, H_f, and *M* and N_T. The analysed data are presented in Table 3.2.

Table 3.2 Instrumentation configurations of some CFRDs

Dam	H_f (m)	M	N_T
Bastyan	75	3	4
Berg River	67	3	12
Kürtün	133	4	21
La Yesca	220	4	45
Lower Pieman	122	4	5
Mackintosh	75	3	6
Murchison	94	3	4
Shuibuya	233	5	38
Tanyeri	103.5	3	22
Tianshengqiau-I	176	4	16
Tullabardine	26	3	4
Xingo	140	3	12
Zipingpu	156	4	30

Linear regression analyses were conducted for the aforementioned relationship with R^2 values of 0.70 for the following equations:

$$M = 0.009H_f + 2.408 \tag{3.1}$$

$$N_T = 0.189H_f - 6.722 \tag{3.2}$$

where H_f is in meters.

It should be noted that the above relationships give only a preliminary information and lack to provide information about the number of sensors on each layer and the locations of sensors within the dam cross-section.

3.5 Concluding Remarks

Lifetime monitoring of a CFRD will provide essential data for assessing the dam behaviour and allow sufficient time for remedial actions to be taken before the occurrence of any unwanted incident. Monitoring is also vital for the verification of the design and development of the future designs as the current practices mainly depend on the empirical approaches and expert judgements (Yanmaz and Arı, 2011).

As explained before in detail, CFRDs are prone to overtopping and seepage induced failures. These failure modes in fact are related with the unexpected movement and excessive settlement of the dam body. Settlement may lead to the decrease of freeboard which increases the risk of overtopping and cracking of the face slab causing leakage problems. That is why the scope of this study is to develop a decision support system for optimal design of stress monitoring system.

In the following section, the developmental stages of an algorithm for positioning the total pressure cells is considered. Pore water pressure and uplift measuring sensors are omitted from the decision support system because in most of the designs, face slabs are considered as completely impermeable. Because of the zero uplift forces within the completely dry fill material, effective stresses are equal to the total stresses. From this fact, it is believed that an abrupt change in the effective stress readings from more than one sensor could provide information about a possible leakage problem from the impervious upstream face slab. Therefore, giving priority to the use of total pressure cells is reasonable.

The deformations and the movement of the face slab and individual panels can be monitored with inclinometers, tiltmeters and crack meters. However, the detailed analyses and the possible optimal instrumentation scheme of the face slab is out of scope of this study. In the light of the facts stated above, an algorithm is proposed for optimal layout of stress measuring sensors in the Chapter 4.

CHAPTER 4

DEVELOPMENT OF OPTIMIZATION ALGORITHM

4.1 Scope and Expected Benefits of the Study

The scope of this study is to find the optimal configuration of the internal stress monitoring system of a CFRD. The algorithm will provide the required number of sensors and the location of the layers to be equipped with these sensors within a CFRD cross-section. It will also give information about the number and the location of the stress measuring sensors.

In order to achieve the desired scope of the study, the proposed algorithm uses the quality of the information by measuring the difference between the true stress distribution obtained via software used and the measured stress distribution. It also takes into account the cost of the proposed monitoring system configuration by considering both the cost of the sensor and the cost of the sensor cable.

The expected benefit of this algorithm is to provide the designers a tool which can be used fast and effortlessly to obtain a configuration for the stress monitoring system of a CFRD. It is believed that this configuration would provide adequate long-time information for both realistic assessment of dam behaviour and verification of structural models. It is obvious that every project in water resources engineering is unique; thus the monitoring requirement may vary from case to case. However, the user would get an initial idea about the instrumentation configuration and then modify it according to the local characteristics and requirements of the project.

4.2 PLAXIS

Effective stress distribution throughout the dam body under a particular loading condition can be determined from a software. To this end, PLAXIS (Brinkgreve and Broere, 2008) was used.

4.2.1 Brief History of PLAXIS

PLAXIS development was started in 1987 by the Technical University of Delft with the help of the Dutch Department of Public Works and Water Management (Brinkgreve and Broere, 2008). The main objective was to form a user-friendly code to solve 2D finite element problems. In 1993, PLAXIS b.v was founded in order to satisfy the growing requirements of business (Brinkgreve and Broere, 2008). The development of PLAXIS continued steadily by covering most of the areas of geotechnical engineering and even 3D finite element codes are released.

4.2.2 Basics of PLAXIS

PLAXIS 2D is a widely used geotechnical engineering tool, which includes PLAXIS Dynamics and PLAXIS PlaxFlow. PLAXIS 2D is a finite element analysis package aimed to analyse various geotechnical applications. With the help of the advanced models, PLAXIS 2D package can solve the non-linear, anisotropic, and time-dependent behaviour of soil (Brinkgreve et.al, 2010).

The main features of PLAXIS are as follows (Brinkgreve et.al, 2010):

- Different structural elements (anchors, plates, and geogrids)
- Elasto-plastic behaviour for structural elements
- Unlimited combination of forces (point loads and distributed loads)

- Automatic identification of soil layers
- Automatic finite element mesh generation with updated mesh (Lagrange) analyses
- Consolidation and groundwater analyses
- Safety factor analysis

The Basic soil models used in PLAXIS are as follows:

- Linear Elastic
- Mohr-Coulomb

More realistic and advanced soil models are also employed in PLAXIS:

- Compression and shear hardening (Hardening soil model)
- Creep behaviour
- Cam-Clay Model
- User-defined models

In early times, rockfill is simply modelled as a linear elastic material. However, this is not a realistic approach because rockfill behaviour is highly non-linear. Duncan and Chang (1970) developed a hyperbolic model for rockfill and is updated by Kulhawy and Duncan (1972). This model, however, does not include plastic behaviour of rockfill. In order to take the plastic behaviour of rockfill into account, hardening soil model (compression and shear hardening) was developed on the basis of hyperbolic approach of Duncan and Chang (1970). The most important difference is that this model uses theory of plasticity rather than theory of elasticity. That is why PLAXIS is generally used for modelling of CFRDs (Özkuzukıran, 2005).

PLAXIS Dynamics module is used to analyse the effects of seismic loading and the vibrations of the nearby construction activities. With the help of dynamic simulations, the effects of wave propagation in soil media can be estimated (Brinkgreve et.al, 2010).

The features of PLAXIS Dynamics module are as follows (Brinkgreve et.al, 2010):

- Absorbent boundaries
- Wave velocities
- Dynamic loading inputs from
- Harmonic loads
- Real earthquake data
- User-defined loading
- Solution in a predefined time domain
- Automatic time stepping
- Displacements
- Velocities
- Time curves
- Spectra

PLAXIS PlaxFlow module is specifically designed to analyse the time-dependent groundwater flow. It is obvious that groundwater flow also has an indispensable effect on the possible deformations of the saturated and partially saturated soils. With the help of this module, time-dependent effects of flow and pore water pressures are also taken into account during simulations of deformations. These time-dependent analyses are based on Biot's theory of consolidation (Brinkgreve et.al, 2010).

The main features of PLAXIS PlaxFlow module are as follows (Brinkgreve et.al, 2010):

- Modelling with screens, wells and drains
- Different boundary conditions (time-dependent, linear, harmonic, and user-defined)
- Prescribed heads
- Inclusion of inflow and outflow
- Inclusion of precipitation and evaporation
- Different models for soil (linear and Van Genuchten)
- Anisotropic flow conditions
- Automatic time stepping
- Combining results with deformation analyses.

4.2.3 Modelling with PLAXIS

4.2.3.1 General Modelling Features

Points: They are the beginnings and ends of the lines and also used for locating structural elements and forces (Brinkgreve and Broere, 2008).

Lines: They are used to define the geometry, boundaries, soil discontinuities, structures, and constructional stages (Brinkgreve and Broere, 2008).

Clusters: They are the areas formed by closed set of lines. The code forms it automatically and assumes the soil properties in a cluster to be uniform (Brinkgreve and Broere, 2008).

Elements: Before calculations, PLAXIS should form the finite element mesh and form triangular elements. These triangles can be divided into 15-node elements or 6-node

elements. The former provides accuracy in calculations, whereas the latter is useful for quick computing (Brinkgreve and Broere, 2008).

Nodes: In finite element analysis, displacements in 2D are calculated for all nodes (Brinkgreve and Broere, 2008).

Stress Points: 15-node triangular elements consist of 12 stress points and 6-node triangular elements consist of 3 stress points (Brinkgreve and Broere, 2008). The nodes and stress points are shown in Figure 4.1.

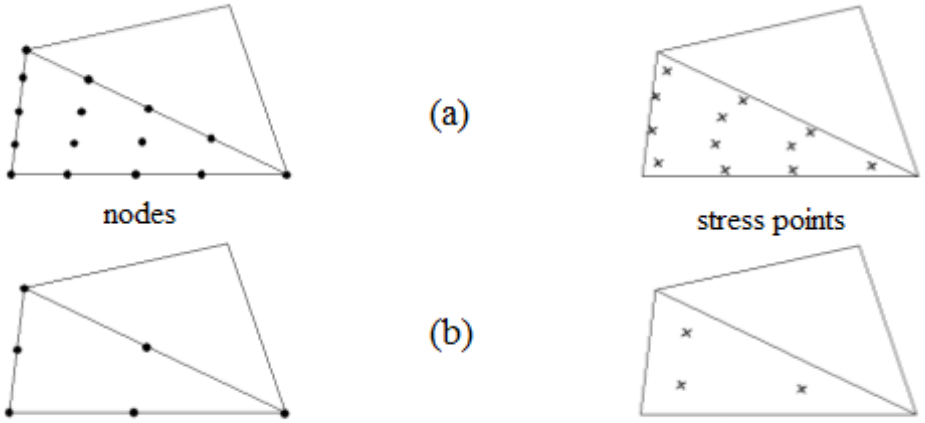

Figure 4.1 Nodes and stress points for (a) 15-node (b) 6-node triangular elements (Brinkgreve and Broere, 2008)

4.2.3.2 Input Procedure

In PLAXIS four types of inputs are available to user (Brinkgreve and Broere, 2008):

- Geometry objects
- Text
- Values
- Selections

In Figure 4.2 and Figure 4.3, the main input window and toolbars of PLAXIS are shown, respectively.

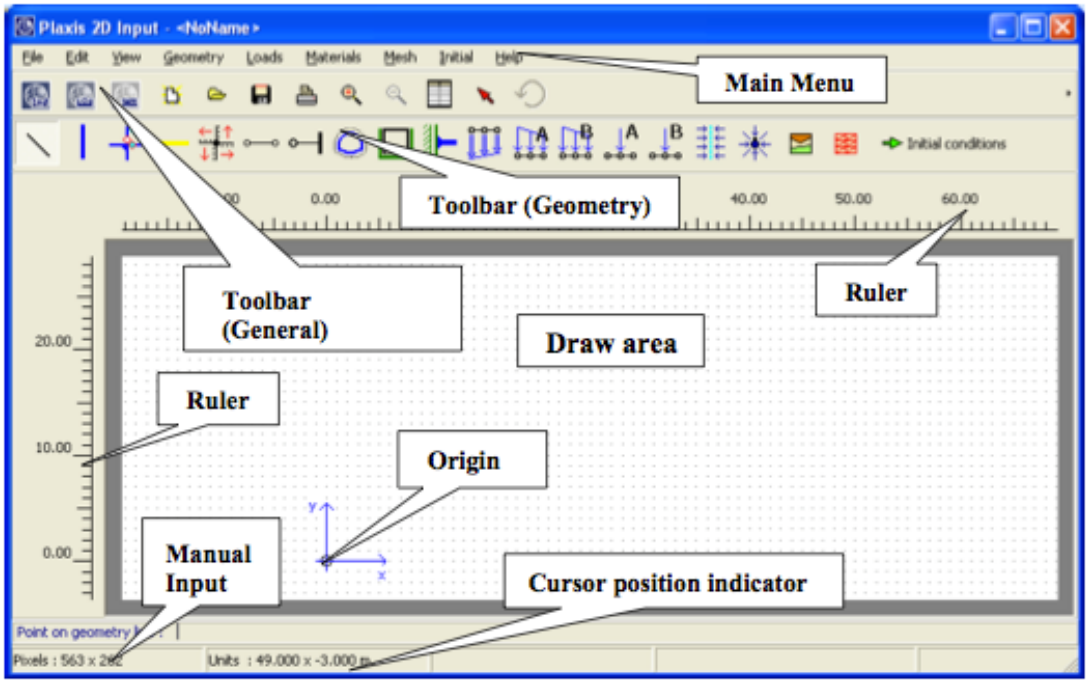

Figure 4.2 Main input window (Brinkgreve and Broere, 2008)

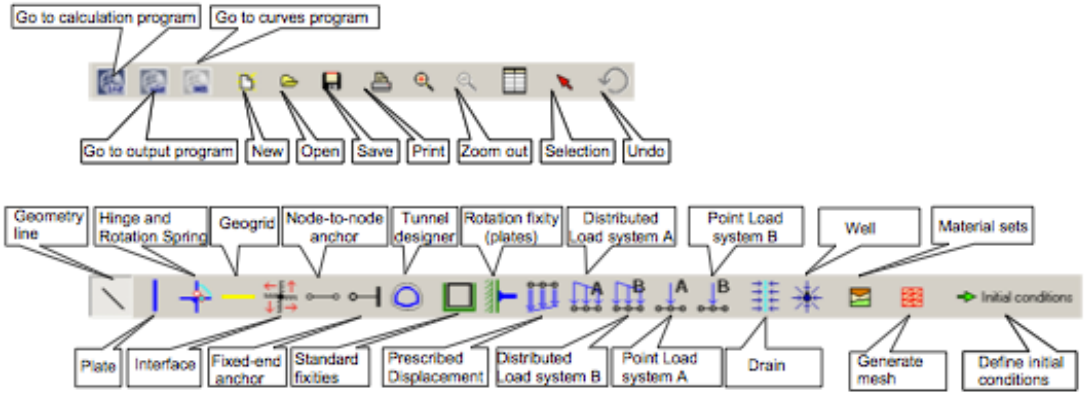

Figure 4.3 Input window toolbar (Brinkgreve and Broere, 2008)

4.2.3.3 Calculations Module

After entering the input data (geometry, loads, etc.), the user forms the mesh and saves the input file. The calculate button in toolbar closes the input window and opens the calculations window of PLAXIS. It is used to define and execute the calculation phases (Brinkgreve and Broere, 2008). Typical view of calculations window is shown in Figure 4.4.

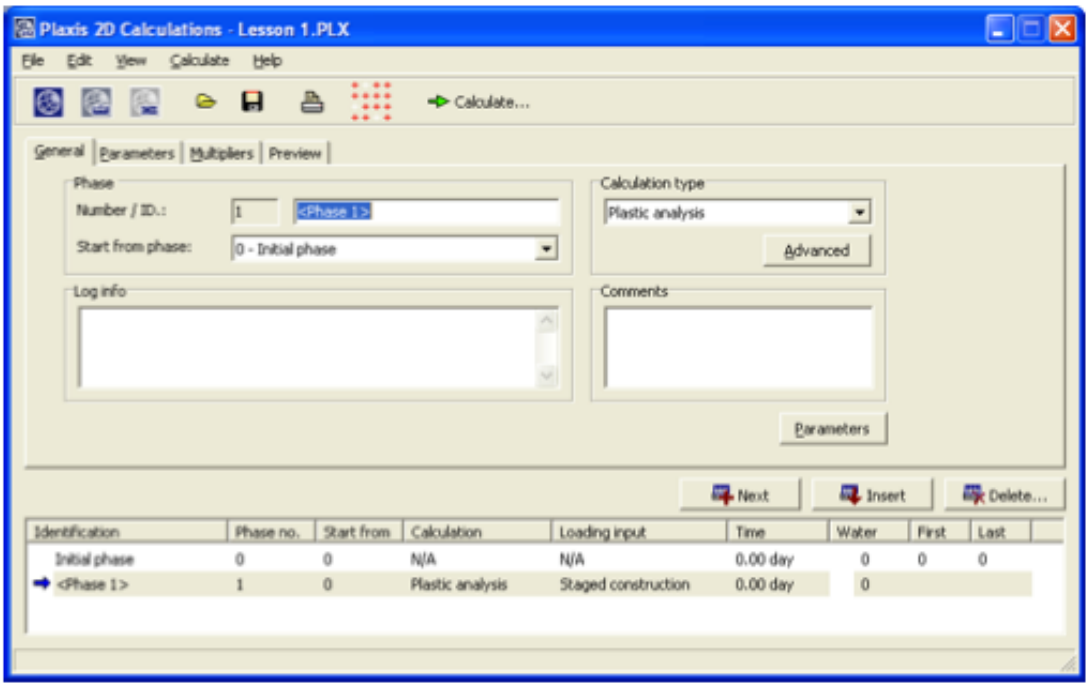

Figure 4.4 Calculations window (Brinkgreve and Broere, 2008)

There are several tabs provided for defining the calculation phase. These can be loading, construction, excavation, or consolidation phases (Brinkgreve and Broere, 2008).

4.2.3.4 Viewing Results

Upon completion of the calculations, one can get the results of the analyses in the output window. In the output window, the user can get the resultant displacements and stresses in the full geometry or in a desired cross-section and in structural elements (Brinkgreve and Broere, 2008).

A view of a deformed mesh in output windows is presented in Figure 4.5.

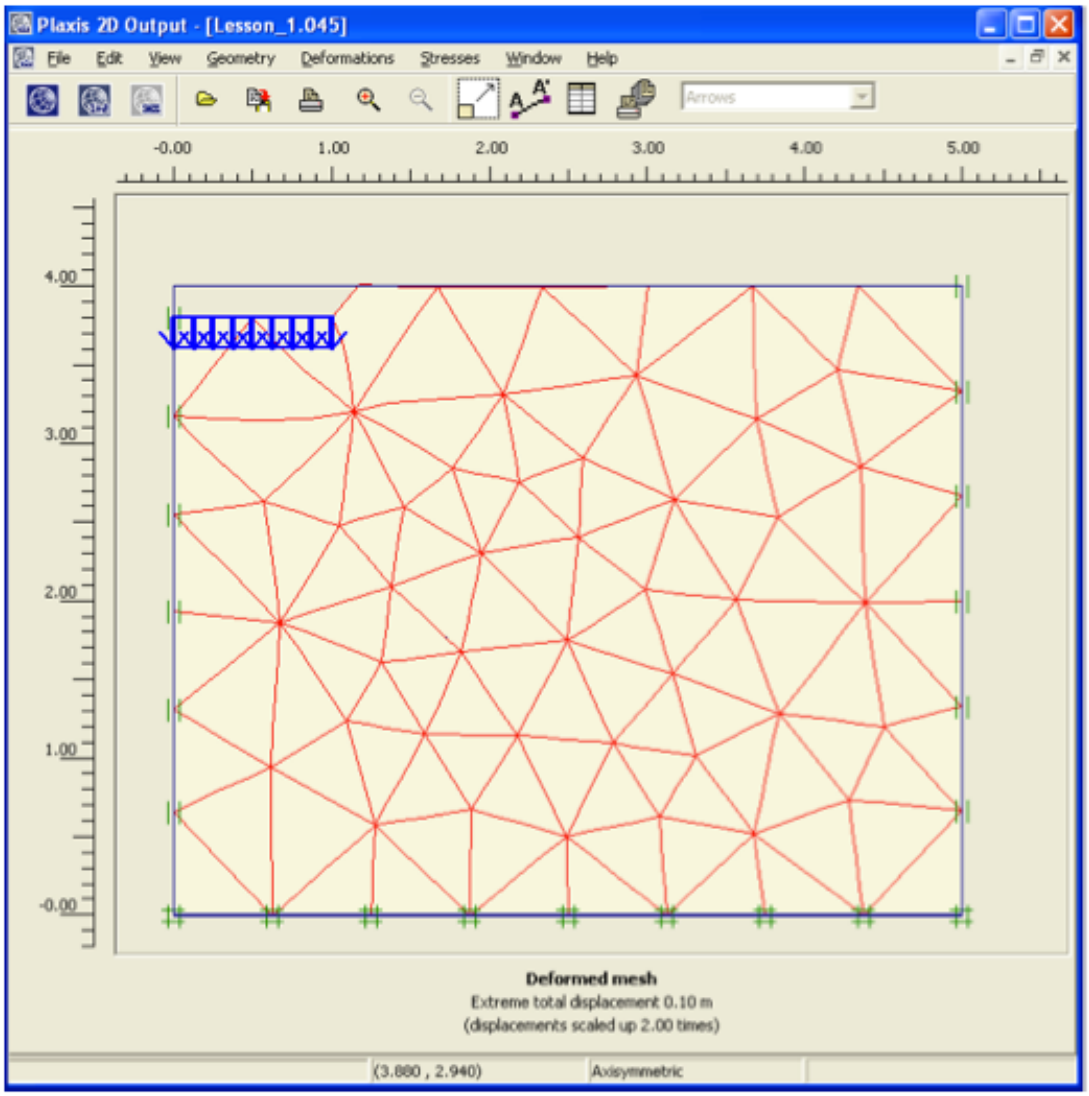

Figure 4.5 Deformed mesh (Brinkgreve and Broere, 2008)

4.3 Assumptions of the Study

The following assumptions are accepted throughout this study unless otherwise stated:

i. Dam body is assumed as homogeneous fill, which is characteristic composition of such dams.

ii. Reservoir level is full, upstream slab is intact and impervious (no cracks initially)

iii. The CRFD cross-sections are symmetrical having side slopes of 1V:1.5H on upstream and downstream faces.

iv. 9 cross-sections were analysed, starting from 40 m up to 200 m-high from thalweg and increasing with 20 m increments.

v. The width of the crest of the CFRD cross-sections are constant and 15 m for all heights.

vi. The relation between the dam height measured from thalweg (H_t) versus the height from foundation (H_f) was obtained with reference to the geometric characteristics of various existing rockfill dams in Turkey (provided in Appendix B) and formulated as (R^2=0.9484):

$$H_f = 1.16H_t \tag{4.1}$$

where H_f and H_t are in meters.

vii. The rockfill was modelled with hardening soil model in PLAXIS. The material type was defined as “drained” with an equal unsaturated and saturated specific weight of 27.79 kN/m^3 and with a reference cohesion value of 1.00 KN/m^2.

viii. Stiffness parameters of PLAXIS hardening soil model are provided in Figure 4.6.

ix. The impervious upstream slab was modelled as “elastic plate” with the properties presented in Figure 4.7.

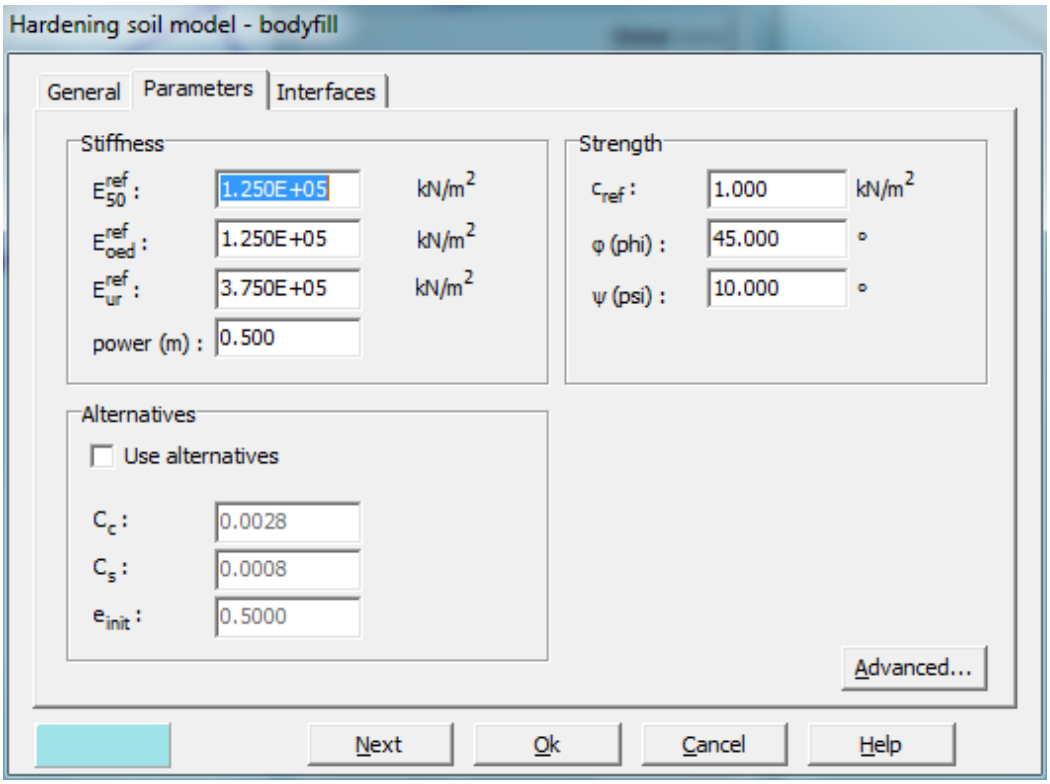

Figure 4.6 Hardening soil model parameters

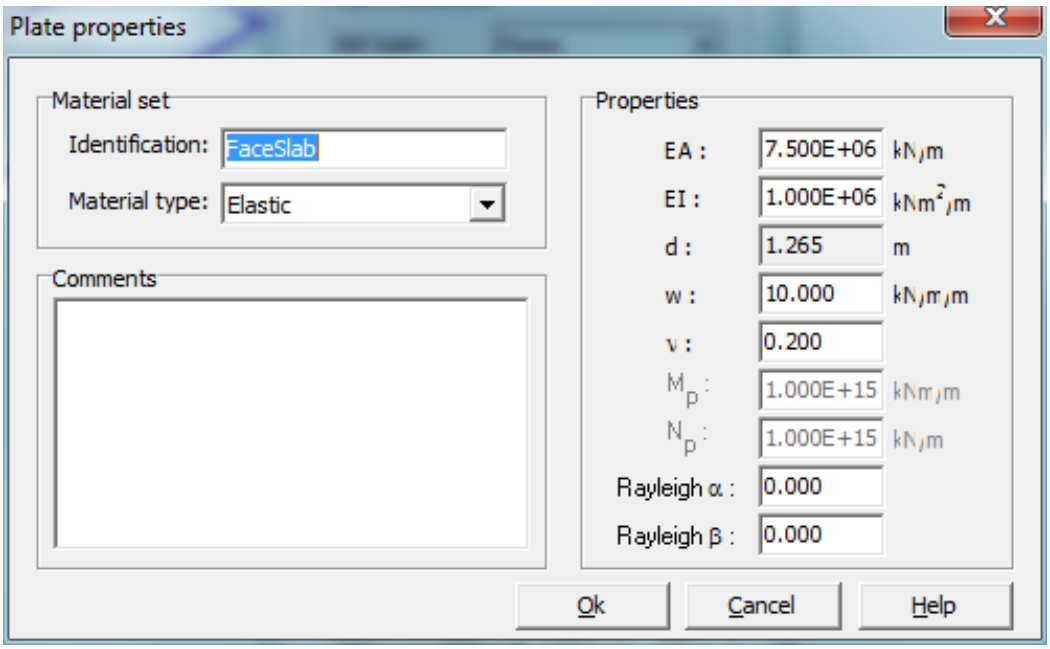

Figure 4.7 Parameters for impervious upstream slab

x. The loading case includes self-weight of the dam and the hydrostatic forces resulted from a reservoir at maximum operating level. The maximum water level is assumed to be 5 m below the dam crest elevation. The loads not considered herein were discussed in sensitivity analysis section (Section 4.7).

xi. Sensors are placed on a layer symmetrically with equal distances between them.

4.4 Vertical Projection of Sensors

4.4.1 Introductory Remarks

Study of vertical projection of the effective stress distribution at the mid-axis of the dam body provides a mean for determining the number of horizontal layers to be equipped with sensors within the dam body. The readings obtained from the sensors will be useful for determining the horizontal pressure and deformation on a vertical projection.

Three different approaches were considered in the developmental stage of the algorithm. Figure 4.8 represents the sectional details of the effective stress distributions. The cross-section “a-a” is used for determining the number of layers for instrumentation, whereas the cross-section “b-b” is utilized for obtaining the number of sensors at a particular layer. In this figure, P_h' and P_v' stand for effective horizontal and vertical force, respectively.

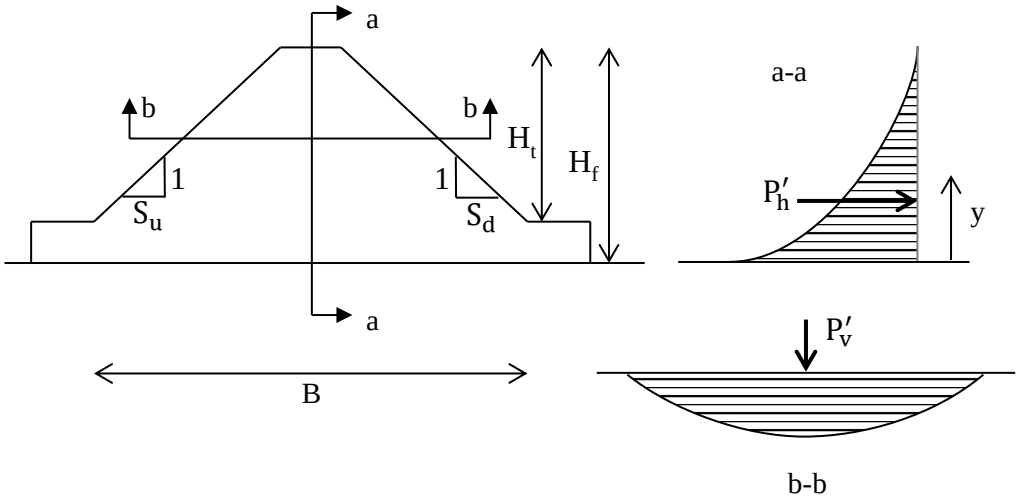

Figure 4.8 Sectional details of the effective stress distributions

4.4.2 Effective Stress Variation on a Vertical Plane

Variation of the effective stress acting on section a-a (Figure 4.8) with respect to varying dam height was modelled and generalized by the regression analysis. Effective stress values were obtained from PLAXIS and provided in Appendix C. Dimensionless parameters are formed and the relation between the effective pressure variations for different dam heights were defined as following:

$$f\left(\frac{y}{H_f}\right) = \frac{\sigma_h'}{\gamma B} \tag{4.2}$$

where;

y : height from the foundation level of the dam (Figure 4.8),

H_f : height of the dam from foundation (Figure 4.8),

γ : specific weight of water,

B : base width of the dam (Figure 4.8), and

σ_h' : horizontal effective stress obtained from PLAXIS.

Base width of the dam is computed by considering the 1V:1.5H symmetric side slopes and 15 m width of dam crest:

$$B = 3H_t + 15 \tag{4.3}$$

where H_t and B are in meters.

The results of the effective stress distributions on section a-a gathered from PLAXIS were analysed for obtaining a dimensionless relationship (Figure 4.9 and Table 4.1).

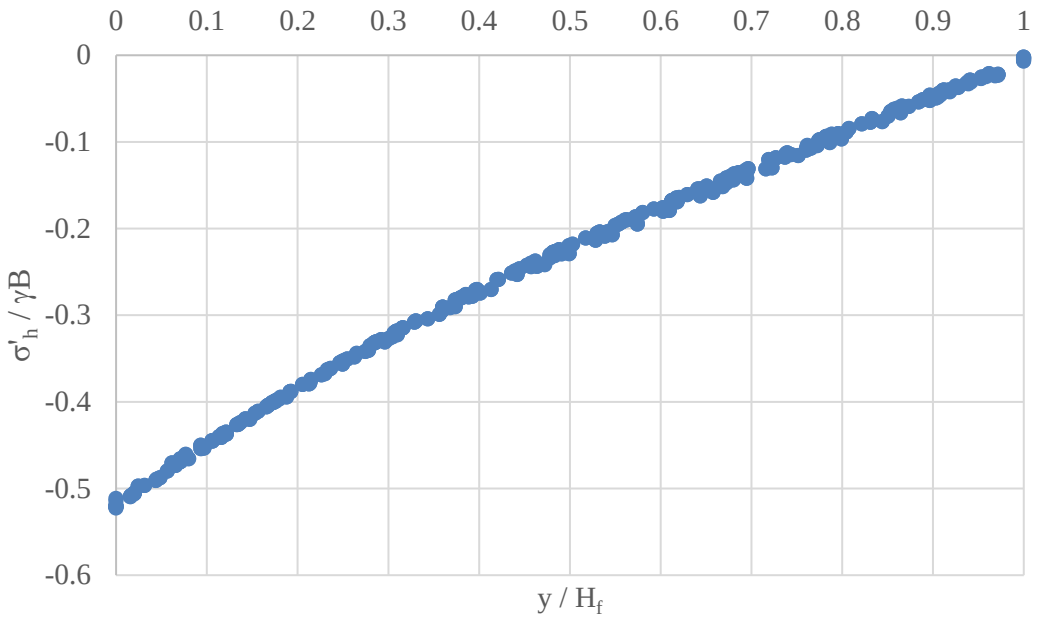

Figure 4.9 Graphical representation of dimensionless function

Table 4.1 Tabular representation of dimensionless function data

H_t = 40 m		H_t = 60 m		H_t = 80 m		H_t = 100 m		H_t = 120 m		H_t = 140 m		H_t = 160 m		H_t = 180 m		H_t = 200 m	
$\sigma'_h/\gamma B$	y/H_f	$\sigma'_h/\gamma B$	y/H_f	$\sigma'_h/\gamma B$	y/H_f	$\sigma'_h/\gamma B$	y/H_f	$\sigma'_h/\gamma B$	y/H_f	$\sigma'_h/\gamma B$	y/H_f	$\sigma'_h/\gamma B$	y/H_f	$\sigma'_h/\gamma B$	y/H_f	$\sigma'_h/\gamma B$	y/H_f
-0.0022	1.0000	-0.0063	1.0000	-0.0068	1.0000	-0.0046	1.0000	-0.0036	1.0000	-0.0034	1.0000	-0.0049	1.0000	-0.0022	1.0000	-0.0028	1.0000
-0.0213	0.9619	-0.0423	0.9188	-0.0269	0.9531	-0.0290	0.9419	-0.0238	0.9686	-0.0233	0.9719	-0.0290	0.9410	-0.0219	0.9718	-0.0238	0.9588
-0.0214	0.9619	-0.0417	0.9188	-0.0270	0.9531	-0.0310	0.9419	-0.0233	0.9686	-0.0223	0.9719	-0.0296	0.9410	-0.0221	0.9718	-0.0249	0.9588
-0.0494	0.9037	-0.0474	0.9060	-0.0374	0.9281	-0.0331	0.9391	-0.0404	0.9180	-0.0442	0.9069	-0.0359	0.9252	-0.0251	0.9536	-0.0289	0.9408
-0.0494	0.9037	-0.0480	0.9060	-0.0368	0.9281	-0.0315	0.9391	-0.0399	0.9180	-0.0440	0.9069	-0.0355	0.9252	-0.0255	0.9536	-0.0290	0.9408
-0.0766	0.8443	-0.0522	0.8968	-0.0454	0.9086	-0.0321	0.9375	-0.0539	0.8844	-0.0514	0.8891	-0.0409	0.9117	-0.0401	0.9123	-0.0462	0.8968
-0.0766	0.8443	-0.0523	0.8968	-0.0454	0.9086	-0.0319	0.9375	-0.0540	0.8844	-0.0513	0.8891	-0.0410	0.9117	-0.0402	0.9123	-0.0463	0.8968
-0.0967	0.7993	-0.0666	0.8646	-0.0705	0.8507	-0.0592	0.8736	-0.0746	0.8341	-0.0613	0.8650	-0.0651	0.8536	-0.0407	0.9110	-0.0586	0.8660
-0.0967	0.7993	-0.0666	0.8646	-0.0705	0.8507	-0.0592	0.8736	-0.0746	0.8341	-0.0614	0.8650	-0.0651	0.8536	-0.0407	0.9110	-0.0589	0.8660
-0.1301	0.7229	-0.1008	0.7865	-0.1044	0.7725	-0.0774	0.8313	-0.0905	0.7956	-0.0793	0.8218	-0.0846	0.8076	-0.0613	0.8610	-0.0626	0.8572
-0.1301	0.7229	-0.1008	0.7865	-0.1044	0.7725	-0.0774	0.8313	-0.0905	0.7956	-0.0792	0.8218	-0.0846	0.8076	-0.0612	0.8610	-0.0625	0.8572
-0.1421	0.6949	-0.1159	0.7518	-0.1074	0.7656	-0.0888	0.8047	-0.1146	0.7384	-0.0918	0.7916	-0.0987	0.7742	-0.0731	0.8330	-0.0913	0.7887
-0.1421	0.6949	-0.1158	0.7518	-0.1074	0.7656	-0.0888	0.8047	-0.1146	0.7384	-0.0918	0.7916	-0.0987	0.7742	-0.0731	0.8330	-0.0913	0.7887
-0.1583	0.6579	-0.1311	0.7161	-0.1095	0.7606	-0.1075	0.7609	-0.1204	0.7247	-0.1041	0.7617	-0.1139	0.7383	-0.0932	0.7855	-0.0937	0.7830
-0.1583	0.6579	-0.1312	0.7161	-0.1095	0.7606	-0.1074	0.7609	-0.1204	0.7247	-0.1042	0.7617	-0.1139	0.7383	-0.0932	0.7855	-0.0937	0.7830
-0.1792	0.6097	-0.1516	0.6684	-0.1439	0.6803	-0.1147	0.7437	-0.1328	0.6956	-0.1185	0.7271	-0.1331	0.6935	-0.0976	0.7751	-0.0942	0.7818
-0.1793	0.6097	-0.1516	0.6684	-0.1440	0.6803	-0.1148	0.7437	-0.1328	0.6956	-0.1185	0.7271	-0.1331	0.6935	-0.0976	0.7751	-0.0942	0.7818
-0.1949	0.5745	-0.1623	0.6438	-0.1472	0.6728	-0.1176	0.7370	-0.1455	0.6660	-0.1397	0.6773	-0.1358	0.6873	-0.1126	0.7395	-0.1205	0.7192
-0.1949	0.5745	-0.1624	0.6438	-0.1472	0.6728	-0.1176	0.7370	-0.1455	0.6660	-0.1397	0.6773	-0.1358	0.6873	-0.1126	0.7395	-0.1205	0.7192
-0.2073	0.5469	-0.1801	0.6029	-0.1765	0.6059	-0.1408	0.6829	-0.1547	0.6447	-0.1417	0.6725	-0.1381	0.6819	-0.1311	0.6966	-0.1370	0.6812
-0.2073	0.5469	-0.1801	0.6029	-0.1765	0.6059	-0.1408	0.6829	-0.1547	0.6447	-0.1417	0.6725	-0.1381	0.6819	-0.1311	0.6966	-0.1369	0.6812
-0.2291	0.4994	-0.2088	0.5388	-0.1909	0.5738	-0.1463	0.6703	-0.1669	0.6167	-0.1510	0.6509	-0.1609	0.6295	-0.1357	0.6858	-0.1545	0.6410
-0.2291	0.4994	-0.2089	0.5388	-0.1909	0.5738	-0.1463	0.6703	-0.1669	0.6167	-0.1510	0.6509	-0.1609	0.6295	-0.1357	0.6858	-0.1545	0.6410

Table 4.1 (continued)

H_t = 40 m		H_t = 60 m		H_t = 80 m		H_t = 100 m		H_t = 120 m		H_t = 140 m		H_t = 160 m		H_t = 180 m		H_t = 200 m	
$\sigma'_h/\gamma B$	y/H_f	$\sigma'_h/\gamma B$	y/H_f	$\sigma'_h/\gamma B$	y/H_f	$\sigma'_h/\gamma B$	y/H_f	$\sigma'_h/\gamma B$	y/H_f	$\sigma'_h/\gamma B$	y/H_f	$\sigma'_h/\gamma B$	y/H_f	$\sigma'_h/\gamma B$	y/H_f	$\sigma'_h/\gamma B$	y/H_f
-0.2417	0.4725	-0.2136	0.5285	-0.2116	0.5284	-0.1691	0.6182	-0.1775	0.5927	-0.1643	0.6205	-0.1865	0.5724	-0.1380	0.6805	-0.1648	0.6176
-0.2417	0.4725	-0.2135	0.5285	-0.2116	0.5284	-0.1691	0.6182	-0.1775	0.5927	-0.1643	0.6205	-0.1865	0.5724	-0.1380	0.6805	-0.1648	0.6176
-0.2704	0.4134	-0.2436	0.4640	-0.2292	0.4911	-0.1761	0.6026	-0.1965	0.5501	-0.1678	0.6126	-0.1951	0.5534	-0.1546	0.6425	-0.1816	0.5803
-0.2704	0.4134	-0.2436	0.4640	-0.2292	0.4911	-0.1761	0.6026	-0.1966	0.5501	-0.1678	0.6126	-0.1951	0.5534	-0.1546	0.6425	-0.1816	0.5803
-0.2901	0.3738	-0.2745	0.4013	-0.2530	0.4421	-0.1900	0.5718	-0.2056	0.5302	-0.1900	0.5628	-0.2043	0.5337	-0.1660	0.6167	-0.1904	0.5610
-0.2902	0.3738	-0.2744	0.4013	-0.2531	0.4421	-0.1900	0.5718	-0.2056	0.5302	-0.1900	0.5628	-0.2043	0.5337	-0.1660	0.6167	-0.1904	0.5610
-0.2991	0.3563	-0.2913	0.3683	-0.2782	0.3928	-0.2037	0.5418	-0.2182	0.5031	-0.2110	0.5176	-0.2304	0.4783	-0.1679	0.6124	-0.2244	0.4883
-0.2991	0.3563	-0.2913	0.3683	-0.2781	0.3928	-0.2037	0.5418	-0.2182	0.5031	-0.2110	0.5176	-0.2304	0.4783	-0.1679	0.6124	-0.2244	0.4883
-0.3309	0.2963	-0.3251	0.3043	-0.3043	0.3436	-0.2313	0.4833	-0.2402	0.4572	-0.2273	0.4832	-0.2514	0.4360	-0.1929	0.5569	-0.2271	0.4827
-0.3310	0.2963	-0.3251	0.3043	-0.3043	0.3436	-0.2313	0.4833	-0.2402	0.4572	-0.2273	0.4832	-0.2514	0.4360	-0.1929	0.5569	-0.2272	0.4827
-0.3565	0.2497	-0.3481	0.2629	-0.3226	0.3100	-0.2338	0.4781	-0.2590	0.4199	-0.2377	0.4621	-0.2588	0.4215	-0.2041	0.5328	-0.2275	0.4820
-0.3565	0.2497	-0.3481	0.2629	-0.3226	0.3100	-0.2338	0.4781	-0.2590	0.4199	-0.2376	0.4621	-0.2588	0.4215	-0.2041	0.5328	-0.2275	0.4820
-0.3677	0.2301	-0.3690	0.2265	-0.3406	0.2783	-0.2440	0.4575	-0.2705	0.3978	-0.2711	0.3963	-0.2799	0.3808	-0.2199	0.4992	-0.2279	0.4813
-0.3677	0.2301	-0.3689	0.2265	-0.3407	0.2783	-0.2440	0.4575	-0.2705	0.3978	-0.2711	0.3963	-0.2799	0.3808	-0.2199	0.4992	-0.2278	0.4813
-0.4045	0.1670	-0.4038	0.1683	-0.3793	0.2128	-0.2730	0.4000	-0.2799	0.3799	-0.2776	0.3839	-0.2910	0.3601	-0.2425	0.4528	-0.2762	0.3854
-0.4045	0.1670	-0.4038	0.1683	-0.3793	0.2128	-0.2731	0.4000	-0.2799	0.3799	-0.2776	0.3839	-0.2910	0.3601	-0.2425	0.4528	-0.2763	0.3854
-0.4501	0.0934	-0.4109	0.1567	-0.4203	0.1476	-0.2790	0.3887	-0.3067	0.3305	-0.3150	0.3154	-0.3080	0.3288	-0.2466	0.4446	-0.2824	0.3739
-0.4502	0.0934	-0.4109	0.1567	-0.4203	0.1476	-0.2790	0.3887	-0.3067	0.3305	-0.3150	0.3154	-0.3080	0.3288	-0.2466	0.4446	-0.2824	0.3739
-0.4607	0.0770	-0.4196	0.1428	-0.4534	0.0970	-0.2944	0.3598	-0.3283	0.2922	-0.3183	0.3095	-0.3206	0.3065	-0.2490	0.4399	-0.3308	0.2868
-0.4607	0.0770	-0.4197	0.1428	-0.4534	0.0970	-0.2944	0.3598	-0.3283	0.2922	-0.3183	0.3095	-0.3206	0.3065	-0.2490	0.4399	-0.3308	0.2868
-0.4706	0.0617	-0.4659	0.0709	-0.4894	0.0449	-0.3272	0.3003	-0.3353	0.2800	-0.3191	0.3081	-0.3506	0.2548	-0.2823	0.3754	-0.3315	0.2857

Table 4.1 (continued)

H_t = 40 m		H_t = 60 m		H_t = 80 m		H_t = 100 m		H_t = 120 m		H_t = 140 m		H_t = 160 m		H_t = 180 m		H_t = 200 m	
$\sigma'_h/\gamma B$	y/H_f	$\sigma'_h/\gamma B$	y/H_f	$\sigma'_h/\gamma B$	y/H_f	$\sigma'_h/\gamma B$	y/H_f	$\sigma'_h/\gamma B$	y/H_f	$\sigma'_h/\gamma B$	y/H_f	$\sigma'_h/\gamma B$	y/H_f	$\sigma'_h/\gamma B$	y/H_f	$\sigma'_h/\gamma B$	y/H_f
-0.4706	0.0617	-0.4659	0.0709	-0.4894	0.0449	-0.3272	0.3003	-0.3353	0.2800	-0.3191	0.3081	-0.3506	0.2548	-0.2823	0.3754	-0.3316	0.2857
-0.5116	0.0000	-0.4974	0.0246	-0.5212	0.0000	-0.3419	0.2748	-0.3526	0.2508	-0.3548	0.2467	-0.3615	0.2366	-0.2907	0.3599	-0.3316	0.2855
		-0.4974	0.0246			-0.3419	0.2748	-0.3526	0.2508	-0.3548	0.2467	-0.3615	0.2366	-0.2907	0.3599	-0.3315	0.2855
		-0.5144	0.0000			-0.3785	0.2136	-0.3743	0.2148	-0.3880	0.1928	-0.3989	0.1765	-0.3146	0.3164	-0.3323	0.2841
						-0.3785	0.2136	-0.3743	0.2148	-0.3880	0.1928	-0.3990	0.1765	-0.3146	0.3164	-0.3323	0.2841
						-0.3944	0.1880	-0.3799	0.2057	-0.3884	0.1922	-0.4007	0.1738	-0.3441	0.2653	-0.3629	0.2328
						-0.3944	0.1880	-0.3799	0.2057	-0.3884	0.1922	-0.4006	0.1738	-0.3441	0.2653	-0.3948	0.1814
						-0.4373	0.1218	-0.3988	0.1757	-0.3887	0.1918	-0.4059	0.1658	-0.3534	0.2496	-0.3949	0.1814
						-0.4374	0.1218	-0.3989	0.1757	-0.3886	0.1918	-0.4059	0.1658	-0.3534	0.2496	-0.4010	0.1719
						-0.4411	0.1161	-0.4263	0.1333	-0.4241	0.1369	-0.4401	0.1139	-0.3628	0.2342	-0.4010	0.1719
						-0.4411	0.1161	-0.4264	0.1333	-0.4241	0.1369	-0.4401	0.1139	-0.3627	0.2342	-0.4132	0.1533
						-0.4657	0.0801	-0.4368	0.1177	-0.4449	0.1059	-0.4540	0.0937	-0.3966	0.1799	-0.4132	0.1533
						-0.4657	0.0801	-0.4368	0.1177	-0.4449	0.1059	-0.4540	0.0937	-0.3966	0.1799	-0.4693	0.0704
						-0.4876	0.0485	-0.4698	0.0693	-0.4686	0.0716	-0.4799	0.0566	-0.4262	0.1346	-0.4694	0.0704
						-0.4877	0.0485	-0.4698	0.0693	-0.4686	0.0716	-0.4799	0.0566	-0.4262	0.1346	-0.5083	0.0166
						-0.4909	0.0440	-0.4966	0.0315	-0.5054	0.0201	-0.5062	0.0202	-0.4350	0.1214	-0.5082	0.0166
						-0.4908	0.0440	-0.4966	0.0315	-0.5054	0.0201	-0.5062	0.0202	-0.4350	0.1214	-0.5205	0.0000
						-0.5226	0.0000	-0.5195	0.0000	-0.5201	0.0000	-0.5210	0.0000	-0.4453	0.1064		
														-0.4453	0.1064		
														-0.4735	0.0658		
														-0.4735	0.0658		
														-0.5095	0.0159		
														-0.5095	0.0159		
														-0.5213	0.0000		

Dimensionless representation of the effective stress distribution of the dam along section (a-a) having H_t ranging from 40 m to 200 m can be expressed by (R^2=0.9996):

$$\frac{\sigma_h'}{\gamma B} = 0.13\left(\frac{y}{H_t}\right)^3 - 0.34\left(\frac{y}{H_t}\right)^2 + 0.65\left(\frac{y}{H_t}\right) - 0.52 \qquad (4.4)$$

where;

H_t : height of dam from thalweg.

The horizontal projected force, P_h', were computed analytically from distribution of the horizontal effective stresses, σ_h'. The results are presented in Table 4.2, and in Figure 4.10 for the aforementioned dam heights.

Table 4.2 Projected horizontal effective forces versus H_t

H_t (m)	**P_h' (kN/m)**
40	14688.28
60	31717.55
80	55307.06
100	84999.08
120	120132.75
140	162415.60
160	211269.55
180	266184.17
200	326790.43

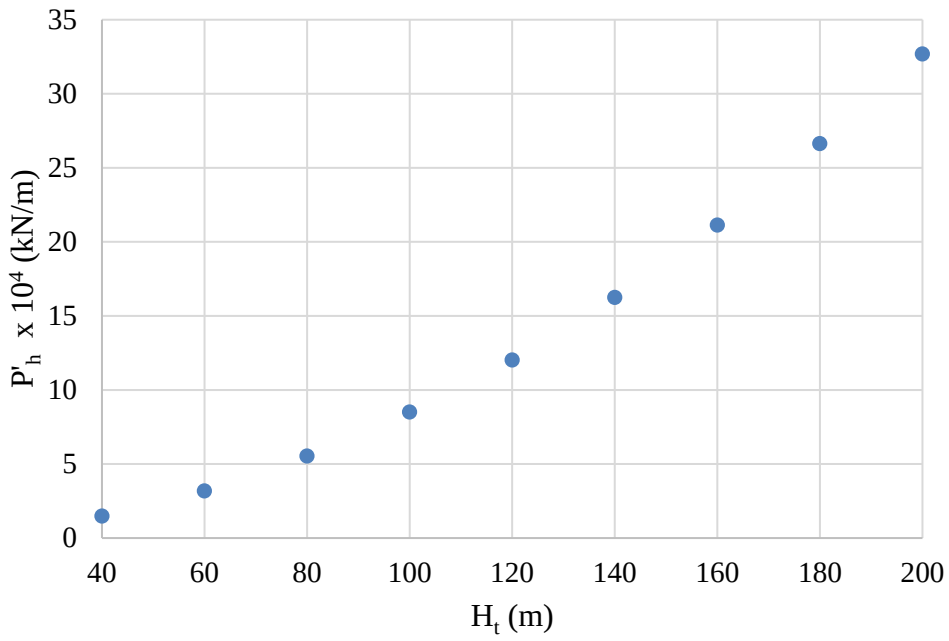

Figure 4.10 Projected horizontal effective forces versus H_t

The areas under the pressure distribution curves were computed for the aforementioned dam heights to obtain the projected force, P'_h, with R^2=0.9999:

$$P'_h = 7.86{H_t}^2 + 64.34H_t - 379.63 \quad (4.5)$$

where H_t is in meters and P'_h is in kN/m

4.4.3 The First Approach

Sensor outputs are used to estimate the true horizontal effective stress distribution as accurate as possible. The sensors are located symmetrically inside the dam body and provide information about the point loads at various points on the cross-section. However, no sensors would provide data about the end points (top and bottom points) of the cross-section. Horizontal pressure on the crest of the dam can be taken as zero. The stress distribution curves between sensors are assumed to be linear. In this approach, the stress distribution below the lowest sensor is assumed as continuous with

the same slope before the lowest sensor till the base of the dam cross-section (See Figure 4.11 and Figure 4.12).

1-Layer Formulation

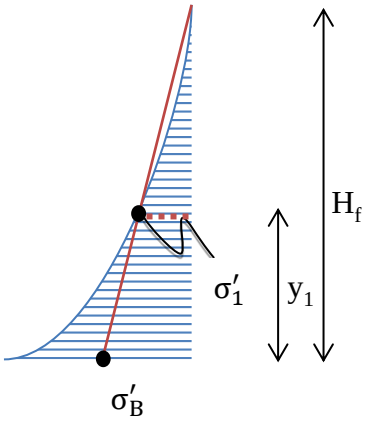

Figure 4.11 Stress distribution modelling with 1 layer

The areas under the effective stress distribution are obtained using the following formulation:

$$\frac{\sigma'_1}{(H_f - y_1)} = \frac{\sigma'_B}{H_f} \qquad \sigma'_B = \frac{\sigma'_1 H_f}{(H_f - y_1)} \tag{4.6}$$

$$P'_1 = \frac{\sigma'_B H_f}{2} \tag{4.7}$$

$$P'_1 = \frac{\sigma'_1 H_f^2}{2(H_f - y_1)} \tag{4.8}$$

2-Layer Formulation

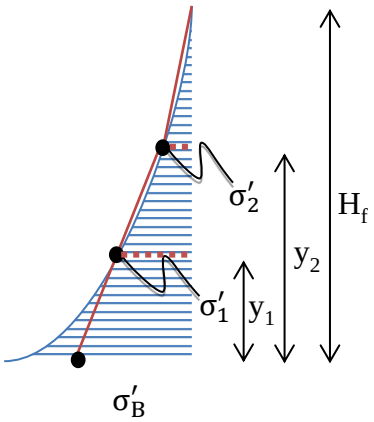

Figure 4.12 Stress distribution modelling with 2 layers

$$P_2^{'} = \frac{\sigma_2'(H_f - y_2)}{2} + \sigma_2' y_2 + \frac{y_2^2(\sigma_1' - \sigma_2')}{2(y_2 - y_1)} \tag{4.9}$$

3-Layer Formulation

$$P_3^{'} = \frac{\sigma_3'(H_f - y_3)}{2} + \frac{(\sigma_3' + \sigma_2')(y_3 - y_2)}{2} + \sigma_2' y_2 + \frac{y_2^2(\sigma_1' - \sigma_2')}{2(y_2 - y_1)} \tag{4.10}$$

4-Layer Formulation

$$P_4^{'} = \frac{\sigma_4'(H_f - y_4)}{2} + \frac{(\sigma_4' + \sigma_3')(y_4 - y_3)}{2} + \frac{(\sigma_3' + \sigma_2')(y_3 - y_2)}{2} + \sigma_2' y_2 + \frac{y_2^2(\sigma_1' - \sigma_2')}{2(y_2 - y_1)} \tag{4.11}$$

5-Layer Formulation

$$P_5^{'} = \frac{\sigma_5'(H_f - y_5)}{2} + \frac{(\sigma_5' + \sigma_4')(y_5 - y_4)}{2} + \frac{(\sigma_4' + \sigma_3')(y_4 - y_3)}{2} + \frac{(\sigma_3' + \sigma_2')(y_3 - y_2)}{2} + \sigma_2' y_2 + \frac{y_2^2(\sigma_1' - \sigma_2')}{2(y_2 - y_1)} \quad (4.12)$$

6-Layer Formulation

$$P_6^{'} = \frac{\sigma_6'(H_f - y_6)}{2} + \frac{(\sigma_6' + \sigma_5')(y_6 - y_5)}{2} + \frac{(\sigma_5' + \sigma_4')(y_5 - y_4)}{2} + \frac{(\sigma_4' + \sigma_3')(y_4 - y_3)}{2} + \frac{(\sigma_3' + \sigma_2')(y_3 - y_2)}{2} + \sigma_2' y_2 + \frac{y_2^2(\sigma_1' - \sigma_2')}{2(y_2 - y_1)} \quad (4.13)$$

4.4.4 The Second Approach

The only difference of the second approach from the first one is that the effective stress distribution at the last segment is assumed to be constant and the same as the lowest sensor readout (See Figure 4.13, Figure 4.14, and Figure 4.15).

1-Layer Formulation

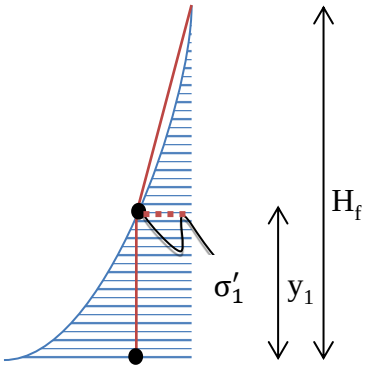

Figure 4.13 Stress distribution modelling with 1 layer

$$P_1^{'} = \frac{\sigma_1'(H_f - y_1)}{2} + \sigma_1' y_1$$

$$P_1^{'} = \frac{\sigma_1'(H_f + y_1)}{2} \tag{4.14}$$

2-Layer Formulation

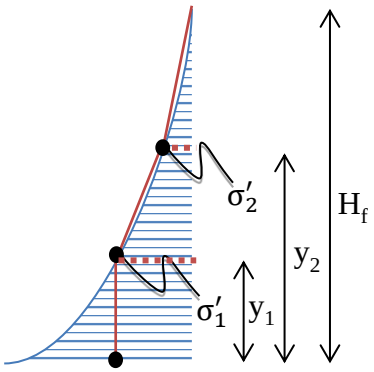

Figure 4.14 Stress distribution modelling with 2 layers

$$P_2' = \frac{\sigma_2'(H_f - y_2)}{2} + \frac{(\sigma_2' + \sigma_1')(y_2 - y_1)}{2} + \sigma_1' y_1$$

$$P_2' = \frac{\sigma_2' H_f - \sigma_2' y_2 + \sigma_1' y_2 - \sigma_1' y_1 + \sigma_2' y_2 - \sigma_2' y_1}{2} + \sigma_1' y_1$$

$$P_2' = \frac{\sigma_2' H_f + \sigma_1' y_2 - \sigma_2' y_1 + \sigma_1' y_1}{2}$$

$$P_2' = \frac{\sigma_2'(H_f - y_1) + \sigma_1'(y_2 + y_1)}{2} \qquad (4.15)$$

3-Layer Formulation

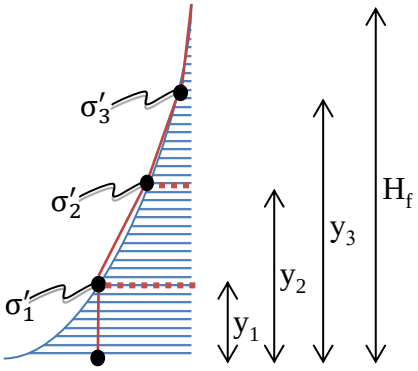

Figure 4.15 Stress distribution modelling with 3 layers

$$P_3' = \frac{\sigma_3'(H_f - y_3)}{2} + \frac{(\sigma_3' + \sigma_2')(y_3 - y_2)}{2} + \frac{(\sigma_2' + \sigma_1')(y_2 - y_1)}{2} + \sigma_1' y_1$$

$$P_3' = \frac{\sigma_3'(H_F - y_2) + \sigma_2'(y_3 - y_1) + \sigma_1'(y_2 + y_1)}{2} \qquad (4.16)$$

4-Layer Formulation

$$P_4' = \frac{\sigma_4'(H_f - y_4)}{2} + \frac{(\sigma_4' + \sigma_3')(y_4 - y_3)}{2} + \frac{(\sigma_3' + \sigma_2')(y_3 - y_2)}{2} + \frac{(\sigma_2' + \sigma_1')(y_2 - y_1)}{2} + (\sigma_1' y_1)$$

$$P_4' = \frac{\sigma_4'(H_F - y_3) + \sigma_3'(y_4 - y_2) + \sigma_2'(y_3 - y_1) + \sigma_1'(y_2 + y_1)}{2} \quad (4.17)$$

5-Layer Formulation

$$P_5' = \frac{\sigma_5'(H_F - L_4) + \sigma_4'(y_5 - y_3) + \sigma_3'(y_4 - y_2) + \sigma_2'(y_3 - y_1)}{2} + \frac{\sigma_1'(y_2 + y_1)}{2} \quad (4.18)$$

4.4.5 The Third Approach

This approach assumes that base and crest level horizontal effective stresses are known and the sensors located between base and crest are used to determine the shape of the stress distribution. More points provide more accurate representation of the shape of the stress distribution (See Figure 4.16, Figure 4.17, and Figure 4.18).

1-Layer Formulation

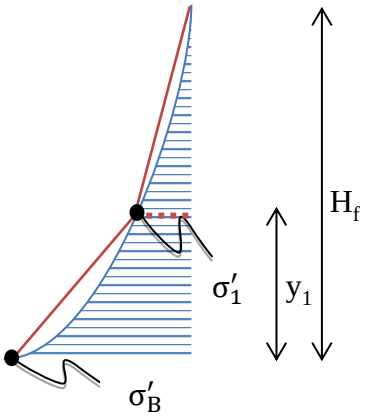

Figure 4.16 Stress distribution modelling with 1 layer

$$P_1' = \frac{\sigma_B' y_1 + \sigma_1' H_f}{2} \quad (4.19)$$

2-Layer Formulation

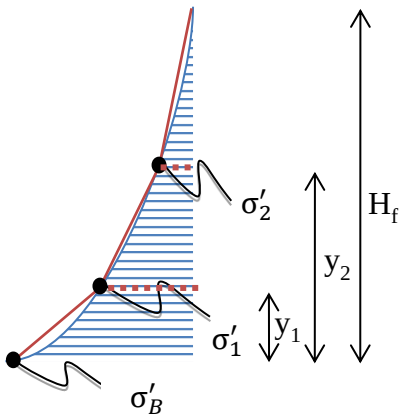

Figure 4.17 Stress distribution modelling with 2 layers

$$P_2' = \frac{y_1(\sigma_B' + \sigma_1')}{2} + \frac{(\sigma_1' + \sigma_2')(y_2 - y_1)}{2} + \frac{\sigma_2'(H_f - y_2)}{2}$$

$$P_2' = \frac{\sigma_B' y_1 + \sigma_1' y_2 - \sigma_2' y_1 + \sigma_2' H_f}{2} \qquad (4.20)$$

3-Layer Formulation

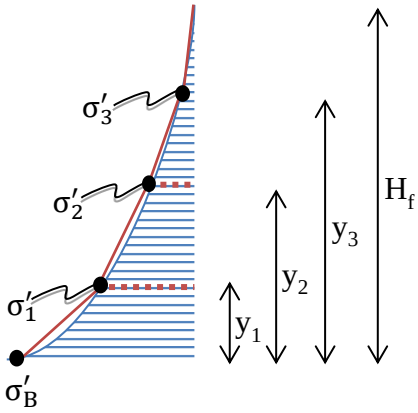

Figure 4.18 Stress distribution modelling with 3 layers

$$P_3' = \frac{y_1(\sigma_B' + \sigma_1')}{2} + \frac{(\sigma_1' + \sigma_2')(y_2 - y_1)}{2} + \frac{(\sigma_2' + \sigma_3')(y_3 - y_2)}{2} + \frac{\sigma_3'(H_f - y_3)}{2}$$

$$P_3' = \frac{\sigma_B' y_1 + \sigma_1' y_2 - \sigma_2' y_1 + \sigma_2' y_3 - \sigma_3' y_2 + \sigma_3' H_f}{2} \tag{4.21}$$

4.4.6 Evaluation of the Error of Approaches

Errors of the approaches were evaluated by comparing the modelled areas with the true areas below the effective stress distributions and presented in Table 4.3, Table 4.4, and Table 4.5.

As it can be observed from these tables, the third approach gives the lowest error. Thus the third approach was chosen to be employed in the following algorithm development process. The next part is devoted to the description of the horizontal projection of the sensors on a layer.

Table 4.3 Percent error of the first approach

H_t (m)	Number of Layers					
	1	**2**	**3**	**4**	**5**	**6**
40	8.37	6.38	4.81	4.00	3.53	3.23
60	7.73	5.72	4.14	3.32	2.85	2.54
80	7.17	5.14	3.56	2.73	2.26	1.95
100	6.75	4.72	3.13	2.30	1.82	1.51
120	6.43	4.39	2.80	1.96	1.48	1.18
140	6.19	4.14	2.54	1.71	1.22	0.92
160	5.99	3.94	2.34	1.50	1.02	0.71
180	5.83	3.78	2.17	1.34	0.85	0.54
200	5.70	3.65	2.04	1.20	0.71	0.41

Table 4.4 Percent error of the second approach

H_t (m)	Number of Layers					
	1	**2**	**3**	**4**	**5**	**6**
40	38.04	23.66	17.59	14.34	12.35	11.01
60	37.60	23.12	17.01	13.74	11.73	10.39
80	37.22	22.65	16.50	13.21	11.20	9.84
100	36.94	22.30	16.13	12.82	10.79	9.44
120	36.72	22.04	15.84	12.53	10.49	9.13
140	36.56	21.83	15.62	12.30	10.26	8.89
160	36.42	21.67	15.45	12.11	10.07	8.70
180	36.32	21.54	15.30	11.97	9.92	8.55
200	36.23	21.43	15.19	11.84	9.79	8.42

Table 4.5 Percent error of the third approach

H_t (m)	Number of Layers					
	1	**2**	**3**	**4**	**5**	**6**
40	1.54	0.20	0.86	1.19	1.38	1.49
60	2.25	0.51	0.16	0.49	0.68	0.80
80	2.87	1.11	0.44	0.11	0.08	0.20
100	3.34	1.57	0.90	0.56	0.37	0.25
120	3.69	1.92	1.24	0.91	0.72	0.60
140	3.96	2.18	1.51	1.17	0.98	0.86
160	4.18	2.40	1.72	1.38	1.19	1.07
180	4.35	2.57	1.89	1.55	1.36	1.24
200	4.50	2.71	2.03	1.69	1.50	1.38

4.5 Horizontal Projection of Sensors

4.5.1 Introductory Remarks

Effective stress distribution of any horizontal layer under the loading case concerned can be obtained from the finite element analysis package, PLAXIS. Shape of the effective stress distribution of a symmetric homogeneous CFRD cross-section tends to be a high-degree polynomial (Figure 4.19).

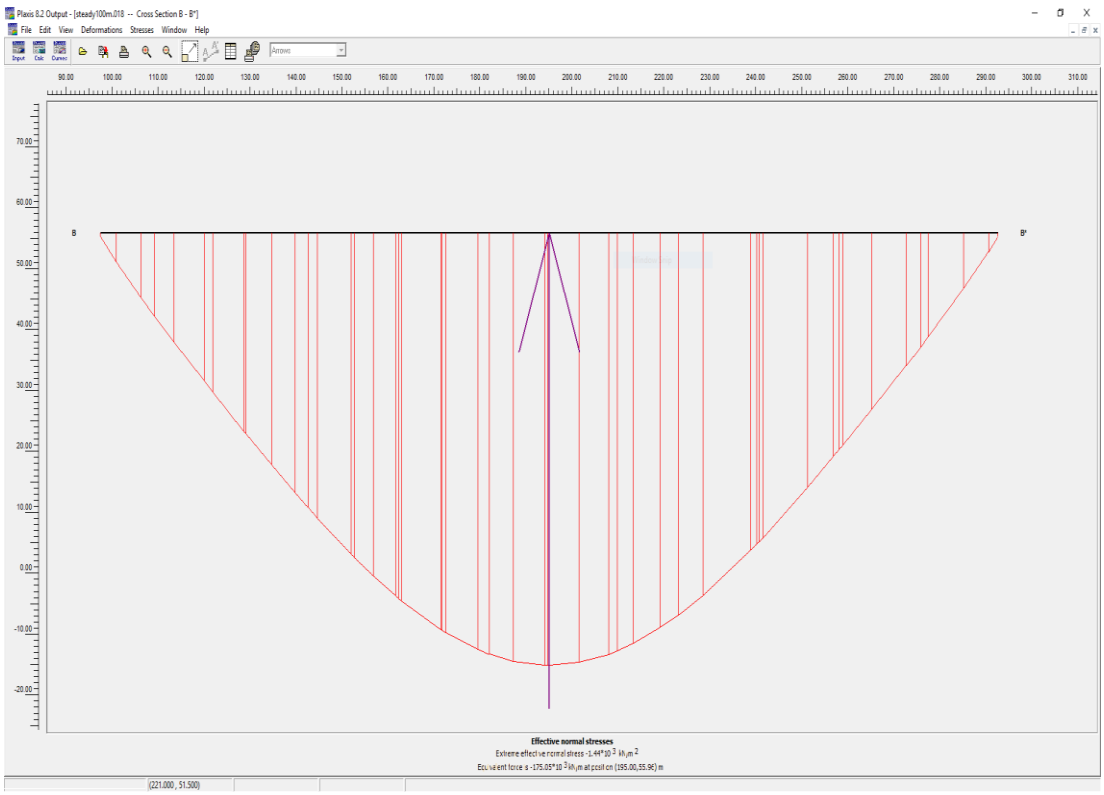

Figure 4.19 PLAXIS output showing the effective stress distribution

4.5.2 Modelling of Effective Stress Distribution

The datasets of the effective stress distribution were obtained from the PLAXIS. The equation of the effective stress distribution at any horizontal layer can be formulated by:

$$\sigma_v'(x) = ax^6 + bx^5 + cx^4 + dx^3 + ex^2 + fx + g \qquad (4.22)$$

where *a*, *b*, *c*, *d*, *e*, *f*, and *g* are coefficients obtained from the regression analysis with R^2 values ranging from 0.72 to 0.98. The coefficients *a*, *b*, *c*, *d*, *e*, *f*, and, *g* are variable with different horizontal cross-section heights within one standard cross-section.

Figure 4.20 represents the arbitrary horizontal cross-sections within a standard CFRD cross-section. It could be noticed that all parameters of different horizontal cross-sections are unique.

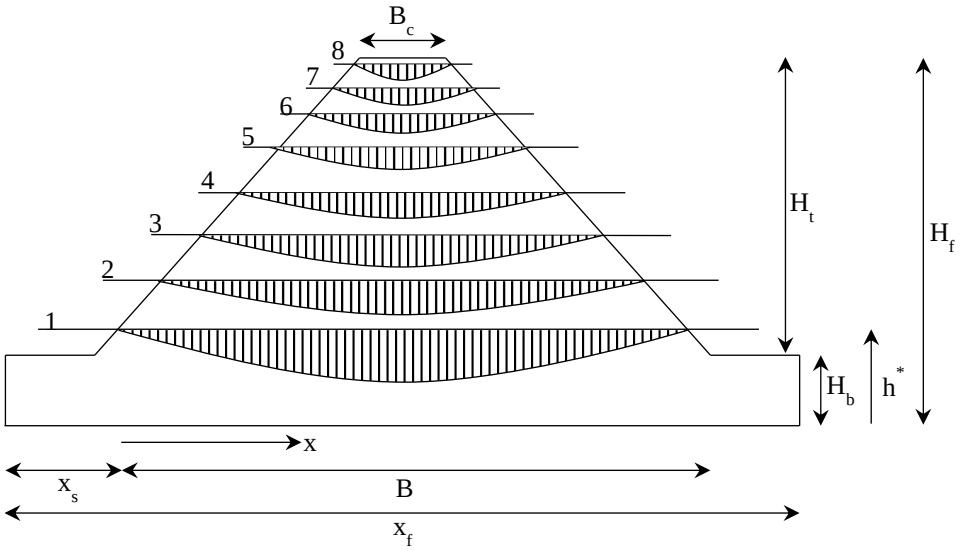

Figure 4.20 Parameters of generalization

In order to search for a possible relationship between the parameters and coefficients, 8 arbitrary horizontal cross-sections were chosen and analysed. Table 4.6. summarizes the raw data obtained from PLAXIS for 40 m-high standard cross-section.

The vertical effective stress distribution data of other cross-sections are presented in Appendix D.

Table 4.6 Vertical effective stresses of arbitrary cross-sections 1 to 4 (h*) of 40-m-high cross-section

h* = 10.134 m		**h* = 14.992 m**		**h* = 20.006 m**		**h* = 25.008 m**	
x (m)	σ'_v **(kN/m²)**	**x (m)**	σ'_v **(kN/m²)**	**x (m)**	σ'_v **(kN/m²)**	**x (m)**	σ'_v **(kN/m²)**
35.621	-4.865	42.934	-4.833	50.482	-4.515	58.011	-3.160
35.940	-11.977	43.918	-23.863	51.658	-26.264	59.438	-28.100
35.940	-12.081	43.918	-22.995	51.658	-25.720	59.438	-28.033
36.797	-28.633	46.971	-71.133	55.374	-76.339	62.917	-71.228
36.797	-29.227	46.971	-71.450	55.374	-76.334	62.917	-71.246
39.374	-71.249	47.561	-78.631	55.971	-83.899	63.142	-73.674
39.374	-71.083	47.561	-78.323	55.971	-83.271	63.142	-73.767
40.095	-81.700	51.085	-120.168	56.140	-85.445	63.355	-75.965
40.095	-82.617	51.085	-120.071	56.140	-85.283	63.355	-76.028
41.232	-98.190	55.230	-163.459	56.317	-87.326	68.043	-122.307
41.232	-98.113	55.230	-163.472	56.317	-87.304	68.043	-122.264
44.951	-141.628	55.637	-167.603	57.704	-102.368	71.089	-149.808
44.951	-141.638	55.637	-167.548	57.704	-102.369	71.089	-149.829
48.941	-183.688	56.238	-173.467	61.773	-143.732	74.426	-177.111
48.941	-183.607	56.238	-173.447	61.773	-143.718	74.426	-177.092
50.640	-200.474	59.629	-205.802	62.416	-149.818	77.044	-196.884
50.640	-200.479	59.629	-205.809	62.416	-149.848	77.044	-196.864
52.027	-214.048	61.055	-218.951	67.322	-194.574	80.545	-220.244
52.027	-214.057	61.055	-218.928	67.322	-194.576	80.545	-220.258
56.103	-253.312	63.952	-245.021	68.896	-208.011	81.454	-225.876
56.103	-253.339	63.952	-245.012	68.896	-208.020	81.454	-225.873
57.048	-262.316	65.834	-261.338	70.955	-224.798	85.361	-247.221
57.048	-262.308	65.834	-261.352	70.955	-224.814	85.361	-247.161
59.710	-287.167	68.267	-281.785	74.579	-252.841	85.768	-249.146
59.710	-287.189	68.267	-281.778	74.579	-252.794	85.768	-249.174
60.488	-294.346	69.479	-291.680	77.054	-270.205	89.891	-265.973
60.488	-294.314	69.479	-291.691	77.054	-270.223	89.891	-265.899
62.834	-315.565	71.183	-305.024	79.193	-284.167	90.305	-267.283
62.834	-315.567	71.183	-305.028	79.193	-284.183	90.305	-267.306
65.265	-336.742	73.217	-320.461	80.380	-291.450	91.077	-269.547

Table 4.6 (continued)

h* = 10.134 m		h* = 14.992 m		h* = 20.006 m		h* = 25.008 m	
x (m)	σ'_v (kN/m^2)	x (m)	σ'_v (kN/m^2)	x (m)	σ'_v (kN/m^2)	x (m)	σ'_v (kN/m^2)
65.265	-336.791	73.217	-320.456	80.380	-291.436	91.077	-269.574
66.378	-346.265	75.183	-334.471	82.766	-304.911	93.495	-275.370
66.378	-346.241	75.183	-334.500	82.766	-304.926	93.495	-275.360
69.076	-368.430	76.161	-341.226	83.972	-311.106	95.495	-278.083
69.076	-368.441	76.161	-341.224	83.972	-311.100	95.495	-278.079
70.585	-380.268	79.308	-361.257	86.910	-324.295	96.243	-278.746
70.585	-380.268	79.308	-361.208	86.910	-324.306	96.243	-278.701
72.867	-397.394	79.350	-361.454	87.823	-327.831	97.189	-279.030
72.867	-397.409	79.350	-361.512	87.823	-327.844	97.189	-279.040
73.720	-403.556	79.854	-364.449	92.072	-340.306	98.898	-278.787
73.720	-403.545	79.854	-364.436	92.072	-340.270	98.898	-278.778
76.059	-419.640	82.955	-381.263	92.166	-340.497	101.523	-275.605
76.059	-419.655	82.955	-381.227	92.166	-340.374	101.523	-275.611
77.952	-431.689	83.185	-382.364	92.182	-340.407	102.004	-274.737
77.952	-431.707	83.185	-382.397	92.182	-340.474	102.004	-274.728
79.943	-443.469	86.232	-395.913	92.219	-340.546	103.634	-270.794
79.943	-443.433	86.232	-395.904	92.219	-340.658	103.634	-270.785
81.774	-453.341	86.585	-397.274	96.117	-345.866	105.359	-265.661
81.774	-453.327	86.585	-397.287	96.117	-345.806	105.359	-265.642
84.193	-464.918	89.151	-406.135	98.341	-346.148	106.021	-263.274
84.193	-464.951	89.151	-406.137	98.341	-346.191	106.021	-263.299
86.281	-473.524	91.637	-412.425	101.200	-343.631	108.653	-252.598
86.281	-473.497	91.637	-412.529	101.200	-343.636	108.653	-252.617
88.581	-481.481	92.803	-414.756	102.484	-341.538	111.121	-240.387
88.581	-481.469	92.803	-414.698	102.484	-341.537	111.121	-240.403
91.179	-488.235	95.850	-418.309	104.605	-336.511	112.415	-233.381
91.179	-488.274	95.850	-418.314	104.605	-336.524	112.415	-233.417
92.688	-491.217	97.654	-418.987	105.957	-332.652	117.253	-202.799
92.688	-491.182	97.654	-418.919	105.957	-332.648	117.253	-202.755
95.045	-494.298	100.791	-416.853	107.283	-327.970	117.854	-198.624
95.045	-494.307	100.791	-416.877	107.283	-327.948	117.854	-198.540
97.561	-495.348	102.188	-415.067	109.573	-318.722	118.393	-194.676

Table 4.6 (continued)

h* = 10.134 m		h* = 14.992 m		h* = 20.006 m		h* = 25.008 m	
x (m)	σ'_v (kN/m^2)	x (m)	σ'_v (kN/m^2)	x (m)	σ'_v (kN/m^2)	x (m)	σ'_v (kN/m^2)
97.561	-495.368	102.188	-415.032	109.573	-318.727	118.393	-194.707
98.993	-495.083	103.511	-412.415	111.356	-310.146	123.184	-157.137
98.993	-495.080	103.511	-412.393	111.356	-310.133	123.184	-157.064
101.588	-492.481	106.146	-405.792	113.557	-298.551	123.302	-156.077
101.588	-492.471	106.146	-405.794	113.557	-298.555	123.302	-156.107
102.648	-490.909	108.726	-396.646	116.490	-280.694	126.558	-127.266
102.648	-490.910	108.726	-396.661	116.490	-280.708	126.558	-127.319
103.484	-489.264	109.987	-391.578	117.858	-271.777	129.945	-94.769
103.484	-489.258	109.987	-391.566	117.858	-271.753	129.945	-94.796
106.395	-482.080	111.153	-386.228	119.485	-260.374	130.997	-84.058
106.395	-482.083	111.153	-386.220	119.485	-260.394	130.997	-84.359
109.460	-471.189	113.901	-372.442	122.146	-240.906	131.486	-78.697
109.460	-471.187	113.901	-372.443	122.146	-240.894	131.486	-78.792
110.220	-468.125	116.807	-355.262	123.689	-228.798	136.418	-16.785
110.220	-468.143	116.807	-355.266	123.689	-228.795	136.418	-17.094
110.964	-464.793	117.898	-348.371	126.207	-208.181	136.988	-8.614
110.964	-464.822	117.898	-348.365	126.207	-208.163	136.988	-8.001
114.072	-449.745	119.105	-340.256	129.519	-179.333	137.088	-6.350
114.072	-449.750	119.105	-340.256	129.519	-179.336		
117.212	-431.498	121.889	-320.705	130.376	-171.535		
117.212	-431.474	121.889	-320.703	130.376	-171.535		
117.957	-426.859	124.140	-303.536	135.815	-119.081		
117.957	-426.870	124.140	-303.547	135.815	-119.454		
118.737	-421.778	125.779	-290.595	135.992	-117.561		
118.737	-421.792	125.779	-290.578	135.992	-117.286		
121.838	-400.586	127.620	-275.415	136.248	-114.452		
121.838	-400.577	127.620	-275.426	136.248	-114.671		
124.767	-378.474	129.169	-262.383	141.472	-54.234		
124.767	-378.468	129.169	-262.363	141.472	-54.162		
125.668	-371.422	132.506	-233.015	144.591	-4.874		
125.668	-371.418	132.506	-233.018				
126.798	-362.267	133.266	-226.170				

Table 4.6 (continued)

h* = 10.134 m		h* = 14.992 m	
x (m)	σ'_v (kN/m^2)	x (m)	σ'_v (kN/m^2)
126.798	-362.265	133.266	-226.144
129.585	-339.120	137.146	-190.043
129.585	-339.115	137.146	-189.986
131.057	-326.339	137.451	-187.086
131.057	-326.334	137.451	-187.138
134.277	-297.507	141.324	-148.415
134.277	-297.516	141.324	-148.492
136.108	-280.599	143.770	-122.713
136.108	-280.573	143.770	-123.064
139.229	-251.151	147.770	-74.066
139.229	-251.143	147.770	-74.030
141.509	-229.142	152.112	-7.218
141.509	-229.166		
143.938	-205.392		
143.938	-205.397		
146.172	-183.190		
146.172	-183.212		
149.134	-152.746		
149.134	-153.018		
150.511	-137.607		
150.511	-137.464		
154.291	-91.637		
154.291	-90.907		
156.032	-65.664		
156.032	-65.899		
159.399	-5.823		

Table 4.7 Vertical effective stresses of arbitrary cross-sections 5 to 8 (h*) of 40-m-high cross-section

h* = 29.989 m		**h* = 34.952 m**		**h* = 39.988 m**		**h* = 44.983 m**	
x (m)	**σ'_v (kN/m^2)**	**x (m)**	**σ'_v (kN/m^2)**	**x (m)**	**σ'_v (kN/m^2)**	**x (m)**	**σ'_v (kN/m^2)**
65.509	-3.949	72.981	-4.537	80.561	-4.423	87.933	-5.175
65.670	-6.819	73.853	-17.399	81.497	-18.270	89.490	-20.855
65.670	-6.786	73.853	-17.361	81.497	-17.903	89.490	-20.610
67.544	-33.818	75.641	-38.787	84.260	-46.482	91.091	-23.108
67.544	-33.673	75.641	-38.724	84.260	-46.862	91.091	-22.896
69.701	-58.743	77.352	-56.533	84.411	-48.183	92.463	-23.986
69.701	-58.721	77.352	-56.430	84.411	-47.805	92.463	-24.184
71.382	-75.452	80.233	-81.314	84.441	-48.102	94.192	-23.524
71.382	-75.404	80.233	-81.298	84.441	-47.863	94.192	-23.522
74.292	-102.568	80.699	-85.013	84.511	-48.370	95.805	-23.281
74.292	-102.583	80.699	-85.133	84.511	-48.246	95.805	-23.752
77.252	-127.063	85.689	-117.674	87.767	-67.186	97.561	-23.383
77.252	-127.080	85.689	-117.625	87.767	-67.265	97.561	-23.162
79.676	-145.308	86.011	-119.455	89.989	-76.447	99.947	-23.804
79.676	-145.294	86.011	-119.269	89.989	-76.409	99.947	-23.714
82.212	-161.941	86.184	-120.221	91.836	-82.548	102.954	-24.304
82.212	-161.937	86.184	-120.353	91.836	-82.556	102.954	-23.854
83.913	-172.082	86.495	-121.909	94.309	-88.045	104.804	-21.654
83.913	-172.072	86.495	-122.018	94.309	-88.044	104.804	-21.946
87.428	-190.199	91.661	-144.320	95.759	-90.251	105.891	-19.684
87.428	-190.239	91.661	-144.270	95.759	-90.278	105.891	-19.220
89.448	-198.950	92.948	-148.108	96.938	-90.990	107.126	-4.691
89.448	-198.938	92.948	-148.095	96.938	-90.975		
90.862	-204.214	95.188	-153.053	99.871	-89.511		
90.862	-204.203	95.188	-153.117	99.871	-89.522		
92.145	-208.138	96.505	-154.409	104.094	-80.004		
92.145	-208.163	96.505	-154.373	104.094	-79.751		
93.644	-211.963	99.469	-153.618	104.112	-79.706		
93.644	-211.949	99.469	-153.610	104.112	-79.517		
95.560	-215.012	103.703	-143.450	104.166	-79.335		

Table 4.7 (continued)

h* = 29.989 m		h* = 34.952 m		h* = 39.988 m	
x (m)	σ'_v (kN/m^2)	x (m)	σ'_v (kN/m^2)	x (m)	σ'_v (kN/m^2)
95.560	-215.048	103.703	-143.307	104.166	-79.601
97.636	-216.140	103.768	-143.092	108.256	-62.648
97.636	-216.099	103.768	-143.081	108.256	-62.633
99.781	-214.811	103.858	-142.755	109.418	-56.006
99.781	-214.855	103.858	-142.840	109.418	-56.076
103.479	-206.698	107.501	-127.617	112.609	-30.121
103.479	-206.698	107.501	-127.607	112.609	-30.359
104.429	-203.720	109.706	-116.183	114.619	-5.168
104.429	-203.653	109.706	-116.210		
104.952	-201.735	110.914	-109.189		
104.952	-201.807	110.914	-109.170		
109.309	-182.428	113.906	-89.167		
109.309	-182.440	113.906	-89.107		
109.963	-179.124	113.976	-88.564		
109.963	-178.974	113.976	-88.615		
110.050	-178.522	117.065	-63.020		
110.050	-178.545	117.065	-62.776		
110.391	-176.690	120.132	-31.716		
110.391	-176.747	120.132	-31.411		
113.804	-156.509	121.239	-18.822		
113.804	-156.514	121.239	-18.493		
114.850	-149.481	122.171	-5.075		
114.850	-149.438				
117.364	-131.364				
117.364	-131.427				
122.353	-89.119				
122.353	-89.052				
122.758	-85.232				
122.758	-85.503				
122.952	-83.467				
122.952	-83.969				
124.845	-64.220				

Table 4.7 (continued)

h* = 29.989 m	
x (m)	σ'_v **(kN/m^2)**
124.845	-64.502
128.746	-18.961
128.746	-18.633
129.152	-13.482
129.152	-12.429
129.617	-4.899

The values of *x* and *h** in Table 4.6 and Table 4.7 represent the horizontal and vertical distance measured from the bottom left corner of the cross-section (0, 0), respectively. Column for σ'_v is provided for effective stress in kN/m^2 and the (-) sign represents compression. The parameters H_f, H_t, and H_b are constant in a single standard cross-section, whereas *h**, *B**, x_s, x_f, σ'_{vmax}, and σ'_{vmin} are variable between the arbitrary horizontal cross-sections. These parameters are defined as:

h* : height of the horizontal cross-section from the base of the dam cross-section (See Figure 4.20).

B* : width of the cross-section at any horizontal layer. Defined as:

$$B^* = (S_u + S_d)\left(H_f - h^*\right) + B_c \tag{4.23}$$

S_d : horizontal run for 1 m-rise at downstream side slope

S_u : horizontal run for 1 m-rise at upstream side slope

B_c : width of the crest

x_s : distance of the beginning of the horizontal cross-section from X=0

x_f : distance of the end of the horizontal cross-section from X=0

σ'_{vmax} : maximum value of the effective stress of the horizontal layer

σ'_{vmin} : minimum value of the effective stress of the horizontal layer

A number of operations were conducted in order to define a dimensionless effective stress distribution. The governing equation was proposed by the functional relationship with reference to the dimensionless plot of the relevant data as shown in Figure 4.21. Legend shows *h** values of 8 arbitrary horizontal layers.

$$f\left(\frac{2(x-x_s)}{B^*}-1\right)=\frac{\sigma_v'}{\sigma_{vmax}'} \tag{4.24}$$

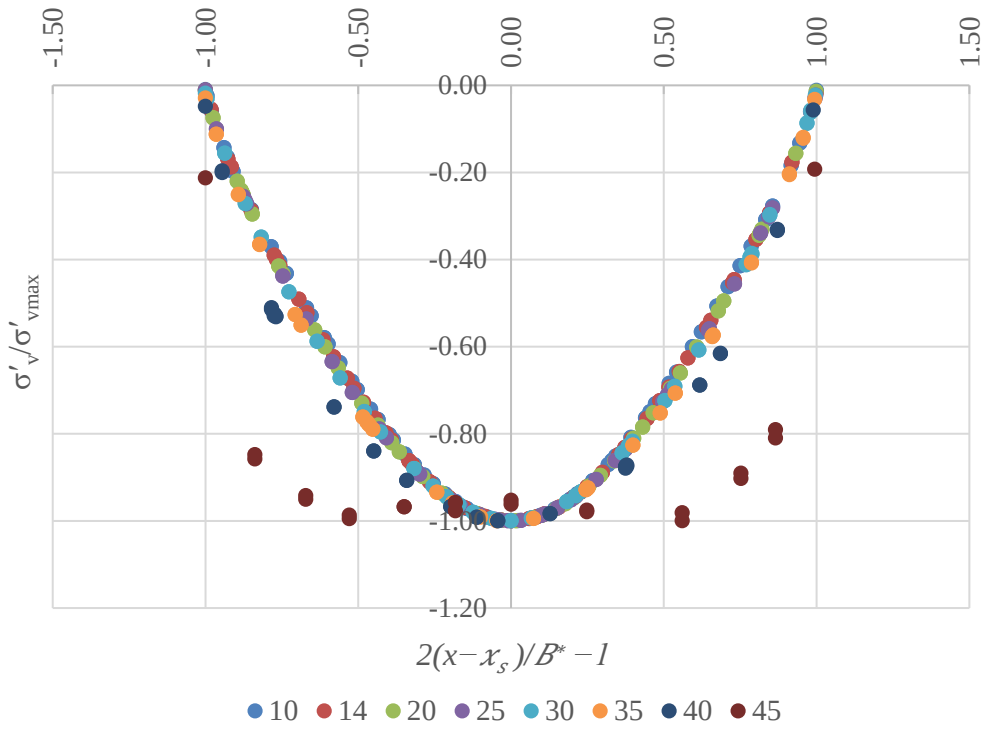

Figure 4.21 Graphical representation of the governing equation for 8 arbitrary horizontal layers of 40 m-high cross-section

As it can be observed from Figure 4.21, the data tend to follow a trend except the levels close to the dam crest elevation. The effective stress distributions of all individual and arbitrary horizontal cross-sections were expressed by a 6th degree polynomial with LINEST function of MS EXCEL, which uses the data given in Table 4.8 with the least squares method. In Table 4.8:

$$\alpha = \frac{(h^* - H_b)}{H_f} \tag{4.25}$$

Table 4.8 Coefficients of the effective stress distributions given in Figure 4.22

α	**a**	**b**	**c**	**d**	**e**	**f**	**g**
0.09	0.5296	-0.0074	-0.9558	0.0093	1.4085	-0.0032	-1.0021
0.21	0.4553	-0.0035	-0.8125	0.0059	1.3391	-0.0018	-1.0012
0.34	0.4222	-0.0008	-0.7304	0.0040	1.2911	-0.0008	-1.0010
0.47	0.3844	-0.0110	-0.6514	0.0126	1.2475	-0.0010	-0.9998
0.59	0.3776	-0.0070	-0.6090	0.0053	1.2093	0.0030	-0.9974
0.71	0.3772	0.0106	-0.5293	-0.0140	1.1264	0.0099	-0.9988
0.84	0.4997	-0.0203	-0.4181	0.0218	0.8837	0.0108	-1.0000
0.96	2.0503	0.0403	-1.5487	-0.0137	0.2813	-0.0020	-0.9762

The true dimensionless effective forces, P'_{vt}, below the effective stress distributions were defined as:

$$P'_{vt} = \frac{\int_{x_s}^{x_f} \sigma'_v(x)dx}{\sigma'_{vmax}B^*} \tag{4.26}$$

The true dimensionless effective forces, P'_{vt}, were also analysed and presented in Figure 4.22 with the other parameters. Finally, the procedure was held for all standard cross-sections ranging from 40 m to 200 m heights and the results are summarized in Table 4.9.

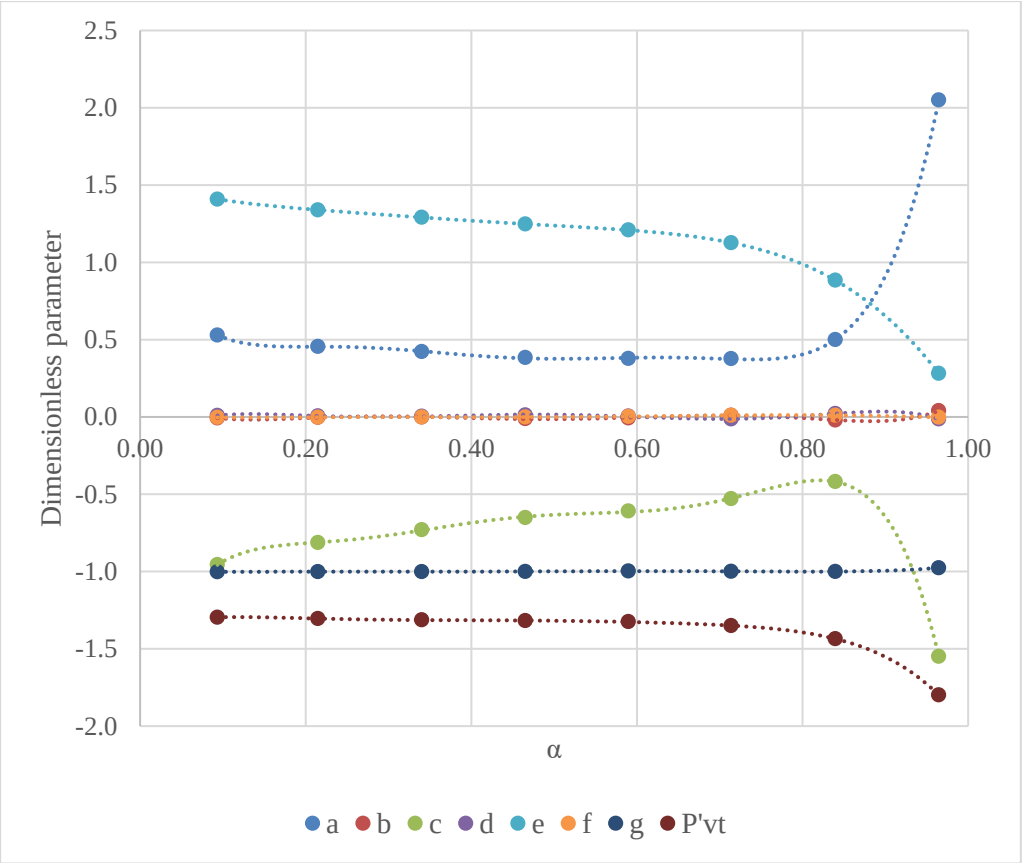

Figure 4.22 α versus parameters a through g and true dimensionless effective forces

Table 4.9 Summary of the values of parameters of all cross-sections

H_t (m)	α	a	b	c	d	e	f	g	P'_{vt}
40	0.093	0.530	-0.007	-0.956	0.009	1.409	-0.003	-1.002	-1.296
	0.215	0.455	-0.004	-0.813	0.006	1.339	-0.002	-1.001	-1.305
	0.340	0.422	-0.001	-0.730	0.004	1.291	-0.001	-1.001	-1.313
	0.465	0.384	-0.011	-0.651	0.013	1.248	-0.001	-1.000	-1.319
	0.590	0.378	-0.007	-0.609	0.005	1.209	0.003	-0.997	-1.324
	0.714	0.377	0.011	-0.529	-0.014	1.126	0.010	-0.999	-1.351
	0.840	0.500	-0.020	-0.418	0.022	0.884	0.011	-1.000	-1.435
	0.965	2.050	0.040	-1.549	-0.014	0.281	-0.002	-0.976	-1.799

Table 4.9 (continued)

H_t (m)	α	a	b	c	d	e	f	g	P'_{vt}
60	0.089	0.523	-0.006	-0.934	0.001	1.393	0.007	-1.003	-1.301
	0.190	0.449	0.004	-0.794	-0.009	1.326	0.009	-1.002	-1.310
	0.374	0.356	0.013	-0.619	-0.020	1.243	0.014	-1.003	-1.324
	0.474	0.324	-0.006	-0.556	-0.004	1.208	0.013	-1.001	-1.326
	0.574	0.319	0.010	-0.532	-0.021	1.185	0.018	-1.000	-1.332
	0.674	0.324	0.017	-0.505	-0.033	1.145	0.025	-1.000	-1.346
	0.823	0.330	-0.010	-0.312	-0.010	0.913	0.031	-1.001	-1.424
	0.956	1.857	-0.179	-1.819	0.215	0.758	-0.018	-1.002	-1.697
80	0.028	0.606	-0.014	-1.082	0.009	1.458	0.003	-1.004	-1.296
	0.152	0.458	0.001	-0.824	-0.004	1.345	0.006	-1.003	-1.307
	0.278	0.376	0.002	-0.673	-0.004	1.275	0.006	-1.003	-1.318
	0.403	0.290	-0.004	-0.524	0.002	1.210	0.006	-1.002	-1.324
	0.528	0.266	-0.003	-0.471	0.000	1.177	0.008	-1.001	-1.329
	0.653	0.300	-0.020	-0.468	0.014	1.140	0.009	-1.000	-1.341
	0.777	0.297	-0.023	-0.336	0.016	0.995	0.015	-1.003	-1.392
	0.903	0.181	-0.082	0.430	0.062	0.264	0.027	-0.996	-1.592
100	0.100	0.506	0.004	-0.902	-0.003	1.381	0.001	-1.003	-1.302
	0.200	0.431	-0.005	-0.752	0.005	1.307	-0.001	-1.003	-1.312
	0.300	0.338	0.005	-0.593	-0.003	1.238	0.000	-1.003	-1.321
	0.400	0.293	-0.001	-0.505	0.002	1.192	0.000	-1.002	-1.327
	0.500	0.256	-0.016	-0.428	0.015	1.153	-0.002	-1.001	-1.332
	0.600	0.255	-0.005	-0.396	0.006	1.119	-0.001	-1.000	-1.340
	0.700	0.269	-0.011	-0.357	0.010	1.059	-0.002	-1.001	-1.362
	0.800	0.296	0.005	-0.203	-0.006	0.864	0.001	-0.997	-1.415
	0.899	-0.125	0.053	0.925	-0.081	0.085	0.027	-0.987	-1.584
120	0.133	0.477	0.006	-0.853	-0.010	1.359	0.006	-1.003	-1.305
	0.216	0.418	0.005	-0.738	-0.009	1.303	0.007	-1.003	-1.314
	0.298	0.343	0.004	-0.606	-0.006	1.243	0.006	-1.003	-1.321
	0.382	0.266	0.008	-0.478	-0.015	1.190	0.009	-1.003	-1.328
	0.465	0.264	-0.004	-0.454	-0.004	1.172	0.008	-1.004	-1.334
	0.549	0.239	0.008	-0.402	-0.017	1.139	0.012	-1.002	-1.336
	0.632	0.246	0.020	-0.376	-0.031	1.104	0.017	-1.002	-1.347
	0.843	0.211	-0.043	0.056	0.024	0.667	0.019	-1.001	-1.474

Table 4.9 (continued)

H_t (m)	α	a	b	c	d	e	f	g	P'_{vt}
140	0.090	0.511	0.003	-0.919	-0.005	1.390	0.004	-1.003	-1.300
	0.198	0.439	-0.002	-0.773	-0.002	1.318	0.005	-1.003	-1.310
	0.305	0.338	0.005	-0.599	-0.007	1.242	0.006	-1.002	-1.320
	0.411	0.279	0.012	-0.487	-0.012	1.189	0.007	-1.002	-1.327
	0.519	0.280	-0.013	-0.464	0.007	1.166	0.005	-1.003	-1.335
	0.628	0.231	0.004	-0.365	-0.012	1.106	0.010	-1.002	-1.346
	0.736	0.261	-0.002	-0.310	-0.003	1.011	0.011	-1.001	-1.377
	0.841	0.237	-0.083	0.021	0.068	0.673	0.007	-0.996	-1.467
160	0.091	0.495	0.001	-0.883	-0.003	1.370	0.004	-1.003	-1.304
	0.184	0.416	0.009	-0.736	-0.013	1.303	0.006	-1.003	-1.313
	0.277	0.359	0.007	-0.624	-0.012	1.249	0.007	-1.003	-1.321
	0.372	0.272	0.004	-0.486	-0.007	1.194	0.006	-1.003	-1.328
	0.465	0.248	0.005	-0.434	-0.011	1.164	0.008	-1.002	-1.331
	0.557	0.212	0.011	-0.365	-0.018	1.133	0.011	-1.004	-1.339
	0.654	0.239	0.000	-0.363	-0.010	1.098	0.011	-1.001	-1.347
	0.747	0.250	0.000	-0.287	-0.010	1.001	0.015	-1.001	-1.377
180	0.107	0.498	0.002	-0.872	-0.004	1.361	0.004	-1.003	-1.305
	0.219	0.390	0.006	-0.681	-0.007	1.278	0.005	-1.004	-1.317
	0.328	0.306	0.004	-0.534	-0.007	1.211	0.006	-1.003	-1.324
	0.440	0.228	0.008	-0.409	-0.013	1.158	0.008	-1.002	-1.331
	0.551	0.205	-0.004	-0.359	-0.003	1.128	0.007	-1.001	-1.335
	0.663	0.215	-0.008	-0.327	-0.002	1.082	0.009	-1.001	-1.349
	0.772	0.319	-0.005	-0.311	-0.007	0.962	0.014	-1.000	-1.392
	0.883	-0.112	-0.067	0.800	0.014	0.208	0.037	-0.992	-1.558
200	0.101	0.512	0.004	-0.898	-0.007	1.372	0.004	-1.003	-1.305
	0.201	0.414	-0.003	-0.722	0.000	1.292	0.004	-1.003	-1.315
	0.300	0.312	0.000	-0.555	-0.003	1.223	0.005	-1.003	-1.323
	0.400	0.298	-0.006	-0.501	0.003	1.188	0.004	-1.002	-1.328
	0.502	0.226	0.000	-0.389	-0.004	1.142	0.006	-1.001	-1.332
	0.602	0.209	-0.006	-0.344	-0.004	1.109	0.008	-1.002	-1.342
	0.700	0.237	-0.007	-0.318	-0.001	1.054	0.010	-1.005	-1.367
	0.802	0.321	-0.028	-0.208	0.014	0.849	0.014	-0.996	-1.419

The graph showing the trend of parameters *a*, *b*, *c*, *d*, *e*, *f*, and *g* is presented in Figure 4.23. Regression analysis was implemented for modelling the parameters as 9-degree polynomials with R^2 values ranging from 0.72 to 0.98. These coefficients and true vertical effective force, P'_{vt}, are presented as Equations 4.26 to 4.33.

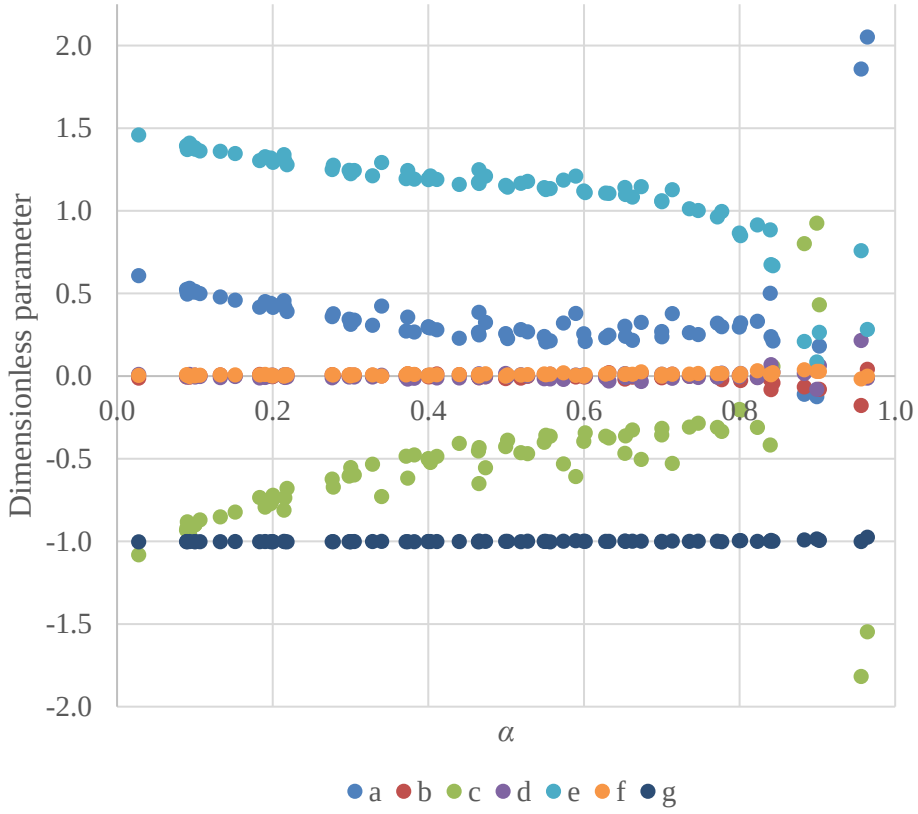

Figure 4.23 Parameters of Eq.4.22 of all cross-sections

$$a = 13215.2\alpha^9 - 53568.49\alpha^8 + 91030.86\alpha^7 - 84270.12\alpha^6 + 46217.74\alpha^5 - 15292.63\alpha^4 + 2973.97\alpha^3 - 313.91\alpha^2 + 14.18\alpha + 0.39 \quad (4.27)$$

$$b = 728\alpha^9 - 3241.33\alpha^8 + 6116.43\alpha^7 - 6361.34\alpha^6 + 3968.09\alpha^5 - 1513.57\alpha^4 + 345.19\alpha^3 - 44.16\alpha^2 + 2.81\alpha - 0.07 \quad (4.28)$$

$$c = -16962.29\alpha^9 + 67907.76\alpha^8 - 113791.92\alpha^7 + 103699.22\alpha^6 \\ -55875.36\alpha^5 + 18118.17\alpha^4 - 3440.83\alpha^3 \\ +351.92\alpha^2 - 14.37\alpha - 0.89 \quad (4.29)$$

$$d = -416.55\alpha^9 + 2010.21\alpha^8 - 4064.37\alpha^7 + 4476.63\alpha^6 \\ -2922.72\alpha^5 + 1153.53\alpha^4 - 269.37\alpha^3 + 34.98\alpha^2 - 2.24\alpha + 0.05 \quad (4.30)$$

$$e = 4097.75\alpha^9 - 15794.47\alpha^8 + 25278.33\alpha^7 \pm 21791.18\alpha^6 \\ +10967.13\alpha^5 - 3263.44\alpha^4 + 553.42\alpha^3 - 47.54\alpha^2 + 0.70\alpha + 1.47 \quad (4.31)$$

$$f = -232.38\alpha^9 + 918.04\alpha^8 - 1519.17\alpha^7 + 1371.32\alpha^6 - 737.09\alpha^5 \\ +241.62\alpha^4 - 47.39\alpha^3 + 5.19\alpha^2 - 0.26\alpha + 0.01 \quad (4.32)$$

$$g = 165.05\alpha^9 \pm 732.87\alpha^8 + 1366.68\alpha^7 - 1390.63\alpha^6 + 840.17\alpha^5 \\ -307.59\alpha^4 + 66.82\alpha^3 - 8.07\alpha^2 + 0.47\alpha - 1.01 \quad (4.33)$$

$$P'_{vt} = 52.78\alpha^9 - 137.57\alpha^8 + 77.63\alpha^7 + 93.81\alpha^6 - 153.32\alpha^5 \\ +87.14\alpha^4 - 24.04\alpha^3 + 3.25\alpha^2 - 0.29\alpha - 1.29 \quad (4.34)$$

4.5.3 Forming the Optimization Algorithm

The optimization for determining the number of stress measuring devices was conducted by the minimization of the total cost of the system, C_T:

$$C_T = C_E + C_P \quad (4.35)$$

where C_E and C_P are the cost of equipment and the cost of penalty, respectively.

Cost of penalty is a measure of how well the pressure distribution is represented by the instrument configuration concerned. As mentioned before, the actual stress distribution is of a high degree polynomial. However, the outputs of an instrumentation system compromise a finite number of sensors connected to each other with straight lines (Figure 4.24).

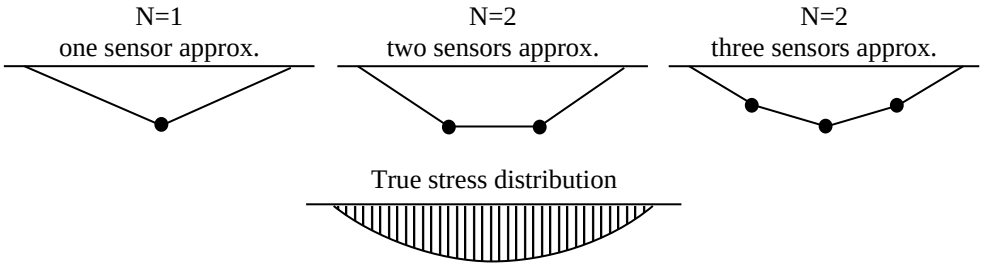

Figure 4.24 Representation of sensor approximations and true stress distribution

Cost of penalty reflects the quality of the information. With the implementation of minimum number of allowable sensors (i.e. one), the cost of the instrumentation system will be lowest which provides poor information about the structural behaviour. On the contrary, with the increasing number of sensors, the cost of the instrumentation system and the quality of the information will increase. Cost of penalty is then defined as the multiplication of the percent difference between the actual area and the computed area under the true effective stress distribution and the linear representation by the instrumentation system, respectively, and the cost difference between the system with maximum and minimum allowed number of sensors.

Cost of equipment is the sum of cost of each sensor C_s and the cost of cable C_c. Switchbox is assumed to be located at the downstream face of the dam with the same height of the horizontal layer. The cables are single-core; thus all sensors use their individual cables for connection to the switchbox. The cost of all instruments and the additional equipment used in this study are provided in Appendix A.

The projected vertical effective forces obtained from the different sensor combinations were calculated by the trapezoidal rule. Then the projected vertical effective forces were generalized. Figure 4.24 illustrates the projected vertical effective stress distributions with finite number of instruments and the comparison with the true vertical effective stress distribution. In this figure, *N* is the number of instruments.

N=1

$$P_v' = \frac{B^*}{N+1}(\sigma_1') \tag{4.36}$$

$$\sigma_1' = \sigma_v'\left(\frac{B^*}{N+1}\right) \tag{4.37}$$

$$C_E = NC_S + N\left(\frac{B^*}{N+1}\right)C_C \tag{4.38}$$

N=2

$$P_v' = \frac{B^*}{N+1}(\sigma_1' + \sigma_2') \tag{4.39}$$

$$\sigma_2' = \sigma_v'\left(\frac{2B^*}{N+1}\right) \tag{4.40}$$

$$C_E = NC_S + \left(\frac{B^*}{N+1}\right)(N^2-1)C_C \tag{4.41}$$

N=3

$$P_v' = \frac{B^*}{N+1}(\sigma_1' + \sigma_2' + \sigma_3') \tag{4.42}$$

$$\sigma_3' = \sigma_v'\left(\frac{3B^*}{N+1}\right) \tag{4.43}$$

$$C_E = NC_S + \left(\frac{B^*}{N+1}\right)(N^2-3)C_C \tag{4.44}$$

N=4

$$P_v' = \frac{B^*}{N+1}(\sigma_1' + \sigma_2' + \sigma_3' + \sigma_4') \tag{4.45}$$

$$\sigma_4' = \sigma_v'\left(\frac{4B^*}{N+1}\right) \tag{4.46}$$

$$C_E = NC_S + \left(\frac{B^*}{N+1}\right)(N^2-6)C_C \tag{4.47}$$

N=5

$$P_v' = \frac{B^*}{N+1}(\sigma_1' + \sigma_2' + \sigma_3' + \sigma_4' + \sigma_5') \tag{4.48}$$

$$\sigma_5' = \sigma_v'\left(\frac{5B^*}{N+1}\right) \tag{4.49}$$

$$C_E = NC_S + \left(\frac{B^*}{N+1}\right)(N^2 - 10)C_C \tag{4.50}$$

N=6

$$P_v' = \frac{B^*}{N+1}(\sigma_1' + \sigma_2' + \sigma_3' + \sigma_4' + \sigma_5' + \sigma_6') \tag{4.51}$$

$$\sigma_6' = \sigma_v'\left(\frac{6B^*}{N+1}\right) \tag{4.52}$$

$$C_E = NC_S + \left(\frac{B^*}{N+1}\right)(N^2 - 15)C_C \tag{4.53}$$

The form of the cost of the equipment, C_E, is then given by:

$$C_E = NC_S + \left(\frac{B^*}{N+1}\right)\left(N^2 - \frac{(N^2 - N)}{2}\right)C_C \tag{4.54}$$

In general form, cost of equipment for various number of instruments, *N*, can be expressed by the following function:

$$C_E(N) = N\left(C_S + C_C\frac{B^*}{2}\right) \tag{4.55}$$

The modelled vertical effective force can also be generalized as function below for various number of instruments on a layer:

$$P_v'(N) = \left(\frac{B^*}{N+1}\right)\sum_{i=1}^{N}\sigma_v'\left(\frac{B^*(i)}{N+1}\right) \tag{4.56}$$

Finally, the objective function can be expressed by:

Minimize

$$C_T = C_E + C_P \tag{4.35}$$

Subject to:

$$N \geq 1 \tag{4.57}$$

$$N \leq {B^*}/{2} \tag{4.58}$$

$$P_v'(N) = \left(\frac{B^*}{N+1}\right)\sum_{i=1}^{N} \sigma_v'\left(\frac{B^*(i)}{(N+1)}\right) \tag{4.56}$$

$$\sigma_v'(x) = ax^6 + bx^5 + cx^4 + dx^3 + ex^2 + fx + g \tag{4.22}$$

$$C_E(N) = N\left(C_S + C_C\frac{B^*}{2}\right) \tag{4.55}$$

$$C_{Diff} = C_E\left(\frac{B^*}{2}\right) - C_E(1) \tag{4.59}$$

$$Err(N) = \frac{P_{vt}' - P_v'(N)}{P_{vt}'} \tag{4.60}$$

$$C_P(N) = C_{Diff}Err(N) \tag{4.61}$$

where;

B^* : width of a horizontal layer

$P'_v(N)$: modelled vertical dimensionless effective force function

This objective function can be solved in MS EXCEL environment without any need for complex linear or non-linear solvers. A detailed view of the working spreadsheet is provided in Appendix E.

4.6 The Outcomes of the Algorithm

4.6.1 Algorithm Outputs

The proposed algorithm was applied to the aforementioned CFRD cross-sections. The third approach was selected for the determination of the number of the horizontal projections to be equipped with sensors. The optimal number of horizontal projections and the number of sensors were computed from the algorithm and the maximum of the ratio of percent error reduction to percent cost increase (E↓ / C↑) was chosen as an optimum solution.

Table 4.10 provides detailed information about the percent error decreases and cost increases for different number of horizontal projections, *M*, of CFRD cross-sections with heights ranging from 40 m to 120 m from thalweg.

Table 4.10 Determination of the optimum number of layers and instruments

H_t (m)	M	Error (%)	N_T	Cost Per Sensor ($)	Error ↓ (%)	Cost ↑ (%)	E↓ / C↑
40	1	1.54	3	880.00			
	2	0.20	6	880.00	1.34	0.00	133.60
	3	0.86	10	888.40	0.00	0.95	0.00
	4	1.19	12	896.80	0.00	0.95	0.00
	5	1.38	15	894.93	0.00	0.00	0.00
	6	1.49	19	896.42	0.00	0.17	0.00
	7	1.57	22	895.27	0.00	0.00	0.00
60	1	2.25	4	964.00			
	2	0.51	7	976.00	1.75	1.24	1.40
	3	0.16	11	975.45	0.34	0.00	34.35
	4	0.49	14	978.40	0.00	0.30	0.00
	5	0.68	18	978.00	0.00	0.00	0.00
	6	0.80	22	986.91	0.00	0.91	0.00
	7	0.88	25	994.24	0.00	0.74	0.00
80	1	2.87	4	1,048.00			
	2	1.11	9	1,060.44	1.76	1.19	1.48
	3	0.44	12	1,076.00	0.67	1.47	0.46
	4	0.11	16	1,073.20	0.33	0.00	33.08
	5	0.08	21	1,074.67	0.04	0.14	0.26
	6	0.20	24	1,080.00	0.00	0.50	0.00
	7	0.28	28	1,078.00	0.00	0.00	0.00
100	1	3.34	4	1,132.00			
	2	1.57	9	1,147.56	1.77	1.37	1.29
	3	0.90	13	1,148.15	0.67	0.05	12.94
	4	0.56	17	1,166.59	0.33	1.61	0.21
	5	0.37	21	1,165.33	0.19	0.00	19.01
	6	0.25	27	1,174.22	0.12	0.76	0.16
	7	0.17	31	1,172.65	0.08	0.00	8.12

Table 4.10 (continued)

H_t (m)	M	Error (%)	N_T	Cost Per Sensor ($)	Error ↓ (%)	Cost ↑ (%)	E↓ / C↑
120	1	3.69	5	1,216.00			
	2	1.92	9	1,234.67	1.77	1.54	1.15
	3	1.24	15	1,249.60	0.68	1.21	0.56
	4	0.91	19	1,253.14	0.33	0.28	1.18
	5	0.72	23	1,267.13	0.19	1.12	0.17
	6	0.60	29	1,268.14	0.12	0.08	1.51
	7	0.51	33	1,269.45	0.08	0.10	0.78

The summary of the results of the number of horizontal projections, *M*, is presented in Table 4.11.

Table 4.11 Number of horizontal projections

H_t (m)	M
40	2
60	3
80	4
100	5
120	6
140	6
160	6
180	6
200	6

Figure 4.25 shows the breakdown of the total cost into cost of equipment and penalty for H_T = 80 m and h* = 30 m. As can be seen, the optimum number of sensors is 7 for this case.

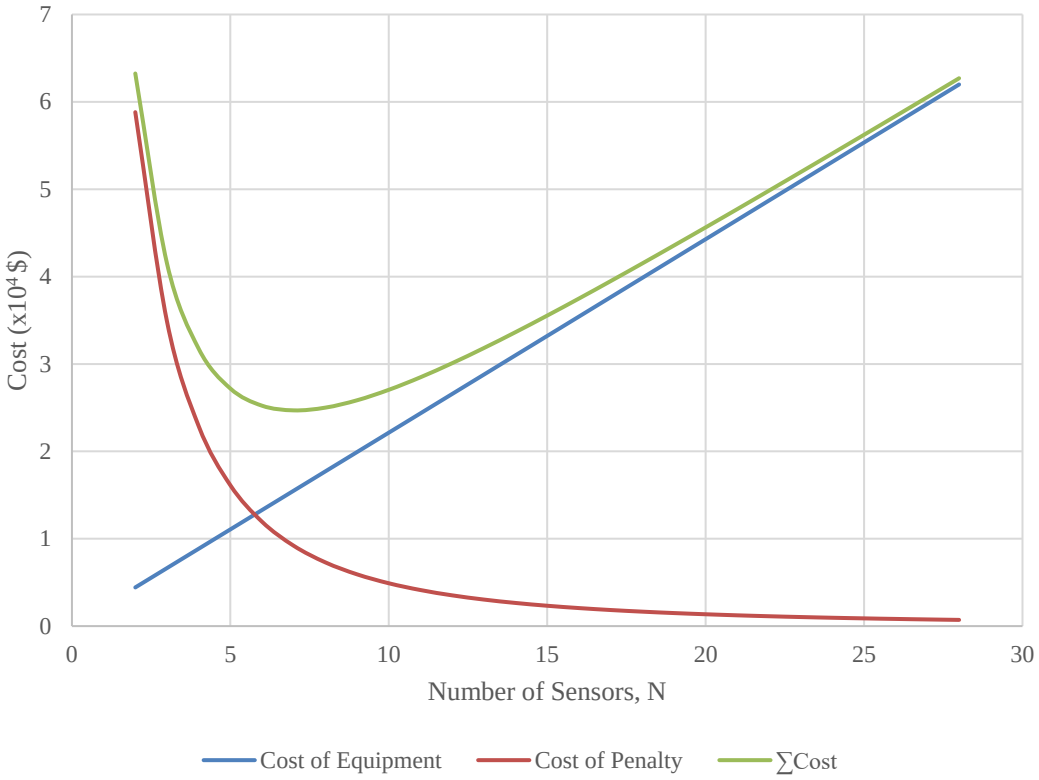

Figure 4.25 Graphical representation of the elements of the total cost

The number of instruments at each horizontal layer are presented in Table 4.12.

Table 4.12 The results of algorithm

H_t (m)	**M**	**h* (m)**	**N**	**N_T**
40	2	19.73	3	6
		33.07	3	
60	3	24.60	4	11
		39.60	4	
		54.60	3	
80	4	28.80	5	16
		44.80	4	
		60.80	4	
		76.80	3	

Table 4.12 (continued)

H_t (m)	M	h* (m)	N	N_T
100	5	32.67	5	21
		49.33	5	
		66.00	4	
		82.67	4	
		99.33	3	
120	6	36.34	6	29
		53.49	6	
		70.63	5	
		87.77	5	
		104.91	4	
		122.06	3	
140	6	42.40	6	29
		62.40	6	
		82.40	5	
		102.40	5	
		122.40	4	
		142.40	3	
160	6	48.46	7	32
		71.31	6	
		94.17	6	
		117.03	5	
		139.89	4	
		162.74	4	
180	6	54.51	7	33
		80.23	6	
		105.94	6	
		131.66	5	
		157.37	5	
		183.09	4	
200	6	60.57	7	35
		89.14	7	
		117.71	6	
		146.29	6	
		174.86	5	
		203.43	4	

The locations of the sensors (not to scale) within the dam body are presented as decision-making information in Table 4.13.

Table 4.13 Decision-making chart

H_t (m)	M	N_T	Definition Sketch
40	2	6	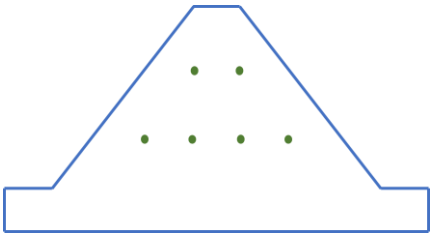
60	3	11	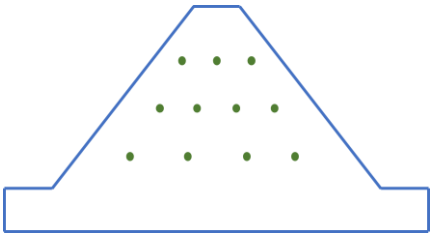
80	4	16	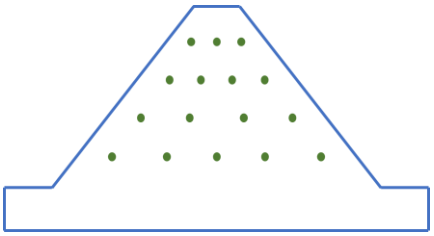
100	5	21	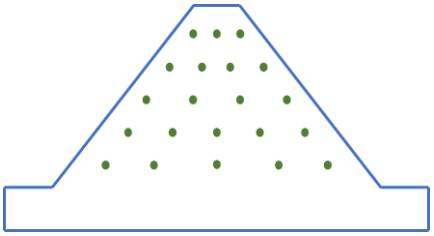
120	6	29	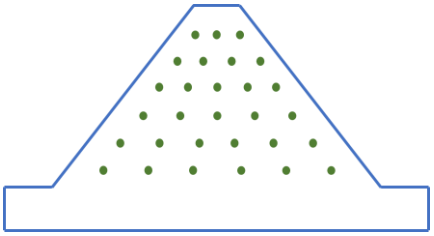

Table 4.13 (continued)

H_t (m)	M	N_T	Definition Sketch
140	6	29	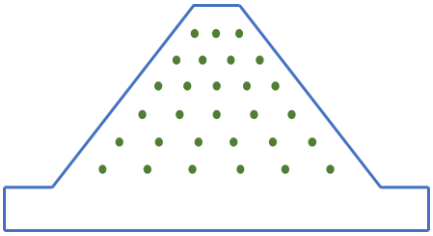
160	6	32	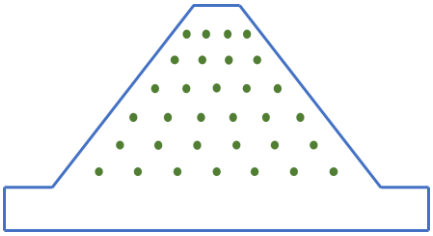
180	6	33	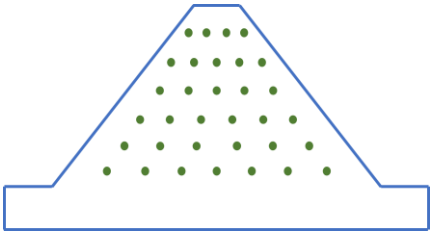
200	6	35	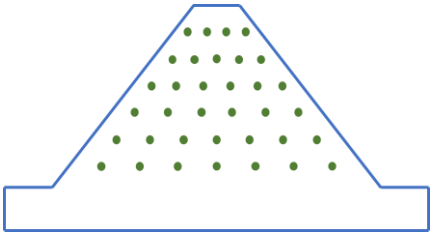

4.7 Evaluation of the Consequences of External Effects

Some external interventions, such as seepage and earthquake loading were also analysed. As mentioned before, the readouts of stress measurement sensors can be used for assessing the possibility of increased leakage. The effects of the seepage and the earthquake loading on the sensor configuration will be analysed in the following sections. Evaluation of the alternative sensor placement is also considered in terms of both accurate modelling of stress distribution and cost.

4.7.1 Effect of Seepage

The design principles of CFRDs dictate that the concrete upstream face is watertight during the lifetime of the dam. Moreover, the dam body consists of homogeneous rockfill without any impervious core. The lack of impervious core and its filters makes CFRDs immune to any seepage through the dam body which might occur from possible cracking of the concrete upstream face.

In order to assess the internal effective stress changes within the dam body in case of any possible leakage through the concrete upstream face, a number of analyses were conducted. The plate element was modified to allow water to seep through from different locations, such as at a location at maximum reservoir level (Figure 4.26-b), half (Figure 4.26-c), and one fourth (Figure 4.26-d) of the dam height and the model was rerun. Results of these analyses were compared with no-seepage case (Figure 4.26-a). Sensor locations are also shown in these figures by white dots.

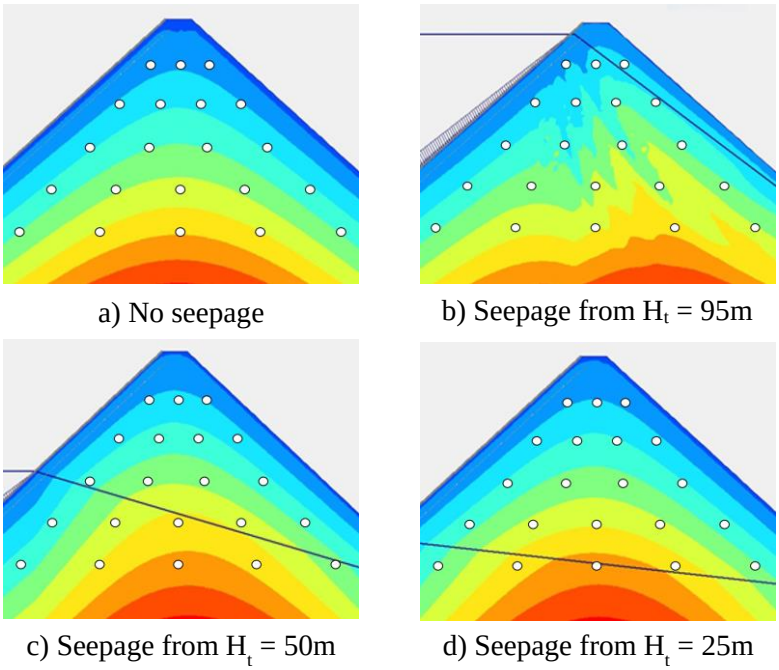

a) No seepage

b) Seepage from H_t = 95m

c) Seepage from H_t = 50m

d) Seepage from H_t = 25m

Figure 4.26. Comparison of the internal stresses of four cases

It is observed that the extreme effective stress values were decreased around 30% for case b, described in Figure 4.26 due to pore water pressures induced as a result of cracking. Because of lower crack elevations for cases c and d, the majority of the dam body was not influenced significantly from seepage. The effective stress values were observed to decrease around zones close to the upstream face of the dam.

As a result of this analysis, it can be said that a possible seepage would not create a safety deficiency within the dam body, whereas there may be some significant economic consequences due to the loss of water. It is also believed that the proposed sensor layout is capable of capturing the effective stress decrease caused from a possible seepage. This decrease is to be considered as a warning remark for possible cracking of the upstream face slab. Remedial actions can then be taken with reference to visual observations at the upstream face block and rate of seepage.

4.7.2 Effect of Earthquake

CFRDs are considered as one of the well-performing dam types during large magnitude earthquakes (ICOLD, 2005) because of the dam fill body being not under the effect of uplift pressure. As a result of this fact, earthquake loading was not taken into account during algorithm building procedures.

For assessing and verifying the assumptions, a dynamic earthquake analysis was conducted to a 100-meter-high cross-section with PLAXIS. A sample data for a strong motion displacement is considered. For this purpose, a strong earthquake occurred in Van, Turkey on 23.10.2011 with a Richter magnitude of 7.2 was analysed. The extreme horizontal displacements of the dam body were compared before and after the earthquake and the residual earthquake displacement after the earthquake was observed to be smaller than 1 cm. This result also proves the resistance ability of the CFRDs against dynamic earthquake loading. In order to trigger the stress/strain measuring sensors and fully assess the real earthquake response of the dam body, it is

advised to use three accelerometers at each dam. Darbre (1995) recommends mounting one accelerometer to the crest of the dam, second one to the foundation of the same cross-section with the first one, and the last one to the close vicinity of the dam body as a free-field accelerometer.

4.8 Effect of Alternative Placement of Sensors

In order to visualize the effect of possible modifications of the height of the horizontal layers, thus the number of the sensors, an arbitrary cross-section was analysed. To this end, 80-meter-high dam was taken into account and several alternative horizontal layers were considered. In the optimal solution, the algorithm output gave 4 horizontal layers with 16 sensors. In the first alternative, only the height of the first horizontal layer was changed. It was shifted to a place 5 m higher than the original height. In the second alternative, all horizontal layers were shifted downwards by 4 m, whereas in the third alternative they were shifted upwards by 4 m.

Table 4.14. Summary of the effect of alternative placement

Case	h* (m)	Average Error (%)	Cost per sensor ($)
Optimal Solution	28.8	2.40	1,073.20
	44.8		
	60.8		
	76.8		
First Alternative	33.8	2.56	1,060.08
	44.8		
	60.8		
	76.8		
Second Alternative	24.8	2.18	1,109.27
	40.8		
	56.8		
	72.8		
Third Alternative	32.8	2.57	1,039.60
	48.8		
	64.8		
	80.8		

It can be observed that these changes either lower the average error or the cost per sensor but not both at the same time. It can, therefore, be said that the optimal solution gave the best combination of lowest percent modelling error and lowest cost per instrument. The summary of the effect of alternative placement of the sensors is presented in Table 4.14.

4.9 Concluding Remarks

In this chapter, an algorithm for optimal design of stress measuring sensors was developed. The logic behind this algorithm is to find out the best combination of the quality of the information gained and the total cost of the configuration.

This algorithm gives the optimum configuration of a monitoring system consists of total pressure cells and settlement cells, because the stress and the strain is related with each other and these two types of instruments are interchangeable during the design of the instrument system according the specific monitoring interests.

Leakage measuring sensors are omitted from the decision support system because in most of the designs, face slabs are considered as completely impermeable. It is expected that total pressure cells can provide information about an abrupt change in the effective stresses which is an indication of a possible leakage problem from the impervious upstream face slab.

In the following chapter, this algorithm was applied to a number of existing CFRDs around the world and the results of the proposed algorithm were compared with those of the existing cases.

CHAPTER 5

APPLICATION OF THE ALGORITHM

5.1 Introductory Remarks

The outcomes of this study were compared with the instrumentation layout of a number of existing dams. The existing layouts and the proposed layouts were compared in a number of terms. Only total pressure cells and settlement cells located in the dam body are taken into account while evaluating the existing configurations. Contact pressure cells, settlement cells and strain meters located in and around close vicinity of concrete face slab are not considered in this study.

5.2 Verification and Discussion

5.2.1 Shuibuya Dam, China

Shuibuya Dam is 233 m-high from foundation and has a base width of 623 m. In the existing configuration, 38 strain measuring sensors (settlement cells) were installed on five horizontal projections along with other types of instruments (Wei et al., 2010). The locations of the aforementioned sensors are shown in Figure 5.1 (dimensions are in meters).

The proposed algorithm was run with the dimensions of Shuibuya Dam and a six-horizontal layer configuration was obtained.

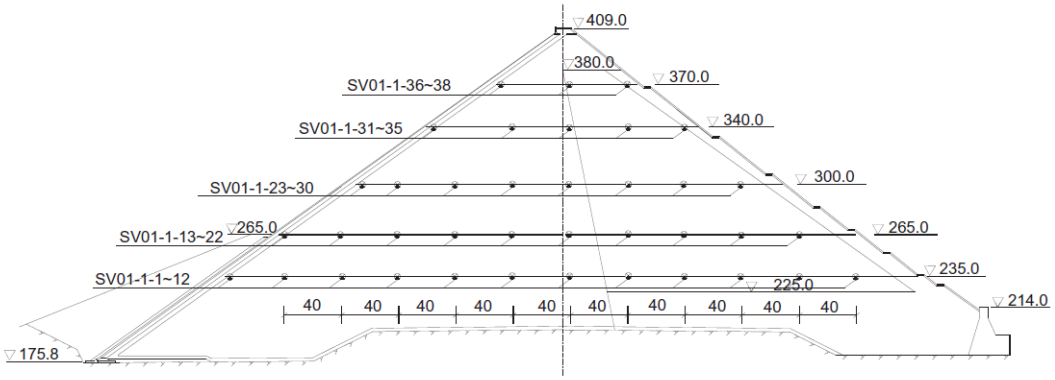

Figure 5.1 Shuibuya Dam settlement cell locations (Wei et al, 2010)

In the existing case, Shuibuya Dam has a total of 38 strain (settlement) measuring sensors on 5 horizontal layers. However, the algorithm recommended that a similar dam cross-section should be equipped with 35 sensors on 6 horizontal projections. Cost of the existing configuration was also evaluated in Table 5.1 with the assumption of switchboxes being provided at the downstream of the dam for each layer and the sensors use their own single-core cables.

Table 5.1 Comparison of existing and proposed configurations of Shuibuya Dam

Existing Configuration			
Layer	**h* (m)**	**N**	**COST ($)**
1	59.2	12	
2	89.2	10	
3	124.2	8	
4	164.2	5	
5	194.2	3	
TOTAL		38	65,062.64

Proposed Configuration			
Layer	**h* (m)**	**N**	**COST ($)**
1	60.8	7	
2	89.5	7	
3	118.2	6	
4	146.9	6	
5	175.6	5	
6	204.3	4	
TOTAL		35	56,977.59

It can be observed that the proposed configuration has not only lower total cost compared to the existing configuration but also provides lower cost per instrument as $1628 compared to the $1712 of existing configuration. The location of the first two horizontal projections are very close to each other for both configurations. However, the advantage of the proposed configuration can be identified when the information gained from sensors with the inclusion of an additional horizontal layer is considered.

5.2.2 Tanyeri Dam, Turkey

Tanyeri Dam is a 100 m-high CFRD from thalweg. It is one of the dams of Fatsa projects and located in the Eastern Black Sea Region of Turkey. The maximum reservoir level is 98 m. Upstream face slope is 1V:1.41H, whereas the downstream slope is 1V:1.4H.

The dam body was designed with a contemporary approach as zoned fill. At the mid-axis, the dam body is equipped with 11 total pressure cells and 11 settlement cells, a total number of 22 stress and strain (settlement) monitoring sensors. Each total pressure cell is installed along with a settlement cell in 3 horizontal levels.

The proposed algorithm was run with the dimensions of Tanyeri Dam and a five-horizontal layer configuration was obtained. The algorithm recommended that a similar dam cross-section should be equipped with 21 sensors on 5 horizontal projections. The comparison and the cost of the existing and proposed configuration is presented in Table 5.2.

Table 5.2 Comparison of existing and proposed configurations of Tanyeri Dam

Existing Configuration			
Layer	**h* (m)**	**N**	**COST ($)**
1	46.0	10	
2	89.2	6	
3	124.2	6	
TOTAL		22	24,492.51

Proposed Configuration			
Layer	**h* (m)**	**N**	**COST ($)**
1	32.7	5	
2	49.3	5	
3	66.0	4	
4	82.7	4	
5	99.3	3	
TOTAL		21	24,472.00

It can be observed that the cost and the number of instruments are nearly identical between the existing and proposed configurations. However, because of having more horizontal layers, it is obvious that the proposed algorithm will provide a better picture of the overall stress behaviour within the dam body.

5.2.3 Zipingpu Dam, China

Zipingpu Dam is a 134 m-high CFRD from thalweg and located 60 km northwest of Chengdu of Sichuan Province (Xu et al., 2012). The height from foundation is 156 m and the ratio between H_f and H_t is 1.16 which is fully compatible with the assumption of this study. The crest width is 12 m and the maximum reservoir level is 127 m. The upstream face slope is 1V:1.4H, whereas the downstream slope is 1V:1.5H.

At the mid-axis, the dam body is equipped with 30 settlement cells, installed in 4 horizontal levels. All settlement cells are also mated with horizontal displacement meters.

The proposed algorithm was run with the dimensions of Zipingpu Dam and a six-horizontal layer configuration was obtained. The algorithm recommended that a similar dam cross-section should be equipped with 29 sensors on 6 horizontal projections. The comparison and the cost of the existing and proposed configuration is presented in Table 5.3.

Table 5.3 Comparison of existing and proposed configurations of Zipingpu Dam

Existing Configuration			
Layer	**h* (m)**	**N**	**COST ($)**
1	32.0	10	
2	68.0	9	
3	92.0	7	
4	122.0	4	
TOTAL		30	45,176.80

Proposed Configuration			
Layer	**h* (m)**	**N**	**COST ($)**
1	40.7	6	
2	59.9	6	
3	79.2	5	
4	98.4	5	
5	117.6	4	
6	136.8	3	
TOTAL		29	38,724.80

It can be observed that the number of instruments are very close in the existing and proposed configurations. However, because of having fewer horizontal layers, the cost of the existing configuration is more than the cost of the proposed configuration. This is an expected result because of the dominance of the cost of the cable.

As a summary, it can be said that the result of the algorithm decreases the cost of the instrumentation system while maintaining the accuracy of the modelling of stress behaviour within the dam body.

5.2.4 Tianshengqiao-I Dam, China

Tianshengqiao-I Dam is a 176 m-high CFRD from foundation and located on the Nanpan river. At the maximum cross-section, the dam body is equipped with 16 settlement cells for vertical strain (settlement) monitoring. Vertical displacement sensors are placed in 4 horizontal levels.

The proposed algorithm was run with the dimensions of Tianshengqiao-I Dam and a six-horizontal layer configuration was obtained. The algorithm recommended that a similar dam cross-section should be equipped with 32 sensors on 6 horizontal projections. The comparison and the cost of the existing and proposed configuration is presented in Table 5.4.

Table 5.4 Comparison of existing and proposed configurations of Tianshengqiao-I Dam

Existing Configuration			
Layer	**h* (m)**	**N**	**COST ($)**
1	50.0	1	
2	77.0	6	
3	110.0	6	
4	143.0	3	
TOTAL		16	23,594.00

Proposed Configuration			
Layer	**h* (m)**	**N**	**COST ($)**
1	46.0	7	
2	67.7	6	
3	89.5	6	
4	111.2	5	
5	132.9	4	
6	154.6	4	
TOTAL		32	45,219.20

The existing configuration of the Tianshengqiao-I Dam comprises considerably less amount of sensors compared to the proposed configuration. A high CFRD, such as Tianshengqiao-I Dam should have been monitored in more detail. However, this result might also be related with the sensor availability and the unit prices of the sensors

during the era when the dam is constructed (between 1992-1998). It can be easily said that the proposed algorithm will provide a much better visualization of the overall stress behaviour within the dam body.

5.2.5 Berg River Dam, South Africa

Berg River Dam is a 67 m-high dam on the Berg River. It was constructed between 2004 and 2009. The existing configuration consists of 12 sensors located on 3 layers. The first layer has 6 sensors, the second one has 4 sensors, and the last one has 2 sensors.

The proposed algorithm was executed with the dimensions of Berg River Dam and a three-horizontal layer configuration was obtained. The algorithm recommended that a similar dam cross-section should be equipped with 11 sensors on 3 horizontal projections. The proposed configuration can be considered as similar to the existing case.

5.2.6 Kürtün Dam, Turkey

Kürtün Dam is a 133 m-high dam from foundation. It is located on the Harşit River. The existing configuration, excluding the contact pressure cells at the face slab, comprises 7 total pressure cells and 12 settlement cells on 4 layers.

The comparison of the existing and proposed configurations is presented in Table 5.5. The proposed algorithm output for a dam with similar dimensions consist of 22 sensors for stress monitoring on 5 horizontal projections. The algorithm recommends 3 more sensors in a symmetrical placement. The cost of existing and proposed configurations are very close to each other.

Table 5.5 Comparison of existing and proposed configurations of Kürtün Dam

Existing Configuration			
Layer	**h* (m)**	**N**	**COST ($)**
1	38.0	7	
2	58.0	7	
3	83.0	4	
4	108.0	1	
TOTAL		19	25,407.28

Proposed Configuration			
Layer	**h* (m)**	**N**	**COST ($)**
1	41.3	6	
2	59.7	5	
3	78.0	4	
4	96.3	4	
5	114.7	3	
TOTAL		22	25,908.08

5.2.7 Nam Ngum 2 Dam, Laos

Nam Ngum 2 Dam is a 181 m-high dam from foundation. The construction was completed on 2011. It is located on the Nam Ngum River. The existing configuration consists of 14 sensors located on 3 layers. The first layer has 3 sensors, second one has 6, and the last one has 5 sensors.

Table 5.6 Comparison of existing and proposed configurations of Nam Ngum 2 Dam

Existing Configuration			
Layer	**h* (m)**	**N**	**COST ($)**
1	7.0	3	
2	59.0	6	
3	119.0	5	
TOTAL		14	20,441.40

Proposed Configuration			
Layer	**h* (m)**	**N**	**COST ($)**
1	37.9	7	
2	61.7	7	
3	85.6	6	
4	109.4	5	
5	133.3	5	
6	157.1	4	
TOTAL		34	53,892.83

The proposed algorithm was executed with the dimensions of Nam Ngum 2 Dam and a six-horizontal layer configuration was obtained. The algorithm recommended that a similar dam cross-section should be equipped with 34 sensors. It can be said that Nam Ngum 2 Dam is under-instrumented comparing with the other CFRDs. The comparison of the existing and proposed configurations is presented in Table 5.6.

5.2.8 Cethana Dam, Australia

Cethana Dam is a 110 m-high dam from foundation. It is located on the Forth River at north-western Tasmania. The construction was completed on 1971. The existing configuration comprises 4 total pressure cells on 2 layers. Comparison of the existing and proposed configurations is presented in Table 5.7.

Table 5.7 Comparison of existing and proposed configurations of Cethana Dam

Existing Configuration			
Layer	**h* (m)**	**N**	**COST ($)**
1	25.0	2	
2	50.0	2	
TOTAL		4	5,216.70

Proposed Configuration			
Layer	**h* (m)**	**N**	**COST ($)**
1	31	5	
2	46.8	5	
3	62.6	4	
4	78.4	4	
5	94.2	3	
TOTAL		21	40,149.66

The proposed algorithm output for a dam with similar dimensions consist of 21 sensors for stress monitoring on 5 horizontal projections. Because of being a relatively old dam, Cethana Dam is under-instrumented when compared to the more recent designs.

5.2.9 Salvajina Dam, Colombia

Salvajina Dam is a 148 m-high dam from foundation. The construction was completed on 1985. It is located on the Cauca River. The existing configuration consists of 25 sensors located on 6 layers.

The proposed algorithm was executed with the dimensions of Salvajina Dam and a six-horizontal layer configuration was obtained. The algorithm recommended that a similar dam cross-section should be equipped with 29 sensors. The number of sensors are close to each other in both configurations. The comparison of the existing and proposed configurations is presented in Table 5.8.

Table 5.8 Comparison of existing and proposed configurations of Salvajina Dam

Existing Configuration			
Layer	**h* (m)**	**N**	**COST ($)**
1	31.0	3	
2	47.0	8	
3	61.0	3	
4	80.0	6	
5	94.0	1	
6	110.0	4	
TOTAL		25	29,591.41

Proposed Configuration			
Layer	**h* (m)**	**N**	**COST ($)**
1	38.29	6	
2	56.57	6	
3	74.86	5	
4	93.14	5	
5	111.43	4	
6	129.71	3	
TOTAL		29	37,968.13

5.2.10 Xingó Dam, Brazil

Xingó Dam is a 150 m-high dam from foundation. It is located on the São Francisco River. The construction was completed on 1994. The existing configuration comprises 12 sensors on 3 layers.

The proposed algorithm was executed with the dimensions of Xingó Dam and a six-horizontal layer configuration was obtained. The algorithm recommended that a similar dam cross-section should be equipped with 33 sensors The comparison of the existing and proposed configurations is presented in Table 5.9. It can be said that Xingó Dam is under-instrumented according to the algorithm results.

Table 5.9 Comparison of existing and proposed configurations of Xingó Dam

Existing Configuration			
Layer	**h* (m)**	**N**	**COST ($)**
1	55	5	
2	85	4	
3	110	3	
TOTAL		12	13,430.40

Proposed Configuration			
Layer	**h* (m)**	**N**	**COST ($)**
1	29.1	7	
2	49.3	6	
3	69.4	6	
4	89.6	5	
5	109.7	5	
6	129.9	4	
TOTAL		33	48,404.83

5.3 Comparison of the Results

The outputs of the algorithm have already been compared with the existing configurations. Results of the comparisons are outlined in Table 5.10 together with the results obtained from Eqns. 3.1 and 3.2.

The total number of sensor outputs of the proposed configuration and the results of the preliminary equation were observed to give close results for the dam heights, H_t, higher than 100 m. However, the preliminary information obtained from Eqns. 3.1 and 3.2 tends to propose fewer sensors for the dam heights, H_t, lower than 100 m.

Table 5.10 Comparison of different configurations

Dam	H_f (m)	M (Eqn. 3.1)	N_T (Eqn. 3.2)	Existing		Proposed		
				M	N_T	M	N_T	e (%)
Shuibuya	233	5	37	5	38	6	35	1.38
Tanyeri	103.5	3	13	3	22	5	21	0.15
Zipingpu	156	4	23	4	30	6	29	0.79
Tianshengqiau-I	176	4	27	4	16	6	32	0.99
Berg River	67	3	6	3	12	3	11	0.24
Kürtün	133	4	18	4	21	5	21	0.68
Nam Ngum 2	181	4	22	3	14	6	34	0.97
Cethana	110	3	11	2	4	5	21	0.27
Salvajina	148	4	17	6	25	6	29	0.70
Xingó	150	4	17	3	12	6	33	0.66

A more realistic comparison could have been made if the errors of both existing and proposed configurations were considered. However, in most of the existing configurations, the sensors are not placed according to the symmetrical arrangement on a particular horizontal layer as proposed in this study. Since the developed algorithm is only capable of assessing the error of the aforementioned placement within a dam cross-section, the errors for the existing configurations were not computed.

CHAPTER 6

CONCLUSIONS

6.1 Conclusions

There is not a widely accepted rule set for placement of the sensors within a dam body. The current applications are generally influenced from the past practices and expert judgments. This gap in the related literature enforced the current study to develop an algorithm for optimal design of a stress/strain monitoring system for a CFRD. With this motivation, an algorithm for optimal design of stress monitoring system of a CFRD was developed. This algorithm can be used as a decision support tool during the design of the configuration of the stress measuring sensors of the instrumentation system.

A number of assumptions were made throughout the course of this study. The dam body is assumed as a homogeneous fill with having symmetrical side slopes of 1V:1.5H and a constant freeboard. The rockfill was modelled with the hardening soil model.

The software PLAXIS was executed for various dam heights, H_t, from 40 m to 200 m with 20 m-increments to obtain effective stress distribution throughout the dam body. The relation between the dam height H_f and H_t was obtained using the geometric characteristics of existing rockfill dams of Turkey.

Study of vertical projection of the effective stress distribution at the mid-axis of the dam body provided a mean for determining the number of horizontal layers to be equipped with sensors within the dam body. Three different approaches were considered in the developmental stage of the algorithm and the third approach was chosen to be employed in the algorithm development process with respect to lowest error involved in the modelling.

Effective stress distribution on any horizontal projection was modelled with a six-degree polynomial (Eqn. 4.22). The numerical terms of the aforementioned polynomial were defined as a nine-degree polynomial of the geometrical features of the CFRD cross-section.

The optimization algorithm was formed by the minimization of the sum of cost of equipment and cost of penalty. Cost of penalty was defined as a measure of how well the pressure distribution is represented by the instrument configuration concerned. The actual stress distribution is of a high degree polynomial. However, the output of an instrumentation system compromise a finite number of sensors connected to each other with straight lines. Cost of penalty was defined as the multiplication of the percent difference between the true vertical effective force and the modelled vertical effective force by the instrumentation system and the cost difference between the system with maximum and minimum allowed number of sensors.

In this algorithm, the cost of the instrumentation system and the error that will result from the modelling of true stress distribution as a piece-wise linear distribution is considered. The outcomes of this could provide a basis for number of sensors and their locations in the design stage of instrumentation system of CFRDs ranging from 40 m to 200 m. The results of the proposed configurations are given in Table 4.13.

Effect of seepage and earthquake loading were evaluated. It was observed that the proposed sensor layout is capable of capturing the effective stress decrease caused from a possible seepage. The extreme horizontal displacements of the dam body induced by earthquake effects were compared before and after the earthquake cases and it was observed that the residual earthquake displacement after the earthquake was smaller than 1 cm. Effect of alternative placement of sensors was also studied and it was concluded that the optimal solution gave the best placement combination having lowest percent modelling error and lowest cost per instrument.

The use of the proposed model was tested by applying it to a number of existing dams. The algorithm generally recommended more horizontal projections for a dam body with similar dimensions. The outputs of the algorithm were also observed to give less cost compared to the existing cases.

It is believed that this algorithm would provide a basis for the future enhancements and the further developments would make it a universally accepted practice which can be employed quickly and easily.

6.2 Recommendations for Future Studies

In a possible future research, the proposed algorithm can be enriched with the inclusion of other types of instruments, such as piezometers for placing in foundation and body fill. Placement of the strain meters and joint meters to the face slab could be a subject of another optimization study. Some parameters were kept constant during the development of this algorithm, such as crest width, upstream and downstream side slopes, freeboard, and material properties. The effect of the variation of these parameters on the algorithm results may also be studied in order to determine whether they have a significant effect on the placement of the sensors or not.

A similar procedure can also be developed for concrete type of dams. Concrete dams are more sensitive to the changes at stress levels because of being slenderer structures compared to the embankment dams. Since concrete is a more homogeneous material than embankment fill material, the assumptions related with the material properties could be eliminated during the development of the algorithm.

REFERENCES

Anthiniac, P., Carrere, A., Develay, D., and Andrzejewski, R. H. (2002). The contribution of numerical analysis to the design of CRFDs. *International Journal on Hydropower & Dams*, *9*(4), 127-132.

Arı, O. (2008). *A Study on Dam Instrumentation Retrofitting: Gökçekaya Dam* (M.Sc. Thesis, Middle East Technical University).

Brinkgreve, R. B. J., and Broere, W. (2008). PLAXIS 2D Manual, Version 9.0. *Delft University of Technology and PLAXIS*.

Brinkgreve, R. B. J., Swolfs, W. M., and Engin, E. (2010). Plaxis 2010 reference manual. *Delft University of Technology and PLAXIS*

Bureau, G. (1997). Evaluation methods and acceptability of seismic deformations in embankment dams. In *Transactıons of the Internatıonal Congress on Large Dams* (Vol. 2, pp. 175-200).

Chau Chin, L. (2004). *A Study on Concrete Faced Rockfill Dams* (B.Sc. Dissertation, University of Southern Queensland).

Chen, S. S., and Han, H. Q. (2009). Impact of the '5.12'Wenchuan earthquake on Zipingpu concrete face rock-fill dam and its analysis. *Geomechanics and Geoengineering: An International Journal*, *4*(4), 299-306.

Cooke, J. B. (1984). Progress in rockfill dams. *Journal of Geotechnical Engineering*, *110*(10), 1381-1414.

Darbre, G. R. (1995). "Strong-Motion Instrumentation of Dams." *Earthquake Engineering and Structural Dynamics, 24*(8). 1101-1111G.R. (1995).

DSİ (General Directorate of State Hydraulic Works). (2012). *Dams of Turkey* [Database]. Retrieved from http://www.dsi.gov.tr/baraj-arama

Duncan, J. M., and Chang, C. Y. (1970). Nonlinear analysis of stress and strain in soils. *Journal of the soil mechanics and foundations division*, *96*(5), 1629-1653.

Ergeneman, I. (2012). Dolgu Barajlar Tasarım İlkeleri Rehberi. In *1. Barajlar Kongresi*. Retrieved from http://www.barajlarkongresi.com/

FERC (Federal Energy Regulatory Commission) (1999). *Engineering Guidelines for the Evaluation of Hydropower Projects*, FERC, Washington DC.

Geokon. (2016-a). *Model 4800 Standard Pressure Cell* [digital image]. Retrieved from http://www.geokon.com/4800

Geokon. (2016-b). *Model 4810 Contact Pressure Cell* [digital image]. Retrieved from http://www.geokon.com/4810

Geosense. (2013). *VWS-2100 Embedment Strain Gauge* [digital image]. Retrieved from http://www.geosense.co.uk/products/details/vws-2100-embedment-strain-gauge

Giesecke J., Rommel M., and Soyeaux R. (1991). Seepage flow under dams with jointed rock foundation. In *Proceedings, 17th Congress on Large Dams.*

Hacelas, J. E., Ramirez, C. A., and Regalado, G. (1985). Construction and performance of Salvajina Dam. In *Concrete Face Rockfill Dams—Design, Construction, and Performance* (pp. 286-315). ASCE.

ICOLD (International Commission on Large Dams). (1989). "Rockfill Dams with Concrete Facing-State of Art", *ICOLD Bulletin 70.*

ICOLD (International Commission on Large Dams). (1994) "Use of Granular Filters and Drains in Embankment Dams", *ICOLD Bulletin 95*

ICOLD (International Commission on Large Dams). (2005). "Concrete Face Rockfill Dams-Concepts for Design and Construction." *International Commission on Large Dams, Committee on Materials for Fill Dams (Draft).*

IIC (IIC-GrupoEP). (2007). *Unit Price List for Material Supply*. Retrieved from http://www.iic-grupoep.com/

itmsoil. (2013). *V-Notch Weir User's Manual.* Retrieved from http://www.itmsoil.com.au/images/instruments/pdf/Man152_V-Notch_Weir.pdf

Jiang, G., and Zhao, Z. (2000). High concrete face rock-fill dams in China. In *Proceedings, International Symposium on Concrete Faced Rockfill Dams*.

Korkmaz, S. (2009). *Evaluation of Concrete Face Rockfill Alternative for Dam Type Selection: A Case Study On Gökçeler Dam* (M.Sc. Thesis, Middle East Technical University).

Kulhawy, F. H., and Duncan, J. M. (1972). Stresses and movements in Oroville dam. *Journal of Soil Mechanics and Foundations Div*, *98*(sm7).

Makdisi, F. I., and Seed, H. B. (1977). Simplified procedure for estimating dam and embankment earthquake-induced deformations. In *ASAE Publication No. 4-77. Proceedings of the National Symposium on Soil Erosion and Sediment by Water, Chicago, Illinois, December 12-13, 1977.*

Marulanda, A., and Pinto, N. D. S. (2000). Recent experience on design, construction, and performance of CFRD dams. *Barry Cooke, Volume "Concrete Face Rockfill Dams", Beijing*, 279-299.

Materon, B., (2013, January). Sharing international experiences in CFRDs. *International Water Power & Dam Construction.*

Moll, S., and Straubhaar, R. (2011). Dams and Reservoirs under Changing Challenges. In *Proceedings of the International Symposium on Dams and Reservoirs Under Changing Challenges* (pp. 65-72).

Mori, R. T. (1999). Deformation and cracks in concrete face rockfill dams. In *Proc. 2nd Symp. on CFRD, Florianopolis, Brazil* (pp. 49-61).

Özkuzukıran, R. S. (2005). *Settlement Behaviour of Concrete Faced Rockfill Dams: A Case Study* (M.Sc. Thesis, Middle East Technical University).

Özkuzukıran, S., Özkan, M. Y., Özyazıcıoğlu, M., and Yıldız, G. S. (2006). Settlement behaviour of a concrete faced rock-fill dam. *Geotechnical & Geological Engineering*, *24*(6), 1665-1678.

Pinto, N. D. S., and Marques Filho, P. L. (1998). Estimating the Maximum Face Deflection in CFRDs. *International Journal on Hydropower and Dams*, *5*, 28-32.

Pinto, N. D. S. and Mori, R. T. (1988). A New Concept of a Perimetric Joint for Concrete Face Rockfill Dams. In *Proceedings of the 16th Congress of the International Commission on Large Dams* (pp. 35-51).

Pinto, N. D. S. (2001). Questions to ponder on designing very high CFRDs. *International Journal on Hydropower & Dams*, *8*(5), 61-65.

Roctest. (2016-a). *GEO-LOK Inclinometer Casing*. Retrieved from http://www.roctest.com/en/content/download/1081/35492/file/E50280-160131 - GEO-LOK__.pdf

Roctest. (2016-b). *PROFIL Digital Inclinometer*. Retrieved from http://www.roctest.com/en/content/download/1198/35923/file/E50359-160131 - PROFIL__.pdf

RST Instruments. (2015). *Vibrating Wire Strain Gauge* [digital image]. Retrieved from http://www.rstinstruments.com/Remote/Vibrating-Wire-Strain-Gauge-3.jpg

Sherard, J. L., and Cooke, J. B. (1987). Concrete-face rockfill dam: I. assessment. *Journal of geotechnical engineering*, *113*(10), 1096-1112.

Sisgeo. (2016). *Electrical and Vibrating Wire Crackmeters*. Retrieved from http://www.sisgeo.com/uploads/schede/schede/D313_EN_11_electrical_and_vibrating_wire_crackmeter.pdf

Slope Indicator. (2013). *VW Arc-Weldable Strain Gauge.* Retrieved from http://www.slopeindicator.com/pdf/vw-arc-weldable-strain-gauge-datasheet.pdf

Soil Instruments. (2014). *Vibrating Wire / Water Settlement Cell.* Retrieved from http://www.itmsoilsupport.com/manuals/Man140_Vibrating_Wire_Water_Settlement_Cell.pdf

Souza, R. J. B., Cavalcanti, A. J. C. T., Silva, S. A., and Silveira, J. F. (1999). Xingo concrete face rockfill dam behaviour of the dam on the left abutment. In *Proceedings of the Second Symposium on Concrete Face Rockfill Dams* (pp. 143-157).

Souza, R. J. B., de Vasconcelos, A. A., and Cavalcanti, A. J. C. (2009). Displacements of the Xingó Concrete Face Rockfill Dam-Brazil. In *Modern Rockfill Dams-2009--Proceedings of the 1~(st) International Symposium on Rockfill Dams*.

Straubaar, R., van Gunsteren, E., and Moll, S. (2009). Design Considerations of a High Rockfill Dam Nam Ngum 2 CFRD, Lao PDR. In *1st International Symposium on Rockfill Dams, Chengdu, China*.

Stucky Teknik. (2012). *Fatsa HEPPs Project Tender Design Drawings Tanyeri Dam: Dam Body Monitoring Devices* (Drawing No FATSA.STKY.TNY.DAM.24) [Technical drawing]

Szostak-Chrzanowski, A., and Massiéra, M. (2006). Relation between monitoring and design aspects of large earth dams. In *Proceedings, 3rd IAG Symposium on Geodesy for Geotechnical and Structural Engineering and 12th FIG Symposium on Deformation Measurements. Baden, Austria*.

Telemac. (2016). *PW Series Vibrating Wire Piezometer*. Retrieved from http://www.telemac.fr/en/content/download/1112/37703/file/E50100D-160208 - PWS_.pdf

Thamae, M. (2007). *Importance of Instrumentation in Concrete Faced Rockfill Dams*. Presentation, South Africa.

Thomas, H. S. H., and Ward, W. H. (1969). The design, construction and performance of a vibrating-wire earth pressure cell. *Geotechnique, 19*(1), 39-51.

Wei, Z., Xiaolin, C., Chuangbing, Z., and Xinghong, L. (2010). "Creep analysis of high concrete-faced rockfill dam." *International Journal for Numerical Methods in Biomedical Engineering, 26*(11), 1477-1492.

Wu, G. Y., Freitas, M. S. Jr., Araya, J. A. M., and Huang, Z. Y. (2000). Planning and Construction of Tianshengqiao 1 CFRD (China). In *Proceedings, International Symposium on Concrete Faced Rockfill Dams*.

Xu, B., Zou, D., and Liu, H. (2012). Three-dimensional simulation of the construction process of the Zipingpu concrete face rockfill dam based on a generalized plasticity model. *Computers and Geotechnics, 43*, 143-154.

Yanmaz, A.M. and Arı, O. (2008). *An Overview of the Role of Retrofitted Instruments in Dam Safety*, Famagusta: 8th International Congress on Advances in Civil Engineering.

Yanmaz, A. M., and Arı, O. (2011). A study on dam instrumentation retrofitting. *KSCE Journal of Civil Engineering, 15*(2), 317-325.

Zhang, B., Wang, J. G., and Shi, R. (2004). Time-dependent deformation in high concrete-faced rockfill dam and separation between concrete face slab and cushion layer. *Computers and Geotechnics, 31*(7), 559-573.

APPENDIX A

In Table A.1 the complete price list of all instruments mentioned in this study are given in U.S. Dollars (USD, $) with reference to IIC (2007).

Table A.1 Unit prices of instruments

Equipment Type	Unit price per item ($)
VW Pressure Cell	670.00
VW Piezometer	455.00
V-Notch Weir and Automatic VW Readout Unit	2440.00
Automatic VW Weir Readout Unit	2,177.00
Parshall Flume and Automatic VW Readout Unit	2,672.00
Surface Mount VW Joint meter	625.00
Accelerometer	12,795.00
Common Triggering Unit and Data Recorder for Accelerometers	27,047.00
Surface Mount Clinometer (Tiltmeter)	1,020.00
Instrument Cable	5.60 per meter
Cable Carrier Tray	30.00 per meter
Multiplexer	5,031.00
Data Logger	17,173.00
Software	18,533.00
Handheld Data Readout	6,398.00

APPENDIX B

Table B.1 H_f and H_t values of the rockfill dams in Turkey (DSİ, 2012)

Name of the Dam	**H_f (m)**	**H_t (m)**
Hirfanlı	83.0	78.0
Sille	40.0	39.0
Mamasin	48.4	44.9
Altınapa	31.5	30.5
Devegeçidi	34.8	32.8
Hasanlar	72.8	70.8
Keban	207.0	163.0
Balçova	73.4	63.4
Hasan Uğurlu	175.0	135.0
Bozkır	52.1	47.1
Suat Uğurlu	51.0	38.0
Doğancı	82.0	64.0
Alaca	57.0	44.3
Belpınar	61.2	58.2
Çamlıdere	106.2	101.7
Germeçtepe	49.0	41.5
Kalecik	80.0	77.0
Kozlu	61.3	60.2
Gödet	93.0	64.0
Kestel	65.0	62.5
Altınkaya	195.0	140.0
Geyik	41.0	39.0
Gökçe	61.0	50.0
Hacıhıdır	38.6	32.0
Kılıçkaya	134.0	103.0
Menzelet	156.5	136.5
Adıgüzel	145.0	144.0
Derbent	33.0	29.0
Atatürk	169.0	166.0
Murtaza	41.0	38.0

Table B.1 (continued)

Name of the Dam	**H_f (m)**	**H_t (m)**
Beyler	40.0	31.0
Çatak	35.0	33.0
Kızılcapınar	60.3	54.3
Kuzgun	120.0	114.0
Tahtalı	57.5	54.5
Sazlıdere	47.0	23.0
Madra	106.0	86.0
Armağan	60.5	57.5
Özlüce	144.0	124.0
Yayladağ	47.4	44.4
Sıddıklı	53.0	50.2
Bakacak	60.0	48.0
Sorgun	45.0	33.5
Birecik (1)	63.5	53.5
Kızıldamlar	46.7	40.0
Kürtün	133.0	110.0
Bahçelik	63.5	53.0

APPENDIX C

Table C.1 Horizontal effective stresses of 40-m-high cross-section

x (m)	y (m)	σ'_h (kN/m^2)
98.00	46.40	-2.88
98.00	44.63	-28.14
98.00	44.63	-28.27
98.00	41.93	-65.38
98.00	41.93	-65.37
98.00	39.18	-101.38
98.00	39.18	-101.39
98.00	37.09	-127.91
98.00	37.09	-127.92
98.00	33.54	-172.11
98.00	33.54	-172.10
98.00	32.24	-188.05
98.00	32.24	-188.05
98.00	30.53	-209.40
98.00	30.53	-209.39
98.00	28.29	-237.14
98.00	28.29	-237.15
98.00	26.66	-257.91
98.00	26.66	-257.88
98.00	25.38	-274.24
98.00	25.38	-274.28
98.00	23.17	-303.14
98.00	23.17	-303.14
98.00	21.92	-319.81
98.00	21.92	-319.79
98.00	19.18	-357.74
98.00	19.18	-357.76
98.00	17.35	-383.85
98.00	17.35	-383.89
98.00	16.53	-395.77

Table C.1 (continued)

x (m)	y (m)	σ'_h (kN/m^2)
98.00	16.53	-395.72
98.00	13.75	-437.83
98.00	13.75	-437.89
98.00	11.59	-471.66
98.00	11.59	-471.69
98.00	10.68	-486.44
98.00	10.68	-486.46
98.00	7.75	-535.20
98.00	7.75	-535.19
98.00	4.33	-595.55
98.00	4.33	-595.62
98.00	3.57	-609.48
98.00	3.57	-609.51
98.00	2.87	-622.62
98.00	2.87	-622.57
98.00	0.00	-676.83

Table C.2 Horizontal effective stresses of 60-m-high cross-section

x (m)	y (m)	σ'_h (kN/m^2)
129.90	69.60	-12.10
129.90	63.95	-80.77
129.90	63.95	-79.74
129.90	63.06	-90.52
129.90	63.06	-91.82
129.90	62.41	-99.84
129.90	62.41	-99.94
129.90	60.18	-127.25
129.90	60.18	-127.21
129.90	54.74	-192.68
129.90	54.74	-192.65
129.90	52.32	-221.42
129.90	52.32	-221.36
129.90	49.84	-250.59
129.90	49.84	-250.65

Table C.2 (continued)

x (m)	y (m)	σ'_h (kN/m^2)
129.90	46.52	-289.79
129.90	46.52	-289.77
129.90	44.81	-310.23
129.90	44.81	-310.29
129.90	41.96	-344.23
129.90	41.96	-344.25
129.90	37.50	-399.03
129.90	37.50	-399.12
129.90	36.79	-408.10
129.90	36.79	-408.07
129.90	32.29	-465.55
129.90	32.29	-465.53
129.90	27.93	-524.55
129.90	27.93	-524.44
129.90	25.63	-556.63
129.90	25.63	-556.72
129.90	21.18	-621.23
129.90	21.18	-621.21
129.90	18.29	-665.28
129.90	18.29	-665.26
129.90	15.76	-705.07
129.90	15.76	-705.06
129.90	11.72	-771.61
129.90	11.72	-771.66
129.90	10.91	-785.30
129.90	10.91	-785.28
129.90	9.94	-801.94
129.90	9.94	-802.00
129.90	4.93	-890.36
129.90	4.93	-890.38
129.90	1.71	-950.53
129.90	1.71	-950.45
129.90	0.00	-983.04

Table C.3 Horizontal effective stresses of 80-m-high cross-section

x (m)	y (m)	σ'_h (kN/m^2)
162.24	92.80	-17.04
162.24	88.45	-67.12
162.24	88.45	-67.55
162.24	86.13	-93.51
162.24	86.13	-92.00
162.24	84.32	-113.45
162.24	84.32	-113.41
162.24	78.94	-176.10
162.24	78.94	-176.13
162.24	71.68	-260.91
162.24	71.68	-260.97
162.24	71.05	-268.29
162.24	71.05	-268.29
162.24	70.58	-273.70
162.24	70.58	-273.56
162.24	63.13	-359.68
162.24	63.13	-359.79
162.24	62.43	-367.92
162.24	62.43	-367.89
162.24	56.23	-441.01
162.24	56.23	-440.97
162.24	53.25	-477.04
162.24	53.25	-477.11
162.24	49.03	-528.78
162.24	49.03	-528.77
162.24	45.58	-572.76
162.24	45.58	-572.73
162.24	41.03	-632.33
162.24	41.03	-632.43
162.24	36.45	-695.17
162.24	36.45	-695.08
162.24	31.89	-760.38
162.24	31.89	-760.43
162.24	28.77	-806.26
162.24	28.77	-806.25
162.24	25.83	-851.28

Table C.3 (continued)

x (m)	y (m)	σ'_h (kN/m^2)
162.24	25.83	-851.31
162.24	19.74	-947.98
162.24	19.74	-947.96
162.24	13.69	-1050.30
162.24	13.69	-1050.42
162.24	9.00	-1133.02
162.24	9.00	-1133.07
162.24	4.16	-1223.09
162.24	4.16	-1222.91
162.24	0.00	-1302.50

Table C.4 Horizontal effective stresses of 100-m-high cross-section

x (m)	y (m)	σ'_h (kN/m^2)
195.31	116.00	-14.31
195.30	109.26	-89.62
195.30	109.26	-95.60
195.30	108.94	-102.04
195.30	108.94	-97.24
195.30	108.75	-99.24
195.30	108.75	-98.50
195.29	101.34	-182.65
195.29	101.34	-182.60
195.28	96.43	-239.06
195.28	96.43	-239.08
195.28	93.34	-274.00
195.28	93.34	-274.06
195.27	88.26	-331.81
195.27	88.26	-331.67
195.27	86.27	-354.20
195.27	86.27	-354.24
195.27	85.49	-363.09
195.27	85.49	-363.09
195.26	79.22	-434.71
195.26	79.22	-434.71

Table C.4 (continued)

x (m)	y (m)	σ'_h (kN/m^2)
195.26	77.76	-451.58
195.26	77.76	-451.59
195.25	71.72	-522.10
195.25	71.72	-522.14
195.25	69.90	-543.57
195.25	69.90	-543.58
195.24	66.33	-586.50
195.24	66.33	-586.49
195.24	62.84	-628.89
195.24	62.84	-628.92
195.23	56.07	-714.01
195.23	56.07	-714.11
195.23	55.46	-721.82
195.23	55.46	-721.76
195.23	53.07	-753.18
195.23	53.07	-753.23
195.22	46.40	-842.86
195.22	46.40	-842.96
195.22	45.08	-861.28
195.22	45.08	-861.21
195.21	41.73	-908.92
195.21	41.73	-908.95
195.20	34.83	-1010.00
195.20	34.83	-1010.06
195.20	31.87	-1055.41
195.20	31.87	-1055.42
195.19	24.78	-1168.28
195.19	24.78	-1168.28
195.18	21.81	-1217.44
195.18	21.81	-1217.47
195.17	14.13	-1350.01
195.17	14.13	-1350.13
195.17	13.47	-1361.82
195.17	13.47	-1361.78
195.17	9.29	-1437.60
195.17	9.29	-1437.58

Table C.4 (continued)

x (m)	y (m)	σ'_h (kN/m^2)
195.16	5.63	-1505.31
195.16	5.63	-1505.43
195.16	5.11	-1515.27
195.16	5.11	-1515.23
195.16	0.00	-1613.15

Table C.5 Horizontal effective stresses of 120-m-high cross-section

x (m)	y (m)	σ'_h (kN/m^2)
227.88	139.20	-13.21
227.95	134.83	-87.47
227.95	134.83	-85.78
228.06	127.79	-148.62
228.06	127.79	-146.82
228.13	123.10	-198.20
228.13	123.10	-198.35
228.23	116.11	-274.23
228.23	116.11	-274.34
228.31	110.75	-332.66
228.31	110.75	-332.48
228.43	102.79	-421.14
228.43	102.79	-421.20
228.46	100.88	-442.51
228.46	100.88	-442.52
228.52	96.83	-488.00
228.52	96.83	-487.96
228.58	92.71	-534.56
228.58	92.71	-534.57
228.63	89.74	-568.54
228.63	89.74	-568.50
228.69	85.84	-613.27
228.69	85.84	-613.29
228.74	82.51	-652.21
228.74	82.51	-652.36
228.83	76.57	-722.32

Table C.5 (continued)

x (m)	y (m)	σ'_h (kN/m^2)
228.83	76.57	-722.37
228.87	73.80	-755.65
228.87	73.80	-755.66
228.92	70.03	-802.02
228.92	70.03	-801.92
229.02	63.64	-882.61
229.02	63.64	-882.70
229.10	58.46	-951.99
229.10	58.46	-952.01
229.15	55.37	-993.93
229.15	55.37	-993.95
229.18	52.88	-1028.66
229.18	52.88	-1028.71
229.29	46.00	-1127.09
229.29	46.00	-1127.09
229.37	40.68	-1206.55
229.37	40.68	-1206.54
229.39	38.98	-1232.27
229.39	38.98	-1232.25
229.45	34.91	-1295.71
229.45	34.91	-1295.76
229.53	29.90	-1375.58
229.53	29.90	-1375.67
229.55	28.64	-1396.21
229.55	28.64	-1396.17
229.61	24.46	-1465.77
229.61	24.46	-1465.79
229.70	18.55	-1566.76
229.70	18.55	-1566.86
229.73	16.38	-1605.09
229.73	16.38	-1605.12
229.83	9.64	-1726.59
229.83	9.64	-1726.61
229.91	4.39	-1824.91
229.91	4.39	-1824.94
229.98	0.00	-1909.13

Table C.6 Horizontal effective stresses of 140-m-high cross-section

x (m)	y (m)	σ'_h (kN/m^2)
259.79	162.40	-14.42
259.80	157.83	-99.28
259.80	157.83	-95.09
259.85	147.27	-188.46
259.85	147.27	-187.77
259.86	144.39	-219.15
259.86	144.39	-218.89
259.87	140.47	-261.34
259.87	140.47	-261.58
259.90	133.45	-337.89
259.90	133.45	-337.81
259.92	128.56	-391.29
259.92	128.56	-391.19
259.94	123.71	-443.88
259.94	123.71	-444.03
259.96	118.09	-505.08
259.96	118.09	-505.07
259.99	109.99	-595.40
259.99	109.99	-595.44
260.00	109.22	-604.16
260.00	109.22	-604.10
260.01	105.71	-643.75
260.01	105.71	-643.88
260.03	100.77	-700.36
260.03	100.77	-700.34
260.03	99.49	-715.21
260.03	99.49	-715.26
260.07	91.40	-810.00
260.07	91.40	-809.97
260.10	84.06	-899.54
260.10	84.06	-899.54
260.12	78.47	-969.01
260.12	78.47	-969.00
260.13	75.04	-1013.23
260.13	75.04	-1013.09
260.17	64.36	-1155.65

Table C.6 (continued)

x (m)	y (m)	σ'_h (kN/m^2)
260.17	64.36	-1155.76
260.18	62.35	-1183.42
260.18	62.35	-1183.44
260.23	51.22	-1342.71
260.23	51.22	-1342.78
260.23	50.26	-1356.98
260.23	50.26	-1357.12
260.23	50.03	-1360.45
260.23	50.03	-1360.15
260.27	40.06	-1512.59
260.27	40.06	-1512.63
260.31	31.31	-1653.92
260.31	31.31	-1654.14
260.31	31.22	-1655.67
260.31	31.22	-1655.67
260.31	31.14	-1656.91
260.31	31.14	-1656.65
260.34	22.24	-1807.75
260.34	22.24	-1807.77
260.36	17.20	-1896.69
260.36	17.20	-1896.67
260.38	11.63	-1997.47
260.38	11.63	-1997.50
260.42	3.26	-2154.43
260.42	3.26	-2154.44
260.43	0.00	-2217.14

Table C.7 Horizontal effective stresses of 160-m-high cross-section

x (m)	y (m)	σ'_h (kN/m^2)
291.50	185.60	-23.71
291.52	174.65	-140.69
291.52	174.65	-143.40
291.52	171.72	-174.20
291.52	171.72	-172.20

Table C.7 (continued)

x (m)	y (m)	σ'_h (kN/m^2)
291.53	169.22	-198.32
291.53	169.22	-198.75
291.54	158.44	-315.85
291.54	158.44	-315.88
291.55	149.90	-410.40
291.55	149.90	-410.22
291.56	143.68	-478.78
291.56	143.68	-478.86
291.57	137.03	-552.47
291.57	137.03	-552.40
291.58	128.72	-645.66
291.58	128.72	-645.67
291.58	127.57	-658.54
291.58	127.57	-658.63
291.58	126.56	-670.14
291.58	126.56	-670.10
291.60	116.83	-780.35
291.60	116.83	-780.35
291.61	106.24	-904.75
291.61	106.24	-904.68
291.62	102.72	-946.53
291.62	102.72	-946.60
291.62	99.05	-991.02
291.62	99.05	-991.09
291.63	88.77	-1117.78
291.63	88.77	-1117.79
291.64	80.92	-1219.78
291.64	80.92	-1219.71
291.65	78.23	-1255.39
291.65	78.23	-1255.51
291.66	70.68	-1357.84
291.66	70.68	-1357.78
291.66	66.84	-1411.60
291.66	66.84	-1411.71
291.67	61.03	-1494.30
291.67	61.03	-1494.31

Table C.7 (continued)

x (m)	y (m)	σ'_h (kN/m^2)
291.68	56.88	-1555.16
291.68	56.88	-1555.15
291.69	47.29	-1700.81
291.69	47.29	-1700.82
291.69	43.91	-1753.76
291.69	43.91	-1753.80
291.71	32.76	-1935.16
291.71	32.76	-1935.39
291.71	32.26	-1943.63
291.71	32.26	-1943.53
291.71	30.77	-1968.87
291.71	30.77	-1968.86
291.72	21.13	-2135.14
291.72	21.13	-2135.15
291.73	17.39	-2202.30
291.73	17.39	-2202.40
291.74	10.50	-2327.95
291.74	10.50	-2327.95
291.75	3.74	-2455.47
291.75	3.74	-2455.44
291.75	0.00	-2527.29

Table C.8 Horizontal effective stresses of 180-m-high cross-section

x (m)	y (m)	σ'_h (kN/m^2)
325.27	208.80	-12.20
325.26	202.91	-119.37
325.26	202.91	-120.35
325.25	199.11	-136.31
325.25	199.11	-138.50
325.22	190.48	-218.05
325.22	190.48	-218.90
325.22	190.23	-221.62
325.22	190.23	-221.63
325.20	179.78	-333.18

Table C.8 (continued)

x (m)	y (m)	σ'_h (kN/m^2)
325.20	179.78	-333.05
325.18	173.92	-397.79
325.18	173.92	-397.64
325.16	164.01	-507.13
325.16	164.01	-506.99
325.15	161.84	-530.89
325.15	161.84	-530.90
325.13	154.41	-612.69
325.13	154.41	-612.67
325.11	145.44	-712.90
325.11	145.44	-712.92
325.10	143.20	-738.02
325.10	143.20	-738.21
325.10	142.08	-750.80
325.10	142.08	-750.70
325.08	134.15	-840.92
325.08	134.15	-840.85
325.06	128.77	-902.74
325.06	128.77	-902.90
325.06	127.87	-913.31
325.06	127.87	-913.24
325.03	116.29	-1049.24
325.03	116.29	-1049.21
325.02	111.25	-1110.01
325.02	111.25	-1110.00
325.00	104.23	-1195.91
325.00	104.23	-1195.95
324.97	94.54	-1318.90
324.97	94.54	-1318.99
324.97	92.84	-1341.13
324.97	92.84	-1341.22
324.97	91.84	-1354.33
324.97	91.84	-1354.21
324.93	78.39	-1535.49
324.93	78.39	-1535.51
324.92	75.14	-1581.03

Table C.8 (continued)

x (m)	y (m)	σ'_h (kN/m^2)
324.92	75.14	-1581.11
324.90	66.07	-1711.05
324.90	66.07	-1711.02
324.87	55.40	-1871.52
324.87	55.40	-1871.56
324.86	52.11	-1922.30
324.86	52.11	-1922.37
324.86	48.91	-1973.00
324.86	48.91	-1972.99
324.83	37.56	-2156.92
324.83	37.56	-2156.94
324.80	28.11	-2318.18
324.80	28.11	-2318.17
324.79	25.36	-2366.07
324.79	25.36	-2366.14
324.79	22.22	-2421.93
324.79	22.22	-2421.98
324.76	13.74	-2575.13
324.76	13.74	-2575.20
324.74	3.32	-2771.28
324.74	3.32	-2771.28
324.73	0.00	-2835.09

Table C.9 Horizontal effective stresses of 200-m-high cross-section

x (m)	y (m)	σ'_h (kN/m^2)
357.50	232.00	-17.10
357.53	222.43	-143.70
357.53	222.43	-149.82
357.54	218.26	-173.93
357.54	218.26	-174.53
357.56	208.05	-278.30
357.56	208.05	-278.82
357.58	200.90	-353.13
357.58	200.90	-354.97

Table C.9 (continued)

x (m)	y (m)	σ'_h (kN/m^2)
357.59	198.87	-377.57
357.59	198.87	-376.67
357.63	182.97	-550.52
357.63	182.97	-550.25
357.63	181.66	-564.71
357.63	181.66	-564.89
357.63	181.38	-567.90
357.63	181.38	-567.57
357.67	166.87	-726.11
357.67	166.87	-726.15
357.69	158.03	-825.50
357.69	158.03	-825.23
357.72	148.72	-931.11
357.72	148.72	-931.09
357.73	143.28	-993.23
357.73	143.28	-993.28
357.76	134.63	-1094.47
357.76	134.63	-1094.39
357.77	130.15	-1147.26
357.77	130.15	-1147.31
357.81	113.29	-1352.42
357.81	113.29	-1352.52
357.82	111.99	-1368.66
357.82	111.99	-1369.34
357.82	111.83	-1371.29
357.82	111.83	-1371.21
357.82	111.66	-1373.36
357.82	111.66	-1372.74
357.88	89.42	-1664.92
357.88	89.42	-1665.14
357.88	86.75	-1701.96
357.88	86.75	-1701.83
357.94	66.53	-1993.44
357.94	66.53	-1993.87
357.94	66.28	-1997.68
357.94	66.28	-1998.26

Table C.9 (continued)

x (m)	y (m)	σ'_h (kN/m^2)
357.94	66.24	-1998.77
357.94	66.24	-1997.83
357.94	65.91	-2002.89
357.94	65.91	-2002.83
357.97	54.00	-2187.42
358.00	42.09	-2379.63
358.00	42.09	-2380.10
358.01	39.89	-2416.76
358.01	39.89	-2416.53
358.02	35.56	-2490.27
358.02	35.56	-2490.59
358.07	16.33	-2828.62
358.07	16.33	-2828.82
358.10	3.86	-3063.55
358.10	3.86	-3063.13
358.11	0.00	-3137.17

APPENDIX D

Table D.1 Vertical effective stresses of arbitrary cross-sections 1 to 4 (h*) of 60-m-high cross-section

h* = 14.965 m		**h* = 21.023 m**		**h* = 32.023 m**		**h* = 38.022 m**	
x (m)	σ'_v **(kN/m^2)**	**x (m)**	σ'_v **(kN/m^2)**	**x (m)**	σ'_v **(kN/m^2)**	**x (m)**	σ'_v **(kN/m^2)**
40.548	-5.042	49.634	-7.187	66.134	-11.151	75.133	-8.613
41.281	-25.361	51.983	-55.988	66.664	-20.972	75.141	-8.769
41.281	-24.202	51.983	-55.701	66.664	-21.327	75.141	-8.737
43.635	-69.956	55.130	-102.725	71.207	-88.859	77.522	-48.958
43.635	-69.301	55.130	-102.193	71.207	-88.735	77.522	-48.908
46.326	-114.383	56.702	-123.388	71.723	-94.859	81.311	-96.450
46.326	-113.775	56.702	-124.012	71.723	-94.983	81.311	-96.523
47.329	-128.010	58.248	-144.227	76.156	-145.183	82.744	-112.123
47.329	-127.477	58.248	-143.635	76.156	-145.216	82.744	-112.055
50.543	-170.456	63.216	-200.440	82.328	-207.779	86.191	-147.476
50.543	-170.385	63.216	-200.409	82.328	-207.765	86.191	-147.471
53.810	-208.322	64.651	-216.006	82.750	-211.903	89.255	-177.476
53.810	-208.344	64.651	-216.101	82.750	-211.823	89.255	-177.424
56.231	-235.092	70.074	-270.968	83.058	-214.782	90.016	-184.693
56.231	-235.161	70.074	-271.002	83.058	-214.790	90.016	-184.742
61.298	-287.073	72.291	-292.705	89.140	-270.305	97.365	-249.128
61.298	-287.014	72.291	-292.668	89.140	-270.339	97.365	-248.941
61.761	-291.644	76.430	-331.600	92.154	-296.060	97.451	-249.650
61.761	-291.598	76.430	-331.604	92.154	-296.078	97.451	-249.587
64.148	-315.012	77.911	-345.267	93.637	-308.293	97.461	-249.663
64.148	-314.994	77.911	-345.276	93.637	-308.294	97.461	-249.780
66.572	-338.549	81.833	-380.498	96.102	-327.698	97.475	-249.892
66.572	-338.569	81.833	-380.510	96.102	-327.694	97.475	-249.928
67.178	-344.430	83.362	-393.922	98.288	-344.303	103.460	-294.945

Table D.1 (continued)

h* = 14.965 m		h* = 21.023 m		h* = 32.023 m		h* = 38.022 m	
x (m)	σ'_v (kN/m^2)	x (m)	σ'_v (kN/m^2)	x (m)	σ'_v (kN/m^2)	x (m)	σ'_v (kN/m^2)
67.178	-344.415	83.362	-393.937	98.288	-344.300	103.460	-294.916
70.957	-380.633	86.476	-420.522	99.220	-351.111	105.005	-305.339
70.957	-380.636	86.476	-420.497	99.220	-351.144	105.005	-305.358
75.390	-422.162	88.620	-438.266	103.367	-379.531	109.842	-334.881
75.390	-422.192	88.620	-438.297	103.367	-379.511	109.842	-334.853
75.739	-425.401	91.240	-459.134	105.204	-391.136	110.667	-339.392
75.739	-425.384	91.240	-459.182	105.204	-391.146	110.667	-339.443
76.049	-428.254	94.042	-480.601	109.732	-416.693	111.426	-343.357
76.049	-428.273	94.042	-480.551	109.732	-416.584	111.426	-343.393
79.816	-462.460	97.216	-503.462	109.864	-417.273	117.199	-369.172
79.816	-462.483	97.216	-503.473	109.864	-417.273	117.199	-369.159
82.381	-484.969	100.607	-526.105	109.931	-417.602	118.714	-374.390
82.381	-485.028	100.607	-526.119	109.931	-417.680	118.714	-374.390
83.635	-495.858	104.323	-548.663	114.755	-439.635	124.089	-388.099
83.635	-495.812	104.323	-548.685	114.755	-439.620	124.089	-388.018
86.913	-523.385	107.029	-563.463	116.263	-445.225	124.353	-388.440
86.913	-523.393	107.029	-563.414	116.263	-445.225	124.353	-388.478
90.608	-552.802	110.777	-581.465	120.136	-457.200	125.389	-389.819
90.608	-552.819	110.777	-581.501	120.136	-457.228	125.389	-389.807
94.045	-578.695	113.426	-592.277	121.691	-460.913	129.269	-392.626
94.045	-578.685	113.426	-592.270	121.691	-460.855	129.269	-392.603
97.445	-602.453	115.955	-601.329	126.266	-467.944	130.557	-392.388
97.445	-602.485	115.955	-601.333	126.266	-467.959	130.557	-392.316
99.944	-618.865	120.493	-613.624	126.998	-468.573	134.250	-389.330
99.944	-618.835	120.493	-613.581	126.998	-468.637	134.250	-389.382
103.114	-638.148	121.050	-614.819	132.106	-468.249	139.402	-377.717
103.114	-638.155	121.050	-614.796	132.106	-468.270	139.402	-377.757
107.323	-660.748	121.494	-615.668	134.283	-466.493	140.737	-373.696
107.323	-660.767	121.494	-615.752	134.283	-466.224	140.737	-373.632
109.545	-671.437	126.777	-622.764	134.546	-465.892	141.779	-369.918

Table D.1 (continued)

h* = 14.965 m		h* = 21.023 m		h* = 32.023 m		h* = 38.022 m	
x (m)	σ'_v (kN/m^2)	x (m)	σ'_v (kN/m^2)	x (m)	σ'_v (kN/m^2)	x (m)	σ'_v (kN/m^2)
109.545	-671.421	126.777	-622.690	134.546	-466.021	141.779	-369.954
112.137	-682.253	127.478	-623.162	134.902	-465.450	147.031	-347.874
112.137	-682.293	127.478	-623.243	134.902	-465.642	147.031	-347.848
114.533	-691.384	129.444	-623.625	142.053	-448.739	150.695	-328.135
114.533	-691.358	129.444	-623.610	142.053	-448.634	150.695	-328.202
118.907	-704.403	133.629	-622.134	144.006	-441.561	152.996	-314.435
118.907	-704.341	133.629	-622.101	144.006	-441.553	152.996	-314.402
119.408	-705.593	134.964	-620.621	147.928	-425.111	156.866	-288.470
119.408	-705.615	134.964	-620.632	147.928	-425.104	156.866	-288.459
120.325	-707.624	137.885	-615.749	150.476	-412.140	160.655	-260.495
120.325	-707.665	137.885	-615.784	150.476	-412.256	160.655	-260.488
123.975	-714.254	139.439	-612.541	154.000	-392.238	165.068	-224.218
123.975	-714.231	139.439	-612.510	154.000	-392.201	165.068	-224.241
127.521	-717.464	143.784	-600.152	156.916	-373.873	167.740	-200.959
127.521	-717.427	143.784	-600.159	156.916	-373.895	167.740	-200.950
127.704	-717.518	144.988	-595.984	161.078	-344.730	172.673	-154.530
127.704	-717.558	144.988	-595.969	161.078	-344.726	172.673	-154.511
131.759	-717.634	150.016	-575.051	163.375	-327.605	173.711	-144.297
131.759	-717.689	150.016	-575.021	163.375	-327.591	173.711	-144.306
133.954	-715.969	150.447	-572.952	166.489	-302.819	174.448	-137.086
133.954	-715.920	150.447	-572.981	166.489	-302.841	174.448	-137.247
136.868	-712.230	154.777	-550.470	168.628	-285.080	181.575	-55.542
136.868	-712.221	154.777	-550.504	168.628	-285.051	181.575	-55.428
139.533	-706.889	160.301	-516.253	170.798	-266.347	183.193	-34.894
139.533	-706.934	160.301	-516.274	170.798	-266.345	183.193	-34.206
141.249	-702.762	161.947	-505.276	172.950	-247.360	184.867	-6.371
141.249	-702.739	161.947	-505.257	172.950	-247.380		
144.645	-692.282	163.965	-490.852	177.848	-201.619		
144.645	-692.227	163.965	-490.802	177.848	-201.574		
144.732	-691.923	169.081	-452.237	178.509	-195.229		

Table D.1 (continued)

h* = 14.965 m		h* = 21.023 m		h* = 32.023 m	
x (m)	σ'_v (kN/m^2)	x (m)	σ'_v (kN/m^2)	x (m)	σ'_v (kN/m^2)
144.732	-691.965	169.081	-452.243	178.509	-195.232
148.603	-676.991	172.417	-425.035	181.054	-169.821
148.603	-677.009	172.417	-425.075	181.054	-169.895
149.769	-671.838	174.908	-404.094	185.826	-119.452
149.769	-671.830	174.908	-404.098	185.826	-119.986
153.908	-651.407	178.865	-369.492	186.621	-109.783
153.908	-651.382	178.865	-369.483	186.621	-109.514
155.854	-640.745	182.057	-340.719	193.190	-18.992
155.854	-640.763	182.057	-340.712	193.190	-18.131
160.678	-610.911	186.962	-294.890	193.721	-9.197
160.678	-610.905	186.962	-294.864	193.721	-9.654
162.457	-599.141	186.979	-294.705	193.866	-6.890
162.457	-599.129	186.979	-294.735		
163.902	-588.970	192.720	-238.413		
163.902	-588.982	192.720	-238.324		
169.085	-550.771	193.659	-228.877		
169.085	-550.755	193.659	-228.931		
172.024	-527.239	196.714	-196.636		
172.024	-527.274	196.714	-196.848		
175.076	-501.935	201.545	-142.162		
175.076	-501.904	201.545	-142.258		
178.177	-475.262	202.793	-124.635		
178.177	-475.257	202.793	-124.748		
181.994	-441.114	210.366	-6.784		
181.994	-441.131				
184.500	-418.159				
184.500	-418.134				
188.056	-384.843				
188.056	-384.848				
189.720	-369.062				

Table D.1 (continued)

h* = 14.965 m	
x (m)	σ'_v (kN/m^2)
189.720	-369.041
195.624	-312.056
195.624	-312.081
195.763	-310.725
195.763	-310.726
195.818	-310.184
195.818	-310.279
201.592	-252.529
201.592	-252.462
206.879	-195.828
206.879	-197.037
208.476	-177.228
208.476	-175.670
210.894	-143.932
210.894	-145.410
215.451	-79.020
215.451	-78.696
217.253	-50.363
217.253	-51.010
219.452	-8.470

Table D.2 Vertical effective stresses of arbitrary cross-sections 5 to 8 (h*) of 60-m-high cross-section

h* = 44.037 m		h* = 50.025 m		h* = 58.990 m		h* = 66.983 m	
x (m)	p'_v (kN/m^2)	x (m)	p'_v (kN/m^2)	x (m)	p'_v (kN/m^2)	x (m)	p'_v (kN/m^2)
84.156	-8.814	93.138	-10.216	106.585	-11.445	118.574	-11.014
87.158	-54.119	94.764	-34.635	110.074	-55.923	120.890	-39.132
87.158	-54.068	94.764	-34.166	110.074	-55.863	120.890	-38.893
87.995	-64.772	96.817	-59.938	111.775	-71.558	122.607	-44.505
87.995	-65.000	96.817	-59.574	111.775	-72.042	122.607	-45.081

Table D.2 (continued)

h* = 44.037 m		h* = 50.025 m		h* = 58.990 m		h* = 66.983 m	
x (m)	σ'_v (kN/m^2)	x (m)	σ'_v (kN/m^2)	x (m)	σ'_v (kN/m^2)	x (m)	σ'_v (kN/m^2)
90.601	-93.798	97.867	-71.171	115.974	-101.188	124.009	-42.633
90.601	-93.780	97.867	-71.680	115.974	-101.139	124.009	-43.205
93.147	-119.823	99.233	-85.925	117.743	-110.717	127.752	-46.843
93.147	-119.916	99.233	-85.796	117.743	-110.593	127.752	-48.326
94.271	-130.649	101.749	-109.977	118.849	-115.864	130.700	-48.549
94.271	-130.666	101.749	-110.033	118.849	-115.904	130.700	-48.414
100.059	-183.124	104.327	-132.463	124.175	-135.453	134.870	-44.322
100.059	-183.101	104.327	-132.491	124.175	-135.331	134.870	-43.769
101.368	-193.758	107.356	-156.989	124.856	-136.868	138.406	-38.263
101.368	-193.753	107.356	-156.929	124.856	-137.014	138.406	-39.159
106.331	-231.365	109.111	-169.883	129.548	-141.638	141.426	-9.156
106.331	-231.385	109.111	-169.887	129.548	-141.622		
109.088	-249.502	114.404	-202.988	132.683	-139.281		
109.088	-249.494	114.404	-202.925	132.683	-139.624		
113.844	-276.662	115.202	-207.321	139.686	-119.134		
113.844	-276.498	115.202	-207.350	139.686	-118.901		
113.868	-276.617	119.653	-228.063	140.896	-113.533		
113.868	-276.676	119.653	-228.045	140.896	-113.629		
117.826	-294.960	120.474	-231.265	142.218	-106.936		
117.826	-294.955	120.474	-231.331	142.218	-107.251		
121.977	-309.213	125.311	-244.561	148.589	-63.517		
121.977	-309.175	125.311	-244.582	148.589	-63.872		
122.312	-310.148	126.615	-246.691	153.415	-8.382		
122.312	-310.080	126.615	-246.650				
122.443	-310.412	130.543	-248.305				
122.443	-310.532	130.543	-248.340				
127.458	-318.680	131.146	-248.102				
127.458	-318.669	131.146	-248.013				
129.232	-319.416	131.410	-247.791				
129.232	-319.439	131.410	-247.847				

Table D.2 (continued)

h* = 44.037 m		h* = 50.025 m	
x (m)	σ'_v (kN/m^2)	x (m)	σ'_v (kN/m^2)
132.094	-318.354	135.174	-241.828
132.094	-318.280	135.174	-241.815
134.595	-314.920	138.633	-231.460
134.595	-314.936	138.633	-231.483
139.951	-300.540	139.716	-227.417
139.951	-300.470	139.716	-227.376
139.953	-300.464	143.242	-211.611
139.953	-300.400	143.242	-211.665
139.955	-300.392	145.743	-198.200
139.955	-300.573	145.743	-198.160
145.370	-277.019	149.640	-174.381
145.370	-277.044	149.640	-174.411
148.997	-257.110	157.164	-115.906
148.997	-257.101	157.164	-115.615
151.270	-243.375	157.400	-113.567
151.270	-243.421	157.400	-113.575
154.161	-223.684	157.619	-111.619
154.161	-223.687	157.619	-111.904
158.136	-193.691	165.319	-28.705
158.136	-193.625	165.319	-28.951
161.380	-166.191	166.863	-6.589
161.380	-166.163		
164.843	-135.039		
164.843	-135.319		
169.040	-92.407		
169.040	-92.377		
172.223	-57.379		
172.223	-57.346		
175.844	-6.114		

Table D.3 Vertical effective stresses of arbitrary cross-sections 1 to 4 (h*) of 80-m-high cross-section

h* = 15.040 m		**h* = 24.960 m**		**h* = 35.044 m**		**h* = 45.040 m**	
x (m)	**σ'_v (kN/m^2)**	**x (m)**	**σ'_v (kN/m^2)**	**x (m)**	**σ'_v (kN/m^2)**	**x (m)**	**σ'_v (kN/m^2)**
38.360	2.218	53.240	-10.864	68.366	-8.534	83.360	-10.981
38.537	-5.759	57.632	-94.562	71.759	-74.036	84.684	-36.733
38.537	-23.091	57.632	-94.855	71.759	-73.910	84.684	-36.066
39.023	-31.854	60.629	-141.172	72.956	-93.059	86.372	-62.954
39.023	-26.178	60.629	-140.635	72.956	-93.642	86.372	-63.235
43.807	-126.840	64.748	-194.237	75.531	-128.818	88.542	-92.952
43.807	-126.039	64.748	-194.225	75.531	-128.603	88.542	-94.209
45.195	-152.799	67.746	-230.873	77.958	-158.829	93.234	-150.719
45.195	-150.467	67.746	-230.877	77.958	-158.539	93.234	-150.643
48.158	-195.235	71.813	-277.191	80.499	-188.367	94.801	-168.021
48.158	-194.282	71.813	-277.221	80.499	-188.332	94.801	-168.090
52.649	-250.011	76.792	-329.648	83.355	-220.397	95.506	-175.503
52.649	-250.264	76.792	-329.598	83.355	-220.499	95.506	-175.677
55.812	-285.079	80.194	-363.802	86.252	-251.490	101.123	-233.316
55.812	-285.076	80.194	-363.794	86.252	-251.459	101.123	-233.285
60.394	-334.381	85.129	-412.323	89.977	-289.809	104.757	-269.014
60.394	-334.207	85.129	-412.278	89.977	-289.910	104.757	-268.878
65.491	-385.672	89.017	-449.396	92.151	-311.306	105.179	-272.967
65.491	-385.660	89.017	-449.412	92.151	-311.300	105.179	-272.949
67.666	-407.498	94.436	-499.956	99.267	-379.314	106.143	-282.082
67.666	-407.486	94.436	-499.927	99.267	-379.276	106.143	-282.194
70.450	-435.246	98.459	-536.477	102.186	-405.752	112.873	-342.951
70.450	-435.185	98.459	-536.472	102.186	-405.765	112.873	-342.886
76.315	-494.041	107.376	-613.382	106.002	-439.650	118.318	-388.470
76.315	-494.090	107.376	-613.211	106.002	-439.691	118.318	-388.533
83.455	-564.170	107.498	-614.215	109.118	-466.192	120.356	-404.553
83.455	-564.193	107.498	-614.250	109.118	-466.250	120.356	-404.523
84.850	-577.818	107.610	-615.175	112.378	-493.308	127.228	-454.683
84.850	-577.807	107.610	-615.316	112.378	-493.295	127.228	-454.716
85.567	-584.703	115.749	-679.277	117.930	-536.521	128.242	-461.472
85.567	-584.789	115.749	-679.279	117.930	-536.562	128.242	-461.514

Table D.3 (continued)

h* = 15.040 m		h* = 24.960 m		h* = 35.044 m		h* = 45.040 m	
x (m)	σ'_v (kN/m^2)	x (m)	σ'_v (kN/m^2)	x (m)	σ'_v (kN/m^2)	x (m)	σ'_v (kN/m^2)
93.483	-659.687	117.325	-690.808	120.618	-556.437	136.493	-510.597
93.483	-659.704	117.325	-690.796	120.618	-556.404	136.493	-510.497
96.200	-684.518	123.274	-731.845	126.206	-594.353	136.866	-512.423
96.200	-684.509	123.274	-731.875	126.206	-594.385	136.866	-512.552
101.436	-730.989	125.552	-746.307	128.733	-610.221	137.481	-515.597
101.436	-731.007	125.552	-746.278	128.733	-610.195	137.481	-515.610
106.662	-775.005	130.960	-777.809	133.269	-636.006	144.037	-544.632
106.662	-775.016	130.960	-777.836	133.269	-636.046	144.037	-544.603
108.614	-790.955	133.719	-792.148	136.475	-652.282	148.792	-560.374
108.614	-790.984	133.719	-792.119	136.475	-652.258	148.792	-560.371
112.670	-822.463	139.072	-816.645	139.462	-665.956	150.982	-566.259
112.670	-822.502	139.072	-816.618	139.462	-665.917	150.982	-566.334
116.299	-849.587	142.672	-830.439	144.921	-686.492	154.056	-572.305
116.299	-849.557	142.672	-830.447	144.921	-686.443	154.056	-572.359
117.559	-858.558	149.479	-850.157	145.209	-687.378	158.452	-578.344
117.559	-858.615	149.479	-850.107	145.209	-687.456	158.452	-578.372
124.900	-907.160	149.856	-851.027	150.617	-702.177	161.607	-579.673
124.900	-907.136	149.856	-850.921	150.617	-702.180	161.607	-579.582
126.357	-915.990	150.098	-851.441	152.995	-706.930	166.308	-578.290
126.357	-916.010	150.098	-851.587	152.995	-706.922	166.308	-578.228
132.220	-948.343	156.754	-862.270	159.403	-714.336	171.195	-571.020
132.220	-948.346	156.754	-862.304	159.403	-714.275	171.195	-571.098
133.037	-952.499	161.364	-864.736	159.907	-714.514	172.853	-567.760
133.037	-952.505	161.364	-864.713	159.907	-714.571	172.853	-567.687
133.798	-956.206	165.497	-864.172	166.453	-713.534	179.268	-548.911
133.798	-956.214	165.497	-864.122	166.453	-713.608	179.268	-548.973
139.596	-981.858	170.636	-858.290	170.958	-707.700	180.695	-543.656
139.596	-981.864	170.636	-858.392	170.958	-707.702	180.695	-543.700
141.173	-987.870	172.653	-855.104	174.696	-700.324	185.844	-521.146
141.173	-987.882	172.653	-855.057	174.696	-700.300	185.844	-521.125
147.120	-1006.83	179.492	-837.960	178.262	-690.510	188.866	-506.073

Table D.3 (continued)

h* = 15.040 m		h* = 24.960 m		h* = 35.044 m		h* = 45.040 m	
x (m)	σ'_v (kN/m^2)	x (m)	σ'_v (kN/m^2)	x (m)	σ'_v (kN/m^2)	x (m)	σ'_v (kN/m^2)
147.120	-1006.84	179.492	-837.890	178.262	-690.585	188.866	-505.935
149.334	-1012.32	180.370	-835.122	180.493	-683.465	189.764	-501.043
149.334	-1012.32	180.370	-835.218	180.493	-683.434	189.764	-501.060
153.631	-1020.69	182.985	-825.812	185.707	-662.893	195.710	-465.070
153.631	-1020.51	182.985	-825.805	185.707	-662.875	195.710	-465.123
157.771	-1025.72	188.167	-804.641	187.713	-653.889	197.927	-450.282
157.771	-1025.77	188.167	-804.586	187.713	-653.948	197.927	-450.229
163.646	-1026.86	189.677	-797.557	192.773	-627.393	201.818	-422.363
163.646	-1027.10	189.677	-797.616	192.773	-627.419	201.818	-422.414
168.588	-1023.88	194.633	-771.406	196.586	-605.282	207.721	-376.234
168.588	-1023.64	194.633	-771.416	196.586	-605.203	207.721	-376.162
174.817	-1013.13	198.887	-746.680	197.938	-596.674	208.993	-365.668
174.817	-1013.18	198.887	-746.578	197.938	-596.708	208.993	-365.752
177.756	-1005.61	200.342	-737.328	203.486	-559.143	209.687	-359.849
177.756	-1005.65	200.342	-737.379	203.486	-559.160	209.687	-359.996
180.608	-997.167	206.339	-696.789	205.751	-542.911	215.197	-311.689
180.608	-997.169	206.339	-696.724	205.751	-542.820	220.707	-260.334
184.704	-982.418	206.804	-693.378	206.367	-538.248	220.707	-260.047
184.704	-982.394	206.804	-693.413	206.367	-538.287	221.974	-247.522
185.826	-977.950	212.215	-652.821	213.909	-478.842	221.974	-247.903
185.826	-977.973	212.215	-652.817	213.909	-478.779	224.967	-218.050
187.284	-971.723	214.402	-635.479	214.646	-472.688	224.967	-217.911
187.284	-971.688	214.402	-635.483	214.646	-472.703	231.001	-154.419
192.002	-949.802	220.046	-588.824	216.411	-457.783	231.001	-154.878
192.002	-949.814	220.046	-588.792	216.411	-457.751	239.670	-43.035
197.449	-919.746	220.207	-587.421	223.016	-399.822	239.670	-42.892
197.449	-919.728	220.207	-587.416	223.016	-399.771	240.665	-28.914
199.273	-908.946	220.403	-585.740	226.851	-364.266	240.665	-27.351
199.273	-908.931	220.403	-585.758	226.851	-364.274	241.640	-10.253
201.044	-897.767	226.760	-530.039	232.106	-314.265		
201.044	-897.781	226.760	-530.029	232.106	-314.323		

Table D.3 (continued)

h* = 15.040 m		h* = 24.960 m		h* = 35.044 m	
x (m)	σ'_v (kN/m^2)	x (m)	σ'_v (kN/m^2)	x (m)	σ'_v (kN/m^2)
206.433	-862.103	228.974	-509.944	240.781	-225.403
206.433	-862.098	228.974	-509.938	240.781	-225.942
211.610	-824.003	236.973	-435.521	241.754	-215.439
211.610	-824.000	236.973	-435.460	241.754	-216.069
213.453	-809.922	238.055	-425.117	242.211	-210.186
213.453	-809.904	238.055	-425.220	242.211	-211.514
215.195	-796.087	244.335	-364.166	245.147	-175.226
215.195	-796.091	244.335	-364.062	245.147	-176.304
220.392	-753.739	247.507	-332.421	253.883	-59.047
220.392	-753.724	247.507	-332.236	253.883	-58.258
225.567	-708.803	247.943	-327.921	255.036	-42.224
225.567	-708.747	247.943	-327.917	255.036	-40.405
226.261	-702.619	251.475	-290.829	256.634	-10.682
226.261	-702.627	251.475	-291.180		
229.684	-671.687	257.627	-222.990		
229.684	-671.674	257.627	-223.851		
233.229	-638.988	258.245	-214.702		
233.229	-638.934	258.245	-215.199		
233.649	-635.008	260.984	-178.858		
233.649	-635.100	260.984	-180.460		
242.777	-547.411	267.960	-78.853		
242.777	-547.269	267.960	-79.024		
243.091	-544.179	269.516	-55.508		
243.091	-544.250	269.516	-54.018		
243.563	-539.601	271.760	-11.314		
243.563	-539.684				
251.077	-465.357				
251.077	-465.325				
256.625	-409.765				
256.625	-409.760				
256.643	-409.574				

Table D.3 (continued)

h* = 15.040 m	
x (m)	σ'_v (kN/m^2)
256.643	-409.612
263.526	-340.517
263.526	-340.755
264.272	-333.458
264.272	-333.237
267.238	-302.770
267.238	-303.548
273.027	-238.877
273.027	-240.304
273.948	-226.341
273.948	-225.442
277.067	-183.288
277.067	-187.899
282.930	-94.717
282.930	-91.141
284.827	-60.848
284.827	-52.652
286.640	2.274

Table D.4 Vertical effective stresses of arbitrary cross-sections 5 to 8 (h*) of 80-m-high cross-section

h* = 55.019 m		h* = 65.024 m		h* = 74.986 m		h* = 85.024 m	
x (m)	σ'_v (kN/m^2)	x (m)	σ'_v (kN/m^2)	x (m)	σ'_v (kN/m^2)	x (m)	σ'_v (kN/m^2)
98.33	-12.34	113.34	-8.65	128.28	-12.17	143.34	-13.57
99.33	-29.48	113.55	-13.11	132.66	-71.46	146.40	-58.78
99.33	-29.37	113.55	-13.04	132.66	-71.38	146.40	-58.75
101.31	-57.52	116.34	-55.91	134.76	-93.02	148.81	-79.02
101.31	-58.43	116.34	-56.31	134.76	-93.57	148.81	-79.90
105.43	-108.96	121.33	-112.64	137.37	-117.83	152.57	-95.51
105.43	-108.83	121.33	-112.65	137.37	-117.63	152.57	-95.24
106.69	-123.43	121.61	-115.73	142.97	-158.28	156.10	-102.64

Table D.4 (continued)

h* = 55.019 m		h* = 65.024 m		h* = 74.986 m		h* = 85.024 m	
x (m)	σ'_v (kN/m^2)	x (m)	σ'_v (kN/m^2)	x (m)	σ'_v (kN/m^2)	x (m)	σ'_v (kN/m^2)
106.69	-123.65	121.61	-115.80	142.97	-158.29	156.10	-102.60
108.48	-143.08	121.85	-118.36	145.66	-174.40	162.84	-105.32
108.48	-142.96	121.85	-118.24	145.66	-174.40	162.84	-105.09
114.60	-203.72	128.23	-177.66	151.81	-202.37	163.96	-104.58
114.60	-203.74	128.23	-177.55	151.81	-202.48	163.96	-104.15
117.32	-229.27	131.77	-207.33	154.51	-211.16	168.17	-100.21
117.32	-229.30	131.77	-207.42	154.51	-211.14	168.17	-100.44
122.62	-275.48	140.84	-270.00	160.07	-221.74	170.98	-95.85
122.62	-275.50	140.84	-269.89	160.07	-221.72	170.98	-95.85
125.77	-301.18	142.41	-279.19	164.61	-221.39	171.95	-93.39
125.77	-301.16	142.41	-279.05	164.61	-221.38	171.95	-94.47
131.09	-340.33	144.57	-290.26	168.43	-215.05	177.22	-64.87
131.09	-340.48	144.57	-290.28	168.43	-215.14	177.22	-66.59
138.34	-385.40	149.45	-312.14	174.40	-194.88	181.66	-12.02
138.34	-385.35	149.45	-312.04	174.40	-194.79		
139.77	-393.45	154.16	-327.12	177.16	-182.39		
139.77	-393.27	154.16	-327.14	177.16	-182.60		
141.38	-401.42	155.36	-330.04	179.58	-169.59		
141.38	-401.46	155.36	-330.08	179.58	-170.04		
146.33	-423.65	157.15	-333.28	189.03	-98.78		
146.33	-423.63	157.15	-333.23	189.03	-98.61		
151.77	-441.57	161.67	-337.70	192.57	-64.72		
151.77	-441.52	161.67	-337.68	192.57	-64.25		
152.43	-443.35	165.87	-335.35	196.72	-8.45		
152.43	-443.27	165.87	-335.42				
152.73	-444.01	167.68	-332.95				
152.73	-444.13	167.68	-333.01				
155.00	-448.70	174.79	-313.00				
155.00	-448.69	174.79	-312.92				
160.12	-455.20	175.56	-310.05				
160.12	-455.18	175.56	-309.91				

Table D.4 (continued)

h* = 55.019 m		h* = 65.024 m	
x (m)	σ'_v (kN/m^2)	x (m)	σ'_v (kN/m^2)
160.92	-455.49	176.45	-306.20
160.92	-455.54	176.45	-306.31
167.87	-451.67	183.73	-269.39
167.87	-451.73	183.73	-269.38
171.43	-444.86	186.75	-250.65
171.43	-444.80	186.75	-250.86
175.97	-431.65	193.77	-198.65
175.97	-431.70	193.77	-198.72
180.88	-412.04	195.73	-182.89
180.88	-412.00	195.73	-182.84
183.12	-401.44	197.88	-164.00
183.12	-401.47	197.88	-164.27
184.93	-391.91	204.78	-95.38
184.93	-391.91	204.78	-95.42
191.35	-354.31	211.66	-9.15
191.35	-354.23		
193.73	-338.07		
193.73	-338.06		
198.25	-305.11		
198.25	-305.13		
200.99	-283.04		
200.99	-282.99		
205.19	-247.60		
205.19	-247.55		
212.64	-177.93		
212.64	-178.10		
214.02	-164.33		
214.02	-164.56		
214.94	-154.32		
214.94	-155.18		
224.77	-38.25		

Table D.4 (continued)

h* = 55.019 m	
x (m)	**σ'_v (kN/m^2)**
224.77	-40.06
226.41	-18.17
226.41	-16.37
226.54	-14.71
226.54	-8.55
226.67	-5.91

Table D.5 Vertical effective stresses of arbitrary cross-sections 1 to 4 (h*) of 100-m-high cross-section

h* = 25.99 m		h* = 35.97 m		h* = 46.00 m		h* = 56.00 m	
x (m)	**σ'_v (kN/m^2)**	**x (m)**	**σ'_v (kN/m^2)**	**x (m)**	**σ'_v (kN/m^2)**	**x (m)**	**σ'_v (kN/m^2)**
52.48	-3.00	67.45	-5.06	82.50	-6.80	97.50	-8.46
55.03	-62.09	68.28	-23.08	87.61	-97.25	99.08	-38.12
55.03	-62.50	68.28	-26.21	87.61	-97.04	99.08	-36.50
59.94	-146.44	69.49	-49.02	89.57	-125.42	100.85	-66.21
59.94	-147.00	69.49	-48.81	89.57	-126.51	100.85	-66.34
59.96	-147.22	73.12	-111.51	93.22	-174.43	103.33	-101.23
59.96	-148.63	73.12	-112.47	93.22	-173.75	103.33	-103.33
65.68	-228.69	78.44	-188.53	97.38	-222.78	107.95	-161.68
65.68	-228.86	78.44	-188.46	97.38	-222.72	107.95	-161.16
68.47	-263.21	80.56	-214.30	99.97	-251.08	108.51	-167.69
68.47	-263.21	80.56	-214.45	99.97	-251.10	108.51	-167.31
76.16	-353.29	81.53	-225.92	105.71	-312.32	108.78	-170.36
76.16	-353.17	81.53	-225.96	105.71	-312.20	108.78	-170.29
77.58	-368.24	84.99	-266.28	109.41	-349.33	115.24	-240.85
77.58	-368.41	84.99	-266.37	109.41	-349.33	115.24	-240.88
79.58	-389.18	90.74	-330.05	111.61	-371.02	118.80	-276.81
79.58	-389.13	90.74	-329.94	111.61	-371.04	118.80	-276.81
85.14	-445.65	92.42	-347.76	115.91	-412.09	124.60	-333.65

Table D.5 (continued)

h* = 25.99 m		h* = 35.97 m		h* = 46.00 m		h* = 56.00 m	
x (m)	σ'_v (kN/m^2)	x (m)	σ'_v (kN/m^2)	x (m)	σ'_v (kN/m^2)	x (m)	σ'_v (kN/m^2)
85.14	-445.63	92.42	-347.72	115.91	-412.10	124.60	-333.59
89.30	-486.72	97.94	-404.04	117.72	-429.07	127.34	-359.04
89.30	-486.74	97.94	-404.05	117.72	-429.11	127.34	-359.04
90.81	-501.47	99.44	-418.96	122.02	-468.19	131.65	-398.11
90.81	-501.52	99.44	-418.91	122.02	-468.23	131.65	-398.12
96.43	-555.62	103.41	-457.47	127.30	-514.43	137.09	-444.58
96.43	-555.65	103.41	-457.49	127.30	-514.43	137.09	-444.55
98.46	-574.95	106.29	-484.81	129.00	-529.10	139.94	-468.11
98.46	-574.95	106.29	-484.80	129.00	-529.10	139.94	-468.12
104.65	-633.27	112.36	-541.17	131.79	-552.35	143.80	-498.42
104.65	-633.27	112.36	-541.18	131.79	-552.33	143.80	-498.46
105.25	-638.82	114.04	-556.43	134.80	-576.87	146.80	-520.91
105.25	-638.84	114.04	-556.48	134.80	-576.87	146.80	-520.86
113.27	-712.27	116.20	-575.79	137.64	-599.04	151.97	-557.04
113.27	-712.24	116.20	-575.76	137.64	-599.03	151.97	-557.10
113.86	-717.52	122.63	-632.13	140.79	-623.04	153.12	-564.62
113.86	-717.56	122.63	-632.11	140.79	-623.09	153.12	-564.59
114.84	-726.37	126.71	-666.56	143.06	-639.74	158.33	-596.73
114.84	-726.36	126.71	-666.62	143.06	-639.71	158.33	-596.73
122.29	-791.19	129.76	-691.60	148.25	-675.88	163.63	-625.09
122.29	-791.17	129.76	-691.54	148.25	-675.87	163.63	-625.08
127.42	-833.59	133.87	-724.20	152.22	-701.16	164.05	-627.23
127.42	-833.63	133.87	-724.20	152.22	-701.21	164.05	-627.22
129.11	-847.25	140.73	-775.34	155.15	-718.96	169.40	-651.31
129.11	-847.24	140.73	-775.28	155.15	-718.92	169.40	-651.38
134.35	-888.08	141.11	-778.00	160.01	-745.63	170.49	-655.81
134.35	-888.09	141.11	-778.03	160.01	-745.66	170.49	-655.81
139.90	-928.58	141.52	-780.89	164.11	-765.63	175.74	-674.86
139.90	-928.64	141.52	-780.93	164.11	-765.65	175.74	-674.87
141.89	-942.51	148.12	-825.46	168.35	-783.72	179.23	-684.88

Table D.5 (continued)

h* = 25.99 m		h* = 35.97 m		h* = 46.00 m		h* = 56.00 m	
x (m)	σ'_v (kN/m^2)	x (m)	σ'_v (kN/m^2)	x (m)	σ'_v (kN/m^2)	x (m)	σ'_v (kN/m^2)
141.89	-942.51	148.12	-825.46	168.35	-783.72	179.23	-684.98
145.06	-963.55	153.34	-857.09	171.90	-796.97	186.56	-699.92
145.06	-963.54	153.34	-857.13	171.90	-796.96	186.56	-699.91
148.80	-987.38	154.75	-865.18	176.41	-810.91	188.07	-701.92
148.80	-987.39	154.75	-865.19	176.41	-810.94	188.07	-701.87
151.36	-1002.70	156.31	-873.71	179.79	-819.53	195.88	-705.86
151.36	-1002.69	156.31	-873.68	179.79	-819.50	195.88	-705.83
155.98	-1028.69	161.13	-898.40	183.95	-827.72	196.67	-705.62
155.98	-1028.64	161.13	-898.40	183.95	-827.77	196.67	-705.67
160.49	-1051.27	166.94	-923.91	189.17	-834.33	203.24	-700.19
160.49	-1051.36	166.94	-923.86	189.17	-834.31	203.24	-700.24
162.48	-1060.50	167.54	-926.28	191.68	-836.27	204.70	-697.92
162.48	-1060.43	167.54	-926.32	191.68	-836.30	204.70	-697.87
165.98	-1075.55	173.42	-946.86	193.99	-836.89	209.68	-687.83
165.98	-1075.55	173.42	-946.89	193.99	-836.86	209.68	-687.88
168.69	-1086.00	174.61	-950.57	200.28	-834.99	219.76	-655.05
168.69	-1086.01	174.61	-950.46	200.28	-834.98	219.76	-654.82
172.89	-1100.33	174.72	-950.77	204.96	-829.36	219.97	-653.98
172.89	-1100.33	174.72	-950.90	204.96	-829.39	219.97	-653.91
176.52	-1110.77	182.18	-968.64	207.97	-824.29	220.09	-653.39
176.52	-1110.76	182.18	-968.57	207.97	-824.27	220.09	-653.59
180.31	-1119.71	182.61	-969.35	215.52	-805.39	220.55	-651.57
180.31	-1119.70	182.61	-969.46	215.52	-805.22	220.55	-651.62
184.58	-1127.31	190.38	-978.95	215.66	-804.79	229.80	-607.29
184.58	-1127.32	190.38	-978.93	215.66	-804.90	229.80	-607.24
188.30	-1131.89	191.73	-979.71	216.77	-801.21	235.31	-574.74
188.30	-1131.87	191.73	-979.70	216.77	-801.30	235.31	-574.68
193.09	-1134.77	194.58	-980.24	222.56	-780.12	235.91	-570.96
193.09	-1134.82	194.58	-980.27	222.56	-780.07	235.91	-570.92
196.82	-1134.84	198.43	-979.62	223.20	-777.39	242.83	-523.38

Table D.5 (continued)

h* = 25.99 m		h* = 35.97 m		h* = 46.00 m		h* = 56.00 m	
x (m)	σ'_v (kN/m^2)	x (m)	σ'_v (kN/m^2)	x (m)	σ'_v (kN/m^2)	x (m)	σ'_v (kN/m^2)
196.82	-1134.76	198.43	-979.59	223.20	-777.41	242.83	-523.49
201.01	-1132.54	204.32	-974.19	229.18	-749.82	244.16	-513.89
201.01	-1132.58	204.32	-974.11	229.18	-749.85	244.16	-513.73
207.28	-1124.20	204.97	-973.23	233.58	-726.19	244.22	-513.31
207.28	-1124.24	204.97	-973.32	233.58	-726.21	244.22	-513.28
209.23	-1120.70	208.98	-966.15	237.43	-703.48	244.33	-512.42
209.23	-1120.63	208.98	-966.13	237.43	-703.51	244.33	-512.63
210.99	-1116.70	213.36	-956.24	243.98	-660.62	252.02	-452.18
210.99	-1116.74	213.36	-956.13	243.98	-660.58	252.02	-452.11
216.19	-1103.21	213.88	-954.76	246.73	-641.24	257.43	-406.13
216.19	-1103.20	213.88	-954.85	246.73	-641.22	257.43	-406.14
221.49	-1085.23	215.41	-950.39	248.51	-628.12	258.74	-394.66
221.49	-1085.18	215.41	-950.37	248.51	-628.18	258.74	-394.56
222.91	-1079.89	221.32	-930.76	252.59	-597.10	260.02	-383.22
222.91	-1079.88	221.32	-930.75	252.59	-597.11	260.02	-383.23
223.96	-1075.64	223.70	-921.27	257.70	-556.62	266.53	-322.75
223.96	-1075.71	223.70	-921.24	257.70	-556.57	266.53	-322.83
231.14	-1043.41	228.47	-900.37	261.26	-526.84	275.46	-233.77
231.14	-1043.39	228.47	-900.36	261.26	-526.83	275.46	-233.93
233.26	-1032.52	233.30	-875.86	265.19	-492.94	277.14	-216.13
233.26	-1032.51	233.30	-875.89	265.19	-492.95	277.14	-217.77
239.01	-1000.63	234.20	-871.01	270.85	-442.18	277.94	-207.71
239.01	-1000.63	234.20	-870.98	270.85	-442.20	277.94	-207.37
241.50	-985.52	239.16	-842.37	272.09	-430.97	283.28	-144.42
241.50	-985.50	239.16	-842.41	272.09	-430.87	283.28	-144.95
247.90	-943.91	240.89	-831.71	273.84	-414.55	290.42	-45.95
247.90	-943.93	240.89	-831.62	273.84	-414.48	290.42	-46.98
250.77	-923.84	245.59	-801.06	279.63	-358.93	292.50	-11.23
250.77	-923.79	245.59	-801.04	279.63	-358.84		
257.02	-877.66	252.71	-750.23	283.19	-323.26		

Table D.5 (continued)

h* = 25.99 m		h* = 35.97 m		h* = 46.00 m	
x (m)	σ'_v (kN/m^2)	x (m)	σ'_v (kN/m^2)	x (m)	σ'_v (kN/m^2)
257.02	-877.67	252.71	-750.25	283.19	-323.23
260.73	-848.49	255.88	-726.04	288.11	-272.02
260.73	-848.45	255.88	-726.04	288.11	-272.38
265.06	-813.45	261.00	-685.34	292.12	-228.57
265.06	-813.47	261.00	-685.38	292.12	-229.45
276.45	-714.91	263.06	-668.46	297.04	-169.64
276.45	-714.67	263.06	-668.43	297.04	-168.53
276.61	-713.21	270.62	-603.94	307.50	-9.32
276.61	-713.20	270.62	-603.95		
276.79	-711.58	272.63	-586.34		
276.79	-711.79	272.63	-586.30		
288.53	-603.57	282.58	-495.58		
288.53	-603.54	282.58	-495.51		
295.44	-537.65	282.79	-493.57		
295.44	-537.59	282.79	-493.50		
296.50	-527.40	290.55	-419.10		
296.50	-527.52	290.55	-419.11		
298.39	-509.17	294.75	-377.05		
298.39	-509.15	294.75	-376.97		
303.78	-456.46	298.80	-334.90		
303.78	-456.58	298.80	-334.91		
309.03	-403.93	300.48	-316.58		
309.03	-403.88	300.48	-316.79		
312.19	-370.93	310.81	-198.00		
312.19	-370.75	310.81	-196.61		
313.80	-353.14	313.16	-162.85		
313.80	-354.12	313.16	-163.52		
322.24	-253.70	322.55	-9.25		
322.24	-253.28				
327.56	-184.41				
327.56	-181.40				
333.07	-96.45				
333.07	-94.59				

Table D.5 (continued)

h* = 25.99 m	
x (m)	σ'_v (kN/m^2)
335.09	-59.30
335.09	-59.71
337.52	-3.62

Table D.6 Vertical effective stresses of arbitrary cross-sections 5 to 8 (h*) of 100-m-high cross-section

h* = 65.96 m		h* = 75.99 m		h* = 86.02 m		h* = 95.98 m	
x (m)	σ'_v (kN/m^2)	x (m)	σ'_v (kN/m^2)	x (m)	σ'_v (kN/m^2)	x (m)	σ'_v (kN/m^2)
112.44	-7.48	127.48	-6.83	142.53	-7.71	157.48	-10.27
112.53	-9.25	130.35	-53.36	143.32	-21.99	161.01	-63.03
112.53	-9.25	130.35	-53.22	143.32	-22.26	161.01	-61.32
116.80	-77.32	135.52	-119.02	144.33	-36.34	165.10	-109.91
116.80	-76.52	135.52	-118.80	144.33	-37.33	165.10	-108.33
124.29	-167.76	136.53	-129.92	149.11	-98.09	166.65	-123.47
124.29	-167.61	136.53	-129.82	149.11	-98.08	166.65	-125.30
125.62	-181.67	137.95	-144.69	151.13	-119.99	170.02	-152.66
125.62	-181.65	137.95	-144.87	151.13	-120.78	170.02	-151.52
126.78	-193.58	143.57	-201.20	156.72	-175.10	174.88	-182.93
126.78	-193.64	143.57	-201.03	156.72	-174.97	174.88	-183.05
134.50	-270.17	146.41	-227.98	160.82	-209.73	176.51	-191.55
134.50	-270.12	146.41	-228.02	160.82	-209.65	176.51	-191.58
138.20	-304.11	151.79	-274.86	163.37	-228.83	179.53	-205.01
138.20	-304.11	151.79	-275.00	163.37	-228.85	179.53	-205.06
142.32	-340.63	159.94	-337.47	170.37	-275.73	186.52	-229.76
142.32	-340.69	159.94	-337.39	170.37	-275.60	186.52	-229.62
149.23	-396.93	160.35	-340.40	172.77	-288.81	191.10	-238.30
149.23	-396.92	160.35	-340.06	172.77	-288.85	191.10	-238.44
150.75	-408.65	160.82	-343.27	178.17	-314.95	194.30	-241.09
150.75	-408.60	160.82	-343.48	178.17	-314.93	194.30	-240.89

Table D.6 (continued)

h* = 65.96 m		h* = 75.99 m		h* = 86.02 m		h* = 95.98 m	
x (m)	σ'_v (kN/m^2)	x (m)	σ'_v (kN/m^2)	x (m)	σ'_v (kN/m^2)	x (m)	σ'_v (kN/m^2)
152.98	-425.05	169.39	-394.99	179.56	-320.62	199.53	-237.46
152.98	-425.11	169.39	-394.93	179.56	-320.69	199.53	-237.64
157.46	-455.69	174.28	-418.92	181.66	-328.16	201.26	-234.61
157.46	-455.62	174.28	-419.02	181.66	-328.13	201.26	-234.45
161.81	-482.13	175.83	-425.57	186.87	-343.32	206.20	-221.66
161.81	-482.26	175.83	-425.48	186.87	-343.29	206.20	-221.71
163.72	-492.74	180.45	-442.58	192.57	-351.80	211.67	-199.91
163.72	-492.62	180.45	-442.57	192.57	-351.73	211.67	-199.84
168.55	-517.98	185.67	-456.44	192.82	-351.91	214.79	-184.70
168.55	-518.03	185.67	-456.47	192.82	-351.93	214.79	-184.69
173.18	-538.42	186.46	-458.07	198.46	-350.86	221.62	-138.94
173.18	-538.32	186.46	-458.10	198.46	-350.97	221.62	-138.56
178.82	-558.93	193.05	-465.87	200.24	-348.58	221.63	-138.52
178.82	-558.89	193.05	-465.86	200.24	-348.51	221.63	-142.21
184.31	-572.65	194.66	-466.38	205.52	-337.33	228.48	-68.25
184.31	-572.76	194.66	-466.39	205.52	-337.31	228.48	-69.04
186.14	-576.23	196.60	-465.92	209.38	-324.60	232.52	-10.50
186.14	-576.19	196.60	-465.96	209.38	-324.69		
191.34	-582.42	203.04	-459.03	215.06	-300.01		
191.34	-582.43	203.04	-458.96	215.06	-299.93		
193.57	-583.54	205.94	-452.81	217.88	-285.49		
193.57	-583.53	205.94	-452.83	217.88	-285.47		
199.02	-582.11	211.75	-435.10	221.06	-266.93		
199.02	-582.09	211.75	-435.01	221.06	-266.99		
200.89	-580.40	211.87	-434.57	226.30	-231.65		
200.89	-580.39	211.87	-434.57	226.30	-231.58		
203.30	-577.00	212.00	-434.10	231.56	-190.03		
203.30	-577.04	212.00	-434.20	231.56	-189.89		
207.34	-569.21	218.11	-407.79	233.09	-176.27		
207.34	-569.18	218.11	-407.79	233.09	-176.25		

Table D.6 (continued)

h* = 65.96 m		h* = 75.99 m		h* = 86.02 m	
x (m)	σ'_v (kN/m^2)	x (m)	σ'_v (kN/m^2)	x (m)	σ'_v (kN/m^2)
210.86	-559.72	223.29	-379.98	238.18	-128.24
210.86	-559.70	223.29	-379.94	238.18	-127.37
215.97	-541.91	224.18	-374.74	244.91	-48.71
215.97	-541.89	224.18	-374.91	244.91	-48.86
217.14	-537.16	231.13	-329.59	246.25	-30.26
217.14	-537.23	231.13	-329.69	246.25	-30.06
221.18	-518.96	233.03	-316.41	246.70	-24.14
221.18	-518.93	233.03	-316.20	246.70	-22.47
225.09	-499.24	233.20	-314.93	247.47	-10.16
225.09	-499.19	233.20	-314.71		
225.94	-494.70	233.48	-312.64		
225.94	-494.69	233.48	-312.78		
229.60	-473.63	241.43	-247.35		
229.60	-473.57	241.43	-247.40		
236.20	-431.15	247.04	-195.63		
236.20	-430.95	247.04	-196.00		
237.53	-421.21	248.21	-184.58		
237.53	-421.29	248.21	-184.23		
246.76	-348.57	249.17	-174.47		
246.76	-348.69	249.17	-175.07		
246.77	-348.61	256.45	-94.22		
246.77	-348.40	256.45	-94.83		
246.77	-348.38	262.52	-9.74		
246.77	-348.59				
256.73	-258.20				
256.73	-258.09				
258.30	-243.20				
258.30	-243.32				
260.25	-224.20				
260.25	-224.55				

Table D.6 (continued)

h* = 65.96 m	
x (m)	σ'_v (kN/m^2)
270.96	-104.96
270.96	-104.76
274.02	-66.22
274.02	-66.34
277.56	-10.38

Table D.7 Vertical effective stresses of arbitrary cross-sections 1 to 4 (h*) of 120-m-high cross-section

h* = 35.15 m		h* = 45.09 m		h* = 55.02 m		h* = 65.07 m	
x (m)	σ'_v (kN/m^2)	x (m)	σ'_v (kN/m^2)	x (m)	σ'_v (kN/m^2)	x (m)	σ'_v (kN/m^2)
63.92	-12.12	78.83	-12.70	93.73	-10.39	108.80	-15.90
67.05	-80.10	81.79	-73.89	98.82	-105.76	113.23	-91.26
67.05	-80.01	81.79	-71.79	98.82	-105.47	113.23	-89.13
70.89	-144.61	90.54	-207.20	100.73	-134.94	122.35	-209.84
70.89	-144.74	90.54	-207.34	100.73	-136.50	122.35	-209.79
77.94	-248.94	91.37	-217.76	112.49	-280.55	123.74	-225.20
77.94	-248.19	91.37	-217.84	112.49	-283.49	123.74	-225.42
82.04	-299.82	93.57	-245.00	112.81	-287.59	135.54	-349.73
82.04	-299.45	93.57	-245.13	112.81	-286.87	135.54	-349.65
91.12	-405.27	101.92	-342.45	112.96	-288.89	135.80	-352.17
91.12	-405.00	101.92	-342.44	112.96	-285.55	135.80	-352.33
93.40	-430.16	104.45	-370.55	113.22	-288.37	136.22	-356.46
93.40	-430.01	104.45	-370.75	113.22	-288.71	136.22	-356.40
94.21	-438.83	113.49	-464.01	119.49	-355.43	145.79	-447.80
94.21	-438.68	113.49	-464.03	119.49	-355.39	145.79	-447.80
103.19	-530.45	123.65	-563.33	128.31	-444.62	150.09	-486.64
103.19	-530.59	123.65	-563.20	128.31	-444.55	150.09	-486.65
109.36	-591.20	124.49	-571.16	128.79	-449.10	155.46	-533.59
109.36	-591.10	124.49	-571.18	128.79	-449.16	155.46	-533.59
113.29	-628.87	129.09	-613.93	138.22	-538.02	159.78	-569.69

Table D.7 (continued)

h* = 35.15 m		h* = 45.09 m		h* = 55.02 m		h* = 65.07 m	
x (m)	σ'_v (kN/m^2)	x (m)	σ'_v (kN/m^2)	x (m)	σ'_v (kN/m^2)	x (m)	σ'_v (kN/m^2)
113.29	-628.92	129.09	-613.92	138.22	-538.03	159.78	-569.70
115.43	-649.26	135.52	-672.24	140.60	-559.43	164.73	-608.81
115.43	-649.25	135.52	-672.23	140.60	-559.43	164.73	-608.86
123.69	-726.50	136.25	-678.74	146.48	-611.31	170.73	-654.12
123.69	-726.51	136.25	-678.81	146.48	-611.31	170.73	-654.05
124.39	-732.97	137.59	-690.67	148.92	-632.30	176.81	-695.84
124.39	-732.97	137.59	-690.64	148.92	-632.35	176.81	-695.90
130.10	-785.08	146.86	-770.31	158.44	-710.18	184.17	-741.29
130.10	-785.09	146.86	-770.31	158.44	-710.19	184.17	-741.29
137.18	-847.82	155.42	-839.30	159.82	-721.03	186.62	-755.07
137.18	-847.75	155.42	-839.25	159.82	-720.98	186.62	-755.09
137.55	-851.01	156.40	-846.93	160.19	-723.78	190.54	-775.09
137.55	-851.00	156.40	-846.91	160.19	-723.93	190.54	-775.08
137.88	-853.85	158.70	-864.38	161.52	-734.01	195.56	-798.55
137.88	-853.95	158.70	-864.42	161.52	-733.98	195.56	-798.61
146.06	-923.27	164.44	-906.60	170.46	-798.62	200.31	-817.04
146.06	-923.27	164.44	-906.62	170.46	-798.63	200.31	-816.97
153.26	-980.77	167.60	-928.42	173.66	-819.99	205.61	-834.41
153.26	-980.75	167.60	-928.39	173.66	-819.99	205.61	-834.47
154.95	-993.84	171.84	-956.65	180.23	-860.74	209.33	-843.93
154.95	-993.85	171.84	-956.74	180.23	-860.67	209.33	-843.88
157.18	-1010.66	176.66	-986.38	185.88	-891.88	217.15	-858.54
157.18	-1010.67	176.66	-986.32	185.88	-891.95	217.15	-858.50
163.47	-1056.46	181.50	-1014.30	191.16	-917.49	224.28	-863.98
163.47	-1056.47	181.50	-1014.29	191.16	-917.49	224.28	-864.01
168.43	-1089.85	183.81	-1026.57	194.04	-930.27	225.50	-864.40
168.43	-1089.87	183.81	-1026.60	194.04	-930.31	225.50	-864.39
171.71	-1111.09	190.27	-1057.54	199.17	-950.00	231.96	-863.03
171.71	-1111.08	190.27	-1057.59	199.17	-950.01	231.96	-863.02
174.63	-1128.89	193.32	-1071.01	202.58	-961.66	239.31	-854.41
174.63	-1128.89	193.32	-1070.93	202.58	-961.65	239.31	-854.41
179.40	-1156.58	195.03	-1077.71	204.06	-966.11	240.24	-852.82

Table D.7 (continued)

h* = 35.15 m		h* = 45.09 m		h* = 55.02 m		h* = 65.07 m	
x (m)	σ'_v (kN/m^2)	x (m)	σ'_v (kN/m^2)	x (m)	σ'_v (kN/m^2)	x (m)	σ'_v (kN/m^2)
179.40	-1156.53	195.03	-1077.74	204.06	-966.18	240.24	-852.98
185.27	-1187.13	200.72	-1098.30	212.86	-986.76	247.99	-835.20
185.27	-1187.19	200.72	-1098.29	212.86	-986.78	247.99	-835.19
187.50	-1197.90	205.31	-1111.80	216.15	-992.06	251.05	-825.82
187.50	-1197.90	205.31	-1111.80	216.15	-992.06	251.05	-825.78
194.97	-1229.77	208.93	-1120.92	225.99	-999.28	255.48	-810.57
194.97	-1229.59	208.93	-1120.88	225.99	-999.21	255.48	-810.68
195.06	-1229.94	216.79	-1134.49	226.82	-999.39	264.27	-771.97
195.06	-1230.00	216.79	-1134.56	226.82	-999.20	264.27	-772.03
195.33	-1231.00	218.98	-1137.08	227.05	-999.19	267.56	-755.41
195.33	-1231.07	218.98	-1137.03	227.05	-999.35	267.56	-755.40
202.09	-1254.18	226.47	-1140.96	227.88	-999.18	275.87	-706.17
202.09	-1254.22	226.47	-1140.84	227.88	-999.24	275.87	-706.21
206.03	-1265.02	226.67	-1140.86	235.57	-994.77	281.14	-671.74
206.03	-1264.96	226.67	-1140.99	235.57	-994.75	281.14	-671.65
209.94	-1274.35	233.96	-1138.06	242.89	-983.31	283.00	-658.45
209.94	-1274.39	233.96	-1138.06	242.89	-983.29	283.00	-658.58
212.29	-1278.90	236.40	-1135.72	243.98	-981.10	290.76	-600.76
212.29	-1278.87	236.40	-1135.73	243.98	-981.17	298.53	-537.90
220.53	-1289.60	246.10	-1118.77	255.16	-949.41	298.53	-537.64
220.53	-1289.66	246.10	-1118.72	255.16	-949.28	298.75	-535.75
223.75	-1291.55	247.33	-1115.80	256.14	-945.87	298.75	-536.01
223.75	-1291.45	247.33	-1115.79	256.14	-945.80	298.91	-534.68
229.50	-1291.96	253.96	-1096.50	257.05	-942.38	298.91	-534.74
229.50	-1292.01	253.96	-1096.47	257.05	-942.54	299.55	-529.13
237.98	-1285.04	255.81	-1090.34	269.37	-886.66	299.55	-529.04
237.98	-1285.00	255.81	-1090.30	269.37	-886.38	310.24	-433.84
239.05	-1283.65	256.48	-1087.83	269.55	-885.47	310.24	-433.83
239.05	-1283.55	256.48	-1087.92	269.55	-885.49	318.21	-357.56
239.76	-1282.47	262.72	-1063.41	269.92	-883.52	318.21	-357.49
239.76	-1282.61	262.72	-1063.44	269.92	-883.72	318.87	-351.01
250.12	-1260.38	270.20	-1027.79	279.39	-828.23	318.87	-350.83

Table D.7 (continued)

h* = 35.15 m		h* = 45.09 m		h* = 55.02 m		h* = 65.07 m	
x (m)	σ'_v (kN/m^2)	x (m)	σ'_v (kN/m^2)	x (m)	σ'_v (kN/m^2)	x (m)	σ'_v (kN/m^2)
250.12	-1260.31	270.20	-1027.68	279.39	-828.12	319.61	-343.51
251.60	-1256.05	271.03	-1023.42	286.71	-779.08	319.61	-343.80
251.60	-1256.07	271.03	-1023.40	286.71	-779.21	328.44	-251.31
260.53	-1225.08	271.43	-1021.26	291.42	-744.83	328.44	-251.23
260.53	-1225.09	271.43	-1021.41	291.42	-744.71	336.14	-163.53
262.94	-1215.23	280.06	-971.90	300.53	-673.96	336.14	-162.05
262.94	-1215.22	280.06	-971.91	300.53	-673.91	340.09	-110.43
271.29	-1175.71	283.44	-950.32	307.11	-618.69	340.09	-109.84
271.29	-1175.67	283.44	-950.27	307.11	-618.74	346.20	-11.19
272.60	-1168.95	290.48	-902.62	311.66	-579.44		
272.60	-1168.87	290.48	-902.64	311.66	-579.38		
273.07	-1166.31	297.70	-849.00	318.52	-517.34		
273.07	-1166.44	297.70	-849.03	318.52	-517.35		
281.71	-1116.78	302.58	-811.01	319.93	-504.34		
281.71	-1116.80	302.58	-810.98	319.93	-504.31		
287.54	-1078.96	313.16	-722.72	325.65	-449.78		
287.54	-1078.93	313.16	-722.72	325.65	-449.77		
292.49	-1045.12	314.97	-707.13	329.72	-410.08		
292.49	-1045.09	314.97	-707.04	329.72	-410.18		
304.00	-958.04	318.37	-677.12	336.79	-337.13		
304.00	-957.97	318.37	-677.14	336.79	-337.19		
304.97	-950.29	324.06	-626.07	343.17	-268.49		
304.97	-950.32	324.06	-626.05	343.17	-269.27		
308.59	-920.75	328.56	-584.44	350.79	-174.12		
308.59	-920.67	328.56	-584.45	350.79	-173.76		
317.66	-844.06	332.97	-543.11	361.27	-12.30		
317.66	-843.98	332.97	-543.11				
319.54	-827.45	335.68	-517.21				
319.54	-827.50	335.68	-517.30				
327.01	-760.59	347.76	-395.30				
327.01	-760.61	347.76	-395.16				
330.51	-728.74	349.84	-373.20				

Table D.7 (continued)

h* = 35.15 m		h* = 45.09 m	
x (m)	σ'_v (kN/m^2)	x (m)	σ'_v (kN/m^2)
330.51	-728.69	349.84	-373.59
331.80	-716.79	351.54	-355.50
331.80	-716.77	351.54	-355.61
340.02	-639.87	357.69	-285.42
340.02	-639.88	357.69	-286.21
346.71	-575.77	365.11	-194.94
346.71	-575.85	365.11	-193.04
349.17	-551.86	368.95	-136.84
349.17	-551.85	368.95	-137.23
353.27	-511.22	376.17	-7.12
353.27	-511.22		
358.24	-460.90		
358.24	-461.10		
361.99	-421.73		
361.99	-421.64		
367.71	-358.24		
367.71	-358.80		
373.62	-286.46		
373.62	-286.71		
381.85	-172.59		
381.85	-172.48		
386.24	-109.27		
386.24	-106.17		
391.08	-3.70		

Table D.8 Vertical effective stresses of arbitrary cross-sections 5 to 8 (h*) of 120-m-high cross-section

h* = 74.95 m		**h* = 85.09 m**		**h* = 95.07 m**		**h* = 120.37 m**	
x (m)	σ'_v **(kN/m²)**	**x (m)**	σ'_v **(kN/m²)**	**x (m)**	σ'_v **(kN/m²)**	**x (m)**	σ'_v **(kN/m²)**
123.63	-13.36	138.84	-13.67	153.81	-11.97	191.76	-11.76
123.78	-16.53	139.43	-24.97	155.85	-47.62	191.84	-13.61
123.78	-17.44	139.43	-27.05	155.85	-47.54	191.84	-20.60
124.03	-21.81	140.85	-47.79	159.34	-94.98	192.00	-23.09
124.03	-20.20	140.85	-48.23	159.34	-95.75	192.00	-19.11
129.57	-107.10	147.87	-139.96	167.86	-189.60	198.30	-109.23
129.57	-108.16	147.87	-139.86	167.86	-189.70	198.30	-109.04
135.03	-176.28	150.23	-166.82	169.91	-210.05	200.76	-133.02
135.03	-176.09	150.23	-167.47	169.91	-210.19	200.76	-134.89
137.74	-206.14	153.01	-198.01	171.05	-220.90	206.02	-173.03
137.74	-206.06	153.01	-197.81	171.05	-221.09	206.02	-172.25
140.40	-234.15	162.10	-287.59	183.92	-332.54	211.84	-199.80
140.40	-234.19	162.10	-287.59	183.92	-332.29	211.84	-199.72
148.76	-318.99	165.56	-319.98	184.78	-338.76	219.65	-221.00
148.76	-318.96	165.56	-320.10	184.78	-338.95	219.65	-221.27
153.47	-363.85	178.27	-426.83	194.67	-407.09	222.67	-226.26
153.47	-363.87	178.27	-426.55	194.67	-407.01	222.67	-225.98
154.26	-371.30	178.37	-427.37	195.52	-412.16	224.55	-227.75
154.26	-371.33	178.37	-427.26	195.52	-412.17	224.55	-227.83
157.64	-402.04	178.75	-430.13	203.12	-452.47	232.69	-224.18
157.64	-401.98	178.75	-430.44	203.12	-452.38	232.69	-224.23
161.72	-437.99	189.16	-501.69	203.28	-453.08	238.89	-209.83
161.72	-438.12	189.16	-501.69	203.28	-453.16	238.89	-210.04
171.26	-515.59	191.74	-517.11	209.82	-478.85	244.51	-189.50
171.26	-515.65	191.74	-517.09	209.82	-478.94	244.51	-190.74
175.54	-548.09	197.56	-549.00	215.41	-494.33	250.96	-153.90
175.54	-548.00	197.56	-548.97	215.41	-494.31	250.96	-153.59
181.37	-587.99	201.29	-566.05	219.26	-502.08	255.98	-110.21
181.37	-588.08	201.29	-565.95	219.26	-502.07	255.98	-110.66
186.64	-621.15	206.54	-586.66	222.27	-505.68	263.24	-15.33

Table D.8 (continued)

h* = 74.95 m		h* = 85.09 m		h* = 95.07 m	
x (m)	σ'_v (kN/m^2)	x (m)	σ'_v (kN/m^2)	x (m)	σ'_v (kN/m^2)
186.64	-621.10	206.54	-586.67	222.27	-505.67
191.60	-648.26	212.01	-603.03	228.97	-507.68
191.60	-648.25	212.01	-603.12	228.97	-507.74
195.65	-668.77	214.22	-608.44	233.45	-503.51
195.65	-668.82	214.22	-608.35	233.45	-503.44
198.40	-680.86	220.16	-618.43	237.61	-496.65
198.40	-680.86	220.16	-618.37	237.61	-496.68
205.33	-706.83	226.81	-622.29	240.54	-489.70
205.33	-706.85	226.81	-622.39	240.54	-489.79
211.48	-724.04	227.53	-622.36	250.86	-452.21
211.48	-724.20	227.53	-622.37	250.86	-452.22
214.31	-730.22	234.31	-617.71	255.00	-432.42
214.31	-730.06	234.31	-617.94	255.00	-432.34
219.56	-738.22	245.02	-594.64	262.43	-389.16
219.56	-738.34	245.02	-594.56	262.43	-389.22
232.20	-740.65	245.94	-591.87	263.70	-381.11
232.20	-740.32	245.94	-591.58	263.70	-381.07
232.27	-740.28	247.14	-587.51	272.25	-318.40
232.27	-739.97	247.14	-587.61	272.25	-318.34
232.30	-739.94	257.80	-542.23	274.85	-297.95
232.30	-740.31	257.80	-542.29	274.85	-297.97
232.34	-740.26	263.98	-508.04	279.43	-258.42
232.34	-740.66	263.98	-508.16	279.43	-258.93
246.50	-713.63	267.50	-486.85	284.61	-210.30
246.50	-713.49	267.50	-486.73	284.61	-210.13
251.23	-697.35	275.17	-433.76	292.12	-133.26
251.23	-697.36	275.17	-433.73	292.12	-132.39
257.26	-673.68	276.74	-422.07	296.76	-76.32
257.26	-673.66	276.74	-422.08	296.76	-76.37
261.37	-654.45	282.69	-374.44	301.19	-8.18
261.37	-654.38	282.69	-374.45		
268.42	-616.25	286.17	-344.85		

Table D.8 (continued)

h* = 74.95 m		h* = 85.09 m	
x (m)	σ'_v (kN/m^2)	x (m)	σ'_v (kN/m^2)
268.42	-616.31	286.17	-344.87
276.92	-561.51	287.15	-336.16
276.92	-561.52	287.15	-336.19
278.77	-548.75	295.52	-258.68
278.77	-548.62	295.52	-258.85
290.20	-460.14	298.85	-225.11
290.20	-459.87	298.85	-225.46
290.23	-459.64	305.62	-151.63
290.23	-459.58	305.62	-151.61
299.84	-375.13	308.36	-119.92
299.84	-375.19	308.36	-119.94
306.50	-312.34	311.43	-83.36
306.50	-312.29	311.43	-82.70
306.96	-307.88	316.16	-8.83
306.96	-307.80		
314.94	-226.18		
314.94	-225.85		
316.18	-213.00		
316.18	-213.73		
329.48	-45.72		
329.48	-47.97		
330.17	-38.43		
330.17	-36.25		
330.69	-29.22		
330.69	-21.61		
331.37	-8.28		

Table D.9 Vertical effective stresses of arbitrary cross-sections 1 to 4 (h*) of 140-m-high cross-section

h* = 35.022 m		**h* = 50.069 m**		**h* = 65.116 m**		**h* = 79.970 m**	
x (m)	**σ'_v (kN/m^2)**	**x (m)**	**σ'_v (kN/m^2)**	**x (m)**	**σ'_v (kN/m^2)**	**x (m)**	**σ'_v (kN/m^2)**
61.43	-4.91	84.00	-12.36	106.57	-15.78	128.85	-12.95
70.10	-179.25	84.93	-34.18	109.41	-70.52	134.78	-114.39
70.10	-181.77	84.93	-35.30	109.41	-69.04	134.78	-114.15
72.49	-222.80	86.91	-73.66	114.93	-157.10	137.30	-149.04
72.49	-222.86	86.91	-75.13	114.93	-156.20	137.30	-150.35
75.95	-271.11	93.27	-178.59	118.28	-202.00	144.05	-232.55
75.95	-271.48	93.27	-179.97	118.28	-203.67	144.05	-232.30
85.55	-395.53	96.60	-228.79	120.02	-226.55	148.04	-276.62
85.55	-395.83	96.60	-228.32	120.02	-225.88	148.04	-276.70
96.14	-516.82	104.96	-333.23	130.76	-349.37	150.85	-306.26
96.14	-516.47	104.96	-333.24	130.76	-349.33	150.85	-306.31
98.55	-541.73	108.29	-372.60	133.87	-383.03	159.42	-393.98
98.55	-541.71	108.29	-372.66	133.87	-383.11	159.42	-393.88
100.87	-565.53	113.41	-430.06	137.42	-420.40	166.25	-459.89
100.87	-565.51	113.41	-430.03	137.42	-420.43	166.25	-459.96
108.22	-639.80	120.31	-503.35	147.33	-519.02	170.00	-494.71
108.22	-639.78	120.31	-503.29	147.33	-519.01	170.00	-494.67
111.44	-671.51	128.72	-588.01	153.28	-575.86	177.31	-560.11
111.44	-671.52	128.72	-587.95	153.28	-575.81	177.31	-560.13
117.44	-729.90	130.97	-610.19	159.79	-635.55	178.77	-572.66
117.44	-729.90	130.97	-610.15	159.79	-635.60	178.77	-572.63
124.89	-801.56	133.15	-631.27	167.22	-701.35	185.28	-627.06
124.89	-801.55	133.15	-631.24	167.22	-701.25	185.28	-627.06
130.42	-854.23	139.62	-692.73	167.35	-702.39	192.92	-686.65
130.42	-854.25	139.62	-692.75	167.35	-702.46	192.92	-686.62
137.75	-922.81	144.06	-733.87	167.67	-705.18	194.24	-696.55
137.75	-922.88	144.06	-733.86	167.67	-705.17	194.24	-696.55
141.70	-959.50	149.05	-779.38	176.56	-779.39	196.04	-709.65
141.70	-959.46	149.05	-779.41	176.56	-779.39	196.04	-709.67

Table D.9 (continued)

h* = 35.022 m		h* = 50.069 m		h* = 65.116 m		h* = 79.970 m	
x (m)	σ'_v (kN/m^2)	x (m)	σ'_v (kN/m^2)	x (m)	σ'_v (kN/m^2)	x (m)	σ'_v (kN/m^2)
151.34	-1046.24	153.41	-818.44	178.97	-798.87	203.43	-760.71
151.34	-1046.29	153.41	-818.46	178.97	-798.87	203.43	-760.68
153.23	-1062.90	159.90	-875.27	186.27	-854.92	207.87	-788.53
153.23	-1062.85	159.90	-875.19	186.27	-855.00	207.87	-788.59
161.69	-1135.67	165.80	-925.34	187.70	-865.66	211.55	-810.44
161.69	-1135.65	165.80	-925.36	187.70	-865.66	211.55	-810.39
169.31	-1197.84	176.44	-1010.91	189.15	-876.12	217.08	-840.21
169.31	-1197.92	176.44	-1010.84	189.15	-876.10	217.08	-840.27
173.61	-1231.76	177.00	-1015.24	195.40	-919.85	224.44	-874.59
173.61	-1231.75	177.00	-1015.29	195.40	-919.85	224.44	-874.58
180.75	-1285.37	177.57	-1019.65	197.39	-933.11	225.14	-877.55
180.75	-1285.35	177.57	-1019.70	197.39	-933.18	225.14	-877.49
185.20	-1317.22	188.06	-1096.70	206.26	-987.90	232.72	-905.96
185.20	-1317.21	188.06	-1096.69	206.26	-987.90	232.72	-905.96
194.17	-1376.77	195.51	-1146.29	209.07	-1003.83	235.97	-916.10
194.17	-1376.73	195.51	-1146.38	209.07	-1003.82	235.97	-916.12
194.99	-1381.93	199.19	-1169.50	213.55	-1027.35	240.26	-927.68
194.99	-1382.00	199.19	-1169.48	213.55	-1027.45	240.26	-927.62
203.46	-1432.04	207.36	-1215.96	217.61	-1047.27	244.75	-937.23
203.46	-1432.04	207.36	-1215.92	217.61	-1047.15	244.75	-937.33
207.36	-1453.05	209.83	-1229.17	224.33	-1075.97	252.20	-947.15
207.36	-1453.06	209.83	-1229.14	224.33	-1076.05	252.20	-947.06
213.61	-1483.83	211.08	-1235.43	230.19	-1096.80	255.35	-949.49
213.61	-1483.84	211.08	-1235.51	230.19	-1096.80	255.35	-949.47
215.72	-1493.48	220.91	-1280.53	234.64	-1110.42	257.50	-950.21
215.72	-1493.45	220.91	-1280.54	234.64	-1110.40	257.50	-950.27
222.34	-1521.04	231.44	-1317.36	240.77	-1125.31	268.71	-945.25
222.34	-1521.10	231.44	-1317.28	240.77	-1125.34	268.71	-945.19
229.58	-1545.97	232.67	-1321.03	241.68	-1127.21	269.55	-944.30
229.58	-1546.03	232.67	-1321.09	241.68	-1127.20	269.55	-944.41
232.74	-1555.59	234.51	-1325.96	248.54	-1138.51	269.79	-944.10
232.74	-1555.59	234.51	-1325.99	248.54	-1138.58	269.79	-944.16

Table D.9 (continued)

h* = 35.022 m		h* = 50.069 m		h* = 65.116 m		h* = 79.970 m	
x (m)	σ'_v (kN/m^2)	x (m)	σ'_v (kN/m^2)	x (m)	σ'_v (kN/m^2)	x (m)	σ'_v (kN/m^2)
237.59	-1567.56	244.20	-1347.19	253.74	-1143.27	280.07	-924.96
237.59	-1567.58	244.20	-1347.14	253.74	-1143.26	280.07	-924.90
242.50	-1577.92	248.19	-1352.94	258.16	-1145.35	289.67	-894.65
242.50	-1577.93	248.19	-1352.95	258.16	-1145.34	289.67	-894.83
245.68	-1582.95	260.26	-1359.90	261.11	-1145.17	291.57	-887.90
245.68	-1582.90	260.26	-1359.59	261.11	-1145.19	291.57	-887.80
251.82	-1590.23	260.41	-1359.59	269.24	-1140.46	302.91	-836.94
251.82	-1590.22	260.41	-1359.69	269.24	-1140.41	302.91	-836.81
256.89	-1592.84	260.65	-1359.66	276.33	-1129.83	303.75	-832.51
256.89	-1592.89	260.65	-1359.82	276.33	-1129.82	303.75	-832.54
261.59	-1593.22	270.75	-1353.46	283.68	-1113.26	312.93	-779.68
261.59	-1593.25	270.75	-1353.40	283.68	-1113.27	312.93	-779.68
270.64	-1586.97	277.42	-1343.09	293.18	-1082.66	315.91	-760.98
270.64	-1586.90	277.42	-1343.22	293.18	-1082.75	315.91	-760.89
273.08	-1584.01	282.87	-1331.42	297.73	-1065.01	316.16	-759.22
273.08	-1583.95	282.87	-1331.32	297.73	-1064.91	316.16	-759.40
274.78	-1581.40	290.10	-1310.96	308.96	-1010.99	326.92	-683.65
274.78	-1581.52	290.10	-1311.09	308.96	-1011.15	326.92	-683.58
282.35	-1566.26	298.09	-1281.66	313.34	-986.77	328.25	-673.48
282.35	-1566.35	298.09	-1281.57	313.34	-986.55	328.25	-673.53
286.95	-1554.87	302.67	-1262.50	321.95	-933.49	338.29	-593.13
286.95	-1554.74	302.67	-1262.55	321.95	-933.55	338.29	-593.10
288.17	-1551.19	306.43	-1244.79	331.90	-864.13	339.79	-580.37
288.17	-1551.26	306.43	-1244.77	331.90	-864.17	339.79	-580.31
298.63	-1514.98	319.31	-1174.79	334.15	-847.62	344.91	-535.67
298.63	-1514.91	319.31	-1174.78	334.15	-847.64	344.91	-535.69
300.36	-1508.01	325.79	-1134.13	342.19	-784.67	350.66	-483.99
300.36	-1508.04	325.79	-1134.07	342.19	-784.59	350.66	-484.21
302.52	-1498.71	335.94	-1063.67	351.32	-709.22	363.68	-358.72
302.52	-1498.73	335.94	-1063.77	351.32	-709.04	363.68	-358.56
313.27	-1446.75	341.62	-1021.23	352.81	-696.15	365.08	-344.48
313.27	-1446.72	341.62	-1021.16	352.81	-696.31	365.08	-344.89

Table D.9 (continued)

h* = 35.022 m		h* = 50.069 m		h* = 65.116 m		h* = 79.970 m	
x (m)	σ'_v (kN/m^2)	x (m)	σ'_v (kN/m^2)	x (m)	σ'_v (kN/m^2)	x (m)	σ'_v (kN/m^2)
319.15	-1413.76	349.50	-959.07	354.57	-680.76	365.25	-343.02
319.15	-1413.83	349.50	-958.96	354.57	-680.89	365.25	-343.70
327.49	-1362.24	360.56	-866.33	370.09	-539.08	365.55	-340.41
327.49	-1362.18	360.56	-866.34	370.09	-539.08	365.55	-340.37
332.47	-1329.13	367.00	-809.68	370.63	-533.90	381.39	-160.76
332.47	-1329.14	367.00	-809.75	370.63	-533.98	381.39	-160.33
338.26	-1287.96	374.76	-739.66	382.64	-414.29	390.99	-14.80
338.26	-1288.02	374.76	-739.64	382.64	-414.22	390.99	-14.87
344.84	-1239.00	378.61	-704.05	386.10	-378.51	391.15	-11.73
344.84	-1238.91	378.61	-704.05	386.10	-378.78		
353.92	-1166.84	385.16	-642.23	391.45	-320.65		
353.92	-1166.89	385.16	-642.22	391.45	-321.34		
358.72	-1126.87	390.16	-594.06	402.92	-180.40		
358.72	-1126.79	390.16	-594.14	402.92	-179.09		
366.41	-1060.83	394.10	-555.19	413.43	-14.26		
366.41	-1060.85	394.10	-555.26				
375.86	-976.18	402.47	-469.05				
375.86	-976.14	402.47	-469.15				
378.44	-952.67	414.48	-335.56				
378.44	-952.64	414.48	-336.38				
383.54	-905.38	417.96	-293.92				
383.54	-905.32	417.96	-292.86				
391.93	-826.65	421.67	-241.73				
391.93	-826.63	421.67	-242.51				
398.76	-761.18	436.00	-14.77				
398.76	-761.20						
407.47	-676.81						
407.47	-676.90						
412.24	-629.54						
412.24	-629.48						
427.53	-472.23						
427.53	-472.05						

Table D.9 (continued)

h* = 35.022 m	
x (m)	**σ'_v (kN/m^2)**
431.99	-419.94
431.99	-419.85
445.57	-245.47
445.57	-243.25
450.86	-160.33
450.86	-160.25
458.57	-10.00

Table D.10 Vertical effective stresses of arbitrary cross-sections 5 to 8 (h*) of 140-m-high cross-section

h* = 95.072 m		h* = 110.342 m		h* = 125.416 m		h* = 140.092 m	
x (m)	**σ'_v (kN/m^2)**	**x (m)**	**σ'_v (kN/m^2)**	**x (m)**	**σ'_v (kN/m^2)**	**x (m)**	**σ'_v (kN/m^2)**
151.51	-9.71	174.41	-15.67	197.02	-18.84	219.04	-15.23
151.88	-18.33	176.68	-52.97	200.90	-76.59	226.59	-126.60
151.88	-18.22	176.68	-52.95	200.90	-74.80	226.59	-125.92
156.36	-93.50	181.53	-117.94	209.10	-173.88	228.82	-150.60
156.36	-94.42	181.53	-117.80	209.10	-173.16	228.82	-151.85
165.99	-211.14	187.71	-189.47	211.08	-191.63	232.79	-184.95
165.99	-211.17	187.71	-189.23	211.08	-191.91	232.79	-183.75
166.59	-217.71	192.04	-232.83	218.25	-254.82	236.88	-208.35
166.59	-217.78	192.04	-232.72	218.25	-254.96	236.88	-207.95
166.82	-220.16	200.52	-312.75	226.60	-314.17	241.06	-226.68
166.82	-220.27	200.52	-312.71	226.60	-314.19	241.06	-226.78
167.35	-225.93	204.92	-350.06	229.90	-334.93	244.70	-240.04
167.35	-225.84	204.92	-350.12	229.90	-334.89	244.70	-240.09
178.99	-343.10	211.82	-404.15	231.79	-345.74	247.75	-248.75
178.99	-343.16	211.82	-404.17	231.79	-345.81	247.75	-248.71
186.48	-412.53	215.08	-428.21	239.12	-380.56	252.92	-260.34
186.48	-412.50	215.08	-428.07	239.12	-380.66	252.92	-260.38
188.30	-428.78	218.97	-454.37	243.63	-398.12	259.63	-265.47

Table D.10 (continued)

h* = 95.072 m		h* = 110.342 m		h* = 125.416 m		h* = 140.092 m	
x (m)	σ'_v (kN/m^2)	x (m)	σ'_v (kN/m^2)	x (m)	σ'_v (kN/m^2)	x (m)	σ'_v (kN/m^2)
188.30	-428.76	218.97	-454.42	243.63	-398.11	259.63	-265.69
195.49	-489.54	223.68	-483.75	245.62	-404.10	263.72	-263.89
195.49	-489.68	223.68	-483.69	245.62	-404.04	263.72	-264.04
204.13	-556.06	230.77	-521.34	254.73	-423.18	270.29	-251.32
204.13	-556.01	230.77	-521.33	254.73	-423.10	270.29	-251.21
205.33	-564.75	231.69	-525.87	261.90	-424.97	273.22	-243.85
205.33	-564.69	231.69	-525.89	261.90	-424.94	273.22	-243.54
206.74	-574.57	232.36	-528.98	262.89	-424.36	275.87	-234.99
206.74	-574.68	232.36	-528.95	262.89	-424.37	275.87	-234.93
214.37	-624.13	240.92	-562.43	271.02	-410.98	282.44	-207.44
214.37	-624.04	240.92	-562.47	271.02	-411.00	282.44	-209.55
220.88	-661.53	246.00	-576.02	273.20	-405.27	289.82	-153.63
220.88	-661.65	246.00	-576.02	273.20	-405.38	289.82	-154.46
227.35	-693.38	252.15	-587.17	283.07	-367.61	300.96	-19.64
227.35	-693.39	252.15	-587.07	283.07	-367.67		
235.54	-726.58	259.78	-591.50	287.99	-343.25		
235.54	-726.52	259.78	-591.51	287.99	-343.08		
239.94	-740.36	261.16	-591.25	296.05	-292.69		
239.94	-740.49	261.16	-591.23	296.05	-292.77		
247.03	-755.91	268.61	-584.39	298.38	-275.99		
247.03	-755.94	268.61	-584.44	298.38	-275.74		
251.00	-762.10	274.41	-572.29	307.05	-205.28		
251.00	-761.99	274.41	-572.32	307.05	-203.44		
253.62	-764.41	282.17	-548.39	312.68	-147.18		
253.62	-764.46	282.17	-548.36	312.68	-147.45		
262.26	-766.30	287.68	-525.09	318.03	-84.94		
262.26	-766.28	287.68	-525.08	318.03	-86.19		
266.36	-763.47	294.14	-492.39	322.98	-13.48		
266.36	-763.47	294.14	-492.35				
276.28	-747.15	297.32	-473.73				
276.28	-747.19	297.32	-473.79				
281.59	-732.70	303.67	-432.75				

Table D.10 (continued)

h* = 95.072 m		h* = 110.342 m	
x (m)	σ'_v (kN/m^2)	x (m)	σ'_v (kN/m^2)
281.59	-732.73	303.67	-432.88
295.53	-676.72	307.37	-406.32
295.53	-676.31	307.37	-406.32
296.09	-673.47	316.26	-335.54
296.09	-673.76	316.26	-335.47
296.63	-670.94	320.87	-295.56
296.63	-671.07	320.87	-295.62
309.72	-594.80	322.93	-277.16
309.72	-594.55	322.93	-277.67
313.68	-567.35	331.11	-196.72
313.68	-567.37	339.28	-101.62
320.06	-520.67	339.28	-102.20
320.06	-520.69	341.54	-75.08
326.41	-469.23	341.54	-74.02
326.41	-469.24	343.28	-52.88
330.34	-436.12	343.28	-48.57
330.34	-436.15	345.59	-10.35
336.47	-381.15		
336.47	-381.75		
341.11	-337.69		
341.11	-337.46		
352.86	-219.51		
352.86	-221.66		
353.13	-218.23		
353.13	-216.75		
355.90	-184.49		
355.90	-185.32		
366.23	-50.23		
366.23	-51.31		
368.49	-15.67		

Table D.11 Vertical effective stresses of arbitrary cross-sections 1 to 4 (h*) of 160-m-high cross-section

h* = 40.095 m		**h* = 54.962 m**		**h* = 69.876 m**		**h* = 85.067 m**	
x (m)	σ'_v **(kN/m²)**	**x (m)**	σ'_v **(kN/m²)**	**x (m)**	σ'_v **(kN/m²)**	**x (m)**	σ'_v **(kN/m²)**
66.74	-14.95	89.04	-10.13	111.41	-15.07	134.20	-13.17
72.75	-138.33	94.14	-120.08	112.60	-40.14	142.86	-159.46
72.75	-138.55	94.14	-119.39	112.60	-41.19	142.86	-158.99
86.09	-348.87	97.34	-170.27	116.48	-110.93	144.80	-188.14
86.09	-348.50	97.34	-175.74	116.48	-112.16	144.80	-189.24
86.39	-352.54	104.28	-275.22	121.92	-195.33	149.22	-244.80
86.39	-352.27	104.28	-273.55	121.92	-195.37	149.22	-244.35
86.52	-353.97	109.99	-349.52	123.00	-213.78	157.06	-335.16
86.52	-356.13	109.99	-349.11	123.00	-213.81	157.06	-334.97
86.68	-358.25	112.68	-381.50	127.99	-278.47	160.11	-367.84
86.68	-357.47	112.68	-381.87	127.99	-277.76	160.11	-367.91
102.92	-556.53	128.87	-566.06	135.35	-366.34	169.81	-469.14
102.92	-556.26	128.87	-565.90	135.35	-366.32	169.81	-469.05
104.75	-576.16	129.60	-573.60	137.69	-392.45	172.84	-499.92
104.75	-576.21	129.60	-573.91	137.69	-392.55	172.84	-499.75
107.12	-601.53	130.53	-583.45	151.15	-537.35	174.23	-513.54
107.12	-601.51	130.53	-583.40	151.15	-537.27	174.23	-513.70
115.99	-694.17	144.25	-721.97	153.30	-559.01	184.48	-611.34
115.99	-694.20	144.25	-721.88	153.30	-559.08	184.48	-611.25
120.36	-737.97	150.04	-777.84	157.18	-597.70	191.93	-679.18
120.36	-737.97	150.04	-777.83	157.18	-597.70	191.93	-679.20
129.07	-824.02	153.40	-809.84	164.94	-673.34	199.53	-744.71
129.07	-824.06	153.40	-809.86	164.94	-673.32	199.53	-744.72
131.76	-850.21	161.07	-881.46	169.88	-720.06	205.42	-793.62
131.76	-850.20	161.07	-881.43	169.88	-720.08	205.42	-793.60
140.66	-935.98	162.17	-891.58	174.98	-767.01	213.53	-856.63
140.66	-935.98	162.17	-891.60	174.98	-766.98	213.53	-856.62
145.81	-984.99	165.17	-919.03	182.12	-830.98	216.47	-878.68
145.81	-985.01	165.17	-919.03	182.12	-830.98	216.47	-878.77
154.88	-1070.00	170.70	-968.86	187.96	-881.54	228.03	-957.96

Table D.11 (continued)

h* = 40.095 m		h* = 54.962 m		h* = 69.876 m		h* = 85.067 m	
x (m)	σ'_v (kN/m^2)	x (m)	σ'_v (kN/m^2)	x (m)	σ'_v (kN/m^2)	x (m)	σ'_v (kN/m^2)
154.88	-1070.02	170.70	-968.89	187.96	-881.57	228.03	-957.91
157.64	-1095.70	174.15	-999.28	196.33	-950.76	229.50	-967.30
157.64	-1095.74	174.15	-999.26	196.33	-950.80	229.50	-967.32
160.98	-1126.19	179.25	-1043.59	201.49	-992.17	241.55	-1035.93
160.98	-1126.17	179.25	-1043.64	201.49	-992.14	241.55	-1035.95
169.38	-1201.65	183.10	-1076.39	209.02	-1048.96	244.56	-1050.94
169.38	-1201.64	183.10	-1076.37	209.02	-1049.02	244.56	-1050.93
179.55	-1289.39	189.91	-1132.83	212.69	-1075.64	253.43	-1089.63
179.55	-1289.31	189.91	-1132.83	212.69	-1075.66	253.43	-1089.64
179.97	-1292.85	198.55	-1200.64	214.84	-1090.62	257.53	-1104.85
179.97	-1292.87	198.55	-1200.63	214.84	-1090.60	257.53	-1104.90
180.35	-1296.01	201.24	-1221.22	222.56	-1142.22	264.81	-1127.59
180.35	-1296.09	201.24	-1221.22	222.56	-1142.23	264.81	-1127.54
190.74	-1380.92	203.84	-1240.47	233.12	-1205.02	269.17	-1138.89
190.74	-1380.93	203.84	-1240.50	233.12	-1204.93	269.17	-1139.06
201.63	-1463.55	212.19	-1299.85	234.10	-1210.35	276.97	-1153.79
201.63	-1463.42	212.19	-1299.82	234.10	-1210.36	276.97	-1153.74
202.09	-1466.73	219.69	-1348.71	234.69	-1213.53	283.78	-1162.55
202.09	-1466.79	219.69	-1348.69	234.69	-1213.74	283.78	-1162.46
202.58	-1470.32	220.95	-1356.66	247.87	-1276.87	287.75	-1164.68
202.58	-1470.42	220.95	-1356.69	247.87	-1276.81	287.75	-1164.77
213.88	-1548.33	224.20	-1376.33	249.47	-1283.32	297.23	-1164.33
213.88	-1548.33	224.20	-1376.28	249.47	-1283.35	297.23	-1164.29
222.28	-1600.40	230.71	-1413.60	258.91	-1317.24	301.24	-1161.44
222.28	-1600.47	230.71	-1413.67	258.91	-1317.33	301.24	-1161.41
226.10	-1622.80	232.66	-1424.08	262.14	-1326.76	311.15	-1146.78
226.10	-1622.79	232.66	-1424.06	262.14	-1326.58	311.15	-1146.96
229.62	-1642.00	242.60	-1472.83	269.67	-1345.56	317.92	-1131.03
229.62	-1642.00	242.60	-1472.82	269.67	-1345.63	317.92	-1130.86
238.10	-1685.05	248.20	-1496.14	277.87	-1359.38	325.18	-1109.32
238.10	-1684.98	248.20	-1496.22	277.87	-1359.50	325.18	-1109.33
243.41	-1708.85	252.38	-1512.18	283.95	-1366.32	330.96	-1087.91

Table D.11 (continued)

h* = 40.095 m		h* = 54.962 m		h* = 69.876 m		h* = 85.067 m	
x (m)	σ'_v (kN/m^2)	x (m)	σ'_v (kN/m^2)	x (m)	σ'_v (kN/m^2)	x (m)	σ'_v (kN/m^2)
243.41	-1708.92	252.38	-1512.14	283.95	-1366.17	330.96	-1088.06
250.73	-1737.97	259.55	-1535.72	293.66	-1369.05	340.48	-1046.14
250.73	-1737.96	259.55	-1535.78	293.66	-1368.91	340.48	-1045.99
253.22	-1746.99	264.21	-1548.61	293.80	-1368.89	346.29	-1016.00
253.22	-1747.06	264.21	-1548.53	293.80	-1369.09	346.29	-1016.01
259.61	-1767.02	273.14	-1567.77	303.55	-1362.78	353.20	-975.65
259.61	-1767.04	273.14	-1567.87	303.55	-1362.74	353.20	-975.72
264.81	-1781.30	281.80	-1579.07	307.25	-1358.23	360.34	-930.66
264.81	-1781.27	281.80	-1579.07	307.25	-1358.26	360.34	-930.53
266.80	-1785.89	287.44	-1583.29	312.90	-1348.11	368.53	-873.12
266.80	-1785.95	287.44	-1583.26	312.90	-1348.22	368.53	-873.15
277.37	-1805.18	295.02	-1583.31	321.29	-1328.62	370.13	-861.49
277.37	-1805.21	295.02	-1583.39	321.29	-1328.42	370.13	-861.41
283.42	-1811.34	298.98	-1581.86	330.39	-1299.60	378.00	-800.71
283.42	-1811.34	298.98	-1581.82	330.39	-1299.68	378.00	-800.77
289.62	-1814.79	302.29	-1579.05	340.23	-1259.17	390.48	-696.56
289.62	-1814.76	302.29	-1579.03	340.23	-1259.17	390.48	-696.35
299.81	-1812.23	309.29	-1570.64	351.62	-1201.93	390.71	-694.42
299.81	-1812.16	309.29	-1570.64	351.62	-1201.88	390.71	-694.63
300.81	-1811.47	317.55	-1554.21	359.69	-1154.27	390.91	-692.82
300.81	-1811.50	317.55	-1554.20	359.69	-1154.29	390.91	-692.83
303.12	-1809.31	320.07	-1548.25	367.51	-1103.58	403.63	-576.77
303.12	-1809.28	320.07	-1548.34	367.51	-1103.60	403.63	-576.75
311.18	-1798.68	322.92	-1540.40	370.97	-1079.58	412.61	-490.08
311.18	-1798.64	322.92	-1540.30	370.97	-1079.50	412.61	-490.01
314.37	-1792.61	333.11	-1507.55	378.32	-1026.31	414.86	-467.24
314.37	-1792.62	333.11	-1507.62	378.32	-1026.33	414.86	-467.31
319.68	-1780.85	339.47	-1481.99	390.00	-934.60	426.68	-343.59
319.68	-1780.88	339.47	-1481.96	390.00	-934.58	426.68	-344.68
325.40	-1765.10	352.78	-1417.61	390.86	-927.65	430.85	-296.47
325.40	-1765.05	352.78	-1417.62	390.86	-927.57	430.85	-294.26
329.26	-1753.20	360.40	-1374.31	391.75	-920.21	439.92	-183.62

Table D.11 (continued)

h* = 40.095 m		h* = 54.962 m		h* = 69.876 m	
x (m)	σ'_v (kN/m^2)	x (m)	σ'_v (kN/m^2)	x (m)	σ'_v (kN/m^2)
329.26	-1753.21	360.40	-1374.28	391.75	-920.27
332.70	-1741.09	368.05	-1326.30	403.52	-819.62
332.70	-1741.16	368.05	-1326.39	403.52	-819.62
343.56	-1696.95	373.29	-1291.19	415.59	-710.08
343.56	-1696.86	373.29	-1291.14	415.59	-710.09
347.58	-1678.36	378.63	-1253.53	416.65	-700.27
347.58	-1678.40	378.63	-1253.53	416.65	-700.21
352.37	-1653.95	388.00	-1183.16	417.78	-689.54
352.37	-1653.93	388.00	-1183.19	417.78	-689.57
362.71	-1596.28	390.78	-1161.57	430.87	-561.83
362.71	-1596.25	390.78	-1161.53	430.87	-561.82
372.00	-1537.42	392.88	-1144.77	448.63	-372.28
372.00	-1537.44	392.88	-1144.72	448.63	-372.32
376.28	-1508.65	403.49	-1057.11	449.31	-364.66
376.28	-1508.64	403.49	-1057.11	449.31	-364.59
385.07	-1445.40	416.60	-942.35	449.63	-361.05
385.07	-1445.44	416.60	-942.29	449.63	-361.88
389.60	-1411.51	416.95	-939.14	461.38	-213.57
389.60	-1411.46	416.95	-939.07	473.13	-33.07
392.40	-1389.65	417.24	-936.46	473.13	-35.09
392.40	-1389.57	417.24	-936.60	473.29	-32.60
402.88	-1305.10	430.93	-810.25	473.29	-29.49
402.88	-1305.09	430.93	-810.25	473.41	-27.70
416.03	-1191.79	442.41	-699.94	473.41	-13.61
416.03	-1191.60	442.41	-700.03	473.59	-9.42
416.28	-1189.44	445.78	-666.46		
416.28	-1189.48	445.78	-666.46		
416.60	-1186.60	450.91	-614.15		
416.60	-1186.73	450.91	-614.13		
429.72	-1067.77	458.83	-531.19		
429.72	-1067.77	458.83	-531.19		
438.86	-981.86	464.58	-467.90		

Table D.11 (continued)

h* = 40.095 m		h* = 54.962 m	
x (m)	σ'_v (kN/m^2)	x (m)	σ'_v (kN/m^2)
438.86	-981.85	464.58	-469.09
443.82	-934.73	469.47	-411.54
443.82	-934.69	469.47	-411.32
450.71	-868.51	480.19	-277.99
450.71	-868.51	480.19	-277.29
457.06	-806.83	483.47	-226.67
457.06	-806.80	483.47	-227.47
459.87	-779.38	495.96	-11.28
459.87	-779.38		
471.97	-658.20		
471.97	-658.35		
472.27	-655.30		
472.27	-655.21		
472.85	-649.27		
472.85	-649.40		
486.34	-501.68		
486.34	-503.28		
493.15	-417.23		
493.15	-417.49		
506.21	-240.78		
506.21	-237.18		
510.10	-176.57		
510.10	-176.14		
518.26	-6.04		

Table D.12 Vertical effective stresses of arbitrary cross-sections 5 to 8 (h*) of 160-m-high cross-section

h* = 100.078 m		**h* = 114.673 m**		**h* = 130.175 m**		**h* = 145.141 m**	
x (m)	σ'_v **(kN/m²)**	**x (m)**	σ'_v **(kN/m²)**	**x (m)**	σ'_v **(kN/m²)**	**x (m)**	σ'_v **(kN/m²)**
156.72	-17.75	178.61	-17.76	201.86	-15.56	224.31	-17.70
159.79	-71.72	181.18	-60.42	210.38	-137.34	227.73	-72.01
159.79	-70.21	181.18	-60.35	210.38	-137.08	227.73	-70.36
167.11	-174.33	187.06	-141.36	213.40	-172.82	240.25	-216.41
167.11	-173.03	187.06	-140.82	213.40	-173.73	240.25	-216.26
170.79	-219.27	196.97	-256.57	219.18	-235.77	240.60	-219.53
170.79	-218.80	196.97	-256.40	219.18	-235.43	240.60	-220.00
171.85	-233.44	200.94	-297.17	226.94	-310.61	241.60	-228.87
171.85	-232.86	200.94	-297.07	226.94	-310.49	241.60	-229.04
174.61	-264.05	208.33	-369.74	230.95	-346.10	256.46	-343.59
174.61	-263.73	208.33	-369.70	230.95	-346.22	256.46	-343.49
185.23	-376.11	215.03	-432.70	241.19	-430.05	259.66	-363.86
185.23	-376.15	215.03	-432.75	241.19	-429.85	259.66	-363.87
190.24	-425.56	218.32	-462.17	242.81	-441.82	264.44	-389.86
190.24	-425.54	218.32	-462.16	242.81	-441.97	264.44	-389.84
202.42	-540.92	227.75	-540.41	244.39	-453.13	275.08	-434.42
202.42	-540.82	227.75	-540.39	244.39	-453.21	275.08	-434.36
204.90	-562.86	233.09	-581.23	256.26	-528.52	284.68	-457.63
204.90	-562.95	233.09	-581.27	256.26	-528.63	284.68	-457.61
210.71	-612.66	238.39	-618.31	267.18	-579.21	286.93	-460.74
210.71	-612.67	238.39	-618.27	267.18	-579.42	286.93	-460.79
218.92	-679.67	242.61	-645.88	272.44	-598.51	289.43	-462.35
218.92	-679.66	242.61	-645.94	272.44	-598.27	289.43	-462.37
222.35	-706.16	247.05	-672.22	281.27	-619.93	299.35	-457.46
222.35	-706.23	247.05	-672.18	281.27	-619.90	299.35	-457.41
235.33	-795.88	254.22	-710.84	282.97	-622.67	311.16	-426.24
235.33	-795.87	254.22	-710.90	282.97	-622.66	311.16	-426.05
238.83	-817.65	261.79	-744.32	290.73	-629.11	312.57	-420.87
238.83	-817.54	261.79	-744.37	290.73	-629.16	312.57	-420.83
245.43	-853.94	268.17	-768.07	293.89	-628.90	315.85	-406.94

Table D.12 (continued)

h* = 100.078 m		h* = 114.673 m		h* = 130.175 m		h* = 145.141 m	
x (m)	σ'_v (kN/m^2)	x (m)	σ'_v (kN/m^2)	x (m)	σ'_v (kN/m^2)	x (m)	σ'_v (kN/m^2)
245.43	-854.09	268.17	-768.08	293.89	-628.87	315.85	-406.95
249.02	-872.15	279.19	-794.59	301.94	-621.00	323.28	-370.57
249.02	-872.12	279.19	-794.67	301.94	-621.02	323.28	-370.64
255.65	-901.48	283.13	-800.95	306.37	-611.97	333.51	-304.84
255.65	-901.49	283.13	-800.88	306.37	-611.92	333.51	-304.57
258.26	-912.20	284.98	-802.66	311.24	-599.14	335.23	-292.36
258.26	-912.07	284.98	-802.75	311.24	-599.29	335.23	-292.82
259.03	-915.07	298.33	-803.38	321.22	-560.68	349.25	-162.05
259.03	-915.21	298.33	-803.34	321.22	-560.70	349.25	-161.69
268.99	-947.76	301.68	-799.61	325.28	-541.64	353.79	-112.41
268.99	-947.82	301.68	-799.56	325.28	-541.54	353.79	-112.58
276.36	-964.28	311.00	-781.62	330.01	-515.67	360.69	-14.86
276.36	-964.35	311.00	-781.61	330.01	-515.78		
280.64	-971.27	318.28	-759.57	338.82	-459.89		
280.64	-971.28	318.28	-759.54	338.82	-459.73		
292.39	-978.63	324.51	-735.16	344.73	-417.41		
292.39	-978.64	324.51	-735.20	344.73	-417.43		
295.33	-978.07	334.46	-686.53	350.42	-371.90		
295.33	-978.02	334.46	-686.38	350.42	-371.84		
300.29	-974.24	335.15	-682.53	354.97	-333.08		
300.29	-974.36	335.15	-682.63	354.97	-333.54		
306.58	-966.27	335.96	-677.92	362.84	-260.31		
306.58	-966.14	335.96	-677.97	362.84	-262.08		
314.43	-949.23	344.91	-624.04	365.59	-234.06		
314.43	-949.21	344.91	-624.05	365.59	-232.22		
315.28	-946.89	350.77	-583.42	370.80	-175.43		
315.28	-946.92	350.77	-583.40	370.80	-177.36		
323.72	-919.87	357.08	-536.55	378.65	-80.52		
323.72	-919.90	357.08	-536.60	378.65	-80.09		
332.10	-885.16	368.27	-442.47	380.75	-54.15		
332.10	-885.23	368.27	-442.48	380.75	-51.30		
335.23	-870.96	371.61	-412.94	383.14	-12.26		

Table D.12 (continued)

h* = 100.078 m		h* = 114.673 m	
x (m)	σ'_v (kN/m^2)	x (m)	σ'_v (kN/m^2)
335.23	-870.95	371.61	-412.89
339.09	-851.41	385.45	-278.14
339.09	-851.35	385.45	-277.51
346.74	-808.47	386.28	-269.23
346.74	-808.49	386.28	-270.17
353.52	-764.84	402.34	-80.24
353.52	-764.82	402.34	-77.89
359.93	-720.70	406.39	-10.57
359.93	-720.64		
364.21	-688.71		
364.21	-688.76		
372.56	-621.95		
372.56	-621.92		
376.64	-587.78		
376.64	-587.87		
389.77	-469.14		
389.77	-469.06		
390.30	-464.10		
390.30	-463.74		
391.01	-457.06		
391.01	-457.60		
404.84	-318.14		
404.84	-317.94		
415.38	-202.03		
415.38	-200.84		
418.91	-155.71		
418.91	-154.59		
428.28	-12.17		

Table D.13 Vertical effective stresses of arbitrary cross-sections 1 to 4 (h*) of 180-m-high cross-section

h* = 48.004 m		**h* = 68.145 m**		**h* = 87.929 m**		**h* = 108.011 m**	
x (m)	**σ'_v (kN/m^2)**	**x (m)**	**σ'_v (kN/m^2)**	**x (m)**	**σ'_v (kN/m^2)**	**x (m)**	**σ'_v (kN/m^2)**
76.31	-10.26	106.52	-13.74	136.19	-13.02	166.32	-20.36
79.55	-87.30	109.35	-74.75	140.12	-91.74	174.31	-148.55
79.55	-83.36	109.35	-73.13	140.12	-91.29	174.31	-148.42
85.99	-206.50	113.21	-144.66	146.43	-188.52	179.85	-219.25
85.99	-206.14	113.21	-145.96	146.43	-189.01	179.85	-220.95
94.51	-341.11	118.56	-227.55	152.39	-268.87	185.20	-286.74
94.51	-339.68	118.56	-231.19	152.39	-268.43	185.20	-285.81
101.70	-435.64	122.55	-288.86	154.59	-298.55	196.96	-413.14
101.70	-435.37	122.55	-287.41	154.59	-299.41	196.96	-413.22
114.76	-593.95	130.64	-390.54	157.58	-336.33	198.77	-432.05
114.76	-594.01	130.64	-390.64	157.58	-335.57	198.77	-432.14
118.69	-637.28	140.01	-501.10	171.12	-485.96	211.88	-560.74
118.69	-637.28	140.01	-501.16	171.12	-485.93	211.88	-560.79
129.69	-753.48	143.49	-539.63	173.33	-509.39	216.83	-607.62
129.69	-753.23	143.49	-539.62	173.33	-509.52	216.83	-607.54
134.83	-805.83	151.27	-622.87	185.64	-633.75	228.32	-709.65
134.83	-805.69	151.27	-622.85	185.64	-633.85	228.32	-709.62
136.55	-823.02	156.08	-672.94	191.30	-688.85	229.53	-720.02
136.55	-823.02	156.08	-672.97	191.30	-688.77	229.53	-720.03
149.32	-947.83	159.05	-703.23	199.96	-769.71	238.14	-790.47
149.32	-947.85	159.05	-703.11	199.96	-769.67	238.14	-790.48
153.20	-985.29	168.37	-794.95	213.15	-886.54	241.92	-820.02
153.20	-985.30	168.37	-794.92	213.15	-886.50	241.92	-820.04
163.24	-1080.69	176.71	-874.29	214.53	-898.45	249.50	-875.81
163.24	-1080.66	176.71	-874.27	214.53	-898.37	249.50	-875.91
167.79	-1123.28	179.59	-901.34	216.04	-911.19	259.96	-945.51
167.79	-1123.31	179.59	-901.33	216.04	-911.20	259.96	-945.45
173.84	-1179.37	181.93	-922.99	227.70	-1005.90	262.12	-958.64
173.84	-1179.38	181.93	-923.06	227.70	-1005.86	262.12	-958.71
181.90	-1252.80	190.51	-1000.95	231.69	-1036.47	263.66	-967.71

Table D.13 (continued)

h* = 48.004 m		h* = 68.145 m		h* = 87.929 m		h* = 108.011 m	
x (m)	σ'_v (kN/m^2)	x (m)	σ'_v (kN/m^2)	x (m)	σ'_v (kN/m^2)	x (m)	σ'_v (kN/m^2)
181.90	-1252.77	190.51	-1000.91	231.69	-1036.52	263.66	-967.81
190.98	-1333.09	196.86	-1057.14	238.55	-1086.70	275.91	-1032.64
190.98	-1333.12	196.86	-1057.16	238.55	-1086.73	275.91	-1032.66
192.07	-1342.58	206.68	-1140.76	243.75	-1123.33	280.03	-1050.98
192.07	-1342.61	206.68	-1140.80	243.75	-1123.36	280.03	-1050.90
202.44	-1430.60	213.04	-1193.20	250.54	-1167.74	287.74	-1081.85
202.44	-1430.66	213.04	-1193.18	250.54	-1167.69	287.74	-1081.81
205.01	-1451.73	221.77	-1261.67	257.20	-1208.45	298.02	-1114.48
205.01	-1451.72	221.77	-1261.68	257.20	-1208.48	298.02	-1114.19
216.71	-1544.40	226.09	-1294.40	260.49	-1226.99	298.57	-1115.67
216.71	-1544.44	226.09	-1294.44	260.49	-1227.05	298.57	-1115.90
220.39	-1572.11	236.74	-1370.06	274.87	-1297.90	299.84	-1118.98
220.39	-1572.12	236.74	-1370.05	274.87	-1297.90	299.84	-1118.93
231.09	-1648.81	240.07	-1392.53	277.37	-1308.89	309.75	-1138.69
231.09	-1648.79	240.07	-1392.54	277.37	-1308.56	309.75	-1138.75
234.63	-1672.92	241.52	-1402.00	278.04	-1311.35	313.17	-1143.12
234.63	-1672.93	241.52	-1402.14	278.04	-1311.48	313.17	-1143.07
238.68	-1699.24	252.76	-1470.78	281.99	-1326.50	320.55	-1148.92
238.68	-1699.28	252.76	-1470.76	281.99	-1326.55	320.55	-1148.92
248.13	-1757.38	255.03	-1483.84	289.87	-1353.39	328.98	-1148.48
248.13	-1757.27	255.03	-1483.73	289.87	-1353.33	328.98	-1148.55
254.39	-1792.68	255.47	-1486.18	291.42	-1357.83	332.08	-1146.78
254.39	-1792.67	255.47	-1486.26	291.42	-1357.80	332.08	-1146.76
265.60	-1848.74	264.83	-1535.07	298.86	-1377.06	343.31	-1131.65
265.60	-1848.87	264.83	-1535.08	298.86	-1377.08	343.31	-1131.65
269.85	-1867.86	272.37	-1569.22	306.66	-1391.79	345.05	-1128.42
269.85	-1867.79	272.37	-1569.29	306.66	-1391.80	345.05	-1128.38
280.84	-1910.63	278.07	-1592.45	312.23	-1399.44	345.41	-1127.61
280.84	-1910.68	278.07	-1592.52	312.23	-1399.47	345.41	-1127.71
284.68	-1923.53	293.12	-1640.49	319.22	-1404.49	358.52	-1091.42
284.68	-1923.48	293.12	-1640.31	319.22	-1404.53	358.52	-1091.49
294.88	-1951.79	294.74	-1644.59	326.41	-1406.13	363.85	-1072.05

Table D.13 (continued)

h* = 48.004 m		h* = 68.145 m		h* = 87.929 m		h* = 108.011 m	
x (m)	σ'_v (kN/m^2)	x (m)	σ'_v (kN/m^2)	x (m)	σ'_v (kN/m^2)	x (m)	σ'_v (kN/m^2)
294.88	-1951.82	294.74	-1644.35	326.41	-1406.06	363.85	-1071.91
296.68	-1955.97	295.52	-1646.28	334.98	-1400.85	371.89	-1038.13
296.68	-1955.96	295.52	-1646.38	334.98	-1400.92	371.89	-1038.11
307.23	-1975.24	296.59	-1648.78	339.23	-1396.43	377.53	-1010.59
307.23	-1975.31	296.59	-1649.19	339.23	-1396.45	377.53	-1010.74
311.42	-1980.43	316.19	-1678.41	342.64	-1391.20	384.63	-972.21
311.42	-1980.41	316.19	-1678.20	342.64	-1391.12	384.63	-972.09
324.18	-1987.35	318.65	-1679.56	352.40	-1371.93	389.37	-943.75
324.18	-1987.37	318.65	-1679.62	352.40	-1371.98	389.37	-943.81
328.27	-1987.02	330.49	-1679.68	362.00	-1344.14	394.02	-913.75
328.27	-1986.98	330.49	-1679.64	362.00	-1344.23	394.02	-913.74
334.96	-1982.76	333.44	-1677.75	368.89	-1319.94	403.66	-847.36
334.96	-1982.89	333.44	-1677.75	368.89	-1319.79	403.66	-847.37
341.07	-1976.62	341.72	-1669.11	375.87	-1290.28	412.61	-778.38
341.07	-1976.46	341.72	-1669.00	375.87	-1290.38	412.61	-778.39
351.32	-1958.87	348.11	-1658.46	381.84	-1262.59	420.08	-717.73
351.32	-1958.98	348.11	-1658.49	381.84	-1262.52	420.08	-717.74
358.11	-1942.41	358.57	-1633.45	393.14	-1200.96	430.80	-623.16
358.11	-1942.41	358.57	-1633.57	393.14	-1200.90	430.80	-623.24
369.73	-1905.96	360.64	-1627.75	394.43	-1193.40	439.64	-541.19
369.73	-1905.93	360.64	-1627.65	394.43	-1193.38	439.64	-541.96
374.77	-1886.93	373.01	-1584.82	397.66	-1173.46	446.89	-469.96
374.77	-1886.96	373.01	-1584.60	397.66	-1173.37	446.89	-469.81
382.57	-1853.32	373.21	-1583.82	408.11	-1104.83	462.82	-304.36
382.57	-1853.37	373.21	-1583.95	408.11	-1104.86	462.82	-305.01
388.69	-1824.69	373.97	-1580.87	413.23	-1068.03	464.82	-279.89
388.69	-1824.67	373.97	-1580.91	413.23	-1067.97	464.82	-278.38
399.71	-1765.00	385.80	-1527.67	423.63	-989.62	478.33	-105.71
399.71	-1764.99	385.80	-1527.64	423.63	-989.63	478.33	-104.40
404.59	-1736.57	389.31	-1509.60	433.28	-911.02	482.39	-42.17
404.59	-1736.42	389.31	-1509.57	433.28	-911.09	482.39	-42.12
406.15	-1726.85	398.41	-1459.37	440.68	-847.41	483.68	-20.00

Table D.13 (continued)

h* = 48.004 m		h* = 68.145 m		h* = 87.929 m	
x (m)	σ'_v (kN/m^2)	x (m)	σ'_v (kN/m^2)	x (m)	σ'_v (kN/m^2)
406.15	-1727.01	398.41	-1459.36	440.68	-847.30
411.86	-1690.49	405.16	-1417.98	456.06	-708.00
411.86	-1690.49	405.16	-1418.05	456.06	-707.98
421.69	-1624.32	410.20	-1385.51	458.32	-686.28
421.69	-1624.27	410.20	-1385.46	458.32	-686.38
425.75	-1594.95	417.79	-1333.10	468.75	-584.44
425.75	-1594.87	417.79	-1333.07	479.18	-477.61
434.70	-1527.83	424.08	-1287.42	479.18	-479.19
434.70	-1527.83	424.08	-1287.42	479.52	-475.41
446.66	-1431.92	433.45	-1215.24	479.52	-474.69
446.66	-1431.91	433.45	-1215.23	480.02	-469.08
448.20	-1419.20	434.44	-1207.43	480.02	-469.47
448.20	-1419.13	434.44	-1207.47	499.74	-236.53
449.33	-1409.68	439.54	-1166.08	499.74	-236.01
449.33	-1409.72	439.54	-1165.99	511.92	-52.09
462.26	-1298.60	448.69	-1089.44	511.92	-52.37
462.26	-1298.62	448.69	-1089.38	513.81	-15.79
472.67	-1204.89	450.09	-1077.34		
472.67	-1204.89	450.09	-1077.50		
477.47	-1160.90	455.76	-1027.65		
477.47	-1160.86	455.76	-1027.68		
481.40	-1124.38	467.61	-921.19		
481.40	-1124.39	467.61	-921.12		
493.72	-1008.38	470.28	-896.54		
493.72	-1008.37	470.28	-896.47		
500.46	-943.56	482.45	-780.89		
500.46	-943.54	482.45	-780.82		
508.52	-865.25	484.37	-762.20		
508.52	-865.41	484.37	-762.34		
518.28	-767.05	498.39	-619.68		
518.28	-767.07	498.39	-619.57		
525.32	-694.85	503.39	-567.08		

Table D.13 (continued)

h* = 48.004 m		h* = 68.145 m	
x (m)	σ'_v (kN/m^2)	x (m)	σ'_v (kN/m^2)
525.32	-694.80	503.39	-567.51
531.61	-627.63	509.81	-496.81
531.61	-627.64	509.81	-498.32
544.90	-471.03	526.40	-290.87
544.90	-470.32	526.40	-289.79
548.87	-420.43	541.62	-53.17
548.87	-421.89	541.62	-56.34
560.24	-260.52	542.70	-38.53
571.61	-68.00	542.70	-30.10
571.61	-63.51	543.48	-11.90
572.71	-44.53		
572.71	-34.89		
573.69	-13.32		

Table D.14 Vertical effective stresses of arbitrary cross-sections 5 to 8 (h*) of 180-m-high cross-section

h* = 128.038 m		h* = 148.064 m		h* = 167.718 m		h* = 187.812 m	
x (m)	σ'_v (kN/m^2)	x (m)	σ'_v (kN/m^2)	x (m)	σ'_v (kN/m^2)	x (m)	σ'_v (kN/m^2)
196.36	-18.30	226.40	-17.21	255.88	-13.70	286.02	-18.79
203.00	-121.37	232.21	-106.64	256.12	-18.63	286.91	-37.45
203.00	-119.96	232.21	-105.25	256.12	-18.50	286.91	-39.47
212.38	-238.48	240.88	-210.85	262.34	-116.78	289.67	-83.45
212.38	-238.02	240.88	-209.60	262.34	-117.30	289.67	-86.15
217.12	-288.61	243.04	-233.63	271.75	-222.03	298.68	-187.19
217.12	-288.66	243.04	-234.67	271.75	-220.19	298.68	-185.41
227.08	-390.69	244.51	-250.53	273.76	-240.63	300.73	-205.31
227.08	-390.69	244.51	-249.63	273.76	-241.58	300.73	-206.33
235.03	-466.05	255.89	-358.66	276.01	-261.78	304.63	-223.12
235.03	-466.19	255.89	-358.55	276.01	-261.32	304.63	-220.48
243.33	-540.74	257.62	-374.14	288.07	-349.43	314.65	-241.92

Table D.14 (continued)

h* = 128.038 m		h* = 148.064 m		h* = 167.718 m		h* = 187.812 m	
x (m)	σ'_v (kN/m^2)	x (m)	σ'_v (kN/m^2)	x (m)	σ'_v (kN/m^2)	x (m)	σ'_v (kN/m^2)
243.33	-540.63	257.62	-374.36	288.07	-349.17	314.65	-241.71
248.77	-586.32	262.51	-415.79	297.94	-402.63	323.74	-247.06
248.77	-586.33	262.51	-415.67	297.94	-402.72	323.74	-247.60
253.50	-623.57	271.84	-487.98	303.77	-426.75	331.51	-242.02
253.50	-623.62	271.84	-488.06	303.77	-426.39	331.51	-242.21
263.84	-699.30	276.47	-519.30	313.90	-455.87	337.36	-233.84
263.84	-699.16	276.47	-519.23	313.90	-455.63	337.36	-236.02
269.08	-732.77	287.43	-584.66	321.81	-465.69	340.45	-230.92
269.08	-732.92	287.43	-584.64	321.81	-465.86	340.45	-229.10
277.69	-781.76	299.40	-637.10	331.93	-460.77	356.21	-135.02
277.69	-781.78	299.40	-637.23	331.93	-460.65	356.21	-132.60
283.93	-814.25	303.09	-649.99	334.72	-456.20	361.60	-68.56
283.93	-814.18	303.09	-649.77	334.72	-456.22	361.60	-65.92
290.27	-841.67	314.00	-675.51	337.36	-450.15	362.55	-54.63
290.27	-841.67	314.00	-675.39	337.36	-450.13	362.55	-49.46
297.31	-867.59	315.08	-676.98	348.28	-414.29	363.98	-25.20
297.31	-867.50	315.08	-677.09	348.28	-414.38		
302.34	-881.93	323.93	-683.59	363.27	-334.60		
302.34	-882.01	323.93	-683.55	363.27	-333.54		
307.33	-893.83	328.97	-681.96	363.49	-332.11		
307.33	-893.73	328.97	-682.04	363.49	-333.61		
313.27	-903.78	340.81	-663.65	363.59	-333.00		
313.27	-903.87	340.81	-663.62	363.59	-334.41		
323.40	-911.29	344.33	-654.34	363.92	-332.13		
323.40	-911.17	344.33	-654.34	363.92	-334.72		
324.15	-911.31	349.55	-636.63	378.79	-212.23		
324.15	-911.36	349.55	-636.67	378.79	-210.60		
324.81	-911.32	357.98	-602.27	389.75	-83.94		
324.81	-911.43	357.98	-602.26	389.75	-80.61		
336.18	-903.26	364.30	-569.72	392.31	-43.46		
336.18	-903.27	364.30	-569.75	392.31	-45.02		
344.95	-886.14	369.66	-538.53	394.12	-13.86		

Table D.14 (continued)

h* = 128.038 m		h* = 148.064 m	
x (m)	σ'_v (kN/m^2)	x (m)	σ'_v (kN/m^2)
344.95	-886.23	369.66	-538.49
349.00	-875.74	375.34	-501.04
349.00	-875.78	375.34	-501.25
363.81	-820.23	381.80	-455.14
363.81	-820.00	381.80	-455.21
365.06	-814.39	391.73	-374.33
365.06	-814.14	391.73	-374.29
365.32	-812.90	395.04	-345.47
365.32	-813.49	395.04	-345.36
365.77	-811.19	404.11	-257.61
365.77	-811.36	404.11	-256.41
381.99	-720.35	420.32	-66.68
381.99	-720.06	420.32	-70.49
393.95	-637.61	422.08	-47.49
393.95	-637.66	422.08	-45.37
395.32	-627.14	422.75	-37.18
395.32	-627.19	422.75	-28.99
401.71	-576.07	423.60	-14.36
401.71	-576.07		
410.46	-502.01		
410.46	-501.81		
411.88	-489.41		
411.88	-489.78		
428.55	-329.20		
428.55	-328.90		
429.54	-319.27		
429.54	-319.96		
440.54	-198.82		
451.54	-56.07		
451.54	-60.07		
452.29	-50.22		
452.29	-46.55		

Table D.14 (continued)

h* = 128.038 m	
x (m)	σ'_v (kN/m^2)
452.88	-39.20
452.88	-26.83
453.64	-12.82

Table D.15 Vertical effective stresses of arbitrary cross-sections 1 to 4 (h*) of 200-m-high cross-section

h* = 52.135 m		h* = 72.120 m		h* = 92.085 m		h* = 112.050 m	
x (m)	σ'_v (kN/m^2)	x (m)	σ'_v (kN/m^2)	x (m)	σ'_v (kN/m^2)	x (m)	σ'_v (kN/m^2)
80.20	-9.89	110.18	-4.66	140.13	-23.92	170.07	-17.14
87.23	-164.85	119.40	-189.91	144.72	-107.61	170.15	-18.79
87.23	-158.90	119.40	-189.68	144.72	-104.81	170.15	-22.38
92.48	-253.96	128.02	-323.58	157.27	-296.02	170.85	-35.15
92.48	-254.52	128.02	-321.91	157.27	-296.01	170.85	-32.03
98.87	-355.82	129.99	-347.80	160.94	-340.90	184.25	-241.43
98.87	-354.00	129.99	-347.20	160.94	-341.13	184.25	-240.60
106.90	-464.01	141.94	-497.37	173.26	-484.98	185.26	-256.22
106.90	-464.14	141.94	-497.43	173.26	-484.68	185.26	-255.20
116.71	-586.59	147.06	-556.27	183.87	-599.41	186.50	-270.21
116.71	-586.66	147.06	-556.23	183.87	-599.53	186.50	-270.14
122.03	-649.18	153.69	-629.37	191.72	-679.39	198.62	-409.25
122.03	-649.25	153.69	-629.37	191.72	-679.28	198.62	-409.43
125.39	-687.65	168.61	-786.91	202.09	-781.57	209.04	-519.08
125.39	-687.70	168.61	-786.83	202.09	-781.50	209.04	-519.03
138.56	-826.83	180.13	-900.06	218.39	-933.17	212.38	-553.27
138.56	-826.87	180.13	-900.13	218.39	-933.20	212.38	-553.35
143.56	-878.18	191.60	-1009.63	219.87	-946.35	228.53	-709.88
143.56	-878.18	191.60	-1009.55	219.87	-946.50	228.53	-709.72
153.97	-980.95	201.13	-1097.14	221.09	-957.26	229.45	-718.31
153.97	-980.96	201.13	-1097.19	221.09	-957.26	229.45	-718.20
159.59	-1035.72	217.73	-1243.63	237.57	-1098.46	245.19	-858.39

Table D.15 (continued)

h* = 52.135 m		h* = 72.120 m		h* = 92.085 m		h* = 112.050 m	
x (m)	σ'_v (kN/m^2)	x (m)	σ'_v (kN/m^2)	x (m)	σ'_v (kN/m^2)	x (m)	σ'_v (kN/m^2)
159.59	-1035.77	217.73	-1243.56	237.57	-1098.44	245.19	-858.22
173.19	-1165.89	221.27	-1274.11	244.44	-1153.59	245.35	-859.52
173.19	-1165.91	221.27	-1273.95	244.44	-1153.57	245.35	-859.60
177.70	-1208.55	223.22	-1290.40	252.96	-1219.47	259.36	-973.35
177.70	-1208.59	223.22	-1290.61	252.96	-1219.49	259.36	-973.38
191.70	-1338.48	241.30	-1435.98	264.94	-1304.78	267.73	-1035.43
191.70	-1338.50	241.30	-1435.91	264.94	-1304.80	267.73	-1035.65
194.82	-1366.85	244.38	-1459.38	268.93	-1331.74	283.77	-1142.31
194.82	-1366.89	244.38	-1459.49	268.93	-1331.80	283.77	-1142.12
205.11	-1458.95	261.88	-1583.62	280.16	-1401.03	286.34	-1157.51
205.11	-1458.98	261.88	-1583.35	280.16	-1401.09	286.34	-1157.64
211.62	-1515.66	262.50	-1587.48	285.45	-1431.38	288.39	-1169.24
211.62	-1515.65	262.50	-1587.62	285.45	-1431.60	288.39	-1169.36
215.86	-1552.04	265.10	-1604.39	288.13	-1445.68	304.86	-1252.80
215.86	-1552.13	265.10	-1604.47	288.13	-1445.63	304.86	-1252.85
226.92	-1643.16	280.63	-1697.52	303.00	-1516.44	310.62	-1276.21
226.92	-1643.11	280.63	-1697.55	303.00	-1516.32	310.62	-1276.00
232.71	-1689.51	284.33	-1717.22	314.55	-1559.27	322.74	-1318.05
232.71	-1689.36	284.33	-1717.23	314.55	-1559.41	322.74	-1318.08
234.18	-1700.86	300.96	-1795.39	324.98	-1589.31	336.20	-1349.66
234.18	-1701.06	300.96	-1795.30	324.98	-1589.29	336.20	-1349.40
242.01	-1760.07	306.95	-1818.79	338.84	-1616.06	337.66	-1352.03
242.01	-1760.08	306.95	-1818.85	338.84	-1616.11	337.66	-1352.32
254.59	-1850.22	314.91	-1845.14	343.01	-1621.50	357.74	-1368.53
254.59	-1850.18	314.91	-1845.27	343.01	-1621.54	357.74	-1367.86
257.00	-1866.33	326.25	-1876.23	351.20	-1627.18	357.96	-1367.88
257.00	-1866.36	326.25	-1876.07	351.20	-1627.16	357.96	-1367.72
273.35	-1968.35	337.18	-1896.15	360.27	-1628.75	358.15	-1367.69
273.35	-1968.43	337.18	-1896.23	360.27	-1628.75	358.15	-1368.34
279.76	-2003.78	341.03	-1901.37	366.71	-1624.91	359.19	-1367.92
279.76	-2003.69	341.03	-1901.39	366.71	-1624.84	359.19	-1368.11
291.17	-2061.24	352.90	-1910.17	379.39	-1609.92	377.67	-1350.08

Table D.15 (continued)

h* = 52.135 m		h* = 72.120 m		h* = 92.085 m		h* = 112.050 m	
x (m)	σ'_v (kN/m^2)	x (m)	σ'_v (kN/m^2)	x (m)	σ'_v (kN/m^2)	x (m)	σ'_v (kN/m^2)
291.17	-2061.19	352.90	-1910.09	379.39	-1609.86	377.67	-1349.93
300.04	-2099.43	358.65	-1910.96	397.38	-1565.86	385.57	-1332.66
300.04	-2099.54	358.65	-1911.17	397.38	-1565.78	385.57	-1332.83
304.62	-2117.51	372.12	-1901.72	399.56	-1559.04	390.67	-1319.33
304.62	-2117.48	372.12	-1901.79	399.56	-1558.90	390.67	-1319.34
314.14	-2150.12	381.18	-1889.81	402.01	-1550.46	399.54	-1289.98
314.14	-2150.05	381.18	-1889.73	402.01	-1550.56	399.54	-1290.01
320.70	-2169.05	385.81	-1880.51	416.45	-1492.59	407.43	-1260.03
320.70	-2169.13	385.81	-1880.38	416.45	-1492.53	407.43	-1259.95
336.43	-2201.00	402.30	-1835.77	422.92	-1461.38	409.73	-1250.13
336.43	-2201.07	402.30	-1835.78	422.92	-1461.38	409.73	-1250.06
339.42	-2205.54	412.51	-1797.43	432.56	-1409.29	419.71	-1201.54
339.42	-2205.55	412.51	-1797.49	432.56	-1409.31	419.71	-1201.66
341.70	-2208.08	417.49	-1776.73	442.31	-1350.46	425.84	-1168.52
341.70	-2208.03	417.49	-1776.67	442.31	-1350.47	425.84	-1168.46
359.36	-2217.27	419.81	-1766.11	450.83	-1293.82	428.84	-1150.63
359.36	-2217.23	419.81	-1766.21	450.83	-1293.78	428.84	-1150.64
373.09	-2207.30	435.51	-1686.33	465.88	-1184.19	439.71	-1082.21
373.09	-2207.65	435.51	-1686.31	465.88	-1184.16	439.71	-1082.30
378.38	-2200.76	440.04	-1660.13	472.18	-1134.67	446.39	-1035.97
378.38	-2200.70	440.04	-1660.09	472.18	-1134.67	446.39	-1036.01
397.24	-2158.62	455.33	-1563.27	483.35	-1042.20	457.96	-948.78
397.24	-2158.45	455.33	-1563.31	483.35	-1042.21	457.96	-948.60
400.07	-2150.24	461.36	-1521.23	492.29	-965.51	471.96	-833.85
400.07	-2150.18	461.36	-1521.11	492.29	-965.44	471.96	-833.90
402.54	-2142.19	475.92	-1413.00	497.87	-915.62	479.44	-767.48
402.54	-2142.45	475.92	-1412.98	497.87	-915.74	479.44	-767.41
413.88	-2099.92	485.58	-1335.49	514.12	-763.27	492.23	-649.33
425.23	-2050.72	485.58	-1335.56	514.12	-763.27	492.23	-649.44
425.23	-2050.63	493.54	-1269.57	530.76	-597.64	508.47	-488.37
426.15	-2046.36	493.54	-1269.52	530.76	-597.53	508.47	-488.81
426.15	-2045.83	506.41	-1157.68	540.10	-497.04	516.91	-398.26

Table D.15 (continued)

h* = 52.135 m		h* = 72.120 m		h* = 92.085 m		h* = 112.050 m	
x (m)	σ'_v (kN/m^2)	x (m)	σ'_v (kN/m^2)	x (m)	σ'_v (kN/m^2)	x (m)	σ'_v (kN/m^2)
426.27	-2045.23	506.41	-1157.70	540.10	-498.23	516.91	-396.24
426.27	-2045.74	515.85	-1073.06	554.55	-324.39	523.45	-321.18
446.45	-1935.00	515.85	-1073.12	554.55	-324.09	523.45	-322.32
446.45	-1934.75	534.39	-898.21	566.11	-170.42	536.15	-163.37
447.57	-1927.84	534.39	-898.27	566.11	-171.14	536.15	-161.35
447.57	-1928.07	544.79	-796.95	574.87	-21.50	544.93	-8.80
464.91	-1813.36	544.79	-796.83				
464.91	-1813.29	565.96	-572.27				
468.18	-1789.84	565.96	-572.18				
468.18	-1789.85	568.88	-539.56				
483.09	-1677.32	568.88	-540.08				
483.09	-1677.34	571.18	-514.33				
491.72	-1607.54	571.18	-515.41				
491.72	-1607.50	582.87	-370.73				
502.29	-1518.93	594.57	-198.69				
502.29	-1518.97	594.57	-197.54				
520.96	-1353.45	599.13	-129.04				
520.96	-1353.46	599.13	-129.25				
525.01	-1316.57	604.82	-21.67				
525.01	-1316.49						
527.69	-1291.80						
527.69	-1291.76						
534.67	-1226.62						
534.67	-1226.68						
547.38	-1106.47						
547.38	-1106.41						
563.93	-946.39						
563.93	-946.79						
566.04	-925.93						
566.04	-925.93						
568.48	-901.23						
568.48	-901.21						

Table D.15 (continued)

h* = 52.135 m	
x (m)	σ'_v (kN/m^2)
583.84	-743.42
583.84	-743.65
601.57	-541.09
601.57	-542.86
602.54	-531.26
602.54	-528.38
603.00	-522.98
603.00	-524.87
616.46	-340.94
629.92	-120.56
629.92	-118.03
632.20	-79.64
632.20	-72.92
634.80	-17.86

Table D.16 Vertical effective stresses of arbitrary cross-sections 5 to 8 (h*) of 200-m-high cross-section

h* = 132.409 m		h* = 152.380 m		h* = 172.092 m		h* = 192.322 m	
x (m)	σ'_v (kN/m^2)	x (m)	σ'_v (kN/m^2)	x (m)	σ'_v (kN/m^2)	x (m)	σ'_v (kN/m^2)
200.61	-17.24	230.57	-20.32	260.14	-18.26	290.48	-16.19
203.69	-73.82	243.04	-195.02	264.17	-84.48	297.95	-135.61
203.69	-74.19	243.04	-194.87	264.17	-82.25	297.95	-135.53
210.44	-170.00	247.74	-248.61	269.59	-157.44	313.35	-289.70
210.44	-170.64	247.74	-249.88	269.59	-155.81	313.35	-291.78
217.06	-252.43	254.14	-319.56	272.78	-193.18	314.70	-303.73
217.06	-252.15	254.14	-319.20	272.78	-196.67	314.70	-302.91
219.38	-280.96	267.21	-445.75	277.48	-247.38	315.17	-307.87
219.38	-281.10	267.21	-445.72	277.48	-246.62	315.17	-303.17
222.89	-320.99	275.60	-521.50	282.75	-299.17	315.83	-307.57
222.89	-320.57	275.60	-521.56	282.75	-298.80	315.83	-308.39

Table D.16 (continued)

h* = 132.409 m		h* = 152.380 m		h* = 172.092 m		h* = 192.322 m	
x (m)	σ'_v (kN/m^2)	x (m)	σ'_v (kN/m^2)	x (m)	σ'_v (kN/m^2)	x (m)	σ'_v (kN/m^2)
235.92	-455.50	286.57	-609.45	286.40	-332.29	336.75	-411.69
235.92	-455.46	286.57	-609.39	286.40	-332.40	336.75	-411.50
241.73	-512.98	293.87	-663.10	296.20	-417.02	339.04	-419.51
241.73	-513.39	293.87	-663.20	296.20	-417.12	339.04	-419.62
256.32	-646.62	308.37	-752.64	307.43	-499.35	343.97	-431.66
256.32	-646.66	308.37	-752.82	307.43	-499.65	343.97	-431.88
266.46	-733.86	313.77	-781.49	310.06	-516.74	358.70	-447.97
266.46	-733.66	313.77	-781.45	310.06	-516.83	358.70	-447.87
280.42	-840.01	316.62	-794.59	326.42	-602.77	366.45	-439.05
280.42	-840.06	316.62	-794.72	326.42	-602.57	366.45	-439.05
282.87	-857.27	334.40	-859.96	326.95	-604.78	376.36	-414.28
282.87	-857.16	334.40	-859.82	326.95	-605.32	376.36	-414.44
294.80	-932.54	337.95	-868.27	329.80	-615.85	386.83	-371.73
294.80	-932.79	337.95	-868.21	329.80	-615.75	386.83	-372.32
305.92	-992.18	350.75	-887.51	345.69	-660.17	391.77	-346.86
305.92	-992.19	350.75	-887.54	345.69	-660.01	391.77	-346.43
309.90	-1011.40	354.27	-889.23	348.76	-664.44	404.58	-263.89
309.90	-1011.53	354.27	-889.14	348.76	-664.57	404.58	-258.80
312.23	-1021.78	365.01	-885.80	363.62	-666.14	407.53	-233.26
312.23	-1021.86	365.01	-885.75	363.62	-665.97	407.53	-236.28
327.05	-1076.76	375.49	-869.32	370.67	-655.42	416.94	-129.49
327.05	-1076.73	375.49	-869.52	370.67	-655.43	416.94	-131.72
335.14	-1096.86	387.68	-833.91	381.90	-623.79	424.52	-16.78
335.14	-1096.89	387.68	-833.85	381.90	-624.07		
343.47	-1111.92	394.33	-808.43	386.65	-606.69		
343.47	-1111.84	394.33	-808.33	386.65	-606.35		
353.95	-1120.19	401.90	-772.63	399.84	-541.22		
353.95	-1120.22	401.90	-772.83	399.84	-541.25		
356.69	-1120.73	409.19	-733.08	404.44	-513.82		
356.69	-1120.73	409.19	-732.92	404.44	-513.90		
368.64	-1113.95	420.33	-662.36	417.97	-417.12		
368.64	-1114.03	420.33	-662.46	417.97	-417.25		

Table D.16 (continued)

h* = 132.409 m		h* = 152.380 m		h* = 172.092 m	
x (m)	σ'_v (kN/m^2)	x (m)	σ'_v (kN/m^2)	x (m)	σ'_v (kN/m^2)
372.96	-1108.02	427.96	-607.02	425.66	-354.37
372.96	-1108.00	427.96	-607.22	425.66	-355.44
387.11	-1075.93	450.48	-416.56	442.99	-176.98
387.11	-1075.88	450.48	-416.23	442.99	-177.03
392.36	-1058.81	450.78	-413.42	448.78	-108.05
392.36	-1058.89	450.78	-415.90	448.78	-108.61
404.95	-1007.17	450.99	-413.66	454.86	-20.11
404.95	-1007.19	450.99	-416.14		
408.76	-989.23	453.54	-388.81		
408.76	-988.97	453.54	-386.94		
411.71	-974.00	466.94	-247.90		
411.71	-974.02	480.34	-87.61		
425.21	-896.63	480.34	-86.33		
425.21	-896.52	482.28	-63.14		
438.60	-804.54	482.28	-53.79		
438.60	-804.54	484.43	-19.57		
440.95	-787.18				
440.95	-787.26				
444.97	-756.02				
444.97	-755.73				
460.04	-629.72				
460.04	-630.14				
465.95	-575.23				
465.95	-575.46				
477.44	-466.40				
488.92	-349.86				
488.92	-348.17				
494.70	-283.71				
494.70	-283.32				
514.39	-20.56				

APPENDIX E

A general view of the user interface of the algorithm for optimizing the instruments in one layer, *h**, is presented in Figure E.1.

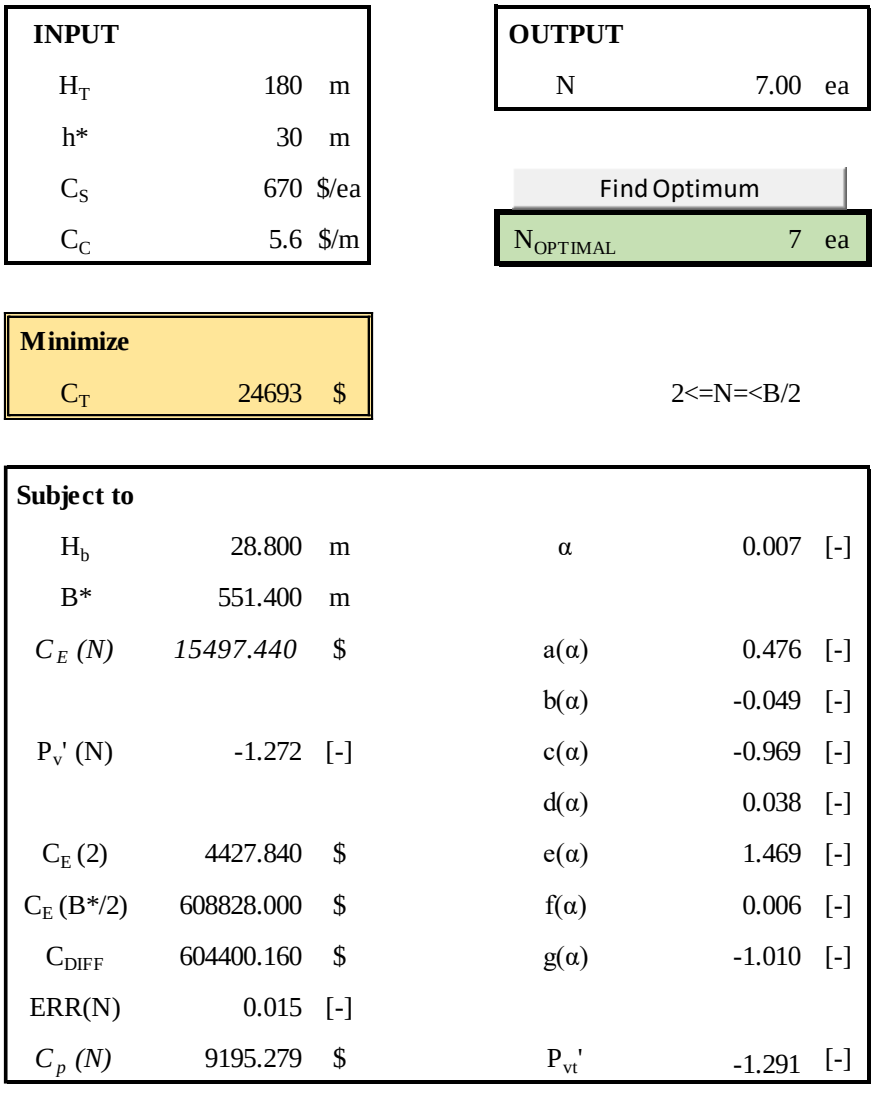

Figure E.1 General view of working spreadsheet

CURRICULUM VITAE

PERSONAL INFORMATION

Surname, Name: Arı, Onur
Nationality: Turkish (TC)
Date and Place of Birth: 1 April 1983, Ankara
Marital Status: Single
Phone: +90 312 498 20 68
Email: onur.ari@me.com

EDUCATION

Degree	Institution	Year of Graduation
MS	QMUL Sustainable Energy Systems	2014
MS	METU Civil Engineering	2008
BS	METU Civil Engineering	2006
High School	Ankara Ataturk Anadolu High School	2001

WORK EXPERIENCE

Year	Place	Enrolment
2015-Present	EnerjiSA	Optimization Specialist
2011-2015	Development Bank of Turkey	Junior Specialist
2006-2011	METU Dept. of Civil Engineering	Research Assistant

FOREIGN LANGUAGES

Advanced English, Intermediate German and French

PUBLICATIONS

1. Yanmaz, A. M., and Arı, O. (2011). A study on dam instrumentation retrofitting. *KSCE Journal of Civil Engineering*, *15*(2), 317-325.

2. Yanmaz, A.M. and Arı, O. (2008). *An Overview of the Role of Retrofitted Instruments in Dam Safety*, Famagusta: 8th International Congress on Advances in Civil Engineering.